



Universiteit
Leiden
The Netherlands

Evolutionary developmental biology of bitterling fish

Yi, W.

Citation

Yi, W. (2022, March 15). *Evolutionary developmental biology of bitterling fish*. Retrieved from <https://hdl.handle.net/1887/3278974>

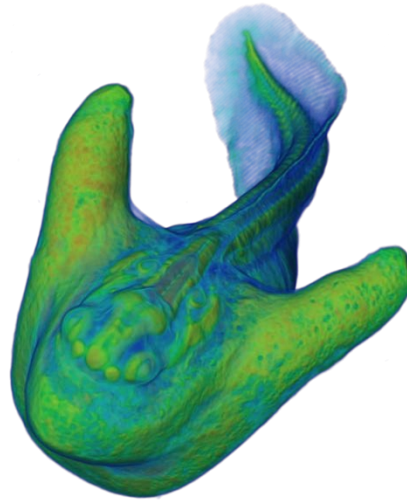
Version: Publisher's Version

License: [Licence agreement concerning inclusion of doctoral thesis in the Institutional Repository of the University of Leiden](#)

Downloaded from: <https://hdl.handle.net/1887/3278974>

Note: To cite this publication please use the final published version (if applicable).

Evolutionary developmental biology of bitterling fish



Wenjing Yi

Printing: Ridderprint, www.ridderprint.nl

Evolutionary developmental biology of bitterling fish

Wenjing Yi

PhD thesis, Institute of Biology (IBL) Leiden University, the Netherlands

Layout by Wenjing Yi

Evolutionary developmental biology of bitterling fish

Proefschrift

ter verkrijging van

de graad van doctor aan de Universiteit Leiden

op gezag van rector magnificus prof.dr.ir. H. Bijl,

volgens besluit van het college voor promoties

te verdedigen op 15 maart 2022

klokke 10.00 uur

door

Wenjing Yi

geboren te Zigui, China

op 13 november 1988

Promotiecommissie

Promotor: Prof.dr. M.K. Richardson

Co-promotor: Dr. M. Rücklin (Naturalis Biodiversity Center)

Promotiecommissie: Prof.dr. G.P. van Wezel

Prof.dr. M.C. de Ruiter

Prof.dr.ir. F.J. Verbeek

Prof.dr. D. Aldridge (University of Cambridge)

Prof.dr. M. Reichard (Czech Academy of Sciences)

Dr. M.J. Spierings

Contents

Chapter 1 Introduction and outline of this thesis.....	7
Chapter 2 Normal stages of embryonic development of a brood parasite, the rosy bitterling <i>Rhodeus ocellatus</i> (Teleostei: Cypriniformes).....	25
Chapter 3 Developmental neuroanatomy of the rosy bitterling <i>Rhodeus ocellatus</i> (Teleostei: Cypriniformes)	73
Chapter 4 Spatial and temporal expression of marker genes during early brain regionalization in the rosy bitterling (<i>Rhodeus ocellatus</i>)	103
Chapter 5 Pre-hatching early embryonic development in the rosy bitterling (<i>Rhodeus ocellatus</i>)	117
Chapter 6 Summary and discussion.....	131
Addendum	139
Nederlandse samenvatting	140
Curriculum vitae	141
List of publications	142

Chapter 1 Introduction and outline of this thesis

Wenjing Yi, Michael K. Richardson

Institute of Biology, University of Leiden, Sylvius Laboratory, Sylviusweg 72, 2333BE, Leiden, the Netherlands.

Manuscript in preparation

General introduction to bitterlings

The bitterlings are a group of Eurasian freshwater teleost fish with approximately 75 species (Nelson et al., 2016). Phylogenetically, the bitterlings are a monophyletic group belonging to the family Acheilognathidae (Cypriniformes: Cyprinoidea). According to recent studies, the family is divided into six clusters, namely: *Acheilognathus*, *Tanakia*, *Paratanakia*, *Pseudorhodes*, *Rhodeus* and an unnamed clade (Chang et al., 2014; Cheng et al., 2014; Kawamura et al., 2014). Among them, the genus *Rhodeus* is strongly supported as being monophyletic. As there are no known diagnostic morphological characters to discriminate *Paratanakia* and *Pseudorhodes* from congeners, we use here the classification and diagnostic key provided by taxonomists (Arai and Yutaka, 1988; Arai et al., 2007; Li and Arai, 2010; Li et al., 2017), and group all bitterling species into three genera: *Acheilognathus*, *Tanakia* and *Rhodeus*.

There are two main hypotheses about the phylogenetic relationships inside the bitterling clade. The original hypothesis is based on the patterns of minute tubercles on the surface of the embryonic skin (Suzuki and Hibiya, 1985a), and on a comparison of the adult cephalic sensory canal system, infraorbital bones, and trunk lateral-line scales (Arai, 2003). It suggests that the basal genus is *Tanakia*, with *Acheilognathus* and *Rhodeus* having evolved within it (Arai, 2003). A more recent alternative hypothesis, supported by molecular data (Chang et al., 2014; Cheng et al., 2014; Kawamura et al., 2014) is that *Acheilognathus* is basal to the *Tanakia-Rhodeus* complex.

Brood parasitism

All bitterling species are brood parasites because they lay eggs in the gills of freshwater mussels (Bivalvia: Unionoida) and rely on the host mussel for the protection of their offspring (Figure 1; Leung, 2014; Mills and Reynolds, 2003; Olt, 1893; Smith, 2016). Other teleosts showing brood parasitism include the snailfish (Liparidae) which oviposit their eggs in the gill chamber of lithodid crabs (Lithodidae; Gardner et al., 2016), and the Japanese tubesnout fish (Hypoptychidae) which lay eggs in the peribranchial cavity of ascidians (Asciacea; Akagawa et al., 2004). Fish that show a preference for brooding in live invertebrates which are termed 'ostracophils' (Balon, 1975). Ostracophils are only parasitic during their early developmental stages (as eggs and larvae); their juveniles and adults are free-living.

Brood parasitism in other animals is represented by cuckoos (*Cuculus canorus*) and parasitic ants (*Harpagoxenus sublaevis*; Davies et al., 1989). Bitterling fish satisfy the criteria of a brood parasite because they reduce the costs of parental care by exploiting the gills of the mussel, and depend on the mussel for their reproduction (Kitamura, Nagata, Nakajima, & Sota, 2012; Rouchet et al., 2017; Smith, 2016). The parasitism causes the mussel host to suffer a significant fitness cost including reduced growth rate (Smith, Reichard, Jurajda, & Przybylski, 2004), oxygen stress (Spence and Smith, 2013), gill epithelium damage, disrupted water circulation (Reichard et al., 2007) and increased mortality (Smith, Reynolds, Sutherland, & Jurajda, 2000).

The mussel gill is multifunctional. The demibranchs (ctenidia) serve as organs of respiration, filter feeding, blood circulation, and as brooding sites. During the mating season, the female mussels brood their own embryos inside the specialized marsupial gill until the glochidia (mussel larvae) are released into the water (Tankersley, 1996; Tankersley and Dimock, 1992). The released glochidia invade fish and temporally parasitize the gills of fish until free-living stages. However, bitterlings have

evolved resistance to infection by glochidia (Mills and Reynolds, 2003). The oily gudgeon (*Sarcocheilichthys variegatus*), a teleost, also uses freshwater mussels as hosts for its embryos. However, in contrast to the bitterlings, the embryos of this species occupy only the mantle cavity and not the gill chamber (Khlopova and Varaksin, 2009).

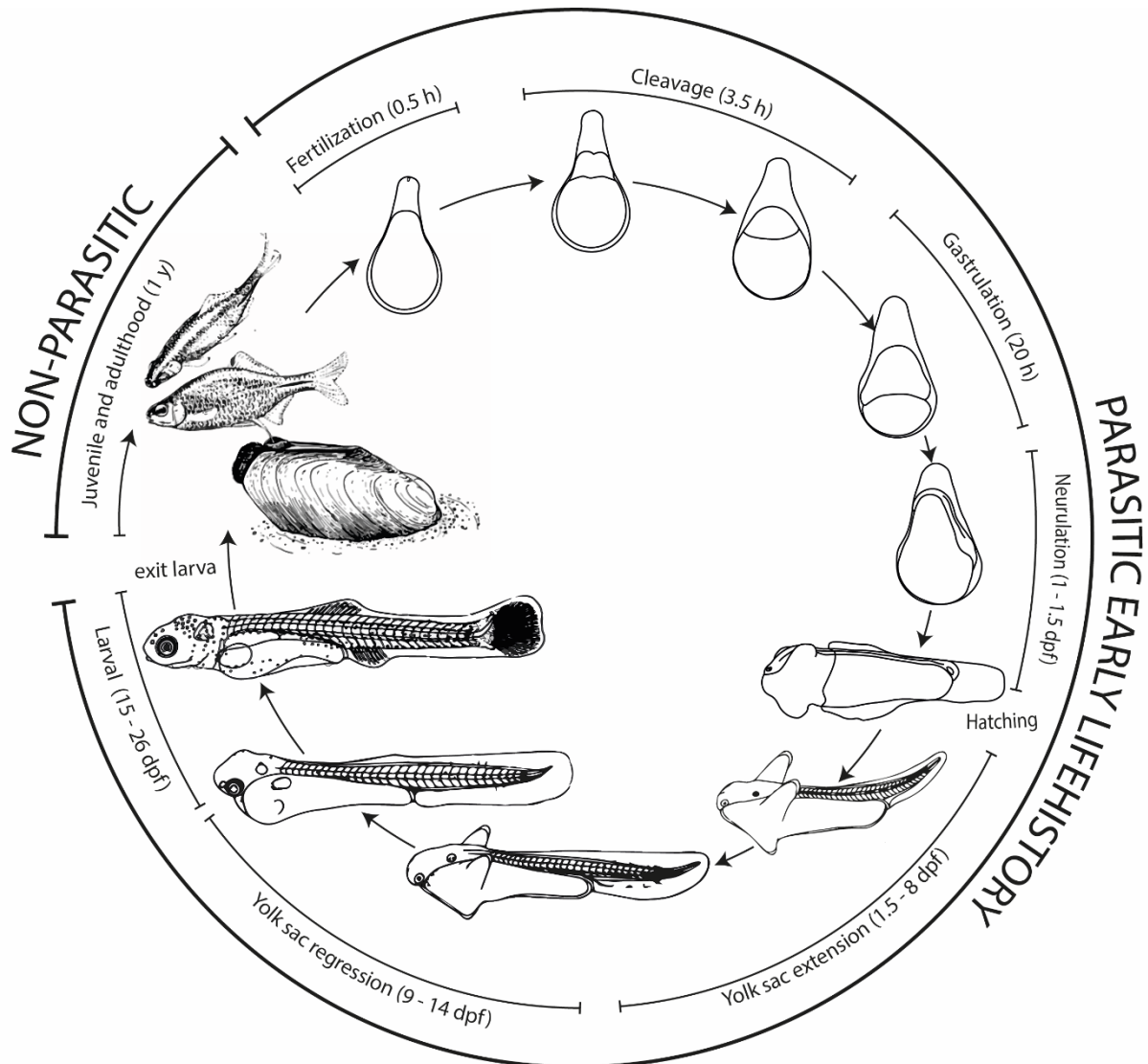


Figure 1 Life history of the bitterling. This figure shows development in the species *Rhodeus ocellatus*. Development progresses clockwise. The parasitic phase takes place inside the mussel while the non-parasitic phase is free-living outside the mussel. Abbreviations: h, hours; dpf, days post fertilization; y, year. Drawn by Wenjing Yi. The figure of adulthood breeding behavior is modified from Boeseman et al. (1938). The figures of periods from hatching until larval period are modified from Kim and Park (1985). Permissions have been granted by the publishers.

The bitterling-mussel interaction as a model system

The distinct bitterling-mussel relationship has been well studied for at least a century (Duyvené de Wit, 1955; Olt, 1893). The reproductive behaviour of *Rhodeus* and its relationship with the mussel were noticed by researchers in Leiden, the Netherlands, including the Nobel Prize winner Nikolaas Tinbergen (Boeseman et al., 1938). Illustrations in that publication presented observations of water

flow, inside the mussel host, that went from the inhalant siphon through the gill chamber to the exhalent siphon (Boeseman et al., 1938). Those authors also observed the behavior of the bitterlings and noted that while the male bitterling inspected and guarded the territory of the mussel host, the female bitterling inserted her ovipositor into the exhalent siphon. Research findings on the European bitterling *Rhodeus amarus* were reviewed by Duyvené de Wit (1955) to motivate worldwide collaboration on studying bitterlings from the aspects of comparative embryology, immunology, behavior, and taxonomy. Smith et al. (2004) reviewed the reproductive ecology of the European bitterling and concluded that the bitterling is a valuable model organism in behavioral, population and evolutionary ecology.

Embryonic adaptations to blood parasitism

In this thesis we study the bitterling from the perspective of evolutionary developmental biology ('evo-devo'). We are particularly interested in the remarkable developmental adaptations that bitterlings show to brood parasitism. The bitterling embryo (Table 1) shows at least two such adaptations: (i) those affecting egg shape or yolk shape, including the remarkable lateral yolk sac extensions (YSEs); (ii) the presence of unicellular tubercles on the epithelium (periderm) that covers the embryo (Fukuhara et al., 1982; Kim et al., 2008; Suzuki and Hibiya, 1984a; Suzuki and Hibiya, 1985b; Suzuki et al., 1986; Suzuki et al., 1989a).

Teleost eggs are usually spherical (Kunz, 2004). Oval and elliptical shapes are often found in bitterlings. The unfertilized eggs of bitterlings are generally ellipsoid. The size and shape vary among genera. (Suzuki, 1958) compared the egg shape of *T. lanceolata*, *A. tabira*, and *R. ocellatus*. According to his measurements, the *T. lanceolata* egg is fusiform, with the highest length/width (l/w) ratio (c. 3.0). *A. tabira* is more rounded (c. 1.6) and *R. ocellatus* is intermediate (c. 2.7). According to (Chi Hong Kim et al., 2006), there are in total 4 types of yolk shape: bulb-like (*Rhodeus*), pear-shaped (*Tanakia*), fusiform (*Tanakia*), and round-oval (*Acheilognathus*).

The shape of the yolk changes during embryonic development in many fish species. In cypriniforms, the initially spherical yolk ball becomes reshaped to form a caudal yolk extension (YE), a cylindrical structure protruding posteriorly from the ball (Virta and Cooper, 2011). According to those authors, the caudal YE is a conserved morphological trait of the order Cypriniformes (carp and minnows). Their experiments with zebrafish (*Danio rerio*) suggested a mechanism underlying formation of the caudal YE: it is likely shaped by the mechanical forces generated by the contractile cell layers of embryonic integument, which exert force on the posterior region of the yolk (Virta and Cooper, 2011). Bitterlings have a caudal YE and two lateral YSEs. It is noticeable that, in *Rhodeus*, the lateral YSEs undergoes the highest level of transformation, forming a pair of prominent wing-like structures on the lateral aspect of the yolk ball (Suzuki, 2004). In *Tanakia*, the lateral YSEs are less developed, having more the appearance of low bulges than projecting wings (Suzuki et al., 1986). *Acheilognathus* has no lateral YSEs (Kim et al., 2018; Suzuki and Jeon, 1991). However, it is still unknown whether the lateral wing-like YSEs shares any homology with the caudal YE.

The teleost epidermis has a complex cellular composition. During development, there are transitory, unicellular hatching gland cells, ion-regulated chloride cells, chromatophores (pigment

Table 1 A summary of yolk sac shape and peridermal features in bitterlings.

Genus	Species	Egg shape	YSEs	EVL tubercles	Ref.
<i>Rhodeus</i>	<i>ocellatus</i>	bulb-like	wing-like	hemispheric	(Kim and Park, 1985; Suzuki and Hibiya, 1984b; Ueda et al., 2001)
	<i>atremius</i>	bulb-like	wing-like	hemispheric	(Suzuki and Hibiya, 1984a)
	<i>suigensis</i>	bulb-like	wing-like	hemispheric	(Suzuki and Hibiya, 1984a)
	<i>uyekii</i>	bulb-like	wing-like	hemispheric	(Suzuki et al., 1985)
	<i>sericeus</i>	bulb-like	wing-like	hemispheric	(Aldridge, 1999)
	<i>pseudo-sericeus</i>	bulb-like	wing-like	hemispheric	(Chi Hong Kim et al., 2006; Kim et al., 2008; Suzuki, 2006)
<i>Sinorhodeus</i>	<i>microlepis</i>	pear-shape	bulge-like	unknown	(Li et al., 2017)
<i>Tanakia</i>	<i>limbata</i>	fusiform	bulge-like	bullet-like	(Suzuki and Jeon, 1988b)
<i>Paratanakia</i>	<i>himantegus</i>	fusiform	bulge-like	bullet-like	(Suzuki et al., 1989a)
<i>Pseudo-rhodeus</i>	<i>tanago</i>	pear-shape	bulge-like	bullet-like	(Suzuki et al., 1986)
<i>Acheilognathus</i>	<i>yamatsutae</i>	round-oval	none	cone shaped	(Suzuki and Jeon, 1987)
	<i>rhombus</i>	round-oval	none	cone shaped	(Kim et al., 2018; Suzuki and Jeon, 1991)
	<i>asmussi</i>	round oval	none	cone shaped	(Suzuki and Jeon, 1989)

Note: YSEs, yolk sac extensions; EVL, enveloping-layer of cells; For shape of the EVL tubercles see Figure 2.

cells), mucus glands, an enveloping-layer of cells (EVL) and adhesive glands cells (which are normally covered by the EVL; (Kunz, 2004)). The caudal YE of zebrafish can be divided into four histological compartments (Virta and Cooper, 2011). The innermost compartment is the yolk ball, which is formed by yolk granules. From deep to superficial, the yolk granules are covered successively by: a

yolk syncytial layer (YSL) or periblast; an intermediate epidermal ectoderm; and a surface layer of simple squamous epithelium called the EVL or periderm. These three layers form the walls of the yolk sac at the ventral side of the yolk ball (Kimmel et al., 1990; Webb et al., 2008). The YSL and EVL are lineage-restricted extra-embryonic structures (Kimmel et al., 1990). But the EVL cells can persist beyond metamorphosis and are slowly renewed by proliferation of basal layer keratinocytes (Fischer et al., 2014). The intermediate epidermal ectoderm will develop into the basal layer of the future adult epidermis (Le Guellec et al., 2004).

In studies of different teleost species, the EVL has a variety of synonyms including: periderm, pavement cells, epithelial cells, epithelial envelope, peripheral cells, outermost flattened layer, skin surface, and surface of the yolk sac (Fukuhara et al., 1982). The EVL of zebrafish and other cypriniform fish is furnished with micro-ridges. These are raised, actin-rich structures that help to maintain a layer of mucus on the surface of the fish (Webb et al., 2008). In bitterlings, the surface of the yolk sac wall is also decorated with micro-ridges. But at the region of the lateral and caudal YSEs these surface cells have a specialized apical surface. The central part of the apex of the cell protrudes as a unicellular tubercle.

The location and micro-ridge structure of the so-called ‘unicellular tubercles on surface of the yolk sac’ leads us to the hypothesis that these surface cells may be specialized EVL cells rather than other cell types found in the developing epithelium. Based on scanning electron microscopy (SEM), there are three types of EVL tubercles (Figure 2): (i) 6.5 - 17.5 μm in height and hemispheric (Kim et al., 2008; Suzuki, 2006); (ii) 15 - 25 μm in height and bullet-like (Suzuki and Hibiya, 1985b; Suzuki et al., 1986; Suzuki et al., 1989a); and (iii) approximately 20 μm in height and conical (Suzuki and Jeon, 1988a).

In summary, the following traits occur in three combinations depending on the bitterling genus: (i) bulb-like eggs with wing-like YSEs and hemispherical EVL tubercles (*Rhodeus*); (ii) fusiform or pear-shaped eggs with bulge-like YSEs and bullet-like EVL tubercles (*Tanakia*); and (iii) round-oval eggs, with no YSEs but with cone-shaped EVL tubercles (*Acheilognathus*).

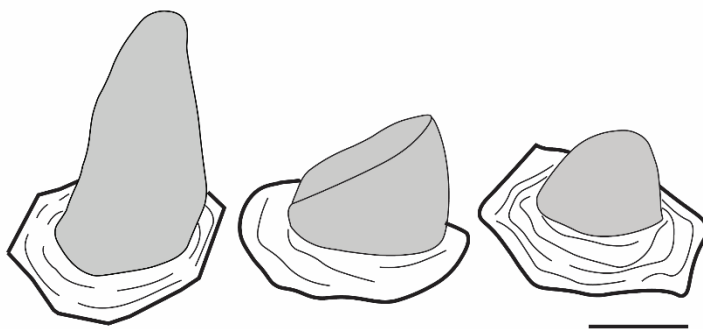


Figure 2 Tubercles of the enveloping-layer of cells (EVL) of bitterling species. From left to right: bullet-like, *Paratanakia himantegus* (Suzuki et al., 1989a); cone shaped, *Acheilognathus rhombeus* (Suzuki and Jeon, 1991); and hemispheric, *Rhodeus uyekii* (Suzuki et al., 1985). The grey colour indicates the protruded tubercles; the narrow lines are the micro-ridges; the broad, dark line is the cell boundary. Scale bar = 10 μm . Drawing by Wenjing Yi based on the references cited.

Host mussel species

We have summarized above the varying developmental adaptations in bitterlings. Previous studies indicated that these differences are related to differences in gill architecture among the mussel host species (Liu et al., 2006). In general, bitterlings spawn inside freshwater bivalve mollusks of the family Unionidae (Bivalvia: Paleoheterodonta: Unionoidea: Unionacea). Some *Rhodeus* individuals have been reported to use mollusks of the family Margaritiferidea as hosts (Smith et al., 2004). A newly-described bitterling species, *Sinorhodeus microlepis*, has been found exploiting the Asian clam *Corbicula fluminea* of the family Corbiculidae (Bivalvia: Heterodonta: Veneroidea: Corbiculoidea). Its larvae were found in the gills of the clam (Dillon, 2000; LemaireGony et al., 1997; Li et al., 2017).

Bivalve mollusks can be divided into four groups according to the complexity of their gill architecture: protobranchia, filibranchia, eulamellibranchia and septibranchia (Lang and Hescheler, 1900). The host mussels for all bitterlings belong to the eulamellibranch group. Eulamellibranchia have the highest degree of gill structural complexity. The lamellae are joined by bars of connective tissue called the interlamellar junctions (septa). The gill filaments are firmly connected by interfilament junctions, and the entire gill has the appearance of a perforated, leaf-like tissue (LemaireGony et al., 1997; McElwain and Bullard, 2014; Medler and Silverman, 2001). The gill chamber between the ascending and descending lamellae is therefore divided by interlamellar junctions into water tubes aligned in parallel.

Reichard et al. (2007) tested interspecific differences among bitterling species in host preference among the eulamellibranch bivalves. They divided bivalves into four types according to the complexity of the water tube: (i) gill without true water tubes or septa (Ableminae); (ii) gill with water tubes and perforated septa (Unioninae); (iii) gill with water tubes and non-perforated septa (Unioninae); (iv) gill with tripartite water tubes and non-perforated septa (Anodontinae). Their results suggest that the host preference of bitterlings is related to gill-structure complexity. For example, *R. ocellatus* embryos, with a well-developed wing-like pair of YSEs, are able to parasitize all mussel species listed above. However, they show a preference for *Anodonta globosula* (type iv), which has the most complex gill type (Reichard et al., 2007).

Liu et al. (2006) mapped bitterling host preference for various East Asian freshwater mussel species of the family Unionidae. In general, *Acheilognathus* and *Tanakia* showed a preference for mussels with a relatively simple gill structure (Ableminae), whereas *Rhodeus* showed a preference for Anodontinae and Unioninae, which have a more complex gill structure.

From the above Introduction, we can make the following conclusions. Phylogenetically, we know that the wing-like YSEs is a synapomorphy supporting the robustness of the genus *Rhodeus*. Ecologically, the fitness advantage associated with the wing-like YSEs is possibly an evolutionary adaptation to the environment of the water tube of the mussel gill. In evolutionary terms, the origin of the YSEs is a speciation event that split the bitterling group. However, the origin of the wing-like YSEs still needs to be explained in terms of developmental mechanisms. To this end, we decided to use the most common species in the genus *Rhodeus*, the rosy bitterling (*R. ocellatus*) as our research organism, and to give special attention to the developmental processes underlying the origin of the lateral wing-like YSEs.

Evolutionary developmental biology (evo-devo) of bitterlings

Evolutionary novelty

The discipline of evolutionary developmental biology (evo-devo) brought evolution and developmental biology together at the time of the discovery of developmental genes in *Drosophila* in the late 1970s (Lewis, 1978). Other stages in the progress of evo-devo include the discovery of the deep homology of developmental regulatory genes across the Metazoa (Creuzet et al., 2005; Ekker et al., 1997; Puschel et al., 1992). This was then linked with conserved metazoan body plans to give the concept of the *zootype* (Graham et al., 2014; Nagashima et al., 2009; Riedel-Kruse et al., 2007) — a definition of the animal body plan in terms of developmental gene expression.

Further, studies on the mechanisms of morphogenesis (Soules and Link, 2005) and organogenesis (Drummond and Davidson, 2016; Ng et al., 2005), provided an opportunity to use developmental tool-kit genes (a small group of transcription factors and secreted peptides and proteins that control embryonic pattern formation; Knoll and Carroll, 1999) to investigate evolution and the origin of evolutionary novelties. For example, Saenko et al. (2008) studied eyespots as an example of an evolutionary novelty in the butterfly (*Bicyclus anynana*). Their research showed that wound healing, a fundamental process, might have been co-opted in the evolution of eyespots via the upregulation of expression of genes *Distal-less*, *engrailed*, and *spalt* in scale-building cells.

In this thesis, the first evo-devo question we ask is the following: is the wing-like YSEs of *R. ocellatus* an evolutionary novelty? According to Mayr (1960), not all particular changes of the phenotype represent the emergence of evolutionary novelties. For example, he suggests that changes in size or pigmentation are not considered to be evolutionary novelties because they are quantitative traits. Traits are only considered novelties if they are new characters, structures, or functions. Therefore, the tentative definition of an evolutionary novelty given by Mayr (1960) is “a change that would permit an organism to perform a new function”. What’s more, modification of the incipient structure is favored by natural selection resulting from a change in the environment.

Accordingly, our hypothesis is as follows. The bitterling YSEs represents a novelty in the following two senses: (i) it represents a morphological change, as the surface of the yolk ball protruded as a pair of wing-like structures; and (ii) because of this morphological change, the bitterling showed a gain of function, namely the ability to parasitize the water tube of the mussel gill. This combined morphological and functional change may be linked to the niche shift of embryonic development from the open water body to the enclosed environment of the mussel body.

From phenotype to genotype

The study of taxon-specific novel phenotypes (shared-derived characters or synapomorphies) is an important topic in evo-devo research. For example, Kupffer’s vesicle (KV) is a teleost-specific embryonic character described by Carl Kupffer (Kupffer, 1868). Histologically, KV is a fluid-filled epithelial sac lined by ciliated cells (Brummett and Dumont, 1978). It is an early, transient embryonic character although its precise stage of appearance is species-specific (Kunz, 2004). It is a useful staging character but was formerly considered to be an embryonic ‘organ of ambiguity’ because of its uncertain function in development (Kimmel et al., 1995; Warga and Stainier, 2002).

More recent research has shown that the function of KV may be related to the normal development of body asymmetry, and might therefore be analogous to the node in mice (formerly called Hensen's node), the gastrocoel roof plate in *Xenopus*, and Hensen's node in the chick (Essner et al., 2002). These regions in all species examined show expression of a dynein gene (*Lrd*, left-right dynein heavy chain). In zebrafish, *lrdr1* (left-right dynein-related1) is first expressed in the dorsal forerunner cells. These cells give rise to KV during the early somitogenesis period. Essner et al. (2002) observed that the node monocilia in KV are motile, and these cilia create a directional fluid flow inside KV. Furthermore, morpholino knockdown of *lrdr1* induces disruption of fluid flow inside KV and perturbs left-right development, suggesting that KV is 'an embryonic organ of asymmetry' (Essner et al., 2005).

The wing-like YSEs of the bitterling is another transient 'embryonic organ of ambiguity' in our view. We aim to uncover the developmental mechanism of YSEs formation. However, to identify candidate genes for a novel phenotype in a non-model organism like the bitterling YSEs is difficult. In the case of the bitterling *R. ocellatus*, there are no genomic data, and no developmental molecular studies have been done. However, the ZFIN (The Zebrafish Information Network) database (Howe et al., 2013a), and the zebrafish reference genome sequence (Howe et al., 2013b) do provide us with mutant phenotypes related to caudal YE development, and therefore a list of candidate genes. For example, the zebrafish caudal YE is shaped by the contraction force of the embryonic integument. One of the contractile cell layers of the integument is the EVL. Previous studies of zebrafish provided reliable EVL related developmental genes (Chang and Hwang, 2011; Eisenhoffer et al., 2017; Fischer et al., 2014; Imboden et al., 1997; Xiong et al., 2014). In zebrafish, the keratin genes *cyt1*, *cyt2*, *krt4*, *krt8* and *krt18* are normally expressed in the EVL whereas the epithelial stem cell marker p63 is specifically expressed in the basal layer. Using such molecular markers can help us to study bitterling tubercle EVL cells on the ridges of wing-like YSEs and identify the homologies of those cells.

Wholemound *in situ* hybridization (WISH) is the method we use to screen candidate genes and to profile gene expression patterns in the bitterling *R. ocellatus*. With mRNA probes, WISH allows the reliable visualization of gene expression during embryo development (Thisse et al., 2004). The expression of orthologous genes allows us to formulate testable hypotheses about mechanisms underlying the development of the wing-like YSEs.

Bitterling developmental staging systems

The next question is how to compare bitterling and zebrafish developmental mechanisms and gene expression in an evolutionary context. The zebrafish is closely related to the bitterlings but is not a brood parasite. Spatial and temporal differences in gene expression, if they exist between the zebrafish and bitterling, could result from interspecific differences arising during the course of evolution. Therefore, we need to have a standard staging series as the basis of comparisons between the two species (Jeffery et al., 2002a; Richardson et al., 2001). One approach to making the dynamic process of embryonic development comparable across species, is to adopt a standard event system to study embryos at stages that are presumed to be comparable (Werneburg, 2009). Another option would be to try to stage bitterling or other teleost embryos using the widely-used zebrafish staging system of (Kimmel et al., 1995).

Kimmel et al. (1995) published what would become the gold standard for zebrafish studies. Those authors use numerical staging characters, believing them to be more accurate, reproducible, and easily compared across species. As is well-known, using 'days' or other time intervals to define a developmental stage is problematic because: (i) the stage at a particular day of development varies with temperature (ii) different species develop at different rates and so, for example, 5 days in the zebrafish is not equivalent in stage to 5 days in a bitterling. Homologous morphological characters such as somite count are not subject to these objections (Jeffery et al., 2002b). That is why each zebrafish stage was based by Kimmel on an identifiable morphological character, combined with a numerical index (for example, 18-somites, and prim-6 etc., where prim = primordium of the lateral line). Later, a postembryonic staging series of the zebrafish, based on externally visible anatomical characters (Parichy et al., 2009) further extended zebrafish staging. Unfortunately, the available bitterling staging systems have not been optimized in this way.

Another problem facing us here is that several key studies of bitterling development are written in languages other than English. For example, two publications on the embryonic developmental stages of the rosy bitterling (*R. ocellatus*) by Uchida (1939) and Nikolsky (1963) are in Japanese and Russian, respectively. Later, Kim and Park (1985) published another study in the Korean language, with English used only in the Abstract and figure legends. Suzuki and Jeon (1988) published another description of the Korean subspecies *R. ocellatus ocellatus*, which covered embryonic, larval, and juvenile development, and also wrote it in Korean.

The most recent English-language description of the developmental stages of the species *R. ocellatus* was given by Nagata and Miyabe (1978). Their study provides us with illustrations of all 30 stages. However, the nomenclature they used is no longer consistent with modern teleost staging systems. For example, one of their criteria is 'embryonic-fin appearing stage', and four other stages based on how far the so-called embryonic fin extends to the cranial region. However, what they call the 'embryonic fin' is actually the median fin fold. Their other criteria, such as 'the formation of the embryonic-fin extends gradually to the more anterior region' is vague and not as clear as if they had said something like: 'extends from the level of somite-15 to somite-10'.

In view of these and other issues, there is a pressing need to produce a new character-based bitterling staging series. Furthermore, the lateral wing-like YSEs appears during the early somite period, persists during development of sensory organs such as ears and eyes, and regresses in the time-window of pectoral fin development. Therefore, the new bitterling staging system should also include the morphogenesis of somites, the lens and optic cups, the otic vesicle, and pectoral fin bud, across several stages. As we show, we can then use this new staging system to study heterochrony.

Sequence heterochrony and transcriptional heterochrony

Heterochrony is any change in developmental timing during evolution (Richardson, 1995). During embryonic development, the embryo has an ever-changing morphology. Changes in embryo morphology can be defined in terms of the occurrence of discrete developmental events such as the appearance of the lens placode, the appearance of the first somite etc.; or they can be defined morphometrically, that is by measuring continuous variables such as the size of a particular part. The order of events is called the 'developmental sequence'. Shifts in the sequence of developmental events during evolution are known as sequence heterochrony (Bininda-Emonds et al., 2002).

Aldridge (1999) found that a discrete event (hatching) occurred earlier in the European bitterling *R. sericeus* compared to another teleost, the common carp (*Cyprinus carpio*), when ages were inferred from body length. On the other hand, retinal pigmentation and melanophore differentiation occurred relatively late in the bitterling. The possible explanation for these heterochronic shifts is that it is related to brood parasitism. The early hatching facilitates direct exposure to dissolved oxygen, while late pigmentation may be because there is no need for camouflage in order to avoid prey in the early stages when the fish is inside the dark interior of the mussel.

These observations led us to ask the following question: is the evolution of brood parasitism associated with changes in developmental timing (sequence heterochrony)? To answer this question, we need to compare the developmental sequences of the bitterling with non-parasitic species to detect sequence heterochrony in a phylogenetic context. For this purpose, we will use the zebrafish (*Danio rerio*). We chose this species because it is well-studied and it belongs to the Cyprinidae Family, a sister-taxon with bitterling species (Mayden et al., 2009). This phylogenetic relation is interesting in two respects. First, if the phylogenetic topology is congruent with heterochrony data, it could mean that there is a phylogenetic signal contained in the developmental sequences. Conversely, if the phylogeny and ontogeny are not congruent, the conflict may indicate adaptation to environmental pressures.

One of the forms of heterochrony we want to study is *transcriptional heterochrony*: a change in the timing of initiation or silencing of gene expression (Richardson, 2012; Richardson et al., 2009). Temporal shifts in the expression of developmental regulatory genes are known to be potential mechanism of phenotypic change. For example, Bickelmann et al. (2012) analyzed the temporal and spatial expression profile of *Sox9* (an early marker of chondrification) in developing forelimbs and hindlimbs of the fossorial talpid mole (*Talpa occidentalis*), a terrestrial shrew (*Cryptotis parva*) and the terrestrial mouse (*Mus musculus*). 'Terrestrial' in this context means dwelling above the ground. The spatial distribution of *Sox9* expression domains was similar in all species investigated. But in the mole, *Sox9* expression was advanced in the forelimb compared to the hind limb, in contrast to synchronous expression in the shrew and mouse. This transcriptional heterochrony may account for the enlarged hands in talpid moles, an adaptation for digging.

Advanced imaging techniques for studying bitterlings development

Three-dimensional (3-D) imaging of embryos is a valuable tool for helping us understand development. One example of this is the ongoing effort to develop a 3-D embryo atlas of the zebrafish. Verbeek et al. (1999) developed a 3-D digital atlas of zebrafish embryos by reconstructing serial histological sections into 3-D images. Histological sectioning has the advantages of high optical resolution, and the ability to use a range of histochemical and other stains (Copper et al., 2018). The disadvantage of histology is that embedding and sectioning are time-consuming and destructive to the samples.

A relatively new and non-destructive technology for the study of developmental anatomy is X-ray micro-computed tomography (microCT) (Metscher, 2009a; Metscher, 2009b). In the area of developmental biology, Metscher (2009a) pioneered a protocol for staining soft tissue, and opened up its application to the study of development. With one-step contrast staining, microCT can produce high-contrast, high-resolution images of embryos. The image dataset, which contains digitally

generated ‘virtual’ sections along all defined anatomical axes of the scanned sample, can be used to give two-dimensional (2-D) histological information. After 3-D volume rendering, the data can be used to visualize anatomical structures. Finally, microCT data can be annotated in 2-D to produce a 3-D model. This method has already been widely used to study mouse development. For example, Wong et al. (2012) created a 3-D mouse embryo atlas which established a baseline of mouse embryo phenotype assessment. (http://www.mouseimaging.ca/technologies/mouse_embryo_atlas.html). Recently, a new zebrafish atlas, Pan-Cellular Tissue Tomography (PANCETTO), has been under construction by the Bio-Atlas team using synchrotron tomography to extend non-destructive methods to a cellular resolution (<http://zfatlas.psu.edu>).

Here, we chose to use microCT to visualize the developmental morphology of the bitterling because this method is more time-efficient than conventional histology, it is non-destructive, and they are optimal for our specimen size (150 μ m to 3 cm). By providing a 3-D view of bitterling development, we hope this research will serve as a navigator and a foundation for further evo-devo research on regional development and comparative embryology.

Advancing the bitterling as an evo-devo model system

With this research, we aim to establish bitterling as a new evo-devo model system. Since bitterlings have such a specialized ecology, they could also be developed into an eco-evo-devo system. Eco-evo-devo is the integrated study of ecology, evolution and development (Gilbert et al., 2015). There are many other evo-devo model species among teleosts. A good example is the blind Mexican cavefish (*Astyanax mexicanus*), a unique species whose surface-dwelling population has normal paired eyes, whereas the cave population is blind due to eye regression. This species has emerged as a good model organism to study eye regression as an adaptive trait driven by natural selection (Krishnan and Rohner, 2017; Yamamoto et al., 2004). The Japanese flounder (*Paralichthys olivaceus*) has a highly-derived asymmetric body morphology and extensive craniofacial transformation, providing a useful model for studying the evolutionary origin of asymmetry and the mechanisms of body shape transformation in vertebrates (Shao et al., 2017). The goldfish (*Carassius auratus*), with morphologically divergent domesticated strains, is a particularly advantageous model organism with which to address how artificial selection and developmental mechanisms are related, and how developmental robustness and genetic diversity are related (Ota and Abe, 2016; Tsai et al., 2013).

There are some promising attempts to link evolution and development with ecology to form the discipline of eco-evo-devo, or ecological evolutionary developmental biology (Abouheif et al., 2014; Gilbert et al., 2015). Eco-evo-devo reminds us of the statement by Lee Van Valen that ‘Evolution is the control of development by ecology’ (Van Valen, 1976). We could paraphrase Van Valen by asking: how does the environment influence development via natural selection to generate novel phenotypes? Here are two examples. Brown planthoppers (*Nilaparvata lugens*) are insects with short-winged and long-winged dimorphism influenced by environmental factors. This dimorphism has been related to the activity of two insulin receptors (InR1 and InR2) on wing bud growth (Xu and Zhang, 2017). The bichir fish (*Polypterus senegalus*) when raised on land, displays behavioral changes that emulate terrestrial locomotion, and anatomical changes that mirror the stem tetrapods of the Devonian period. This suggests that the bichir is a potential evo-devo model of developmental plasticity, which can further be integrated into the study of macroevolutionary change (Standen et al., 2014).

Bitterling have a remarkable brood parasite relationship with bivalves. This gives us an opportunity to use bitterlings model to study adaptation, co-evolution, and developmental plasticity, all in the context of parasitism and the interaction with the host. Bitterling embryos live in a complex environment influenced by both abiotic and biotic environmental factors. The host bivalves can dramatically narrow the space occupied by bitterling embryos by contracting their gill muscles, something which they do normally to regulate the dimensions of their water tube (Medler and Silverman, 2001). This pumping process can even eject embryos before the end of the parasitic period (Kitamura, 2005; Rouchet et al., 2017). When stressed or disturbed, bivalves retract their siphon, close their shell and bury themselves into sediments; therefore, the embryos are forced into a temporarily hypoxic environment (Aldridge, 1999; Smith et al., 2004). Interspecies differences in host preference, and species-specific embryonic adaptation, are potentially interesting evo-devo topics. Furthermore, host-parasite interaction is an ecological factor that influences bitterling development. In summary, the bitterling is a promising candidate model organism for eco-evo-devo research.

Aims of the thesis

First, we develop the bitterling as a unique, well-studied model organism in the area of the evolutionary ecology of brood parasitism. The bitterling-mussel relationship, interspecific mussel host preference, and mussel gill structure are studied in detail, to help understand the developmental adaptation of bitterling embryos in response to their mussel hosts. Further, the study of bitterlings is necessary to provide a better understanding of teleost developmental evolution, teleost evolutionary novelties and their developmental origin. Finally, bitterlings are interesting as evo-devo and eco-evo-devo model organisms. **(This Chapter)**

We revise and expand on the previously-published time-based staging systems by making producing new, character-based systems that are compatible with the widely-used zebrafish staging system. By using microCT, we identify a series of anatomic characters as development landmarks. This allows us to: (i) produce the first 3-D atlas of bitterling embryonic development (ii) update the normal developmental stages of *R. ocellatus* (iii) explore the development of the central neural system in detail. In all of these studies we produce digital 3-D models. **(Chapters 2 and 3)**

We also investigate the early brain regionalization of the rosy bitterling (*Rhodeus ocellatus*) by studying the expression pattern of marker genes *dlx2a*, *fgf8a*, *msx3*, *pax6a*, *shha*, and *sox9b* using whole-mount *in situ* hybridizations (WISH). This allows us to determine the formation of brain subdivisions. To test our hypothesis that the bitterling shows transcriptional heterochrony associated with brood parasitism, we investigate the compare the bitterling gene expression patterns with the zebrafish. **(Chapter 4)**

To study the morphogenetic process of *blastokinesis* in the bitterling embryo, and its possible relation to brood parasitism, we focus on early pre-hatching development and the hatching event of the rosy bitterling (*Rhodeus ocellatus*). We profile the expression of developmental regulatory genes *fgf8a*, *msx3*, *krt8* and *ctslb* by whole-mount *in situ* hybridization (WISH). This allows us to visualize morphogenetic movements during gastrulation and neurulation, and the process of body elongation during somitogenesis. We also analyze the hatching event by time-lapse photography, histology and microCT to explore the phenomenon of blastokinesis and its possible adaptive significance. **(Chapter 5)**

Finally, we summarize and discuss the preceding chapters, and highlight the overarching conclusions of the work described in this thesis. (Chapter 6)

References

- Abouheif, E., Fave, M. J., Ibarraran-Viniegra, A. S., Lesoway, M. P., Rafiqi, A. M. and Rajakumar, R.** (2014). Eco-Evo-Devo: The Time Has Come. *Ecol. Genomics Ecol. Evol. Genes Genomes* **781**, 107–125.
- Akagawa, I., Iwamoto, T., Watanabe, S. and Okiyama, M.** (2004). Reproductive behaviour of Japanese tubenout, *Aulichthys japonicus* (Gasterosteiformes), in the natural habitat compared with relatives. *Environ. Biol. Fishes* **70**, 353–361.
- Aldridge, D. C.** (1999). Development of European bitterling in the gills of freshwater mussels. *J. Fish Biol.* **54**, 138–151.
- Arai, R.** (2003). Gross morphology and evolution of the lateral line system and infraorbital bone in bitterlings (Cyprinidae, Acheilognathinae), with an overview of the lateral line system in the family Cyprinidae. *Bull Mus Tokyo Univ* **40**, 1–42.
- Arai, R. and Yutaka, A.** (1988). *Acheilognathus melanogaster*, a Senior Synonym of *A. moriokae*, with a Revision of the Genera of the Subfamily Acheilognathinae (Cypriniformes, Cyprinidae). *Bull. Natl. Sci. Museum. Ser. A, Zool.* **14**, 199–213.
- Arai, R., Fujikawa, H. and Nagata, Y.** (2007). Four New Subspecies of *Acheilognathus* Bitterlings (Cyprinidae: Acheilognathinae) from Japan. *Bull. Natl. Mus. Nat. Sci. A, Suppl.* **1**, 1–28.
- Balon, E. K.** (1975). Reproductive Guilds of Fishes: A Proposal and Definition. *J. Fish. Res. Board Canada* **32**, 821–864.
- Bickelmann, C., Mitgutsch, C., Richardson, M. K., Jiménez, R., de Bakker, M. A. G., Sánchez-Villagra, M. R., Jimenez, R., de Bakker, M. A. G. and Sanchez-Villagra, M. R.** (2012). Transcriptional heterochrony in talpid mole autopods. *Evodevo* **3**, 16.
- Bininda-Emonds, O. R. P. P., Jeffery, J. E., Coates, M. I. and Richardson, M. K.** (2002). From Haeckel to event-pairing: the evolution of developmental sequences. *Theory Biosci.* **121**, 297–320.
- Boeseman, M. J., Van der Drift, J., Van Roon, J. M., Tinbergen, N. and Ter Pelkwijk, J. J.** (1938). De bittervoorns en hun mossels. *Levende Nat.* **43**, 129–136.
- Brummett, A. R. and Dumont, J. N.** (1978). Kupffer's vesicle in *Fundulus heteroclitus*: A scanning and transmission electron microscope study. *Tissue Cell* **10**, 11–22.
- Chang, W.-J. J. and Hwang, P.-P. P.** (2011). Development of zebrafish epidermis. *Birth Defects Res. Part C Embryo Today Rev.* **93**, 205–214.
- Chang, C. H., Li, F., Shao, K. T., Lin, Y. S., Morosawa, T., Kim, S., Koo, H., Kim, W., Lee, J. S., He, S., et al.** (2014). Phylogenetic relationships of Acheilognathidae (Cypriniformes: Cyprinoidea) as revealed from evidence of both nuclear and mitochondrial gene sequence variation: evidence for necessary taxonomic revision in the family and the identification of cryptic spec. *Mol Phylogenet Evol* **81**, 182–194.
- Cheng, P., Yu, D., Liu, S., Tang, Q. and Liu, H.** (2014). Molecular phylogeny and conservation priorities of the subfamily Acheilognathinae (Teleostei: Cyprinidae). *Zool. Sci* **31**, 300–308.
- Chi Hong Kim, Eon Jong Kang and Kim, J. H.** (2006). Development of Eggs and Early Life History of Korean Bitterling, *Rhodeus pseudosericeus* (Acheilognathinae). *Korean J. Ichthyol.* **18**, 266–272.
- Copper, J. E., Budgeon, L. R., Foutz, C. A., van Rossum, D. B., Vanselow, D. J., Hubley, M. J., Clark, D. P., Mandrell, D. T. and Cheng, K. C.** (2018). Comparative analysis of fixation and embedding techniques for optimized histological preparation of zebrafish. *Comp. Biochem. Physiol. Part C Toxicol. Pharmacol* **208**, 38–46.
- Creuzet, S., Couly, G. and Le Douarin, N. M.** (2005). Patterning the neural crest derivatives during development of the vertebrate head: insights from avian studies. *J Anat* **207**, 447–459.
- Davies, N. B., Bourke, A. F. G. and de L. Brooke, M.** (1989). Cuckoos and parasitic ants: Interspecific brood parasitism as an evolutionary arms race. *Trends Ecol. Evol.* **4**, 274–278.
- Dillon, R. T.** (2000). *The Ecology of Freshwater Molluscs*. Cambridge: Cambridge University Press.
- Drummond, I. A. and Davidson, A. J.** (2016). *Zebrafish kidney development*. Elsevier Ltd.
- Duyvené de Wit, J.** (1955). Some results of investigations into the European Bitterling, *Rhodeus amarus* BLOCH. *Japanese J. Ichthyology* **4**, 94–104.
- Eisenhoffer, G. T., Slattum, G., Ruiz, O. E., Otsuna, H., Bryan, C. D., Lopez, J., Wagner, D. S., Bonkowsky, J. L.,**

- Chien, C. Bin, Dorsky, R. I., et al.** (2017). A toolbox to study epidermal cell types in zebrafish. *J Cell Sci* **130**, 269–277.
- Ekker, M., Akimenko, M. A., Allende, M. L., Smith, R., Drouin, G., Langille, R. M., Weinberg, E. S. and Westerfield, M.** (1997). Relationships among *msx* gene structure and function in zebrafish and other vertebrates. *Mol. Biol. Evol.* **14**, 1008–1022.
- Essner, J. J., Vogan, K. J., Wagner, M. K., Tabin, C. J., Yost, H. J. and Brueckner, M.** (2002). Conserved function for embryonic nodal cilia. *Nature* **418**, 37.
- Essner, J. J., Amack, J. D., Nyholm, M. K., Harris, E. B. and Yost, H. J.** (2005). Kupffer’s vesicle is a ciliated organ of asymmetry in the zebrafish embryo that initiates left-right development of the brain, heart and gut. *Development* **132**, 1247–1260.
- Fischer, B., Metzger, M., Richardson, R., Knyphausen, P., Ramezani, T., Franzen, R., Schmelzer, E., Bloch, W., Carney, T. J. and Hammerschmidt, M.** (2014). p53 and Tap63 Promote Keratinocyte Proliferation and Differentiation in Breeding Tubercles of the Zebrafish. *PLoS Genet.* **10**, e1004048.
- Fukuhara, S., Yoshikazu, N. and Wataru, M.** (1982). Minute Scaly Tubercles on the Yolksac of Rhodeine Cyprinid Fishes in Prolarval Stages. *Japanese J. Ichthyol.* **29**, 232–236.
- Gardner, J. R., Orr, J. W., Stevenson, D. E., Spies, I. and Somerton, D. A.** (2016). Reproductive Parasitism between Distant Phyla: Molecular identification of snailfish (Liparidae) egg masses in the gill cavities of king crabs (lithodidae). *Copeia* **104**, 645–657.
- Gilbert, S. F., Bosch, T. C. G. G. and Ledón-Rettig, C.** (2015). Eco-Evo-Devo: Developmental symbiosis and developmental plasticity as evolutionary agents. *Nat. Rev. Genet.* **16**, 611–622.
- Graham, A., Butts, T., Lumsden, A. and Kiecker, C.** (2014). What can vertebrates tell us about segmentation? *Evodevo* **5**, 24.
- Howe, D. G., Bradford, Y. M., Conlin, T., Eagle, A. E., Fashena, D., Frazer, K., Knight, J., Mani, P., Martin, R., Moxon, S. A., et al.** (2013a). ZFIN, the Zebrafish Model Organism Database: increased support for mutants and transgenics. *Nucleic Acids Res* **41**, D854–60.
- Howe, K., Clark, M. D., Torroja, C. F., Torrance, J., Berthelot, C., Muffato, M., Collins, J. E., Humphray, S., McLaren, K., Matthews, L., et al.** (2013b). The zebrafish reference genome sequence and its relationship to the human genome. *Nature* **496**, 498–503.
- Imboden, M., Goblet, C., Korn, H. and Vríz, S.** (1997). Cytokeratin 8 is a suitable epidermal marker during zebrafish development. *C R Acad Sci III* **320**, 689–700.
- Jeffery, J. E., Bininda-Emonds, O. R. P., Coates, M. I. and Richardson, M. K.** (2002a). Analyzing evolutionary patterns in amniote embryonic development. *Evol. Dev.* **4**, 292–302.
- Jeffery, J. E., Richardson, M. K., Coates, M. I. and Bininda-Emonds, O. R. P.** (2002b). Analyzing developmental sequences within a phylogenetic framework. *Syst. Biol.* **51**, 478–491.
- Kawamura, K., Ueda, T., Arai, R. and Smith, C.** (2014). Phylogenetic relationships of bitterling fishes (Teleostei: Cypriniformes: Acheilognathinae), inferred from mitochondrial cytochrome B sequences. *Zool. Sci* **31**, 321–329.
- Khlopova, A. V. and Varaksin, A. A.** (2009). Peculiarities of reproductive biology of lazy gudgeon (*Sarcocheilichthys sinensis*) and chersky’s gudgeon (*Sarcocheilichthys czerskii*) (Cyprinidae, gobioninae). *Zool. Zhurnal* **88**, 960–967.
- Kim, Y. U. and Park, Y. S.** (1985). Egg development and larvae of the rose bitterling *Rhodeus ocellatus* (KNER). *Korean J. Fish. Aquat. Sci.* **18**, 586–593.
- Kim, C. H., Park, J. Y., Park, M. K., Kang, E. J., Kim, J. H. and Kim, H. S.** (2008). Minute tubercles on the skin surface of larvae in the Korean endemic bitterling, *Rhodeus pseudosericeus* (Pisces, Cyprinidae). *Ecol. Evol.* **24**, 269–275.
- Kim, H. S., Choi, H. S. and Park, J. Y.** (2018). Embryonic development characteristics and host mussel utilization of flat bitterling *Acheilognathus rhombeus* (Cyprinidae) during winter in Korea. *Environ. Biol. Fishes* **101**, 55–66.
- Kimmel, C. B., Warga, R. M. and Schilling, T. F.** (1990). Origin and organization of the zebrafish fate map. *Development* **108**, 581–594.
- Kimmel, C. B., Ballard, W. W., Kimmel, S. R., Ullmann, B. and Schilling, T. F.** (1995). Stages of embryonic development of the zebrafish. *Dev. Dyn.* **203**, 253–310.
- Kitamura, J. I.** (2005). Factors affecting seasonal mortality of rosy bitterling (*Rhodeus ocellatus kurumeus*) embryos on the gills of their host mussel. *Popul. Ecol.* **47**, 41–51.
- Kitamura, J., Nagata, N., Nakajima, J. and Sota, T.** (2012). Divergence of ovipositor length and egg shape in a brood parasitic bitterling fish through the use of different mussel hosts. *J. Evol. Biol.* **25**, 566–573.
- Knoll, A. H. and Carroll, S. B.** (1999). Early animal evolution: emerging views from comparative biology and

- geology. *Science*. **284**, 2129–2137.
- Krishnan, J. and Rohner, N.** (2017). Cavefish and the basis for eye loss. *Philos Trans R Soc L. B Biol Sci* **372**, 20150487.
- Kunz, Y. W.** (2004). *Developmental Biology of Teleost Fishes*. Dordrecht: Springer Netherlands.
- Kupffer, C. v** (1868). Beobachtungen über die Entwicklung der Knochenfische. *Arch. für mikroskopische Anat.* **4**, 209–272.
- Lang, A. and Hescheler, K.** (1900). *Lehrbuch der vergleichenden Anatomie der wirbellosen Thiere*. 2. umgearb. Jena: G. Fisher.
- Le Guellec, D., Morvan-Dubois, G. and Sire, J. Y.** (2004). Skin development in bony fish with particular emphasis on collagen deposition in the dermis of the zebrafish (*Danio rerio*). *Int J Dev Biol* **48**, 217–231.
- Lemaire-Gony, S., Boudou, A., Lemaire-Gony, S. and Boudou, A.** (1997). Mantle and gill fine structure in the freshwater Asiatic clam, *Corbicula fluminea* (Muller). *Ann. Limnol. J. Limnol.* **33**, 163–178.
- Leung, T. L. F.** (2014). Fish as parasites: an insight into evolutionary convergence in adaptations for parasitism. *J. Zool.* **294**, 1–12.
- Lewis, E. B.** (1978). A gene complex controlling segmentation in Drosophila. *Nature* **276**, 565–570.
- Li, F. and Arai, R.** (2010). *Rhodeus shitaiensis*, a new bitterling from China (Teleostei: Cyprinidae). *Ichthyol. Explor. Freshwaters* **21**, 303–312.
- Li, F., Liao, T. Y., Arai, R. and Zhao, L.** (2017). *Sinorhodeus microlepis*, a new genus and species of bitterling from China (Teleostei: Cyprinidae: Acheilognathinae). *Zootaxa* **4353**, 69–88.
- Liu, H. Z., Zhu, Y. R., Smith, C. and Reichard, M.** (2006). Evidence of host specificity and congruence between phylogenies of bitterling and freshwater mussels. *Zool. Stud.* **45**, 428–434.
- Mayden, R. L., Chen, W. J., Bart, H. L., Doozey, M. H., Simons, A. M., Tang, K. L., Wood, R. M., Agnew, M. K., Yang, L., Hirt, M. V., et al.** (2009). Reconstructing the phylogenetic relationships of the earth's most diverse clade of freshwater fishes—order Cypriniformes (Actinopterygii: Ostariophysi): A case study using multiple nuclear loci and the mitochondrial genome. *Mol. Phylogenet. Evol.* **51**, 500–514.
- Mayr, E.** (1960). The emergence of evolutionary novelties. *Evol. after Darwin* **1**, 349–380.
- McElwain, A. and Bullard, S. A.** (2014). Histological Atlas of Freshwater Mussels (Bivalvia, Unionidae): *Villosa nebulosa* (Ambleminae: Lampsilini), *Fusconaia cerina* (Ambleminae: Pleurobemini) and *Strophitus connasau-gaensis* (Unioninae: Anodontini). *Malacologia* **57**, 99–239.
- Medler, S. and Silverman, H.** (2001). *Muscular Alteration of Gill Geometry in vitro: Implications for Bivalve Pumping Processes*.
- Metscher, B. D.** (2009a). MicroCT for developmental biology: a versatile tool for high-contrast 3D imaging at histological resolutions. *Dev Dyn* **238**, 632–640.
- Metscher, B. D.** (2009b). MicroCT for comparative morphology: simple staining methods allow high-contrast 3D imaging of diverse non-mineralized animal tissues. *BMC Physiol* **9**, 11.
- Mills, S. C. and Reynolds, J. D.** (2003). The bitterling-mussel interaction as a test case for co-evolution. *J. Fish Biol.* **63**, 84–104.
- Nagashima, H., Sugahara, F., Takechi, M., Ericsson, R., Kawashima-Ohya, Y., Narita, Y. and Kuratani, S.** (2009). Evolution of the turtle body plan by the folding and creation of new muscle connections. *Science*. **325**, 193–196.
- Nagata, Y. and Miyabe, H.** (1978). Development Stages of the Bitterling, *Rhodeus ocellatus ocellatus* (Cyprinidae). *Mem. Osaka Kyoiku Univ. III, Nat. Sci. Appl. Sci.* **26**, 171–181.
- Nelson, J. S., Grande, T. C. and Wilson, M. V. H.** (2016). *Fishes of the World*. John Wiley & Sons.
- Ng, A. N. Y., de Jong-Curtain, T. A., Mawdsley, D. J., White, S. J., Shin, J., Appel, B., Dong, P. D. S., Stainier, D. Y. R. and Heath, J. K.** (2005). Formation of the digestive system in zebrafish: III. Intestinal epithelium morphogenesis. *Dev. Biol.* **286**, 114–135.
- Nikolsky, G. V** (1963). *The ecology of fishes*. London.
- Ota, K. G. and Abe, G.** (2016). Goldfish morphology as a model for evolutionary developmental biology. *Wiley Interdiscip Rev Dev Biol* **5**, 272–295.
- Parichy, D. M., Elizondo, M. R., Mills, M. G., Gordon, T. N. and Engeszer, R. E.** (2009). Normal table of postembryonic zebrafish development: Staging by externally visible anatomy of the living fish. *Dev. Dyn.* **238**, 2975–3015.
- Puschel, A. W., Gruss, P. and Westerfield, M.** (1992). Sequence and expression pattern of pax-6 are highly conserved between zebrafish and mice. *Development* **114**, 643–651.
- Reichard, M., Liu, H. and Smith, C.** (2007). The co-evolutionary relationship between bitterling fishes and freshwater mussels: insights from interspecific comparisons. *Evol. Ecol. Res.* **9**, 239–259.

- Richardson, M. K.** (1995). Heterochrony and the phylotypic period. *Dev Biol* **172**, 412–421.
- Richardson, M. K.** (2012). A phylotypic stage for all animals? *Dev Cell* **22**, 903–904.
- Richardson, M. K., Jeffery, J. E., Coates, M. I. and Bininda-Emonds, O. R. P.** (2001). Comparative methods in developmental biology. *Zoology* **104**, 278–283.
- Richardson, M. K., Gobes, S. M. H., van Leeuwen, A. C., Polman, J. A. E., Pieau, C., Sanchez-Villagra, M. R. and Sánchez-villagra, M. R.** (2009). Heterochrony in limb evolution: developmental mechanisms and natural selection. *J Exp Zool B Mol Dev Evol* **312**, 639–664.
- Riedel-Kruse, I. H., Müller, C. and Oates, A. C.** (2007). Synchrony dynamics during initiation, failure, and rescue of the segmentation clock. *Science* **317**, 1911–1915.
- Rouchet, R., Smith, C., Liu, H. Z., Methling, C., Douda, K., Yu, D., Tang, Q. Y. and Reichard, M.** (2017). Avoidance of host resistance in the oviposition-site preferences of rose bitterling. *Evol. Ecol.* **31**, 769–783.
- Saenko, S. V., French, V., Brakefield, P. M. and Beldade, P.** (2008). Conserved developmental processes and the formation of evolutionary novelties: examples from butterfly wings. *Philos Trans R Soc L. B Biol Sci* **363**, 1549–1555.
- Shao, C. W., Bao, B. L., Xie, Z. Y., Chen, X. Y., Li, B., Jia, X. D., Yao, Q. L., Orti, G., Li, W. H., Li, X. H., et al.** (2017). The genome and transcriptome of Japanese flounder provide insights into flatfish asymmetry. *Nat. Genet.* **49**, 119–124.
- Smith, C.** (2016). Bayesian inference supports the host selection hypothesis in explaining adaptive host specificity by European bitterling. *Oecologia* **183**, 1–11.
- Smith, C., Reynolds, J. D., Sutherland, W. J. and Jurajda, P.** (2000). Adaptive host choice and avoidance of superparasitism in the spawning decisions of bitterling (*Rhodeus sericeus*). *Behav. Ecol. Sociobiol.* **48**, 29–35.
- Smith, C., Reichard, M., Jurajda, P. and Przybylski, M.** (2004). The reproductive ecology of the European bitterling (*Rhodeus sericeus*). *J. Zool.* **262**, 107–124.
- Soules, K. A. and Link, B. A.** (2005). Morphogenesis of the anterior segment in the zebrafish eye. *BMC Dev. Biol.* **5**, 12.
- Spence, R. and Smith, C.** (2013). Rose bitterling (*Rhodeus ocellatus*) embryos parasitize freshwater mussels by competing for nutrients and oxygen. *Acta Zool.* **94**, 113–118.
- Standen, E. M., Du, T. Y. and Larsson, H. C.** (2014). Developmental plasticity and the origin of tetrapods. *Nature* **513**, 54–58.
- Suzuki, R.** (1958). Sperm activation and aggregation during fertilization in some fishes. V. Spermstimulating factor on the vegetal pole. *Embryologia (Nagoya)*. **34**, 18–23.
- Suzuki, N.** (2004). Development of egg and larvae of bitterling, *Rhodeus spinalis* (Cyprinidae). *J. Sch. Mar. Sci. Technol. Univ.* **2**, 25–30.
- Suzuki, N.** (2006). Egg and larval development of the bitterling, *Rhodeus pseudosericeus* (Cyprinidae). *Japanese J. Ichthyol.* **53**, 47–54.
- Suzuki, N. and Hibiya, T.** (1984a). Development of Eggs and Larvae of Two Bitterlings, *Rhodeus atremius* and *R. suigensis* (Cyprinidae). *Japanese J. Ichthyol.* **31**, 287–296.
- Suzuki, H. and Hibiya, T.** (1984b). Minute tubercles on the skin surface of larvae of *Rhodeus* (Cyprinidae). *Japanese J. Ichthyol.* **31**, 198–202.
- Suzuki, N. and Hibiya, T.** (1985a). Pharyngeal teeth and masticatory process of the basioccipital bone in Japanese bitterlings (Cyprinidae). *Japanese J. Ichthyol.* **32**, 180–188.
- Suzuki, N. and Hibiya, T.** (1985b). Minute Tubercles on the Skin Surface of Larvae of *Acheilognathus* and *Pseudoperilampus* (Cyprinidae). *Japanese J. Ichthyol.* **32**, 335–344.
- Suzuki, N. and Jeon, S. R.** (1987). Development of the bitterling, *Acheilognathus yamatsutae* (Cyprinidae), with notes on minute tubercles on the skin surface and pharyngeal apparatus. *Kor. J. Limnol* **20**, 229–241.
- Suzuki, N. and Jeon, S. R.** (1988a). Development of eggs, larvae and juveniles of *Rhodeus ocellatus* from Ansong-river, Korea (Pisces: Cyprinidae), with a Note on Minute Tubercles on the Skin Surface. *Korean J. Limnol.* **21**, 1–15.
- Suzuki, N. and Jeon, S. R.** (1988b). Development of the bitterling, *Acheilognathus limbata* (Cyprinidae) from Korea and Japan, with notes on minute tubercles on the skin surface and on genetic implication in hybrid embryos. *Korean J Limnol* **21**, 211–229.
- Suzuki, N. and Jeon, S. R.** (1989). Development of the Bitterling, *Acanthorhodus asmussi* (Cyprinidae) with Note on Minute Tubercles on the Skin Surface. *Korean J. Ichthyol.* **1**, 73–82.
- Suzuki, N. and Jeon, S. R.** (1991). Development of the bitterling, *Acheilognathus rhombeus* (Cyprinidae), from Korea. *J. Basic Sci.* **5**, 53–62.
- Suzuki, N., Akiyama, N. and Hibiya, T.** (1985). Development of the Bitterling *Rhodeus uyekii* (Cyprinidae), with

- a Note on Minute Tubercles on the Skin Surface. *Japanese J. Ichthyol.* **32**, 28–34.
- Suzuki, N., Oka, A., Sugoh, Y., Yamakawa, K. and Hibiya, T.** (1986). Development of the Bitterling, *Tanakia tanago* (Cyprinidae), with a Note on Minute Tubercles on the Skin Surface. *Japanese J. Ichthyol.* **33**, 225–231.
- Suzuki, N., Umezawa, K., Yabe, T. and Murai, H.** (1989). Development of the bitterling, *Paracheilognathus himantegus* (cyprinidae), with a note on minute tubercles on the skin surface. *Japanese J. Ichthyol.* **36**, 318–326.
- Tankersley, R. A.** (1996). Multipurpose Gills: Effect of Larval Brooding on the Feeding Physiology of Freshwater Unionid Mussels. *Invertebr. Biol.* **115**, 243.
- Tankersley, R. A. and Dimock, R. V.** (1992). Quantitative Analysis of the Structure and Function of the Marsupial Gills of the Freshwater Mussel *Anodonta cataracta*. *Biol. Bull.* **182**, 145–154.
- Thisse, B., Heyer, V., Lux, A., Alunni, V., Degrave, A., Seiliez, I., Kirchner, J., Parkhill, J. P. and Thisse, C.** (2004). Spatial and temporal expression of the zebrafish genome by large-scale *in situ* hybridization screening. *Methods Cell Biol* **77**, 505–519.
- Tsai, H.-Y. Y., Chang, M., Liu, S.-C. C., Abe, G. and Ota, K. G.** (2013). Embryonic development of goldfish (*Carassius auratus*): A model for the study of evolutionary change in developmental mechanisms by artificial selection. *Dev. Dyn.* **242**, 1262–1283.
- Uchida, K.** (1939). The fishes of Tyosen (Korea). Part I. Nematognathi, Eventognathi. *Bull Fish Exp St Govern-Gen Tyosen* **6**, 1–458.
- Ueda, T., Naoi, H. and Arai, R.** (2001). Flexibility on the karyotype evolution in bitterlings (Pisces, Cyprinidae). *Genetica* **111**, 423–432.
- Van Valen, L.** (1976). Energy and evolution. *Evol. theory* **1**, 179–229.
- Verbeek, F. J., Broeder, M. J. den, Boon, P. J., Buitendijk, B., Doerry, E., Raaij, E. J. van and Zivkovic, D.** (1999). Standard 3D digital atlas of zebrafish embryonic development for projection of experimental data. In *Electronic Imaging*, p. 11. SPIE.
- Virta, V. C. and Cooper, M. S.** (2011). Structural components and morphogenetic mechanics of the zebrafish yolk extension, a developmental module. *J. Exp. Zool. Part B Mol. Dev. Evol.* **316 B**, 76–92.
- Warga, R. M. and Stainier, D. Y. R.** (2002). The Guts of Endoderm Formation. In *Results Probl Cell Differ*, pp. 28–47.
- Webb, A. E., Driever, W. and Kimelman, D.** (2008). psoriasis regulates epidermal development in zebrafish. *Dev Dyn* **237**, 1153–1164.
- Werneburg, I.** (2009). A Standard System to Study Vertebrate Embryos. *PLoS One* **4**, e5887.
- Wong, M. D., Dorr, A. E., Walls, J. R., Lerch, J. P. and Henkelman, R. M.** (2012). A novel 3D mouse embryo atlas based on micro-CT. *Development* **139**, 3248–3256.
- Xiong, F., Ma, W., Hiscock, T. W., Mosaliganti, K. R., Tentner, A. R., Brakke, K. A., Rannou, N., Gelas, A., Souhait, L., Swinburne, I. A., et al.** (2014). Interplay of Cell Shape and Division Orientation Promotes Robust Morphogenesis of Developing Epithelia. *Cell* **159**, 415–427.
- Xu, H. J. and Zhang, C. X.** (2017). Insulin receptors and wing dimorphism in rice planthoppers. *Philos Trans R Soc L. B Biol Sci* **372**, 20150489.
- Yamamoto, Y., Stock, D. W. and Jeffery, W. R.** (2004). Hedgehog signalling controls eye degeneration in blind cavefish. *Nature* **431**, 844–847.

Chapter 2 Normal stages of embryonic development of a brood parasite, the rosy bitterling *Rhodeus ocellatus* (Teleostei: Cypriniformes)

Wenjing Yi¹, Martin Rücklin², Robert Poelman¹, David C. Aldridge³ and Michael K. Richardson¹

1, Institute of Biology, University of Leiden, Sylvius Laboratory, Sylviusweg 72, 2333BE, Leiden, the Netherlands.

2, Naturalis Biodiversity Center, Postbus 9517, 2300 RA Leiden, The Netherlands.

3, Department of Zoology, University of Cambridge, The David Attenborough Building, Pembroke Street, Cambridge, CB2 3QZ, UK.

Published as:

Yi, W., Rücklin, M., Poelmann, R. E., Aldridge, D. C. and Richardson, M. K. (2021). Normal stages of embryonic development of a brood parasite, the rosy bitterling *Rhodeus ocellatus* (Teleostei: Cypriniformes). *J. Morphol.* **282**, 783–819.

Abstract

Bitterlings, a group of freshwater teleosts, provide a fascinating example among vertebrates of the evolution of brood parasitism. Their eggs are laid inside the gill chamber of their freshwater mussel hosts where they develop as brood parasites. Studies of the embryonic development of bitterlings are crucial to deciphering the evolution of their distinct early life-history. Here, we have studied 255 embryos and larvae of the rosy bitterling (*Rhodeus ocellatus*) using *in vitro* fertilization and X-ray microtomography (microCT). We describe 11 pre-hatching and 13 post-hatching developmental stages spanning the first 14 days of development, from fertilization to the free-swimming stage. In contrast to previous developmental studies of bitterlings, the staging system described here is character-based, and therefore more compatible with the widely-used stages described for zebrafish. Our data provide new insights into the polarity of the chorion, and into notochord vacuolization and yolk sac extension in relation to body straightening. This study represents the first application of microCT scanning to bitterling development and provides one of the most detailed systematic descriptions of development in any teleost. Our staging series will be an important tool for heterochrony analysis and other comparative studies of teleost development, and may provide insight into the co-evolution of brood parasitism.

Introduction

The bitterlings are a group of freshwater teleost fish in the family Acheilognathidae (Teleostei: Cypriniformes) which have a brood parasitic life-history (Smith et al., 2004). With their elongated ovipositor, female bitterlings lay eggs in their preferred mussel host species through the exhalant siphon of the mussel (Boeseman et al., 1938; Duyvené de Wit, 1955; Olt, 1893; Rouchet et al., 2017; Wiepkema, 1962). The eggs are introduced directly into the gill chamber by the ovipositor (Chang, 1948). They come to occupy the lumen of the water tube between the gill lamellae (Kim, Park, Park, Kang, & Kim, 2008; Kim, Choi, & Park, 2017; Tankersley, 1996). Later, male bitterlings release their sperm near the inhalant siphon (Boeseman et al., 1938; Smith and Reichard, 2013). The sperm are carried into the mussel by the water flow and fertilize the eggs; subsequently the eggs undergo their early stages of development inside the gill chamber (Liu, Zhu, Smith, & Reichard, 2006; Reichard, Liu, & Smith, 2007). When the larvae are capable of swimming, they migrate into the exhalant cavity and emerge from the host; this marks the end of the parasitic phase of their life (Aldridge, 1999).

Because of their interesting life history, bitterlings have been intensively studied by ecologists and behavioral biologists (Boeseman et al., 1938; Smith et al., 2004; Wiepkema, 1962). Aspects of the bitterling life cycle that have been studied include the parental behavior of bitterlings (Reichard, Smith, & Jordan, 2004) and bitterling-mussel co-evolution (Mills and Reynolds, 2003). For studies of bitterling and mussel phylogeny, see Chang et al. (2014) and Kawamura, Ueda, Arai, and Smith (2014). While there have been many studies of adult bitterlings, their development is less well-known. This is largely because of the difficulties of accessing the early embryos inside the mussel host. Furthermore, when early embryos are dissected out of the mussel, it is difficult to stage them because the precise time of fertilization is unknown (Duyvené de Wit, 1955; Olt, 1893). The unique early life history of bitterlings means that the embryos are subject to a protected but physiologically challenging environment, which may result in deviations from typical teleost embryonic development (Aldridge, 1999). The first description of early developmental stages in the European bitterling (*Rhodeus amarus*) were given by Olt (1893). Olt (1893) noticed the peculiar forms of the yolk and depicted the changing shapes of the yolk stage-by-stage in illustrations, but did not record the precise developmental age of these stage. Fortunately, the techniques of *in vitro* fertilization and time-controlled *in vitro* incubation can be used to obtain embryos of the most widely-distributed oriental bitterling, the rosy bitterling, *Rhodeus ocellatus* (Chang, 1948; Chang & Wu, 1947; Kim & Park, 1985; Nagata & Miyabe, 1978; Park & Han, 2018). Previous studies provided detailed descriptions (Chang, 1948; Chang & Wu, 1947), as well as schematic developmental atlases, of bitterling embryonic stages based on external morphological characters (Kim & Park, 1985; Nagata & Miyabe, 1978; Park & Han, 2018).

Nagata and Miyabe (1978) described 30 developmental stages of *R. ocellatus*: 14 stages before hatching, and 16 post-hatching ('prelarvae') stages. Unfortunately, the illustrations provided by Nagata and Miyabe (1978) are not annotated. Kim and Park (1985) described 20 pre-hatching stages with special emphasis on the period from yolk plug closure to presence of the tailbud (stage O to S in their series). They illustrated the migration and elongation of the rostral end towards the ventral side, but did not indicate the rostral-caudal axis in their illustrations, which means that some of their descriptions are ambiguous.

It is well-known that temperature has a strong influence on the rate of development (Werneburg, 2009). Nagata and Miyabe (1978) recorded the developmental age of bitterlings in terms of hours post fertilization (hpf). Kim and Park (1985) and Park and Han (2018) also used the term hpf for pre-hatching stages, but used 'hours post hatching' (hph) and 'days post hatching' (dph) for later stages. Those three studies differed in the timing that they assigned to certain developmental events. For example, 'hatching' was stated to occur at 27.8 hpf, 39 hpf and 50 hpf by Nagata and Miyabe (1978), Kim and Park (1985) and Park and Han (2018), respectively. We suggest that the difference in the time of hatching recorded in the first two studies is because the rearing temperature was different, namely: 22 ± 1 °C in Nagata and Miyabe (1978), 17-25.5 °C in Kim and Park (1985). The greatest difference in time of hatching is between Park and Han (2018) and Nagata and Miyabe (1978), although the rearing temperature in Park and Han (2018) is 21.5 ± 1 °C, closer to Nagata and Miyabe (1978). The newly-hatched embryo illustrated by Park and Han (2018) corresponds to a later developmental stage in Nagata and Miyabe (1978). Because Kim and Park (1985) used a relatively wide temperature range, we have chosen to use here the developmental age in Nagata and Miyabe (1978) as a guide. In Nagata and Miyabe (1978) and Kim and Park (1985), hatching occurred at the same morphological stage, namely when the embryo has 6-10 somites, Kupffer's vesicle is present, and the tailbud is not yet free from the yolk extension.

In the literature on teleost development, it is sometimes stated that the embryo becomes a larva at hatching (e.g. Ali, Champagne, Spaink, & Richardson, 2011; Ballard, 1981). Kunz-Ramsay (2013) noticed that bitterlings have an ostraphilic reproductive habit (laying eggs in mussels) and have a nidicolous (nest-dwelling) type of hatching. This means that they hatch at a relatively early age and are not capable of independent living by means of free-swimming and foraging (Aldridge, 1999; Li and Arai, 2010). Therefore, the term 'postembryo' is suggested by Kunz-Ramsay (2013) to describe the fish after hatching until the yolk is completely absorbed. After that, when exogenous feeding begins, the fish is termed a larva.

Here, we shall define the embryonic period of bitterlings as beginning at fertilization and ending when the embryos are capable of swimming out of their mussel host. Post-hatching individuals are termed 'embryos' instead of 'larvae' in this thesis (**Figure 1**). Hatching, in this view, implies the breaking of the chorion, and the embryo-to-larva transition is a nutritional definition (when endogenous feeding transitions to exogenous feeding).

In the current study, we make detailed descriptions of developmental stages in *R. ocellatus* in order to expand on the published studies. For post-hatching stages, we use microCT (X-ray microtomography) to reveal the internal structure of the embryos in tomographic sectional view, and to provide 3-D (three-dimensional) visualization of the external morphology of the developing bitterling. In preliminary studies (data not shown) we found that the perivitelline space of bitterlings is quite narrow, and this means that there is little room to perform dechoriation with forceps without damaging the yolk or embryo. Therefore, we decided not to dechorionate the eggs. Because the chorion is highly impermeable to many reagents (Masuda et al., 1986; Masuda et al., 1992), we assumed that the contrast medium needed for microCT would not penetrate. Therefore, we decided not to use microCT for the pre-hatching stages.

Advantages of microCT are that it is less time-consuming than conventional histological sectioning, it does not destroy the samples. Furthermore, larger specimens can be studied than is possible with, for example, confocal microscopy (Bassi et al., 2015; Huisken and Stainier, 2009; Weber et al., 2014). The main disadvantages of microCT are a lack of cellular resolution, the inability to use special stains to identify particular structures or molecules, and the inability to perform *in vivo* tracing. Metscher (2009) has pioneered the application of microCT to developmental biology by developing a soft-tissue staining protocol. MicroCT has been used to study mouse development (see for example the 3-D mouse embryo atlas (Wong et al., 2012)); to compare phenotypic variation of larval and juvenal zebrafish at the histological level (Ding et al., 2019); and to make quantitative morphometric analyses of adult teleost fish (Weinhardt et al., 2018).

By analyzing a developmental series of the rosy bitterling with microCT, we hope to provide a practical guide to staging bitterlings embryos in the lab and field. We also aim to provide a knowledge foundation for future research that focusses on development, comparative embryology, evolutionary developmental biology (evo-devo), and gene expression patterns. Our study may also serve as a model in the emerging discipline of eco-evo-devo, or ecological evolutionary developmental biology, which aims to integrate evolution and development with ecology (Abouheif et al., 2014; Gilbert et al., 2015).

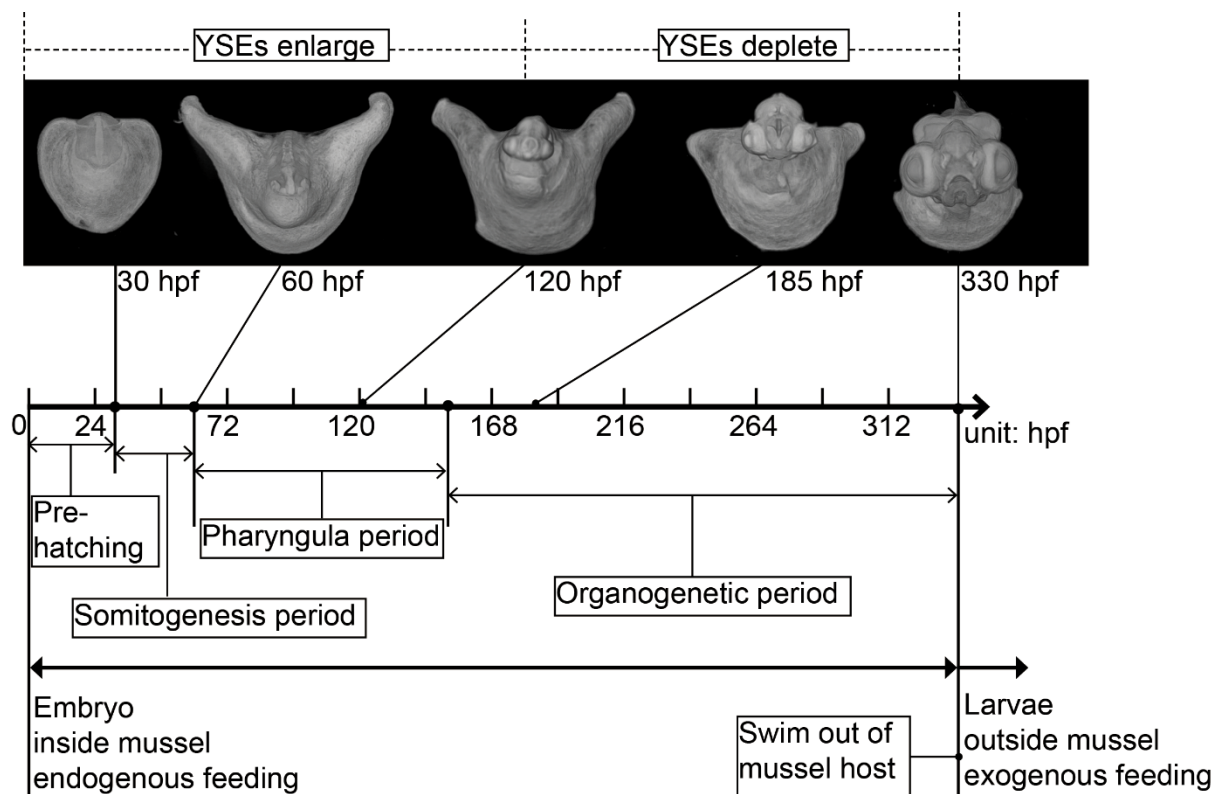


Figure 1 *Rhodnius ocellatus* development timeline. Abbreviations: hpf, hours post fertilization; YSEs, yolk sac extensions.

Materials and Methods

Ethics statement

All animal experimental procedures were conducted in accordance with local and international regulations. The local regulation is the Experiments on Animals Act (*Wet op de dierproeven*). This local regulation serves as the implementation of Guidelines on the protection of experimental animals by the Council of Europe, Directive 86/609/EEC, which excludes fish larvae up to the moment of free-feeding. Because the larvae used here were no more than 15 days old, and at that stage are not yet free-feeding, no license is required by the Council of Europe (1986) Directive 86/609/EEC, or by the Central Authority for Scientific Procedures on Animals, the Netherlands.

The animals were housed at the Institute of Biology, Leiden University. The Leiden University Medical Centre has installed an Animal Welfare Body to oversee the welfare of the laboratory animals; in addition, the Inspectorate of the Ministry of Economic Affairs, the Netherlands, is charged with enforcing the law and associated regulations. Mussels are not covered under the Directive mentioned above. Fish and mussels were all sourced from commercial suppliers and none of them is an endangered species.

Animal husbandry

Rosy bitterlings (*Rhodeus ocellatus*, Kner, 1866) were kept in indoor freshwater aquaria with controlled light and temperature. Adult fish were purchased from Ruinemans Aquarium B.V., Montfoort, NL. At 06:45 and 20:15, the lights were turned on and off, respectively, with a 15 min transition time to avoid sudden shock. The room temperature and water temperature were kept at 22.5 ± 1 °C and the fish were checked every day. Fish were fed daily with frozen chironomid larvae (Ruinemans Aquarium B.V., Montfoort, NL). Duck mussels (*Anodonta anatine*, Linnaeus, 1758) and swan mussels (*Anodonta cygnea*, Linnaeus, 1758) were obtained from Vijver-centrum Enschede, Aquaria Veldhuis, Enschede, NL, and kept indoors with natural light from a window, in a shallow filtration tank without feeding. Water from the filtration tank was fed into the fish tanks to stimulate mating.

In vitro fertilization

Embryos with synchronized development were obtained by *in vitro* fertilization following the method of Nagata and Miyabe (1978). In brief, sexually-mature parental fish were chosen based on the bright mating color of the male and the elongated ovipositor of the female. Eggs were expressed from 35 females into a clean, dry 10 cm Petri dish by gentle abdominal compression. Sperm was harvested from 25 males by gentle abdominal compression. We used a narrow-mouthed pipette to distribute the sperm evenly over each batch of eggs in a clean Petri dish. Fresh aquarium water was then added, so as to synchronously activate embryonic development. Embryos were raised 20 per Petri dish containing embryo water (Kimmel et al., 1995) changed every 24 h. The Petri dish was kept in an incubator with stationary shelves at 22.5 ± 1 °C.

Time-lapse videography

For all pre-hatching stages, we used time-lapse videography of embryos at room temperature with epi-illumination from a fiber-optic lamp (Schott KL 1500 LCD). Photos were taken every 5 min with a

CCD (charge-coupled device) camera (Nikon DS-Fi1-L2) connected to stereo microscope (Nikon SMZ1500). The images acquired had a minimum resolution of 300 dpi (dots per inch) and were stored in JPG format. During the recording, embryos were kept in glass embryo dishes (uncovered, 30 mm diameter x 12 mm deep) filled with embryo water. Because young embryos do not yet show spontaneous movements, it was not necessary to immobilize them with agarose embedding or anesthesia. The water level during the recording period was maintained by adding drops of egg water to the embryo dishes as necessary.

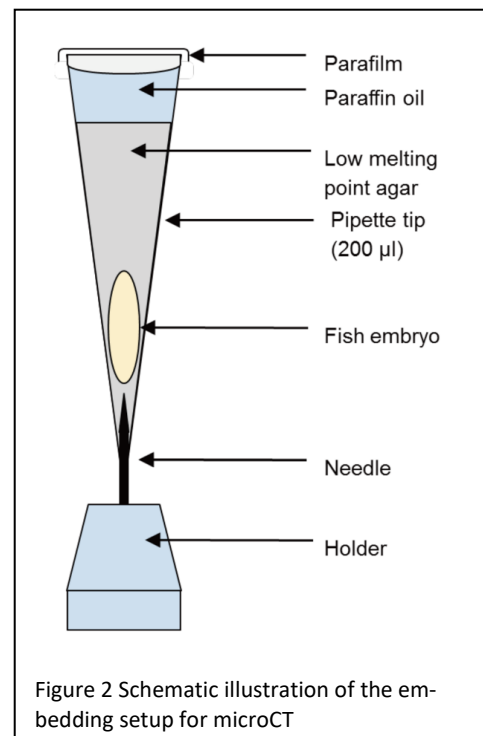
Embryo fixing, processing and microCT scanning

The following protocol is based on Metscher (2009) and Babaei et al. (2016). Post-hatching stages were fixed for microCT at different developmental time points as shown in Table 1. The fixative was 3% paraformaldehyde and 1% glutaraldehyde in 0.1 mol l⁻¹ phosphate buffered saline, pH 7.0 at 4 °C overnight. After rinsing in PBS (2 x 10 min), specimens were stained with iodine-potassium iodide (1% iodine in 2% potassium iodide) for 12 h or phosphotungstic acid (PTA, 0.3% phosphotungstic acid in 70% ethanol) for ≥ 24 h. Staining was carried out on a rotary mixer at 6 rpm. After staining, the embryos were stored at 4 °C in 70% ethanol. Embryos were immobilized in 1% low melting-point agarose, sealed with paraffin oil and parafilm, and stabilized in a polystyrene tube during scanning (see Figure 2).

The raw data for 3-D imaging of the samples were acquired using an Xradia 520 Versa 3-D X-ray microscope (Zeiss). The X-ray source was set to 80/7 or 40/3 (keV/W). A thin LE1 filter was used to avoid beam hardening artifacts. To obtain high resolution images, a CCD optical objective (4x) was used. The acquisition parameters were set according to the developmental stage of the sample stages (Table 1). The isotropic voxel size for overview scanning of the whole embryo was 2-3 μm. For detailed scanning of the head region, the isotropic voxel size was set to < 1.5 μm. Each sample was rotated 180+fan degrees along the anterior-posterior (AP) axis. The projection images acquired were checked for sample drifting then reconstructed if of acceptable quality.

Image processing

Reconstructed tomographic data for each sample were 3-D rendered using Avizo software (Version: 9.5.0; Thermo Fisher Scientific), and further processed for viewing in coronal, sagittal and transverse section planes. The 3-D views were pseudo-colored with the volume rendering module using physics.icol as the colormap in the Avizo software. Annotations were applied to the virtual sections using Adobe InDesign software (Version: 15.0.2, Adobe Systems Inc., San José, California). For complex structures (e.g., the semicircular canals of the inner ear), the segmentation of a region of interest was performed in Avizo from the reconstructed



images, in order to verify the annotations. Anatomical terms, including those used in the annotations of the figures, were based on the ZFIN anatomical ontology (<https://zfin.org/action/ontology/search>, Belmamoune & Verbeek, 2007; van Slyke, Bradford, Westerfield, & Haendel, 2014).

Table 1 Micro-CT scanning parameters for embryos during post-hatching stages

Age (hpf)	Stage name	Scan type	Pixel size (μm)	Voltage (keV/W)	Exp. time (sec.)	Intensity
30	s-10	overview	1.4913	80/7	1.4	5200-6500
36	s-18	overview	1.4908	80/7	1.5	5000-7000
48	s-28	overview	1.4907	80/7	1.8	5000-8000
54	s-32	overview	1.4907	80/7	1.7	5000-7500
60	s-35	overview	1.4908	80/7	1.4	5000-6500
80	4-ovl	overview	1.9688	40/3	7	5000-7500
100	3-ovl	overview	1.9714	40/3	8	5000-8300
135	2-ovl	overview	2.19	40/3	4	5000-9000
150	1-ovl	overview	2.0643	40/3	4.5	5000-10000
165		overview	2.0635	40/3	4	5000-10000
185	pec-bud	overview	1.971	80/7	0.8	5500-8200
210	high-pec	overview	3.5202	40/3	1.6	5000-10000
235	long-pec	overview	3.8545	40/3	1.4	5000-10000
260		overview	1.9707	80/7	0.8	5300-7500
330	pec-fin	overview	3.5214	40/3	1.5	6000-10000
80	4-ovl	head detail	0.99801	40/3	20	5000-5700
100	3-ovl	head detail	0.99916	40/3	24	5000-6200
165		head detail	0.9765	40/3	17	5000-8500
185	pec-bud	head detail	0.9989	80/7	3	5000-6300
210	high-pec	head detail	1.4582	40/3	9.5	5000-10000
235	long-pec	head detail	1.4299	40/3	8.5	5000-10000
260		head detail	1.4782	80/7	1.3	5200-7700
330	pec-fin	head detail	1.3727	40/3	9	5000-8500

Note, hpf, hours post fertilization; sec, second; exp, exposure. Intensity is the ‘light ’intensity that reaches the detector camera. Typically, the exposure time was set so that the intensity was at least 5000 in the darker parts of the sample.

Results

Notes: In the following descriptions, the abbreviations in parentheses are the same as those used in the figure annotations. The developmental age of each stage is recorded as hours post fertilization (hpf) at an incubation temperature of 22.5 °C. The references to zebrafish stages are to Kimmel et al. (1995); we shall refer to them as 'Kimmel' stages. Please note that there is (i) a single *yolk extension* (the yolk extension caudally to the yolk constriction) and (ii) a pair of wing-like *yolk sac extensions* (YSEs) dorsolateral to the yolk ball and mainly formed as thickenings of the yolk sac. 'Somite number' refers to the number of pairs of somites.

Our results are divided into: (i) pre-hatching stages; and (ii) post-hatching stages (Figure 1). The pre-hatching stages begin at fertilization, and include cleavage, blastula, gastrula and neurula periods, and end at hatching. These pre-hatching stages were all studied by time-lapse videography in live embryos. The developmental age was calculated from the time-lapse videos. The post-hatching stages include the somitogenesis, pharyngula and organogenetic periods. These periods were originally applied to zebrafish development by Kimmel et al. (1995). The definition of these 'periods' is arbitrary, but useful for organizing the stages and making comparisons with the zebrafish staging series.

(i) Pre-hatching stages

STAGE 1: 1-cell, 0.4 hpf.

The eggs of *R. ocellatus* are demersal (inclined to sink in water). The chorion is bulb-shaped, with an elongated stalk at the animal pole (Figure 3). The perivitelline space between the embryo and the chorion forms as the latter swells and lifts away from the embryo; it is narrow at the vegetal pole. Activated by fertilization, the yolk-poor cytoplasm streams towards the animal pole (AP), forming the blastodisk. By contrast, the yolk cytoplasm remains at the vegetal pole (VP) forming the yolk ball (Figure 4A). This stage is comparable to Kimmel stage 1-cell.

STAGE 2: 2-cell, 1.3 hpf

Cleavage is meroblastic, as in other teleosts including *Danio rerio* (Kimmel et al., 1995). At the 2-cell stage, the blastodisk becomes divided symmetrically, forming two equally-sized blastomeres (Figure 4A). This stage is comparable to Kimmel stage 2-cell.

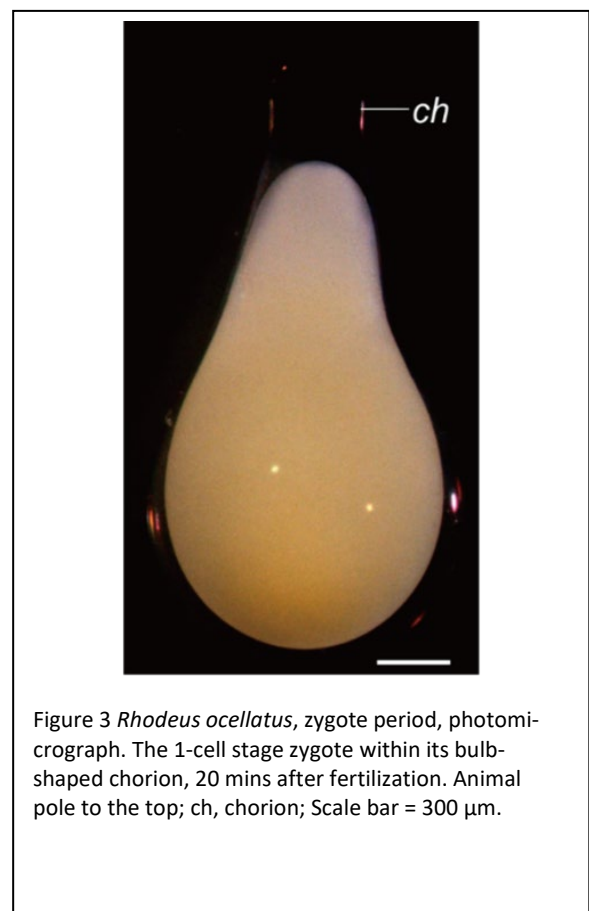


Table 2 Developmental stages and selected characters proposed in this stu for the rosy bitterling (*Rhodeus ocellatus*) and a comparison with the zebrafish (*Danio rerio*).

Stage name (<i>R. ocellatus</i>)	hpf	Staging characters	Stage name (<i>D. rerio</i>)	hpf
Zygote period				
1-cell	0.4	Blastodisk appears	1-cell	0
Cleavage period				
2-cell	1.3	First cleavage division	2-cell	0.75
Blastula period				
Blastula	3.7	Blastoderm forms, irregular tiers of blastomeres	256-cell	2.5
Gastrula period				
50%-epiboly	15	Shield visible	shield	6
90%-epiboly	22.5	Small yolk plug	90% epiboly	9
Convergent	23.5	Yolk plug closure	bud	10
Neurula period				
Extension	23.8	Yolk plug totally disappeared	bud	10
Migration	24.2	Head region at the midpoint of the A-V axis	bud	10
1-somite	24.5	Ventral yolk constriction, first somite furrow		
3-somite	25.5	Discernible optic primordium	3-somite	11
6-somite	27	Small dorsal yolk sac extensions (YSEs), hatching	6-somite	12
Somitogenesis period				
10-somite	30	EL=2.6-2.7 mm, Neural tube, Somite number 10-12, otic placode	10-somite	14
			14-somite	16
18-somite	36	EL=2.8-3.1 mm, roll-like tail bud protrusion, somite number 13-20, chevron-shaped trunk somites, optic vesicle, trigeminal placode, pronephric duct		
28-somite	48	EL=3.2-3.3 mm, tail elongate, somite number 19-29, heart tube, muscular twitches of skeletal muscles, optic cup, lens placode, otic vesicle, cephalic flexure, rhombomeres	18-somite	18
32-somite	54	EL=3.6-3.8 mm, somite number 30-32, otolith, optic stalk, heart cone-shaped, irregular cardiac contraction, nephron primordium, notochord vacuoles, body movements (side-to-side flexing)	21-somite	19.5
35-somite	60	EL= 3.7-4.0 mm, tail blade-shaped, somite number reaches maximum (35), startle response	26-somite	22

Pharyngula period

4-OVL	80	EL= 3.9-4.1 mm, lens formation, median fin fold, blood islands, tubular heart, cloaca		
3-OVL	100	EL= 4.5-4.7 mm, prim-6, red blood cells circulating, telencephalon eversion, heart looping, heartbeat; caudal fin rays, caudal vein plexus	Prim-5	24
2-OVL	135	EL=4.8-4.9 mm, prim-10, pituitary, heart forward, heartbeat rhythmic, aortic arch, ventral aorta, thickened otic vesicle wall, pectoral fin bud primordium, gut a solid endodermal rod	Prim-10	~27
1-OVL	150	EL=5.1 mm, prim-20 to 24, sparse melanophore pigmentation in retina, low pectoral fin bud, semicircular canals, YSEs reaches maximal size	Prim-25	36

Organogenetic period

Pec-bud	185	EL=5.5 mm, head straightening, olfactory bulb, AER of pectoral fin bud, branchial arches, dorsal body pigmentation, regionalization of median fin fold into dorsal and ventral fins, liver tissue appears		
High-pec	210	EL=5.7 mm, lower jaw recognizable, cartilage in mandibular and hyoid arches, pericardium cavity, heart divided into atrium and ventricle	High-pec	42
Long-pec	235	EL=5.8-6.0 mm, head pigmentation, membranous pectoral fin, dorsal fin primordium, mouth open at ventral side, pharyngeal teeth, operculum, gill slits open, gill filaments, gall bladder	Long-pec	48
Pec-fin	330	EL=6.1-6.3 mm, iridophores in iris, YSEs regressing, jaw protruding, mouth opening rostrally, caudal fin rays, melanophores in lateral stripes, three pairs of otoliths, swim bladder	Pec-fin	60

Note, the stages for the zebrafish are taken from Kimmel, Ballard et al. (1995). hpf, hours post fertilization; A-V. animal-vegetal; EL, standard embryo length from rostral to caudal (including the tail); AER, apical ectodermal ridge, OVL, otic vesicle length.

STAGE 3: Blastula, 3.7 hpf.

The blastula stage (Figures 4B and 5) is characterized by the proliferation of blastomeres so that they come to form several layers. A distinct border, the yolk syncytial layer (YSL), appears between the blastodisk and yolk. In late blastula stages, epiboly movements start so that the blastodisk spreads towards the vegetal pole, engulfing the underlying yolk ball. The animal-vegetal (A-V) axis becomes shortened and the shape of the embryo changes from pear-shape to ellipsoid (compare Figures 4A and B). This stage is comparable to Kimmel stage 256-cell.

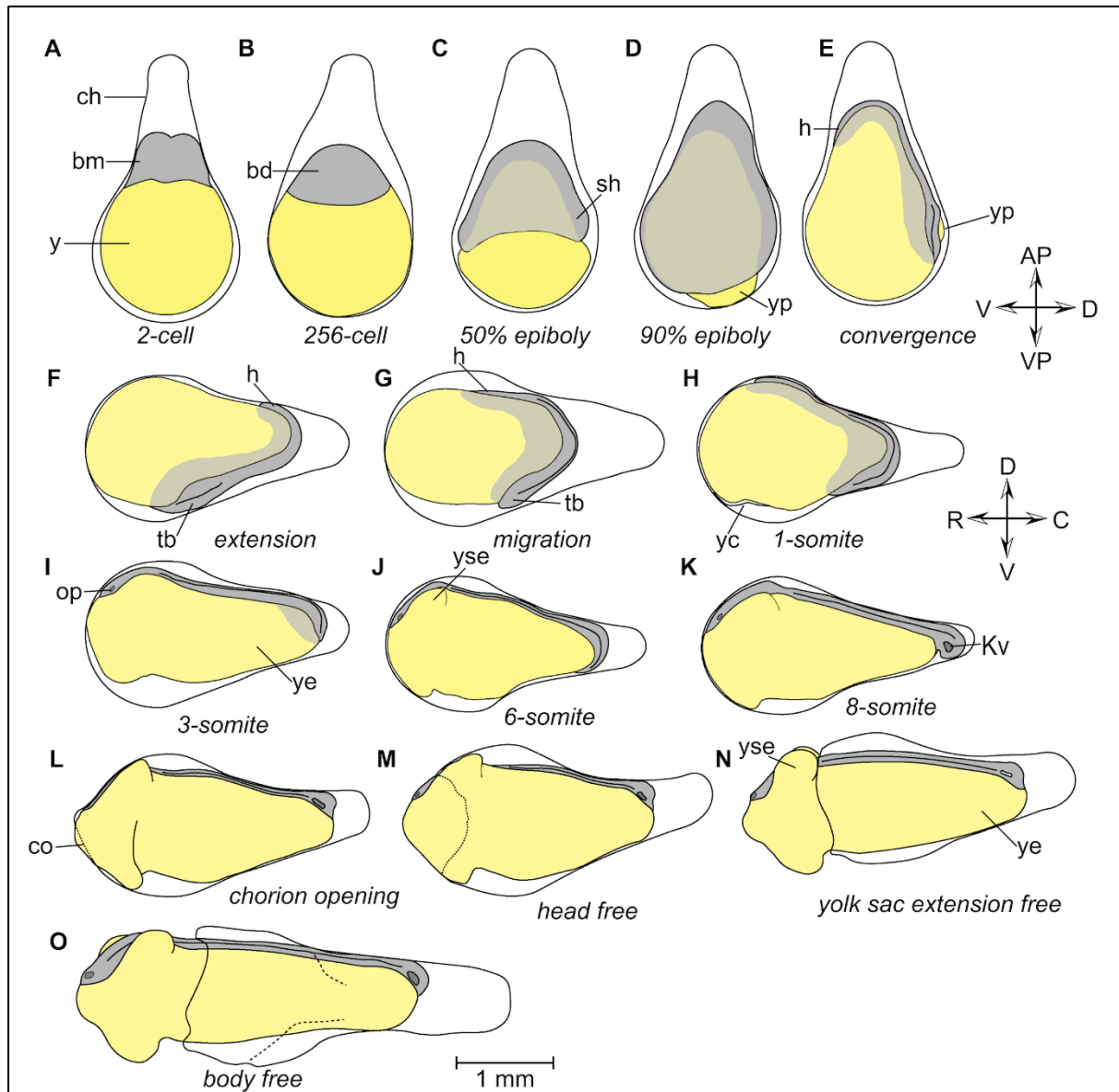


Figure 4 *Rhodeus ocellatus*, pre-hatching stages, schematic illustration based on time-lapse photomicrographs. The transparent chorion is represented by a solid line, the ruptured chorion by a dashed line. The blastoderm, and the tissue derived from it, are shaded in light and dark grey, respectively. The yolk is shown in yellow. A to E are lateral views, with the animal pole at top, ventral to the left. In F to O, the lateral view is rotated 90° clockwise (relative to A-E), with dorsal to the top, rostral to the left. Abbreviations: AP, animal pole; bd, blastoderm; bm, blastomere; C, caudal; Ch, chorion; co, chorion opening; D, dorsal; h, head; Kv, Kupffer's vesicle; op, optic primordium; R, rostral; sh, shield; tb, tail bud; V, ventral; VP, vegetal pole; y, yolk; yc, yolk constriction; ye, yolk extension; yp, yolk plug; yse, yolk sac extension.

STAGE 4: 50% Epiboly, 15 hpf.

Epiboly is coordinated by three morphogenetic movements: spreading, convergence and extension (Xiong et al., 2014). First, the blastoderm covers the yolk by gradually spreading over it. The progress of epiboly can be expressed in terms of the percentage coverage of the yolk ball by the blastodisk margin. At the beginning of epiboly, the blastoderm is uniform in thickness. Later, the spreading cells converge on the dorsal midline of the embryo and the embryonic shield is thereby formed (Figures 4C and 6A). After formation of the shield, the dorsoventral (D-V) and rostrocaudal (R-C) axes are distinct. The shield is now at the caudal end of the dorsal midline. This stage is comparable to Kimmel stage *shield*.

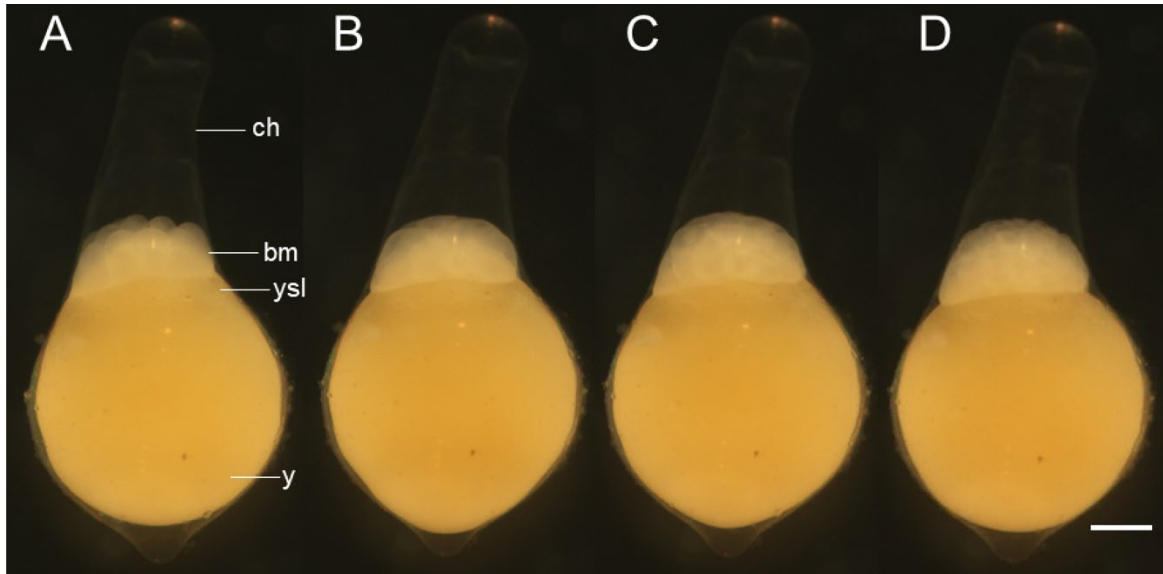


Figure 5 *Rhodeus ocellatus*, embryos during the cleavage period, photomicrographs. Animal pole to the top. A, 16-cell stage (1.75 hpf). B, 32-cell stage (2.2 hpf). C, 64-cell stage (2.65 hpf). D, 128-cell stage (3.1 hpf). Abbreviations: bm, blastomere; ch, chorion; y, yolk; ysl, yolk syncytial layer. Scale bar = 300 μ m.

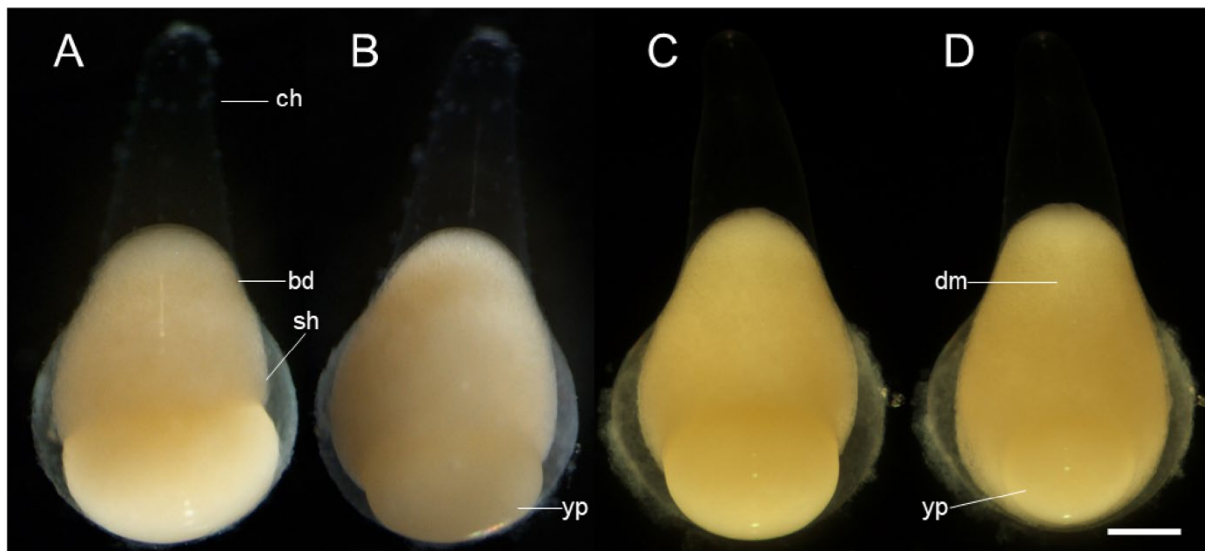


Figure 6 *Rhodeus ocellatus*, embryos during the epiboly period, photomicrographs. A, B, left view, animal pole to the top, dorsal to the left. A, 60% epiboly stage (16 hpf). B, 80% epiboly stage (20 hpf). C, D, dorsal view. C, 80% epiboly stage (20 hpf). D, 90% epiboly stage (22.5 hpf). Abbreviations: bd, blastoderm; ch, chorion; dm, dorsal midline; sh, shield; yp, yolk plug. Scale bar = 400 μ m.

STAGE 5: 90% epiboly, 22.5 hpf.

The margin of the blastoderm is no longer perpendicular to the A-V axis; the ventral part has spread further than the more compact dorsal part. Therefore, the yolk plug is not located precisely at the vegetal pole but on the dorsal side of the A-V axis (Figures 4D, 6D, 7B). Comparable to Kimmel stage 90% Epiboly.

STAGE 6: Convergence, 23.5 hpf.

A small yolk plug is present on the dorsal side of the A-V axis (Figures 4E and 7C); epiboly ends when the yolk plug disappears. The developing head region is becoming visible as a cellular condensation

near the animal pole. The developing neural primordium is visible in the dorsal midline, flanked by on each side by paraxial mesoderm. This stage is comparable to Kimmel stage *bud*.

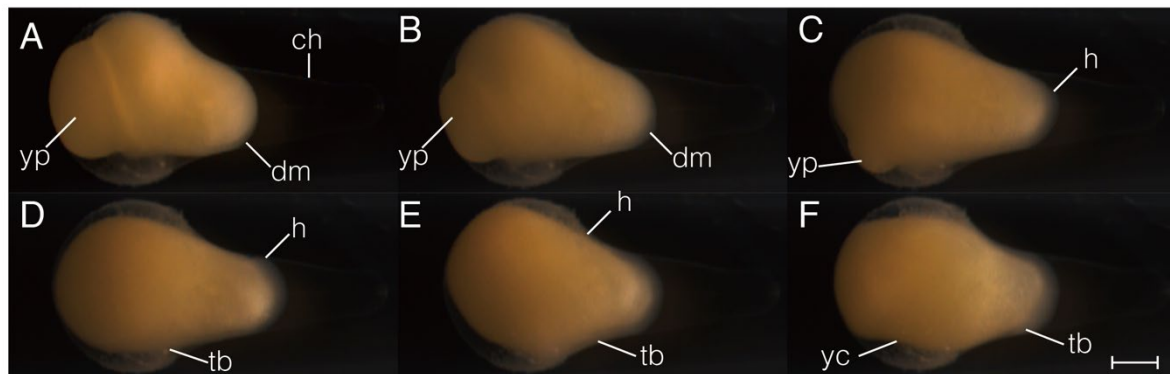


Figure 7 *Rhodeus ocellatus*, embryos from yolk-plug closure to tail bud present, photomicrographs. Lateral views. The position of embryo is changing so that, at the final stage (F) dorsal is at the top, rostral to the left. A, 80% epiboly stage (20 hpf), embryo with a large yolk-plug at the vegetal pole. B, 90% epiboly stage (22.5 hpf), embryonic tissue condensed along the dorsal midline. C, end of epiboly stage (23.5 hpf), embryo with a small yolk plug. The developing head region is at the animal pole, with dorsal to the top, rostral to the left; D, neurula extension stage (23.8 hpf), yolk plug has disappeared, tail bud present, head region extends towards ventral side. E, neurula migration stage (24.2 hpf), head migrates towards the vegetal pole. F, 1-somite stage (24.5 hpf), yolk constriction appears at the ventral side. Abbreviations: AP, animal pole; ch, chorion; dm, dorsal midline; h, head; tb, tail bud; VP, vegetal pole; yc, yolk constriction; yp, yolk plug. Scale bar = 500 μ m.

STAGE 7: Neurula extension, 23.8 hpf.

Neurula stages (Figures 4F, 7D) begin after closure of the yolk plug. At the neurula extension stage, the head region, notochord rudiment, and tailbud are distinguishable. Neurula extension movements cause the head region to become displaced towards the vegetal pole. The head is located near the narrowed part of the chorion. This stage is comparable to Kimmel stage *bud*.

STAGE 8: Neurula migration, 24.2 hpf.

The head region extends along the R-C axis towards the widened part of the chorion. In time-lapse movies, it appears as though the embryonic tissue migrates on the yolk ball surface, driven by the neurula extension movements, and we therefore name this stage the 'neurula migration' stage (Figures 4G, 7E). This stage is comparable to Kimmel stage *bud*.

STAGE 9: 1-somite, 24.5 hpf.

The first somitic furrow appears. Somitogenesis (Figures 4H, 7F) overlaps in time with neurulation. The intersomitic boundaries are not easily discernible under the dissection microscope. Therefore, yolk shape is used to define this stage. The yolk constriction appears at this stage on the ventral side of the embryo and deepens towards the dorsal side. This stage is intermediate between Kimmel stages *bud* and *3-somite*.

STAGE 10: 3-somite, 25.5 hpf.

There are three somite pairs. The head has assumed its definitive location at the end of the wide 'bulb' of the chorion. During neurulation the neural ectoderm develops into the neural plate, which forms the neural keel by primary neurulation (Lowery and Sive, 2004). The neural keel is triangular in cross-section, and initially solid; it later forms the neural rod which has a circular cross-section and is also solid. The eye field, a common primordium of both the left and right eyes (Figure 4I), is the only discernible sensory primordium at this stage. Comparable to Kimmel stage *3-somite*.

STAGE 11: 6-somite, 27 hpf.

There are six somite pairs. A pair of yolk sac extensions (YSEs) is forming ventrolaterally on the trunk. Kupffer's vesicle appears on the ventral aspect of the tailbud just before hatching (Figures 4J, K). Hatching (Figure 4L-O) does not take place at a consistent developmental age and is therefore not part of our series of named stages. The typical time of hatching that we observed here was 28 hpf – 35 hpf. The initial rupture of the chorion always appears in its 'bulb' (Figure 4L); the yolk comes to protrude rostrally from that opening. As the opening in the chorion becomes enlarged, the head region of the embryo also emerges from it (Figure 4M). Then, the widest part of the embryo, that is the region of the YSE, also emerges (Figure 4N). By now, the posterior part of the embryo is still inside the chorion; gradually however, the entire chorion is pushed away by the increasing length of the body and elongation of tail, and by the intermittent side-to-side movements of the tail observed in videography (Figure 4O). Comparable to Kimmel stage 6-somite.

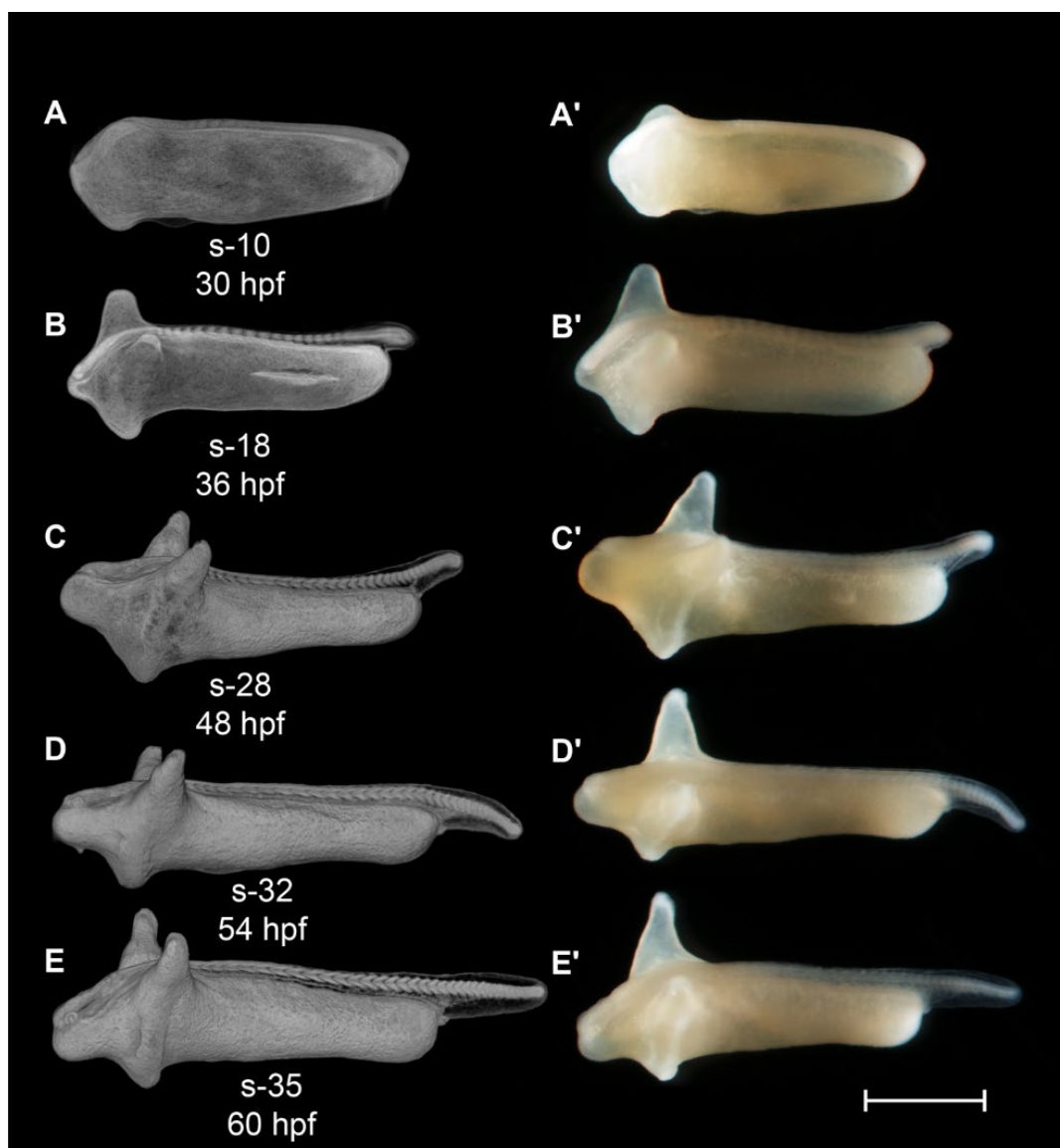


Figure 8 *Rhodnius ocellatus*, stages during the somitogenesis period. A to E, microCT images, volume rendering. A' to E', photomicrographs of the same embryo. A and A', stage 10-somite, 30 hpf. B and B', stage 18-somite, 36 hpf. C and C', stage 28-somite, 42 hpf. D and D', stage 32-somite, 54 hpf. E and E', stage 35-somite, 60 hpf. Lateral view, dorsal up, head to the left. Abbreviations: hpf, hours post-fertilization; s, somite. Scale bar = 1 mm.

(ii) Post-hatching stages

We have divided post-hatching stages into somitogenesis, pharyngula and organogenetic periods.

Somitogenesis period: during the somitogenesis period, segmentation of somites continues and rhombomeres develop. The somite number is a quantal (discrete) staging character and is therefore easy to compare between species (Battle, 1940; Furutani-Seiki and Wittbrodt, 2004; Iwamatsu, 2004; Signore et al., 2009; Tsai et al., 2013). The elongation of the tail during the somitogenesis period is a useful staging character. Embryos before tailbud protrusion have <12 somite pairs (Figure 8A). When the tailbud is elongated and cylindrical, somitogenesis in the truncal region is complete and there are 12-22 somites (Figure 8B). As the tailbud elongates further, caudal somites develop and the body somites reach the final number of 35 (Figure 8C, D and E).

STAGE 12: 10-somite, 30 hpf

There are 10 somite pairs (Figure 9A). The somites are contiguous caudally with unsegmented paraxial mesoderm. The intermediate mesoderm is discernible as two rods on the ventrolateral margin of the somitic mesoderm (Figure 9A and E). The tailbud is not yet free from the yolk (Figure 8A and A'). Kupffer's vesicle is still recognizable ventral to the tailbud (Figure 8A and Figure 9F). The yolk constriction is prominent on the ventral aspect of the yolk, near the head end of the embryo (Figure 8A). The neural tube is differentiated into a brain primordium and narrower spinal cord primordium (Figure 9A and C). The optic primordia extend laterally from the future diencephalon so that the outline of the head in dorsal view is shaped like an arrowhead (Figure 9A and C). Ectodermal placodes first become visible with microCT as thickenings in the ectoderm lateral to the neural tube (Figure 9A). The otic placodes are located midway between the optic primordia and the first somite (Figure 9A and D). There are paired heart primordia in the splanchnic mesoderm (Figure 9D). Most embryos have hatched completely, but in a few cases, the posterior part of the body is still enclosed. This stage is comparable to Kimmel stage *10-somite*.

STAGE 13: 18-somite, 36 hpf

There are 18 somite pairs (Figure 10A). The first post otic somite, and last three somites, are cuboidal in shape, whereas the remaining somites have the characteristic chevron-shape of the adult myotome (Figure 10A). The tailbud projects beyond the yolk, on the dorsal side, forming a cylindrical protrusion (Figure 8B and Figure 10A). Kupffer's vesicle is now decreasing in size. It is now located close to the tip of the tailbud (Figure 10J). The yolk extension is elongated posteriorly. The YSEs project dorsally (Figure 8B and Figure 10A). The neural tube is now cylindrical in transverse section and has a lumen (compare Figure 10D and E). The optic vesicle now has a lumen (optocoele) but is not yet invaginated into a cup (Figure 10D). The otic placodes are condensed, but lack a lumen at this stage (Figure 10G). The trigeminal placodes are present midway between the optic vesicle and otic placode, adjacent to the future rhombomere 2, and posterior to the nascent midbrain-hindbrain boundary (Figure 10A). The cardiac primordia are visible as a pair of hollow tubes (Figure 10G). The notochord has a 'stack-of-coins' appearance (Figure 11A). A pair of pronephric ducts is seen, one on each side of the dorsal aorta (Figure 10I). This stage is comparable to Kimmel stages *14-somite* and *18-somite*.

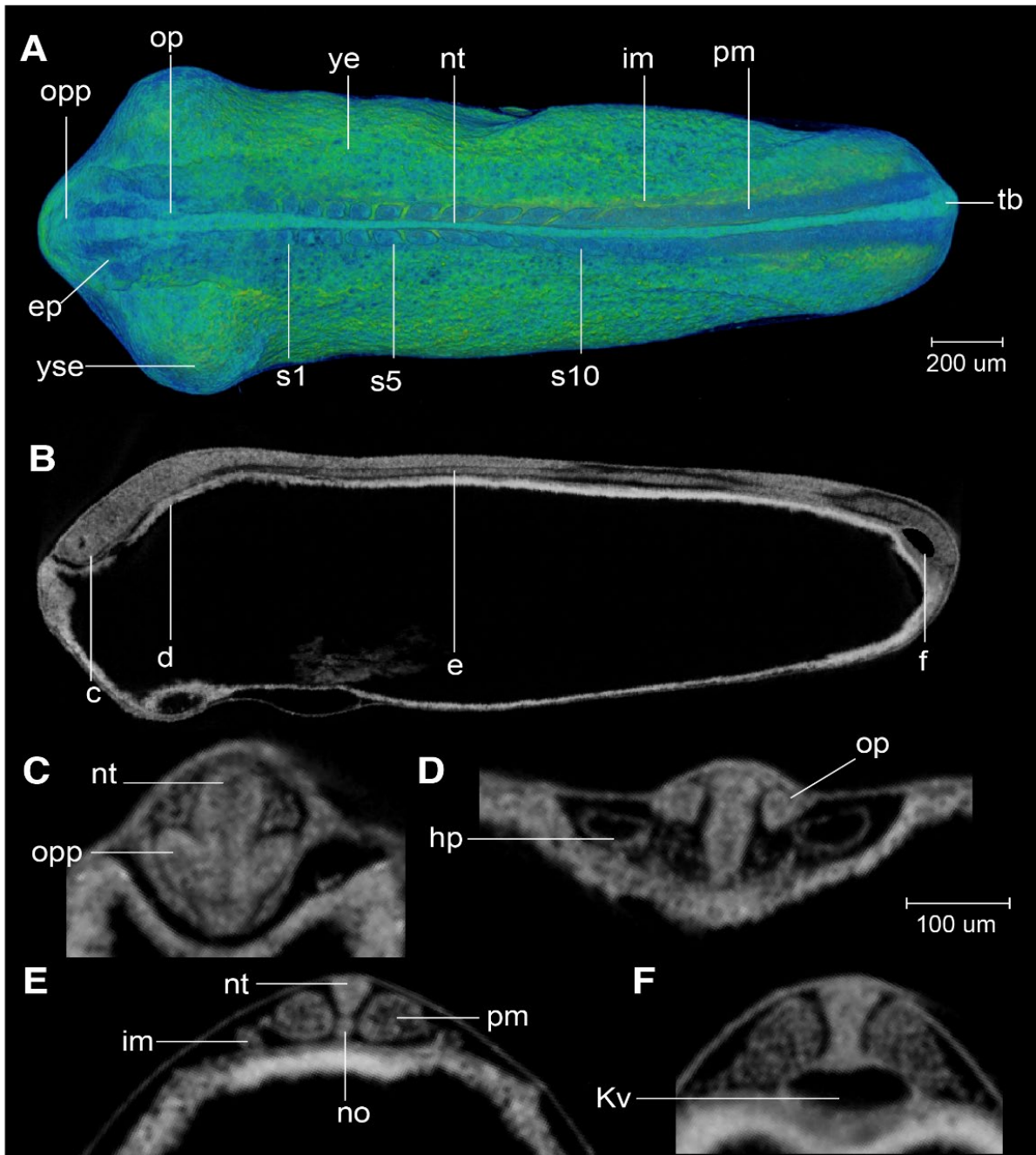


Figure 9 *Rhodeus ocellatus*, stage 10-somite, microCT images. A, volume rendering, dorsal view, rostral to the left. B, virtual section, midsagittal, dorsal to the top, rostral left, letters c to f indicates the section level of the correspondent transverse sections. C to E, virtual sections, transverse, dorsal to the top. Abbreviations: ep, ectoderm placode; hp, heart primordium; im, intermediate mesoderm; Kv, Kupffer's vesicle; no, notochord; nt, neural tube; op, otic placode; opp, optic primordium; pm, paraxial mesoderm; s, somite; tb, tail bud; ye, yolk extension; yse, yolk sac extension.

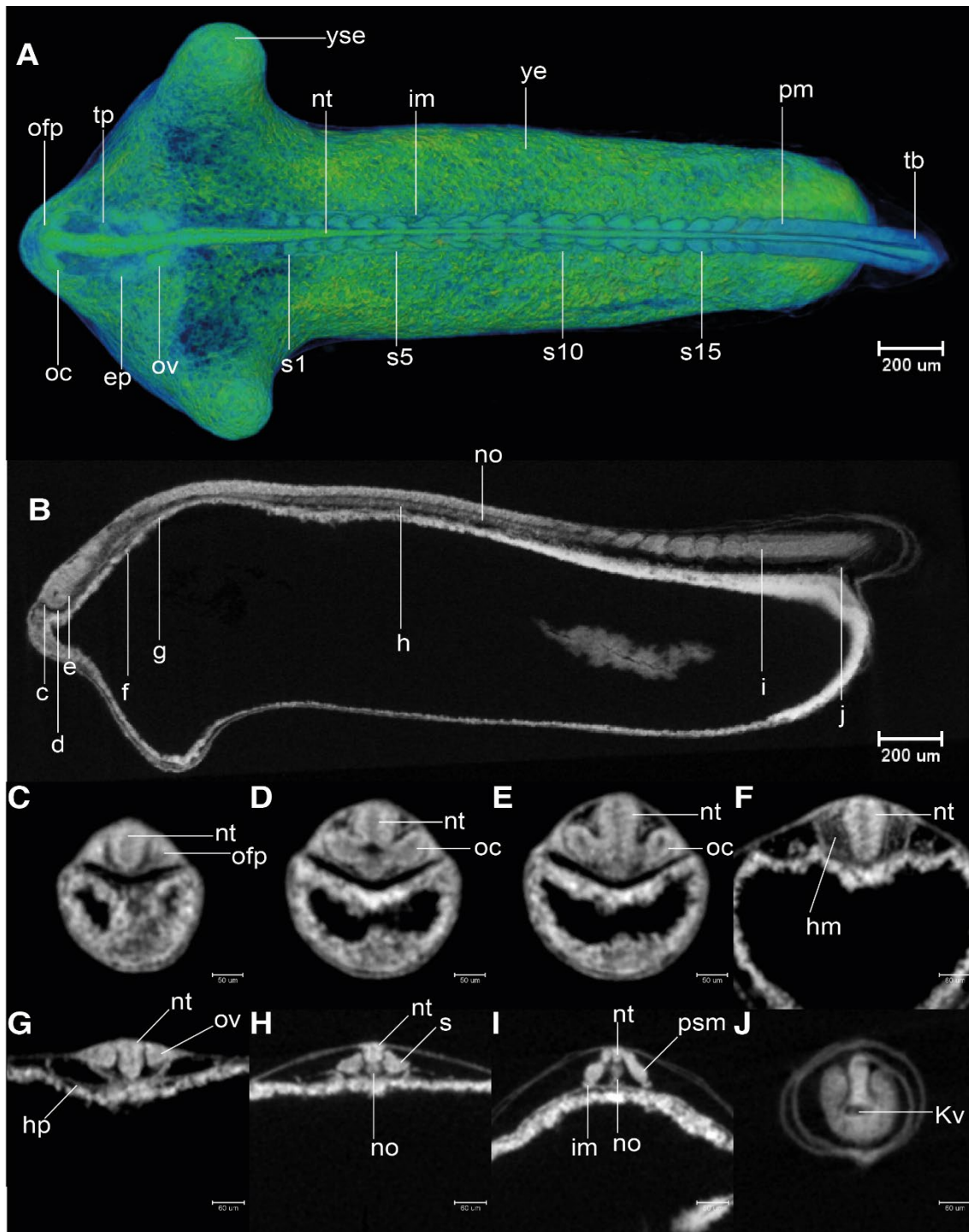


Figure 10 *Rhodeus ocellatus*, stage 18-somite, microCT images. A, volume rendering, dorsal view, rostral to the left. B, virtual section, midsagittal, dorsal to the top, rostral left, letters c to j indicates the section level of the correspondent transverse sections. C-F, virtual sections, transverse, dorsal to the top. Abbreviations: ep, ectoderm placode; hm, head mesoderm; hp, heart primordium; im, intermediate mesoderm; Kv, Kupffer's vesicle; no, notochord; nt, neural tube; oc, optocoele; ofp, olfactory placode; ov, otic vesicle; pm, paraxial mesoderm; psm, presomitic mesoderm; s, somite; t, tail; tg, trigeminal placode; ye, yolk extension; yse, yolk sac extension.

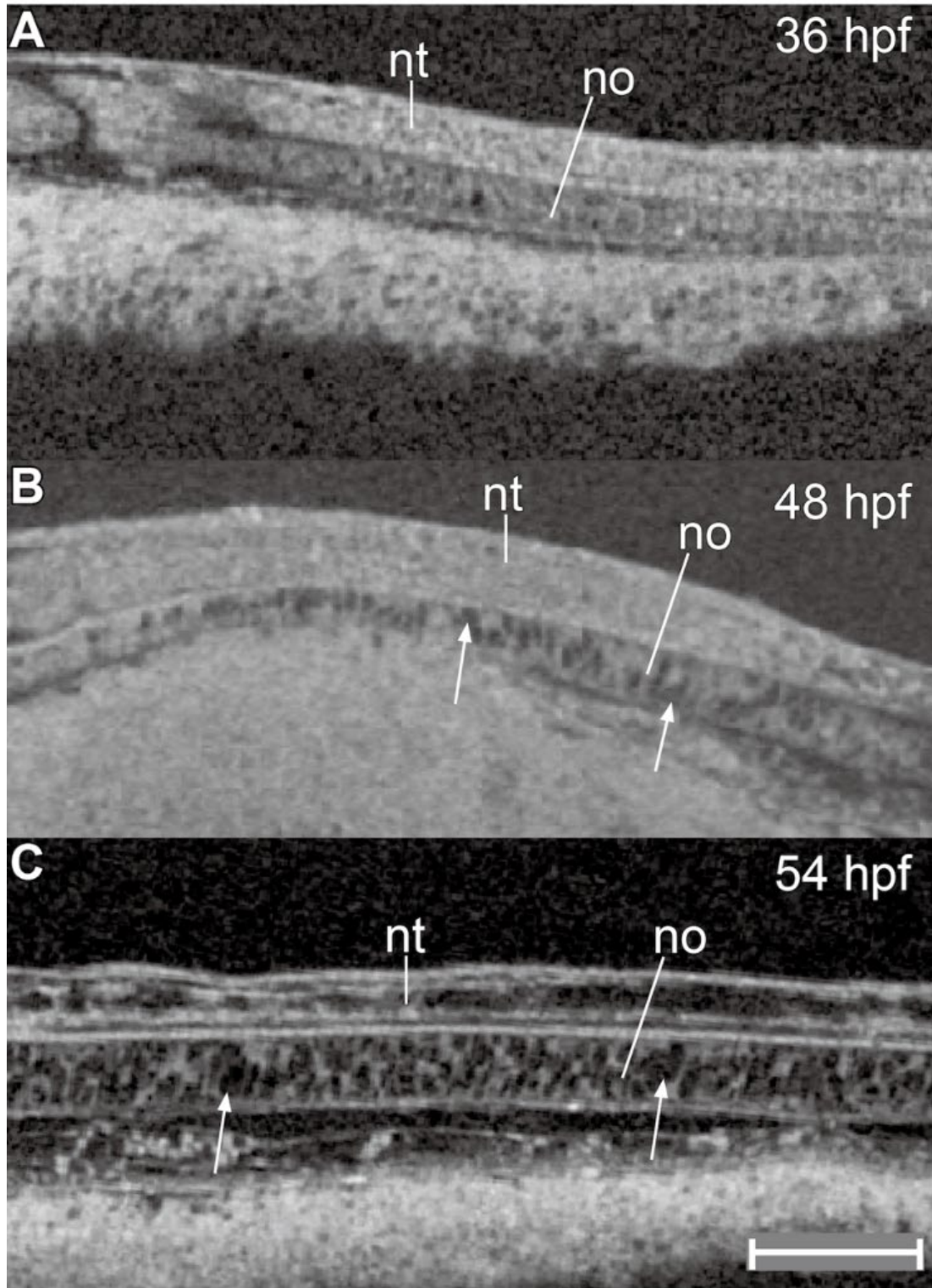


Figure 11 *Rhodeus ocellatus*, development of the notochord, microCT images, virtual sections. A to C, sagittal view, dorsal to the top, rostral left. A, stage 18-somite, 36 hpf. B, stage 28-somite, 48 hpf. C, stage 32-somite, 54 hpf. Abbreviations: no, notochord; nt, neural tube. Vacuolated cells are indicated by arrowheads. Scale bar = 100 μ m.

STAGE 14: 28-somite, 48 hpf (2 dpf).

There are 28 somite pairs. The YSEs are increasingly narrowed at their tips (Figure 8C and Figure 12A). Kupffer's vesicle is no longer visible (Figure 12J). The tailbud is flexed dorsally at its caudal end

(Figure 8C). The median fin fold is now visible as a continuous ridge extending the length of the tail (Figure 8C and Figure 12J). The cephalic flexure of the neural tube is now apparent, dorsal to the hypothalamus (Figure 8B). The neural tube is completely hollow (Figure 12A). Forebrain, midbrain and hindbrain regions are distinct (Figure 12A). The midbrain-hindbrain boundary (mhb or isthmus) is a shallow constriction of the neural tube (Figure 12A). The midbrain and hindbrain ventricles are becoming expanded (Figure 12A). Rhombomeres (neuromeres) 2-6 (r2-6) are visible as shallow indentations of the neural tube (Figure 12A). The olfactory placodes thicken and appear oval in shape; in dorsal view, they are situated between the forebrain and the eyes (Figure 12A and C). The optic vesicle is now cup-shaped (Figure 12A and D). The lens placodes appear and are located within the invaginating optic cups (Figure 12D). The otic vesicle is present at the axial level of r5 and is now a hollow vesicle with a simple, ovoid lumen (Figure 12A and G). Otoliths are not yet visible with microCT. Epibranchial placodes are present ventrolateral to the otic vesicles (Figure 12A and F). The heart is conical with its apex directed dorsally. A medial section through the apex of the cone shows the endocardial organ as a cluster of cells (Figure 12F). There is no detectable cardiac constriction. The stack-of-cells appearance of the notochord is giving way to a vacuolated appearance (Figure 11B). A pair of nephric rudiment appears, one on each side ventral to somite 3 (Figure 12H). The endoderm superficial to the yolk syncytial layer is thin (Figure 12H). This stage is comparable to Kimmel *18-somite* stage.

STAGE 15: 32-somite, 54 hpf (2.25 dpf).

There are 32 somite pairs. The tail tip is flexed ventrally (Figure 8D). The span of the YSEs (the tip-to-tip distance) is c. 50% of the rostrocaudal length of the yolk extension (Figure 13A). The optic rudiment is distinctly cup-shaped (Figure 13A and D). The optic recess (lumen of the optic stalk) is visible at the boundary of telencephalon and diencephalon (Figure 13D). Two pairs of otoliths (the anterior otolith lapillus and the posterior otolith sagitta) are visible in the otic vesicles. Epibranchial placodes and head mesoderm are distinct condensations (Figure 13A and G). The heart is tubular at the axial level of the rhombencephalon (Figure 13F), and exhibits regular peristaltic contraction. At the axial level of somite 3, the nephric primordium has pronephric tubules and pronephric glomeruli (Figure 13). The embryos show irregular spontaneous body movements as the tail thrashes from side-to-side. This stage is comparable to Kimmel stage *21-somite*.

STAGE 16: 35-somite, 60 hpf (2.5 dpf).

The maximum number of 35 somite pairs is present. The tail is straight and blade-like (Figure 8E). A continuous ridge extends around the ventral aspect of the yolk sac connecting the two YSEs (Figure 8E). The ventral edge of the yolk sac bulges caudally and forms the yolk sac ridge (Figure 14B). The caudal aspect of this ridge is becoming hollowed-out (Figure 8E and Figure 14B). As the cephalic flexure increases, ventral bending of the neural axis is more evident (compare Figure 13B and Figure 14B); the hypothalamus and thalamus therefore come to lie ventral to the mesencephalon (Figure 14E). The lens becomes spherical and is partially detached from the surface ectoderm (Figure 14D). The roof of the rhombencephalic ventricle is now thin (Figure 14F and G). The epithelium of the ventral part of the otocyst appears irregular, with cells delaminating as precursors of the statoacoustic ganglion (Figure 14G). The embryos show a touch reflex. This stage is comparable to Kimmel stage *26-somite*.

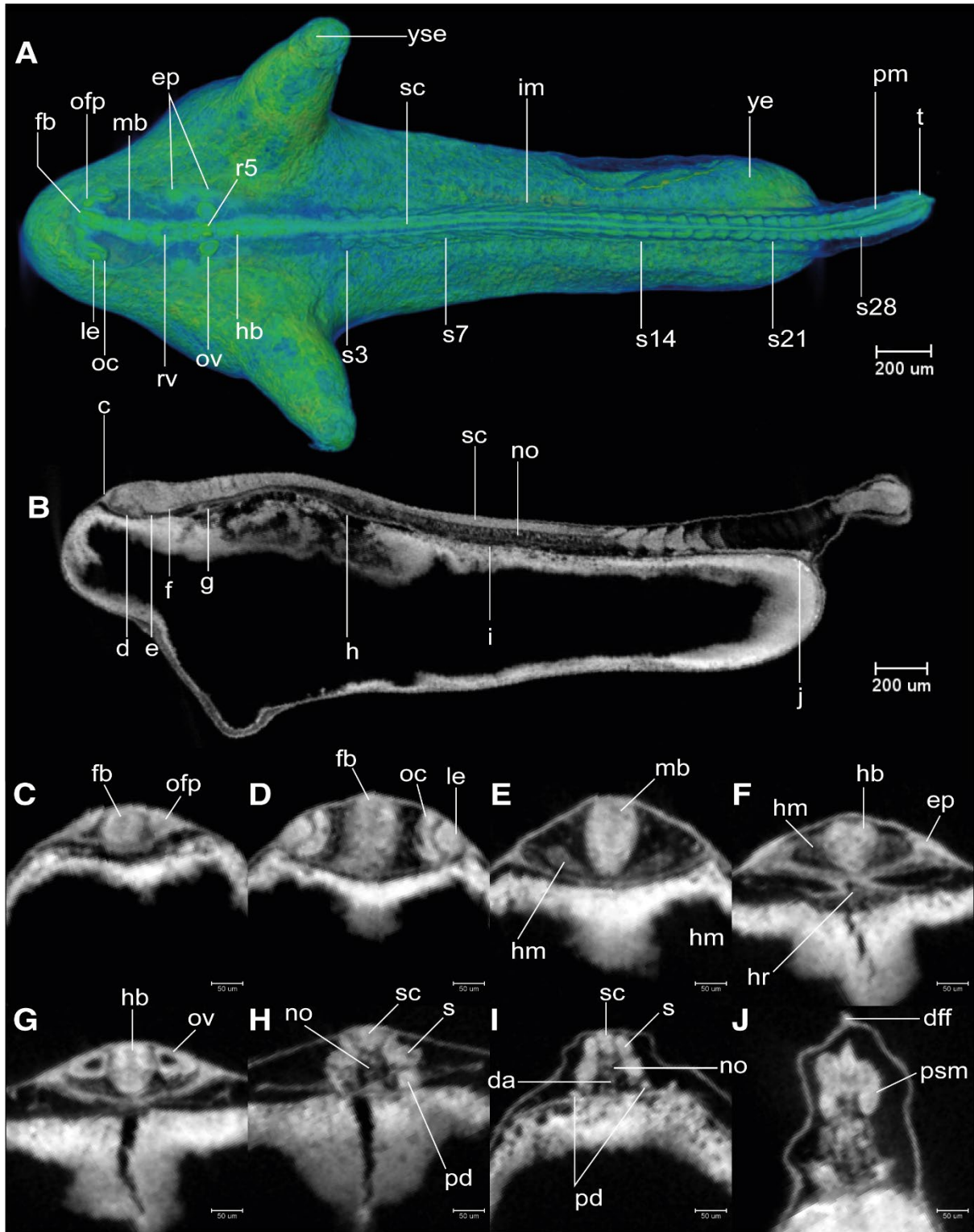


Figure 12 *Rhodnius ocellatus*, stage 28-somite, microCT images. A, volume rendering, dorsal view, rostral to the left. B, virtual section, midsagittal, dorsal to the top, rostral left, letters c to j indicates the section level of the correspondent transverse sections. C to J, virtual sections, transverse, dorsal up. Abbreviations: da, dorsal aorta; dff, dorsal part of median fin fold; ep, ectoderm placode; fb, forebrain; hb, hindbrain; hm, head mesoderm; hr, heart; im, intermediate mesoderm; le, lens; mb, midbrain; no, notochord; nt, neural tube; oc, optic cup; ofp, olfactory placode; ov, otic vesicle; rv, rhombencephalic ventricle; pd, pronephric duct; pm, paraxial mesoderm; psm, presomitic mesoderm; s, somite; sc, spinal cord; t, tail; ye, yolk extension; yse, yolk sac extension.

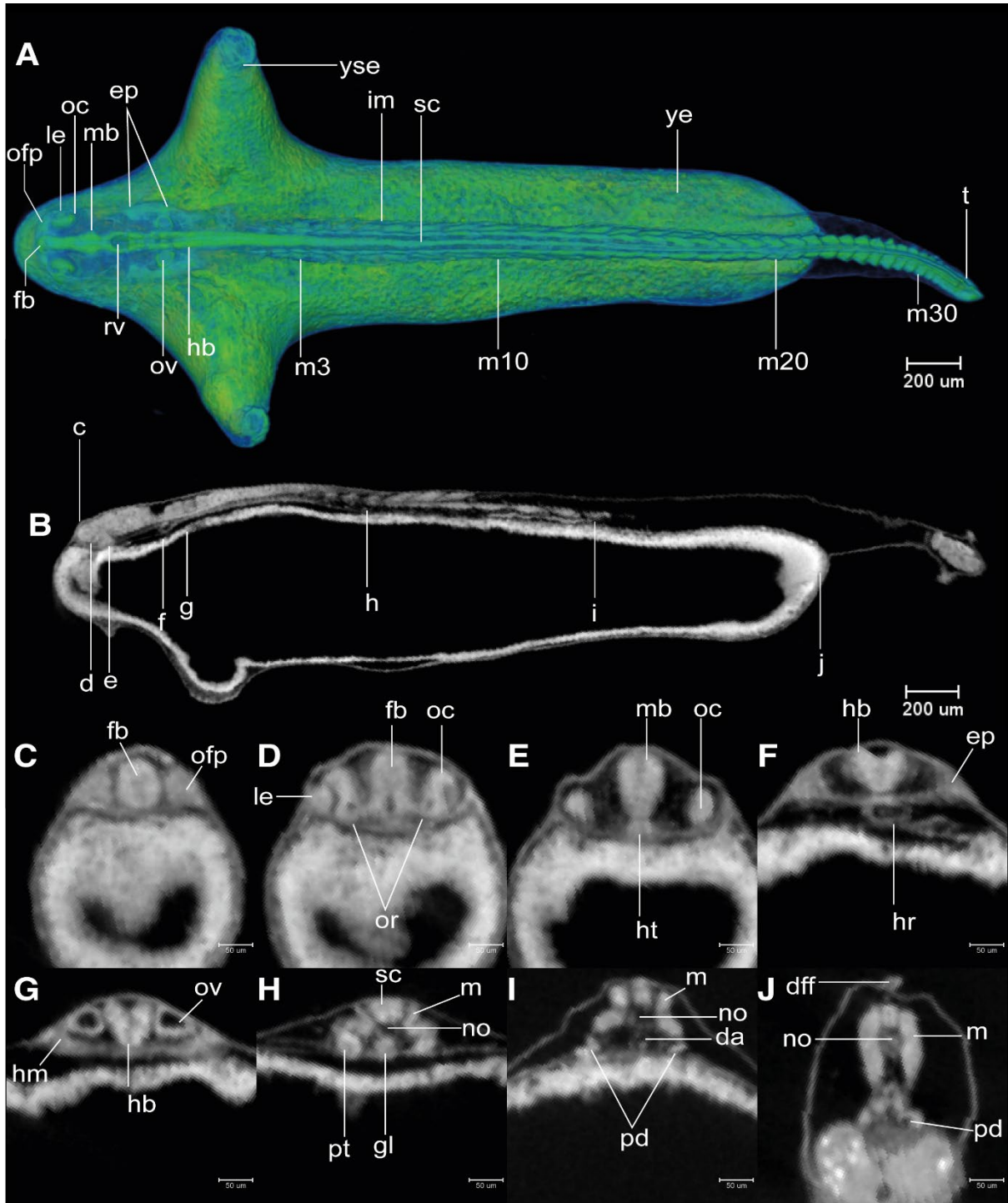


Figure 13 *Rhodeus ocellatus*, stage 32-somite, microCT images. A, volume rendering, dorsal view, rostral to the left. B, virtual section, midsagittal, dorsal to the top, rostral left, letters c to j indicates the section level of the correspondent transverse sections. C to J, virtual sections, transverse, dorsal up. Abbreviations: da, dorsal aorta; dff, dorsal part of median fin fold; ep, ectoderm placodes; fb, forebrain; gl, pronephric glomerulus; hb, hindbrain; hm, head mesoderm; hr, heart; ht, hypothalamus; le, lens; m, myotome; mb, midbrain; no, notochord; nt, neural tube; oc, optic cup; ofp, olfactory placode; or, optic recess; ov, otic vesicle; rv, rhombencephalic ventricle; pd, pronephric duct; pt, pronephric tubule; sc, spinal cord; t, tail; ye, yolk extension; yse, yolk sac extension.

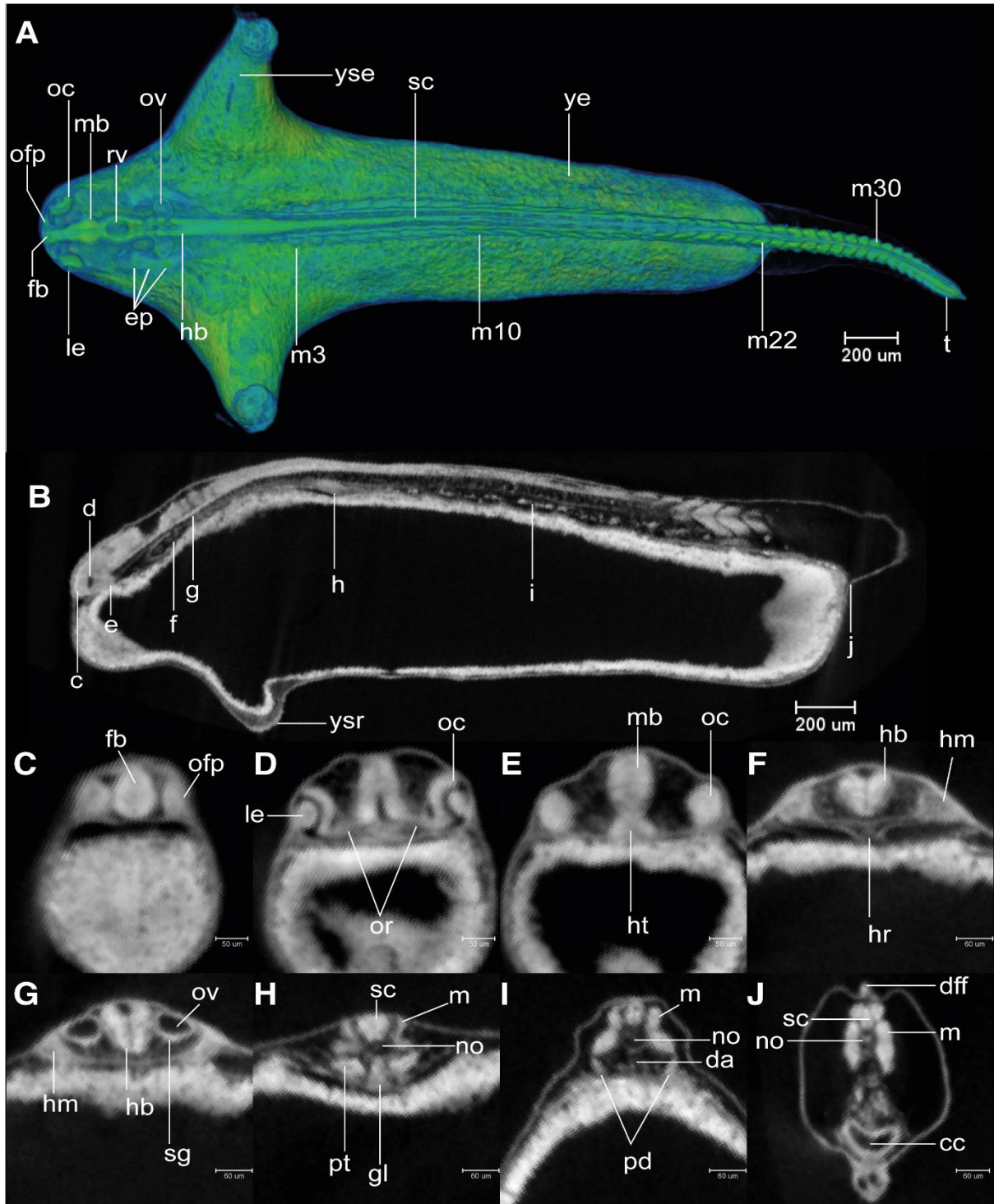


Figure 14 *Rhodius ocellatus*, stage 35-somite, microCT images. A, volume rendering, dorsal view, rostral to the left. B, virtual section, midsagittal, dorsal to the top, rostral left, letters c to j indicates the section level of the correspondent transverse sections. C to J, virtual sections, transverse, dorsal up. Abbreviations: cc, cloaca; da, dorsal aorta; dff, dorsal part of median fin fold; ep, ectoderm placodes; fb, forebrain; gl, pronephric glomerulus; hb, hindbrain; hm, head mesoderm; hr, heart; ht, hypothalamus; le, lens; m, myotome; mb, midbrain; no, notochord; oc, optic cup; ofp, olfactory placode; or, optic recess; ov, otic vesicle; rv, rhombencephalic ventricle; pd, pronephric duct; pt, pronephric tubule; sc, spinal cord; sg, rudiment of statoacoustic ganglion; t, tail; ye, yolk extension; yse, yolk sac extension; ysr, yolk sac ridge.

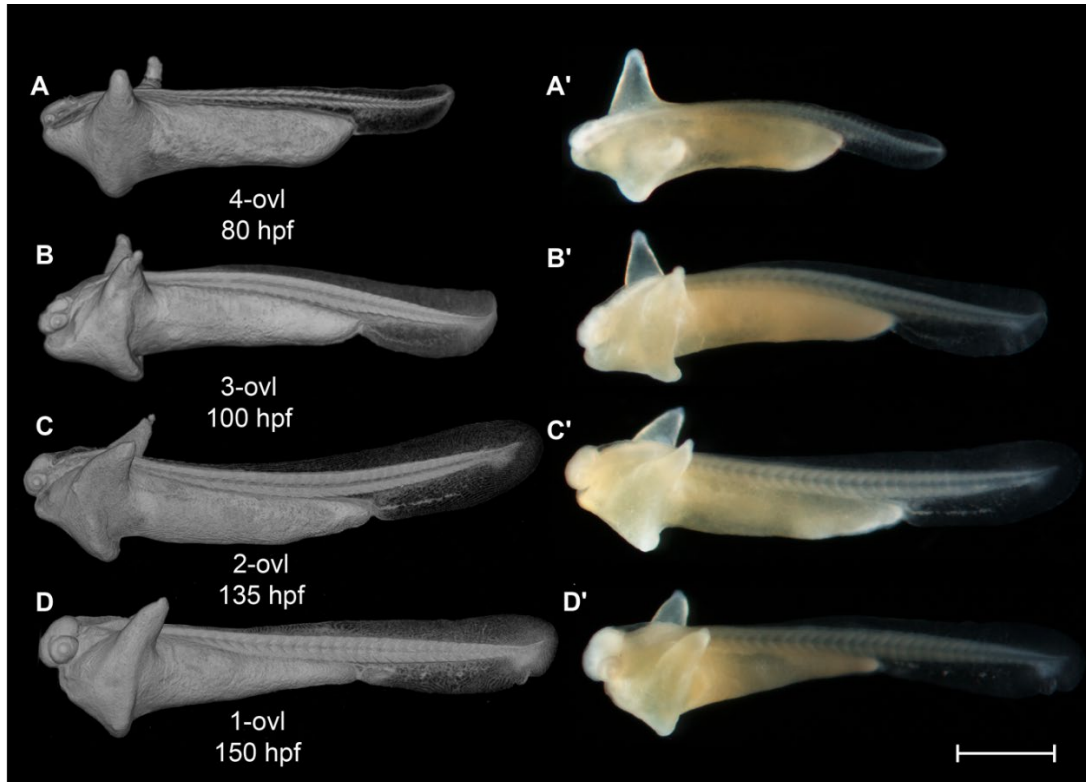


Figure 15 *Rhodeus ocellatus*, stages during the pharyngula period. A to D, microCT images, volume rendering. A' to D', photomicrographs of the same embryo. A and A', stage 4-ovl, 80 hpf. B and B', stage 3-ovl, 100 hpf. C and C', stage 2-ovl, 135 hpf. D and D', stage 1-ovl, 150 hpf. Lateral view, dorsal up, head to the left. The photomicrographs are slightly rotated to the left along the primary axis in order to show both yolk sac extensions. Abbreviations: hpf, hours post-fertilization; ovl, otic vesicle length. Scale bar = 1 mm.

Pharyngula period: in naming this period the 'pharyngula' period, we are following the lead of the Kimmel stages (Kimmel et al., 1995). The term 'pharyngula' was introduced by Ballard (1981) to describe a conserved phase of vertebrate development in which the pharyngeal arches are externally visible (Figure 16). During the pharyngula period, we have named each stage using otic vesicle length (ovl), defined by Kimmel as corresponding to the number of otic vesicle diameters between the optic cup and the otic vesicle itself. Because of the continuous growth of the optic cup and otic vesicles during head-straightening, the value of ovl decreases progressively (Figure 16). For this reason, we defined four stages as follows: 4-ovl, 3-ovl, 2-ovl and 1-ovl.

STAGE 17: 4-ovl, 80 hpf (3.3 dpf).

All somites or myotomes are chevron-shaped (Figure 15A). The caudal vein plexus appears in the anterior-ventral region of the tail, just posterior to the caudal yolk extension (Figure 17A). The cloacal primordium is a funnel-shaped structure near the base of the ventral yolk extension (Figure 15A). Rhombomere 7 now distinct (Figure 16A). The trigeminal (V) ganglia are visible at the axial level of r2, and appear to be connected with the first (mandibular) pharyngeal arch. The pharyngeal arches are visible as three discrete cell condensations at this stage. The first is the mandibular arch, the second is the hyoid arch, and the third is the combined pharyngeal arches 1-5 (Figure 16A). The lens is completely detached from the overlying epidermis (Figure 18D). The tubular heart comprises an inner layer, the endocardial layer; and an outer layer, the trabecular myocardial layer (Figure 18I). The heart tube migrates leftward and begins to loop dextrally (Figure 18P). In the Petri dish, the embryo can swim away a short distance if stimulated by a jet of water from a pipette (is this the same as the

touch reflex you described in the previous stage?). This stage is comparable to a stage intermediate between Kimmel stages *26-somite* and *prim-6*.

STAGE 18: 3-ovl, 100 hpf (4.2 dpf).

The tips of the wing-like YSEs are directed caudally, and covered by skin tubercles (Figure 15B). The caudal yolk extension is markedly tapered at its caudal end (Figure 15B). The median fin fold in the tail becomes taller than the caudal yolk extension (Figure 15B). At the ventral base of the caudal fin fold, the prospective caudal fin rays are appearing (Figure 17B). The dorsally-situated part of the median fin extends rostrally, its rostral margin approaching the axial level of myotomes 6-8 (Figure 19P).

In the bitterling, the telencephalic ventricle undergoes eversion, as it does in other ray-finned fishes including the zebrafish (Mueller and Wullimann, 2009; Wullimann and Puelles, 1999). This is in contrast to the evagination of the ventricle seen in amniotes (Folgueira et al., 2012). Therefore, instead of two lateral ventricles uniting in the midline, the bitterling has a large, fan-shaped telencephalic ventricle everted dorsoventrally (Figure 16B and Figure 19A). The mhb is much deeper than in previous stages (compare Figure 16A and B). The olfactory placodes are oval, with their long axes parallel to the rostrocaudal axis (Figure 16B). The optic tectum expands to the lateral side, overlying the optic cups (Figure 16B).

A pair of common cardinal veins (ducts of Cuvier) are present, and contain blood flowing from the yolk sac to the pole of the heart (sinus venosus). The heart has a regular heart beat and blood circulation. A solid endodermal rod, the primordium of the gut, is appearing (Figure 19N). The posterior lateral line primordia extend to the level of myotomes 5-6. This stage corresponds to Kimmel stage *prim-5*.

STAGE 19: 2-ovl, 135 hpf (5 dpf).

The pericardial cavity bulges prominently from the surface of the yolk sac (Figure 20A). In live specimens, the common cardinal veins are red and contain flowing blood (Figure 15C'). Gill rudiments appear as shallow furrows rostral to the otic vesicle (Figure 15C). The cerebellum is clearly distinguishable at the axial level of r1 (Figure 16C and Figure 20G).

In sagittal microCT virtual sections, the epiphysis appears as a swelling in the midline of the diencephalic roof plate (Figure 20R). The hypophysis is a small, well-defined swelling descending in the ventral midline from the floor of the diencephalon (Figure 20F and R). Otic epithelium cells are condensing to form the sensory maculae (Figure 20K).

The outflow tract of the heart tube migrates to the axial level of the rostral margin of the optic cup (Figure 20A to H). The ventral aorta and the first pair of aortic arch arteries are recognizable in transverse sections (Figure 20H). The pectoral fin buds appear as cell patches at the level of myotome 3, at the base of the YSEs. These buds are indistinct in surface view but distinct in sections as condensed protrusions of the lateral plate mesoderm (Figure 20O). A lumen appears in the gut (Figure 20O). The migrating margin of the posterior lateral line primordia approaches myotome 10. This stage corresponds to Kimmel stage *prim-10*.

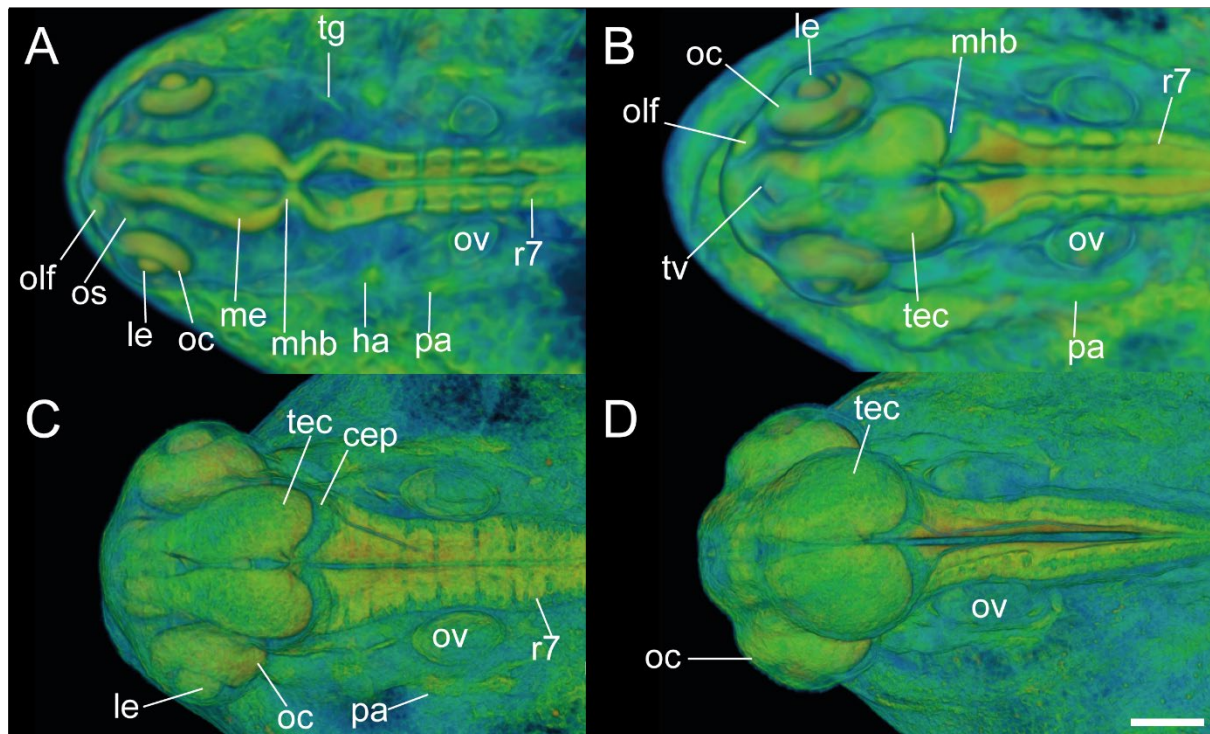


Figure 16 *Rhodeus ocellatus*, embryos during the pharyngula period, microCT images, pseudo-coloured volume-renderings. Dorsal view, rostral to the left. A, 4-ovl, 80 hpf; B, 3-ovl, 100 hpf; C, 2-ovl, 135 hpf; D, 1-ovl, 150 hpf. Abbreviations: cep, cerebellar plate; ha, hyoid arch; le, lens; me, mesencephalon; mhb, midbrain-hindbrain boundary; oc, optic cup; olf, olfactory placode; os, optic stalk; ov, otic vesicle; ovl, otic vesicle length; pa, pharyngeal arch; r, rhombomere; tec, optic tectum; tg, trigeminal ganglion. Scale-bars, 100 μ m in A, 110 μ m in B and C, 130 μ m in D.

STAGE 20: 1-ovl, 150 hpf (6.25 dpf).

This stage represents the maximal extent of the YSEs before they regress at later stages (Figure 15D). The tail is now half as long as the body (Figure 15D). Blood vessels appear in the dorsal part of the tail (Figure 15D). At the ventral base of the tail, the primordia of the caudal fin rays are in a fan-shaped array (Figure 15D). Sporadic melanocytes with faint pigment are appearing in the retina (Figure 15D').

The olfactory placode is semicircular (Figure 21A). In the otic vesicle, there are epithelial projections into the lumen from each wall forming the pillars of the semicircular canals (Figure 21K). The pars inferior of the developing inner ear (primordium of the lagena and saccule) is forming as a ridge on the ventromedial part of the otic vesicle (Figure 21M). The caudal end of the hypothalamus extends dorsally, towards the ventral surface of the medulla oblongata (Figure 21R). This displacement represents the maximum extent of the cephalic flexure. The pectoral fin bud is a shallow dome (Figure 21O). The caudal margin of the migrating posterior lateral line primordia approach myotome 24. This stage corresponds to Kimmel stage *prim-25*.

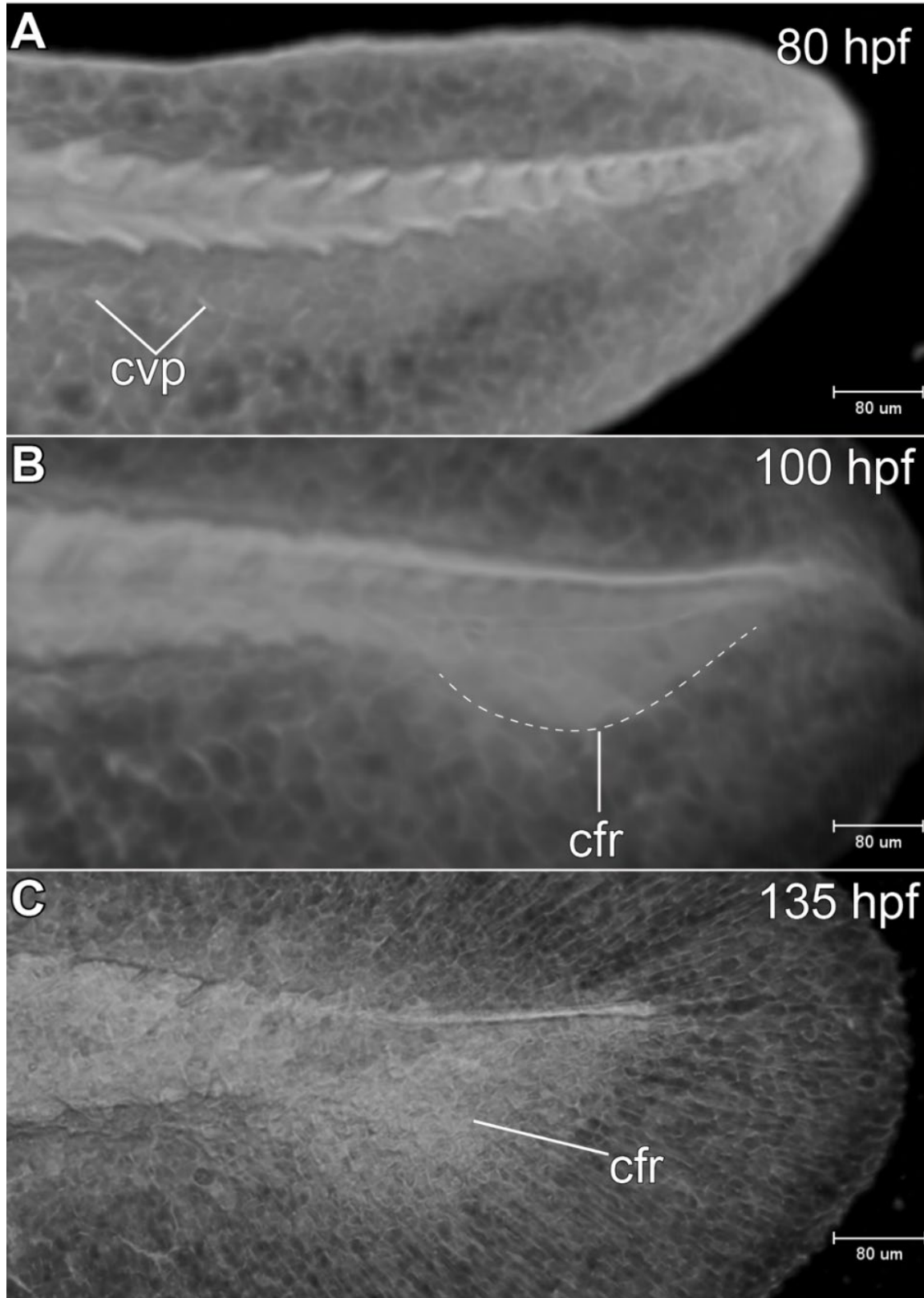


Figure 17 *Rhodeus ocellatus*, tail development, microCT images, virtual sections. A to C, lateral view, dorsal to the top, rostral left. A, 4-ovl, 80 hpf; B, 3-ovl, 100 hpf; C, 2-ovl, 135 hpf. Dashed line in B indicates the margin of the primordia of caudal fin rays. Abbreviations: cfr, primordia of caudal fin rays; cvp, caudal vein plexus.

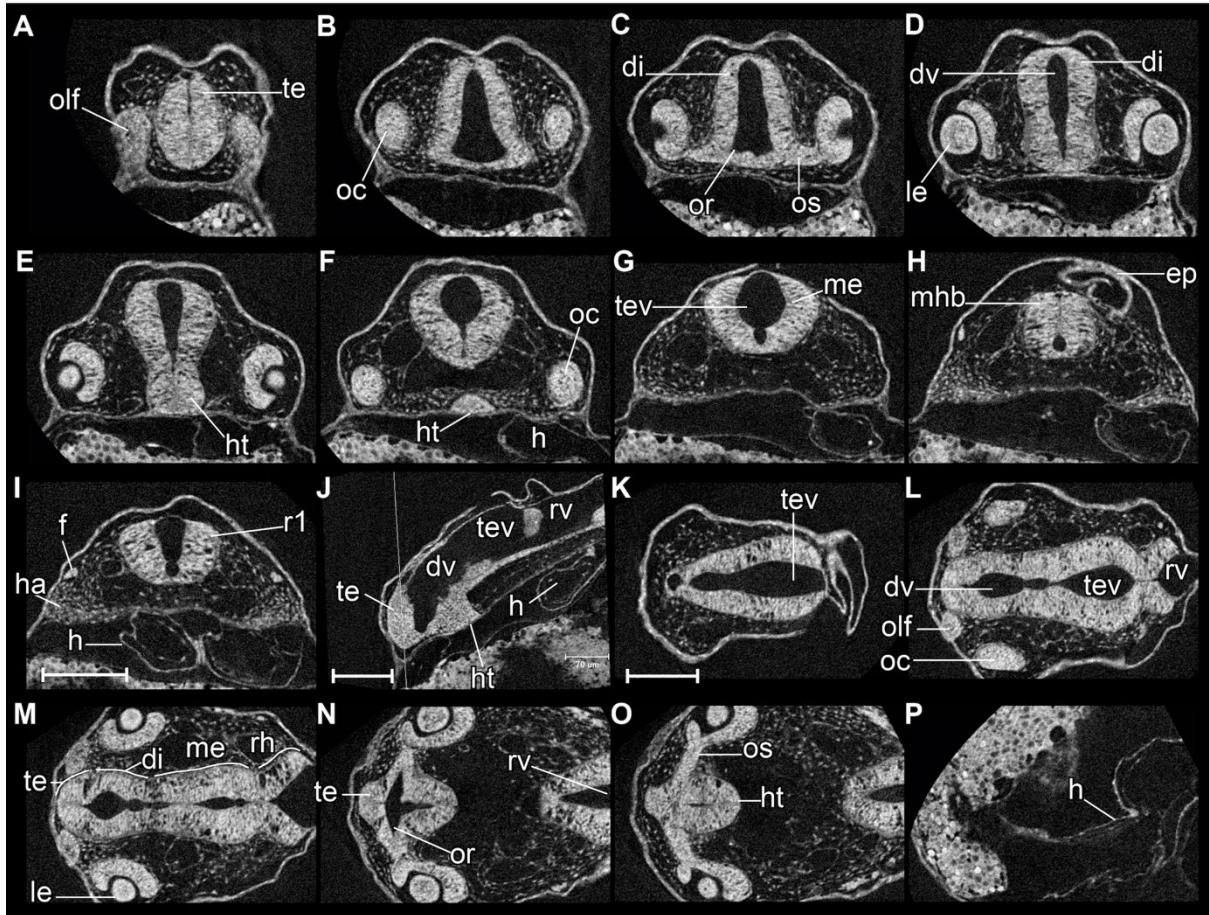


Figure 18 *Rhodius ocellatus*, stages 4-ovl, microCT images, virtual sections. A-I, transverse section views, dorsal towards the top, section plane indicated in J. J, mid-sagittal section view, rostral to the left, dorsal towards the top. K-P, coronal section views, from dorsal to ventral, rostral to the left. Abbreviations: di, diencephalon; dv, diencephalic ventricle; ep, epidermis; f, facial ganglion; h, heart; ha, hyoid arch cartilage; ht, hypothalamus; le, lens; me, mesencephalon; mhb, midbrain-hindbrain boundary; oc, optic cup; olf, olfactory placode; or, optic recess; os, optic stalk; r1 to 7, rhombomeres 1 to 7; rh, rhombencephalon; rv, rhombencephalic ventricle; te, telencephalon; tev, tectal ventricle; tv, telencephalic ventricle. Scale bars, 100 μm .

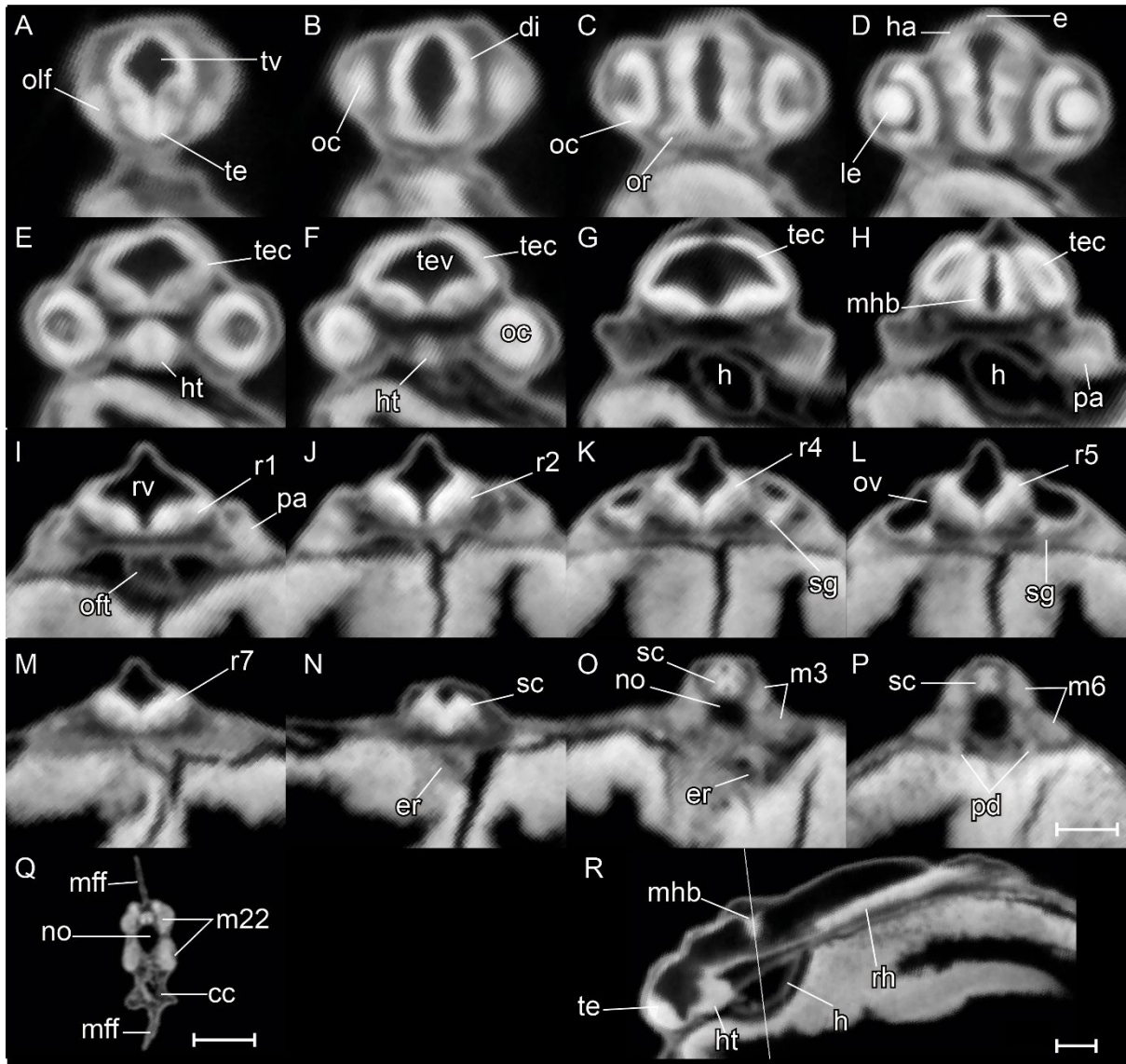


Figure 19 *Rhodeus ocellatus*, stage 3-ovl, microCT images, virtual sections. A-Q, transverse section views, dorsal towards the top, sections from rostral to caudal, direction of section plane indicated by the line in R. R, mid-sagittal section view, rostral to the left, dorsal towards the top. Abbreviations: cc, cloaca; di, diencephalon; e, epiphysis; er, endodermal rod; h, heart; ha, habenula; ht, hypothalamus; le, lens; m, myotome; mff, median fin fold; mhb, midbrain-hindbrain boundary; no, notochord; oc, optic cup; oft, outflow tract; olf, olfactory placode; or, optic recess; ov, otic vesicle; pa, pharyngeal arch; pd, pronephric duct; r1 to 7, rhombomeres 1 to 7; rh, rhombencephalon; rv, rhombencephalic ventricle; sc, spinal cord; sg, statoacoustic ganglion; te, telencephalon; tec, optic tectum; tev, tectal ventricle; tv, telencephalic ventricle. Scale bars, 100 μ m.

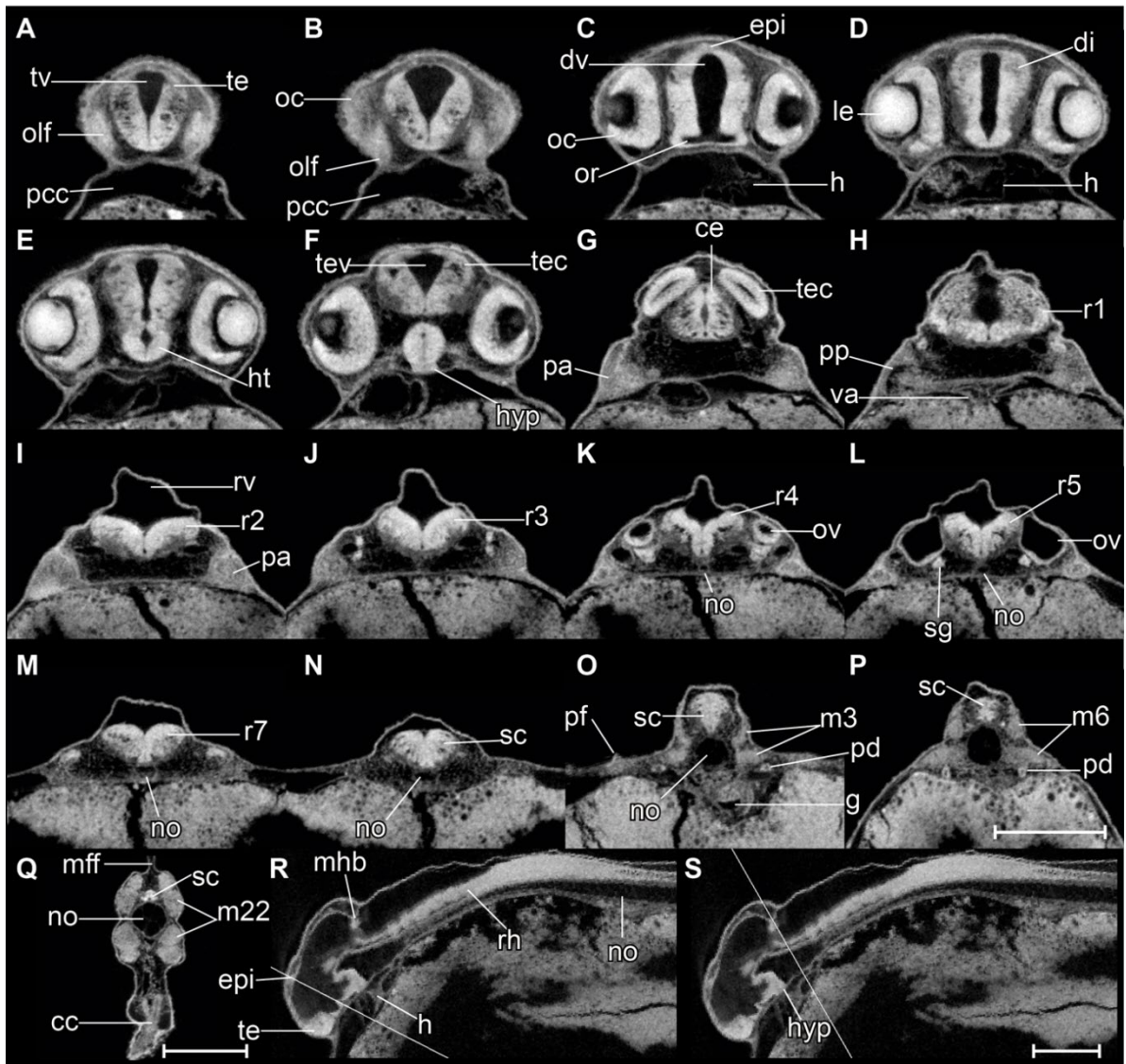


Figure 20 *Rhodeus ocellatus*, stage 2-ovl, microCT images, virtual sections. A-Q, transverse section views, dorsal towards the top, sections from rostral to caudal, direction of section plane from A-F indicated in R; section plane in G-Q indicated in S; R to S, mid-sagittal section views, rostral to the left, dorsal towards the top. Abbreviations: cc, cloaca; ce, cerebellum; di, diencephalon; dv, diencephalic ventricle; epi, epiphysis; g, gut; h, heart; ht, hypothalamus; hyp, hypophysis; le, lens; lv, lateral ventricle; m, myotome; mff, median fin fold; mhb, midbrain-hindbrain boundary; no, notochord; oc, optic cup; olf, olfactory placode; or, optic recess; ov, otic vesicle; pa, pharyngeal arch; pcc, pericardial cavity; pd, pronephric duct; pf, pectoral fin bud; pp, pharyngeal pouch; r1 to 7, rhombomere 1 to 7; rh, rhombencephalon; rv, rhombencephalic ventricle; sc, spinal cord; sg, statoacoustic ganglion; te, telencephalon; tec, optic tectum; tev, tectal ventricle; va, ventral aorta. Scale bars, 200 μm .

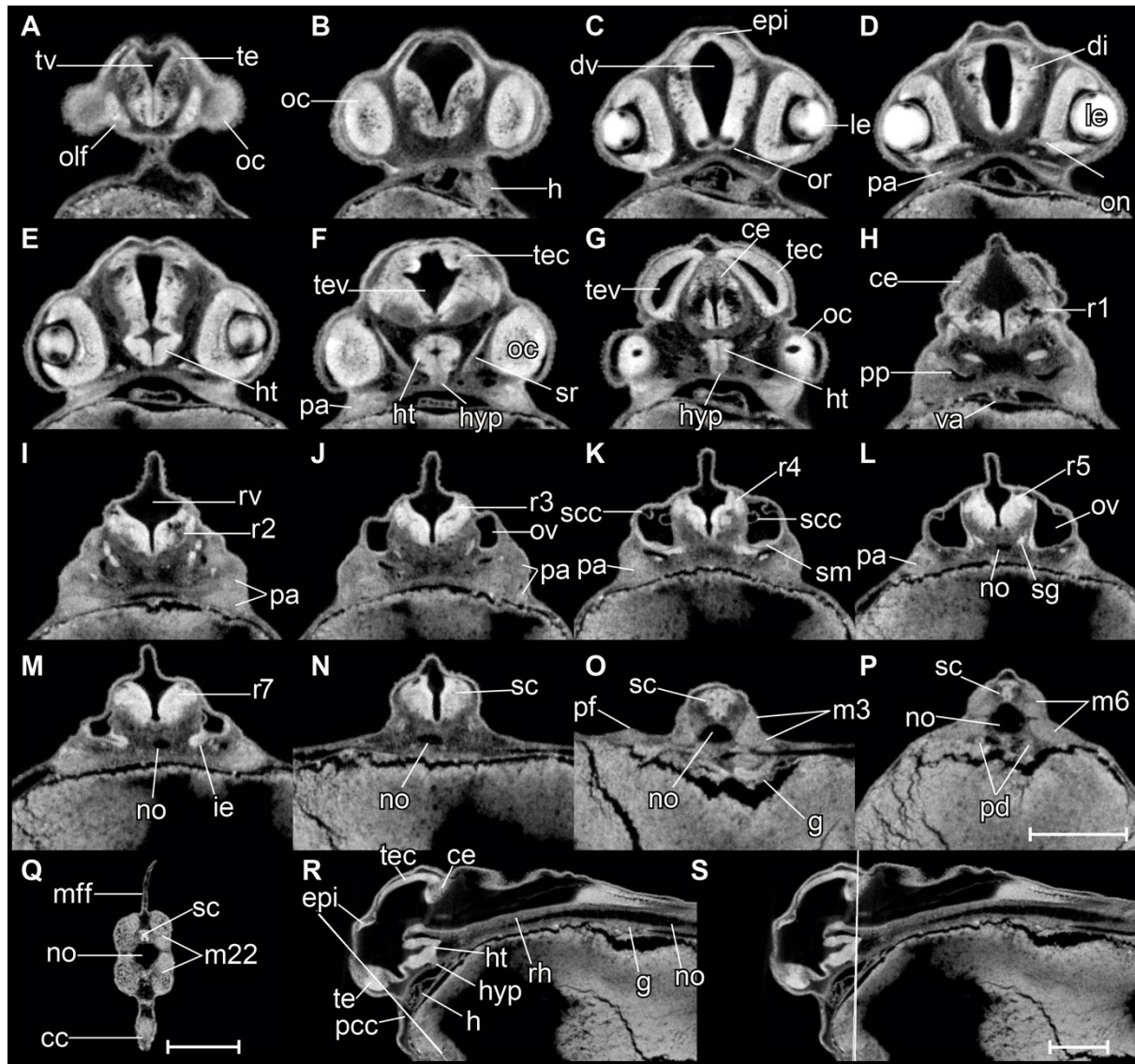


Figure 21 *Rhodius ocellatus*, stage 1-ovl, microCT images, virtual sections. A to Q is transverse section view, dorsal towards the top, sections go from rostral to caudal, direction of section plane from A to F indicated in R, section plane from G to Q indicated in S; R and S are mid-sagittal section view, rostral to the left, dorsal towards the top. Abbreviations: cc, cloaca; ce, cerebellum; di, diencephalon; dv, diencephalic ventricle; epi, epiphysis; g, gut; h, heart; ht, hypothalamus; hyp, hypophysis; ie, pars inferior of inner ear; le, lens; no, notochord; oc, optic cup; olf, olfactory placode; or, optic recess; ov, otic vesicle; pa, pharyngeal arch; pcc, pericardial cavity; pf, pectoral fin bud; pp, pharyngeal pouch; r1 to 7, rhombomere 1 to 7; rh, rhombencephalon; rv, rhombencephalic ventricle; sc, spinal cord; scc, semicircular canal; sg, statoacoustic ganglion; sm, sensory maculae; te, telencephalon; tec, optic tectum; tev, tectal ventricle; tv, telencephalic ventricle; va, ventral aorta; pd, pronephric duct; m, myotome; mff, median fin fold. Scale bars, 200 μ m.

Organogenetic period: throughout the development of the previous (pharyngula) period, many features of body plan of the embryo were established. In the organogenetic period, regional development of organs is marked. We therefore define this as the ‘organogenetic’ period. The key staging character for each stage is the morphology of the pectoral fin bud (Figure 22 and Figure 23), and we have made this consistent with the Kimmel zebrafish stages to facilitate comparison.

During the organogenetic period, we observe lamination of the retina (Figure 28), formation of the extraocular muscles (Figure 29), differentiation of the pharyngeal cartilages (Meckel’s cartilage, palatoquadrate, ceratohyal, hyosymplectic, and ceratobranchials, see Supplemental Figure 1),

morphogenesis of the semicircular canals, and formation of the inferior part of the inner ear (Figure 30). The gut was a solid endodermal rod in the pharyngula period, but in the organogenetic period it develops into an alimentary canal with liver, gall bladder and pancreatic primordia (Figure 31). The swim bladder also develops (Figure 31). At the end of this period, as the bitterling approaches the end of its parasitic life, it has a gaping mouth (Figure 32), a mobile lower jaw, gill filaments on the gill arches, and pointed pharyngeal teeth. The yolk mass is depleted and the wing-like YSEs regress completely (Figure 22).

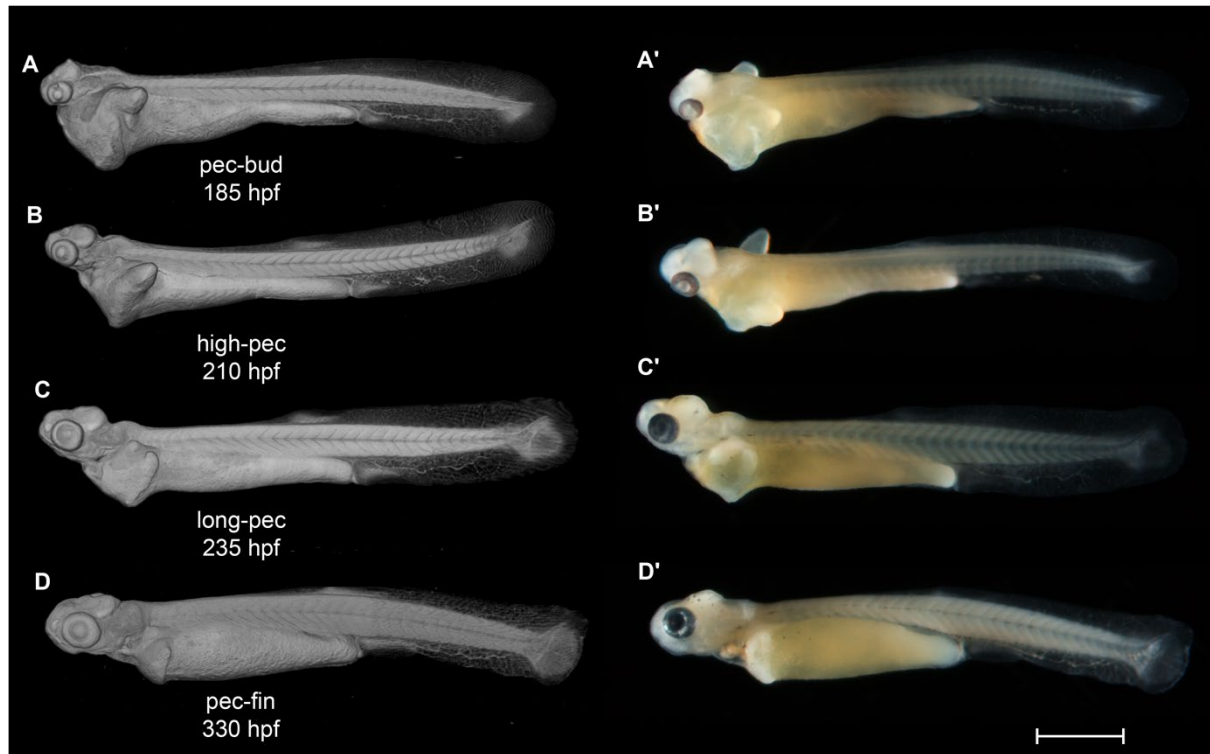


Figure 22 *Rhodeus ocellatus*, stages during the organogenetic period. A to D, microCT images, volume rendering. A' to D', photomicrographs of the same embryo. A and A', stage pec-bud, 185 hpf. B and B', stage high-pec, 210 hpf. C and C', stage long-pec, 235 hpf. D and D', stage pec-fin, 330 hpf. Lateral view, dorsal up, head to the left. Scale bar = 1 mm

STAGE 21: pec-bud, 185 hpf (7.7 dpf).

In dorsal view, the pectoral fin bud is dome-shaped (Figure 23A); its height is equal to its dorsoventral width (Figure 23A and Figure 24N). The apical ectodermal ridge is discernible (Figure 24N). Based on the morphology of the pectoral fin bud, we name this stage 'pec-bud'. The YSEs taper ventro-dorsally. They still extend dorsally but not beyond the level of the dorsal margin of the eye (Figure 22A). Two cell condensations are recognizable in the median fin fold; these are the primordia of the dorsal and anal fins (Figure 22A). On the yolk sac, the bilateral common cardinal vein is fan-shaped, and in live specimens contains vigorously flowing blood. Retinal pigment is now distinct (compare Figure 22A' and Figure 15D').

The olfactory bulb is forming (Figure 24A). What we presume to be the inner plexiform layer of the retina is distinct (Figure 24C and D). There is no mouth opening; the mouth is indicated by a shallow groove (Figure 24S). The protrusions forming anterior and posterior semicircular canals are fused; the common crus and lateral semicircular canal are developing (Figure 24J to L). The liver is visible (Figure 24N). This stage is intermediate between Kimmel *prim-25* and *high-pec* stages.

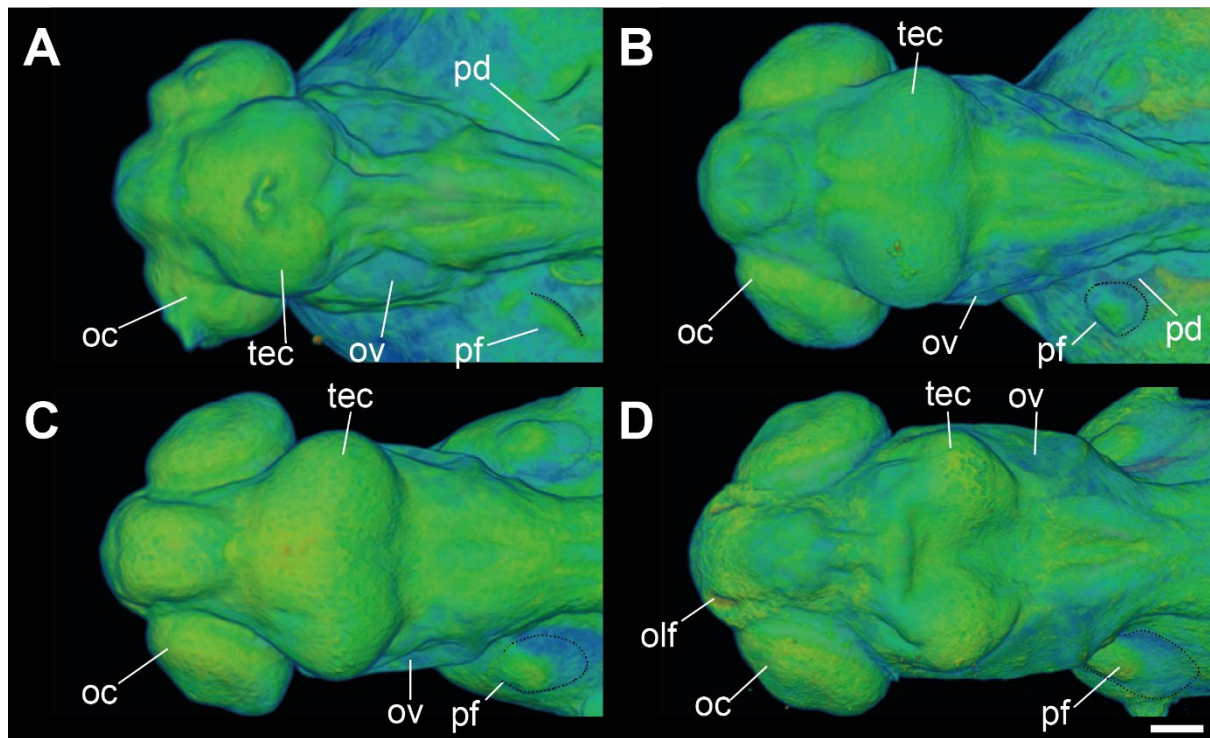


Figure 23 *Rhodeus ocellatus*, embryos during the organogenetic period, microCT images, pseudo-coloured volume-renderings. Dorsal view, rostral to the left. Margins of left pectoral fin bud/fold are illustrated with a dotted line. A, pec-bud, 185 hpf; B, high-pec, 210 hpf; C, long-pec 235 hpf; D, pec-fin, 330 hpf. Abbreviations: le, lens; oc, optic cup; olf, olfactory pit; ov, otic vesicle; pd, pronephric duct; pf, pectoral fin bud/fold; tec, optic tectum. Scale-bars, 100 μ m in A and B, 120 μ m in C and D.

STAGE 22: high-pec, 210 hpf (8.75 dpf)

The pectoral fin bud shows mesenchymal condensations at the central of the fin bud (Figure 25N); its height exceeds its width (Figure 23B). Dense retinal pigmentation, except in the region around the lens, giving the appearance, in light microscopy of whole embryos, of a black ring encircling the limpid lens (Figure 22B'). The pericardial cavity now lies rostral to the yolk mass and so the heart is visible in lateral view (Figure 22B and Figure 25S). Olfactory pit a shallow groove (Figure 22B and Figure 25A). The mouth a small opening, not yet gaping (Figure 25C, D and S, Figure 32A). No gill filaments are present on the branchial arches (Figure 25G and Figure 32A). Rudiments of pharyngeal teeth are appearing on the 5th branchial arch (Figure 25H). Branchial clefts not yet open (compare Figure 25H and Figure 26H). Cells in the liver have the histological features of hepatocytes (Figure 25N). A common chamber of the sacculus and lagena appears (Figure 30B). This stage corresponds to Kimmel *high-pec* stage, on the basis of the morphology of the pectoral fin bud.

STAGE 23: long-pec, 235 hpf (9.8 dpf).

The apical ectodermal ridge of the pectoral fin develops into the fin fold (Figure 23C and Figure 26O). Chondrocytes are differentiating in the pectoral girdle (Figure 26O). The YSEs shrink to vestigial bumps (Figure 22C and Figure 26Q). Melanophores are differentiating in a rostral to caudal gradient in the skin, and are most prominent on the dorsal surface of the head (Figure 22C'). The entire retinal pigment layer is pigmented (Figure 22C').

The olfactory epithelium of the bowl-shaped olfactory pit is connected to the olfactory bulb by a distinct olfactory nerve (Figure 26A). The anterior portion of the trabeculae cranii expand and fuse with

the ethmoid plate to form the trabecula communis (Figure 26A to C). The upper oral valve appears on the pharyngeal aspect of the upper jaw (Figure 26S). The jaw becomes extended rostrally, and the mouth opening therefore becomes located at the axial level of the rostral margin of the optic cup (Figure 32B and B'). The annular ligament appears in the angle between the cornea and the iris (Figure 26D and Figure 28C). The opercular cavity expands and opens into the buccal cavity (Figure 26H). Buds of developing gill filaments are present on all gill arches (Figure 26J and K). The sacculle and lagenae are now distinct as separate structures (Figure 30C). A hollow gallbladder appears ventral to the intestine (Figure 26Q). This stage corresponds to Kimmel *long-pec* stage on the basis of fin morphology.

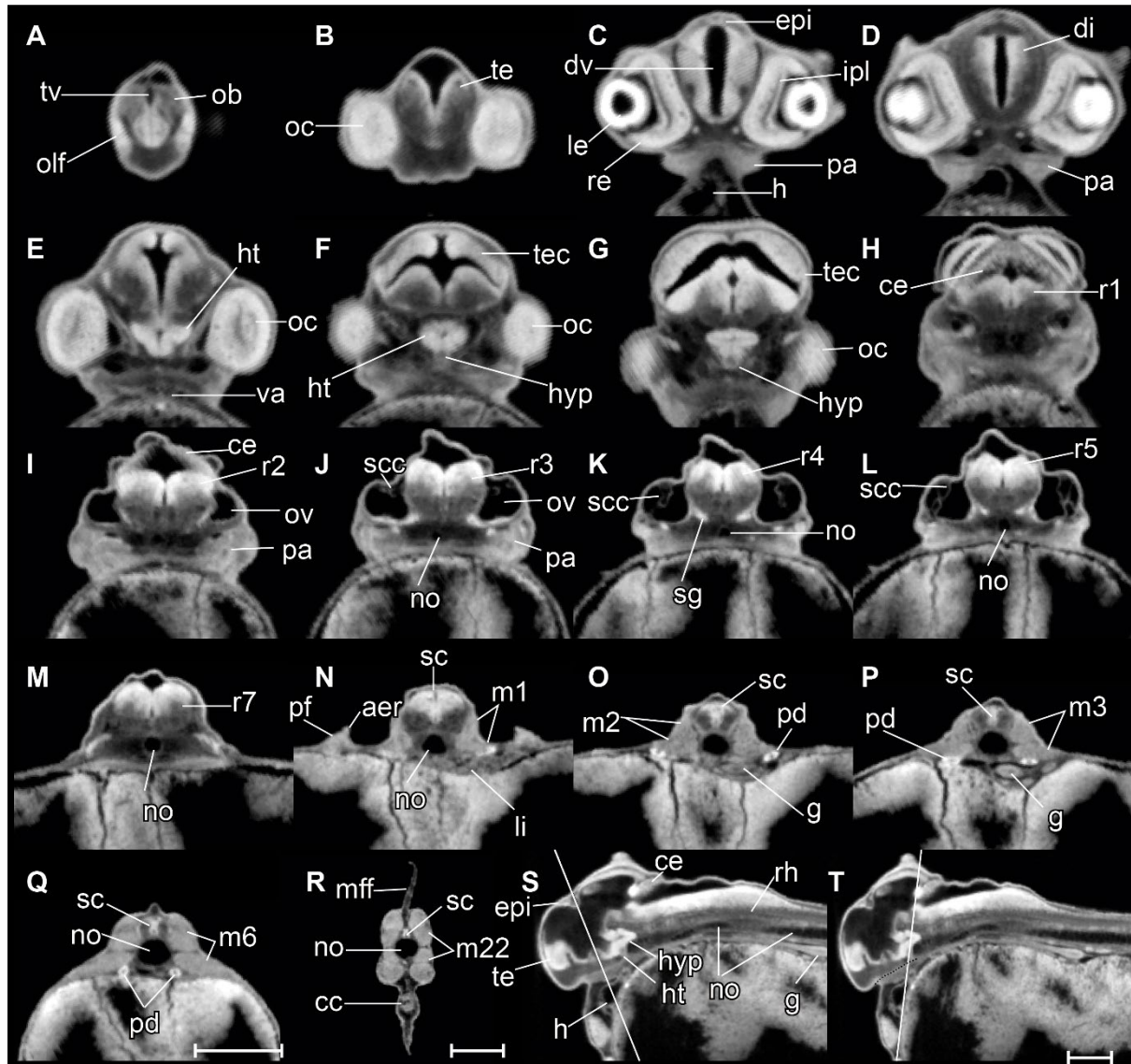


Figure 24 *Rhodeus ocellatus*, stage pec-bud, microCT images, virtual sections. A to R is transverse section view, dorsal towards the top, sections go from rostral to caudal, direction of section plane from A to F indicated in S, section plane from G to R indicated in T; S and T are mid-sagittal section view, rostral to the left, dorsal towards the top. Abbreviations: aer, apical ectodermal ridge; cc, cloaca; ce, cerebellum; di, diencephalon; epi, epiphysis; g, gut; h, heart; ht, hypothalamus; hyp, hypophysis; ipl, inner plexiform layer; li, liver; m, myotome; mff, median fin fold; no, notochord; ob, olfactory bulb; oc, optic cup; le, lens; olf, olfactory epithelium; ov, otic vesicle; pa, pharyngeal arch; pd, pronephric duct; pf, pectoral fin bud; r1 to 7, rhombomere 1 to 7; re, retina; rh, rhombencephalon; sc, spinal cord; scc, semicircular canal; sg, statoacoustic ganglion; te, telencephalon; tec, optic tectum; tv, telencephalic ventricle. Scale-bars equal to 200 μ m.

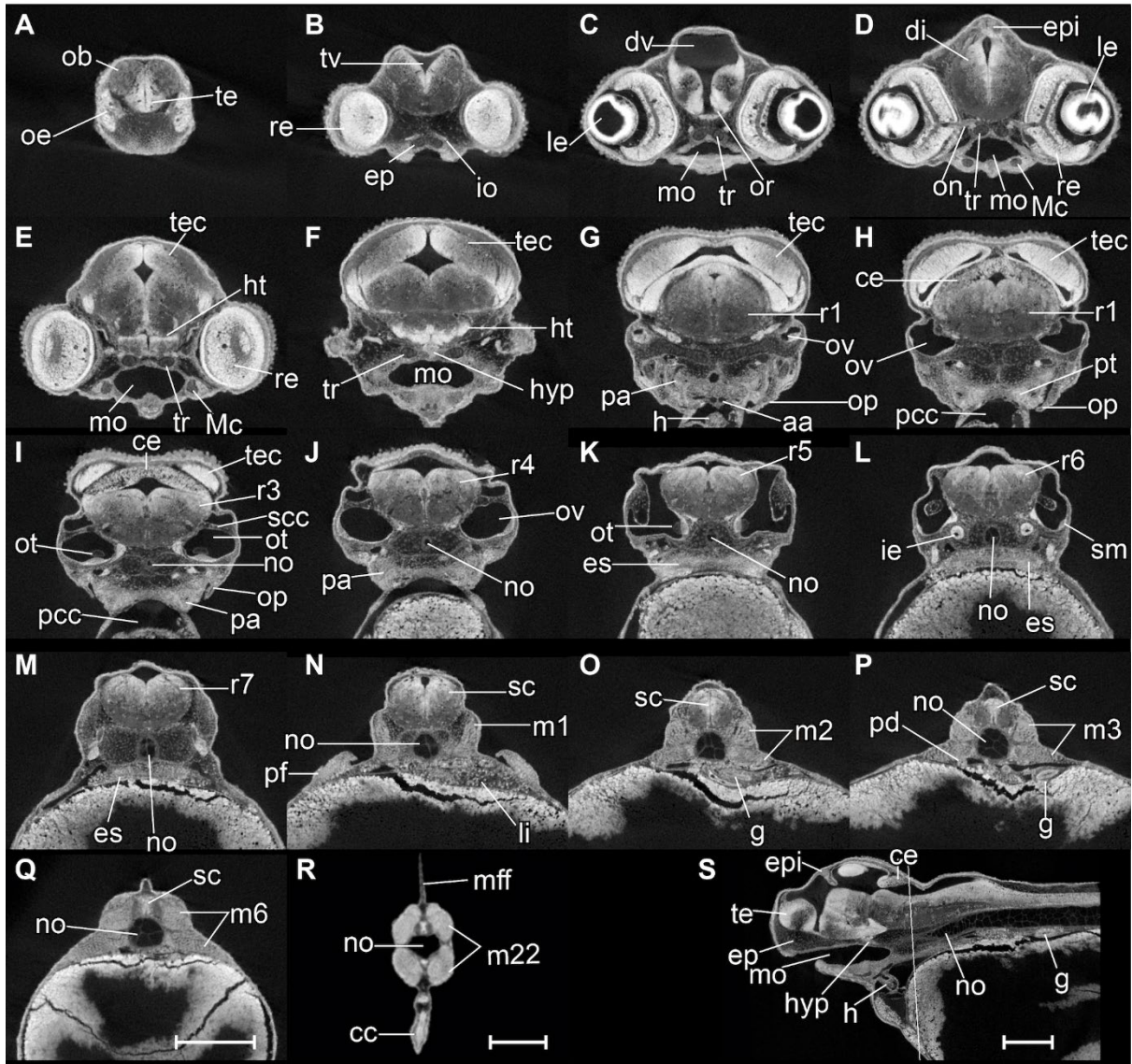


Figure 25 *Rhodeus ocellatus*, stage high-pec, microCT images, virtual sections. A-R, transverse section views, dorsal towards the top, sections from rostral to caudal, direction of section plane indicated in S. S, mid-sagittal section view, rostral to the left, dorsal towards the top. Abbreviations: aa, arch artery; cc, cloaca; ce, cerebellum; di, diencephalon; ep, ethmoid plate; epi, epiphysis; es, esophagus; g, gut; h, heart; ht, hypothalamus; hyp, hypophysis; ie, pars inferior of inner ear; io, inferior oblique muscle; le, lens; li, liver; m, myotome; Mc, Meckel's cartilage; mff, median fin fold; mo, mouth; no, notochord; ob, olfactory bulb; oe, olfactory epithelium; on, optic nerve; op, operculum; or, optic recess; ot, otolith; ov, otic vesicle; pa, pharyngeal arch; pcc, pericardial cavity; pd, pronephric duct; pf, pectoral fin bud; pt, pharyngeal teeth; r1 to 7, rhombomere 1 to 7; re, retina; rh, rhombencephalon; sc, spinal cord; scc, semicircular canal; sg, statoacoustic ganglion; sm, sensory maculae; te, telencephalon; tec, optic tectum; tr, trabeculae cranii; tv, telencephalic ventricle. Scale bars, 200 μ m.

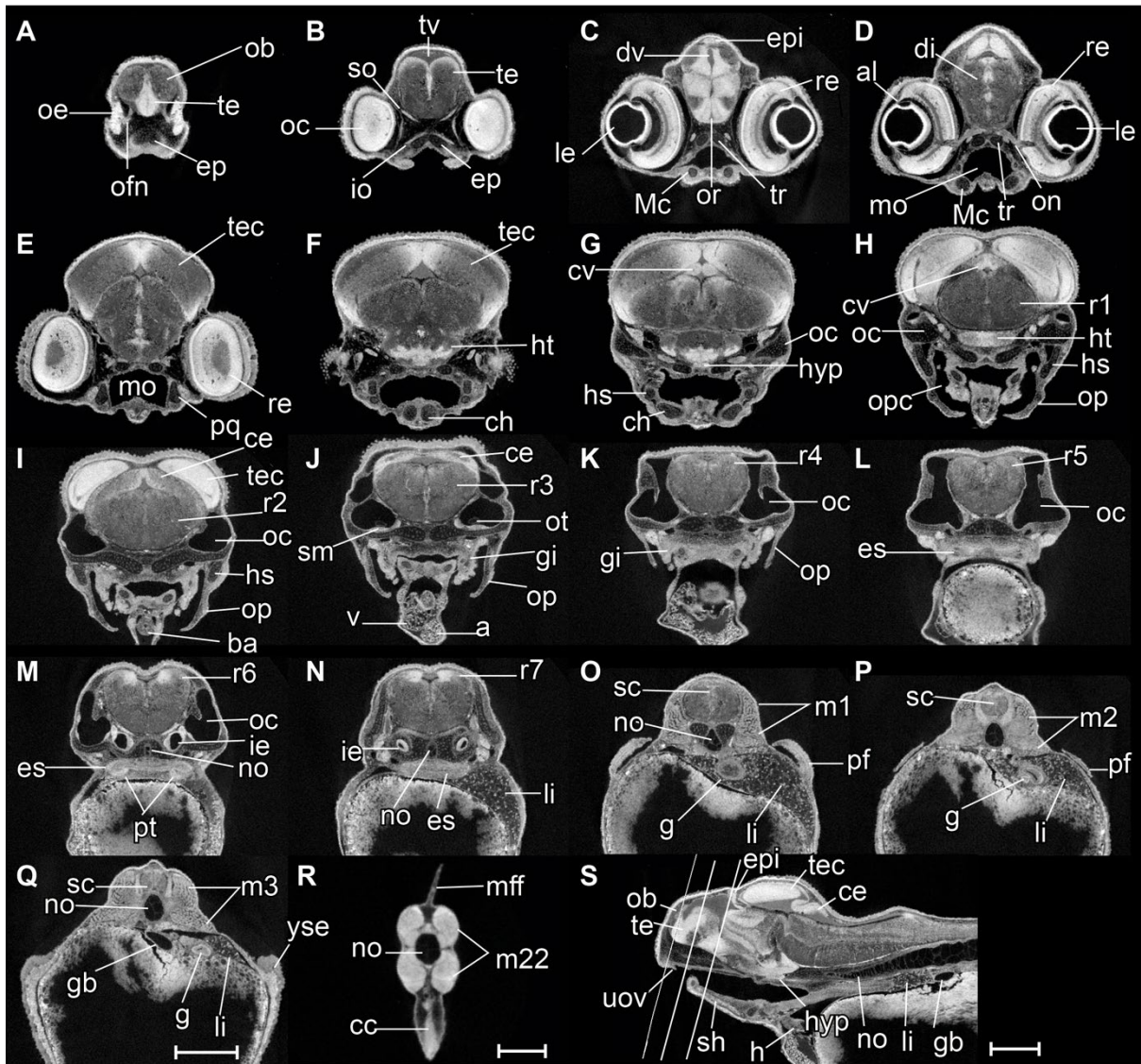


Figure 26 *Rhodius ocellatus*, stage long-pec, microCT images, virtual sections. A-R, transverse section views, dorsal towards the top, sections go from rostral to caudal, direction of section plane indicated in S. S, mid-sagittal section view, rostral to the left, dorsal towards the top. Abbreviations: a, atrium; al, annular ligament; ba, bulbus arteriosus; cc, cloaca; ce, cerebellum; ch, ceratohyal cartilage; di, diencephalon; ep, ethmoid plate; epi, epiphysis; es, esophagus; g, gut; gb, gall bladder; gi, gill; h, heart; hs, hyosymplectic cartilage; ht, hypothalamus; hyp, hypophysis; ie, pars inferior of inner ear; io, inferior oblique muscle; le, lens; li, liver; m, myotome; Mc, Meckel's cartilage; mff, median fin fold; mo, mouth; no, notochord; ob, olfactory bulb; oc, otic capsule; oe, olfactory epithelium; ofn, olfactory nerve; on, optic nerve; op, operculum; opc, opercular cavity; or, optic recess; ot, otolith; pa, pharyngeal arch; pcc, pericardial cavity; pd, pronephric duct; pf, pectoral fin bud; pq, palatoquadrate arch cartilage; pt, pharyngeal teeth; r1 to 7, rhombomere 1 to 7; re, retina; sc, spinal cord; scc, semicircular canal; sg, statoacoustic ganglion; sh, sternohyoid muscle; sm, sensory maculae; so, superior oblique muscle; te, telencephalon; tec, optic tectum; tr, trabeculae cranii; tv, telencephalic ventricle; uov, upper oval valve; v, cardiac ventricle; yse, yolk sac extension. Scale bar, 200 μ m.

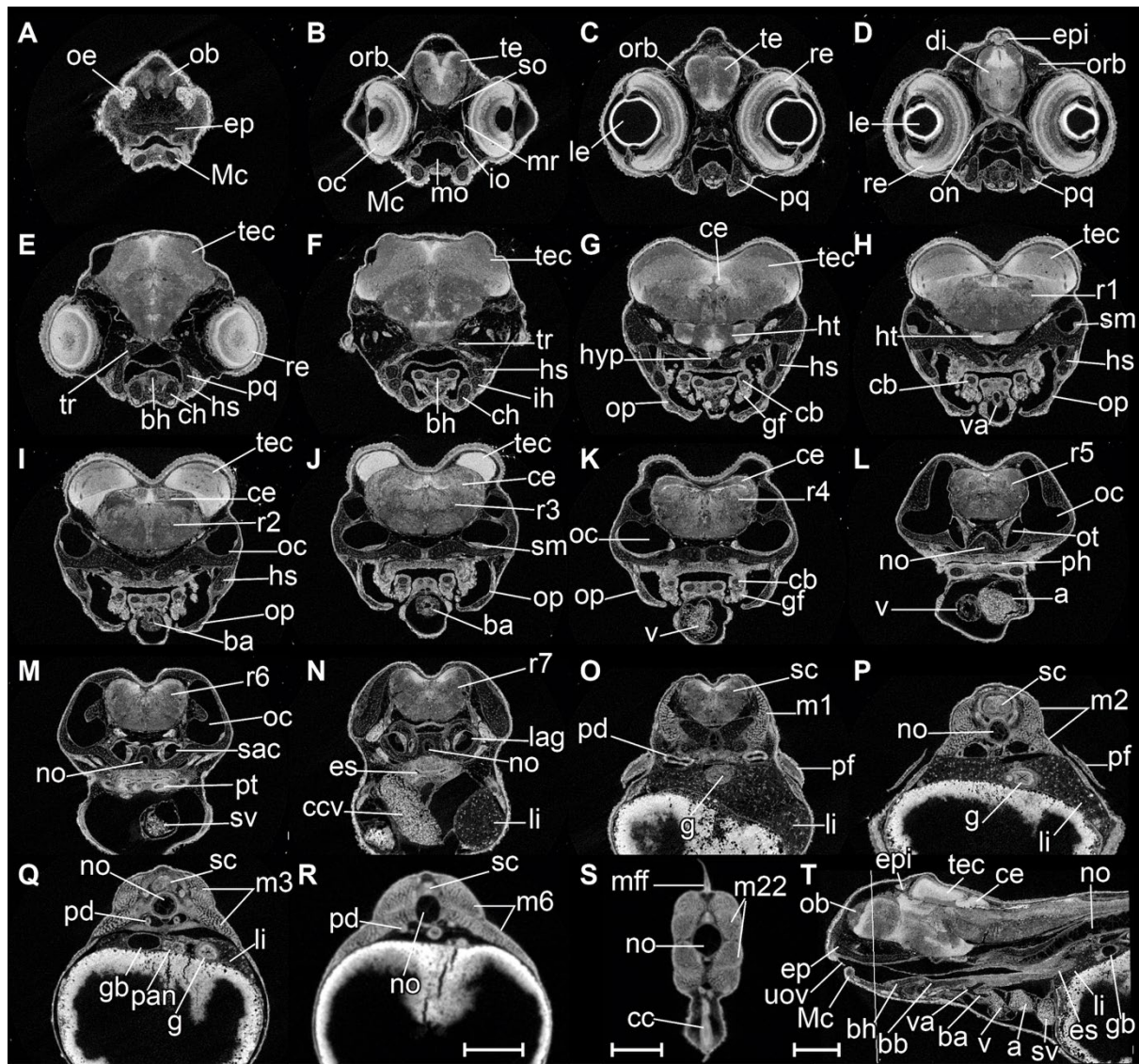


Figure 27 *Rhodeus ocellatus*, stage pec-fin, microCT images, virtual sections. A to S are transverse section view, dorsal towards the top, sections go from rostral to caudal, direction of section plane indicated in T; T is mid-sagittal section view, rostral to the left, dorsal towards the top. Abbreviations: a, atrium; ba, bulbus arteriosus; bb, basibranchial cartilage; bh, basihyal cartilage; cb, ceratobranchial cartilages; cc, cloaca; ccv, common cardinal vein (duct of Cuvier); ce, cerebellum; ch, ceratohyal cartilage; di, diencephalon; ep, ethmoid plate; epi, epiphysis; es, esophagus; g, gut; gb, gall bladder; gf, gill filament; h, heart; hs, hyosymplectic cartilage; ht, hypothalamus; hyp, hypophysis; ih, interhyal cartilage; io, inferior oblique muscle; lag, lagena; le, lens; li, liver; m, myotome; Mc, Meckel's cartilage; mff, median fin fold; mo, mouth; mr, medial rectus muscle; no, notochord; ob, olfactory bulb; oc, otic capsule; oe, olfactory epithelium; ofn, olfactory nerve; on, optic nerve; op, operculum; opc, opercular cavity; or, optic recess; orb, orbital cartilage; ot, otolith; p, proctodeum; pan, pancreas; pcc, pericardial cavity; pd, pronephric duct; pf, pectoral fin bud; ph, pharynx; pq, palatoquadrate arch cartilage; pt, pharyngeal teeth; r1 to 7, rhombomere 1 to 7; re, retina; sac, sacculle; sc, spinal cord; scc, semicircular canal; sg, statocoustic ganglion; sm, sensory maculae; so, superior oblique muscle; sv, sinus venosus; te, telencephalon; tec, optic tectum; tr, trabeculae crani; uov, upper oval valve; v, cardiac ventricle; va, ventral aorta. Scale bar, 200 μ m.

STAGE 24: pec-fin, 330 hpf (13.75 dpf).

The pectoral apical fin folds have the form of asymmetric blades (Figure 23D). Iridophores are present in the iris giving the appearance of a reflective ring around the lens (Figure 22D'). On the trunk and tail, melanophores organize into a lateral stripe at the level of the horizontal myoseptal boundaries (Figure 22D'). Ventral melanocytes appear on the caudal end of the yolk sac (Figure 22D'). In concert with the extension of the jaw (Figure 32), the pericardial cavity extends further rostrally. The heart is elongated in its rostrocaudal axis; this is in contrast to the previous stage, in which the heart was oriented in the dorsoventral plane (compare Figures Figure 26S and Figure 27T). Live specimens (Figure 22D'), in lateral view (Figure 27T), show blood flow in the common cardinal vein (Figure 27N), sinus venosus (Figure 27M), atrium (Figure 27L), ventricle (Figure 27K), bulbus arteriosus (Figure 27I and J), ventral aorta (Figure 27H), and branchial arch arteries (Figure 27G).

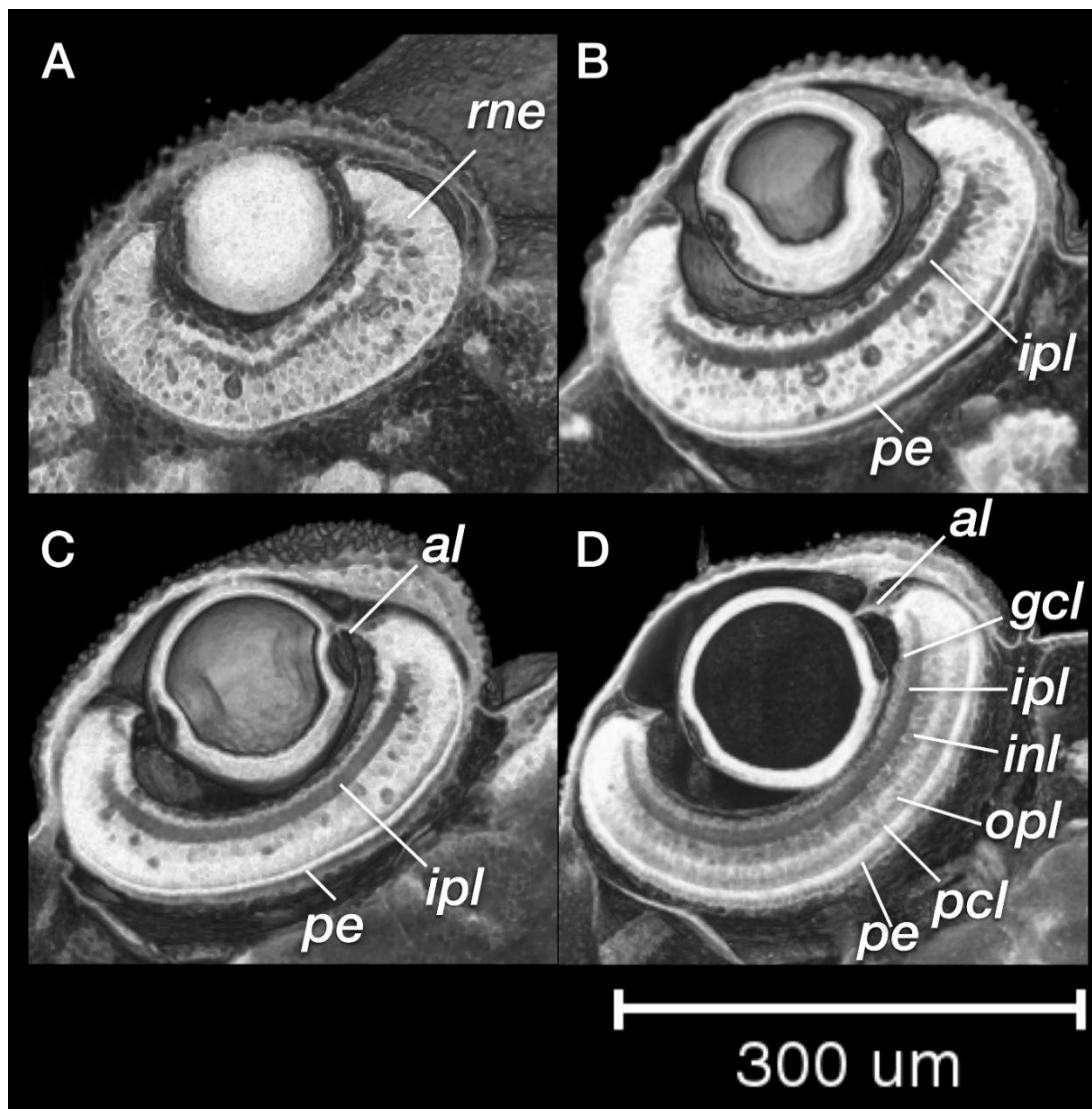


Figure 28 *Rhodeus ocellatus*, retinal lamination at different stages of development. Dorsal view, coronal section plane of volume rendering visualization. A, 165 hpf, B, 210 hpf, C, 235 hpf, D, 330 hpf. Abbreviations: al, annular ligament; gcl, ganglion cell layer; inl, inner nuclear layer; ipl, inner plexiform layer; le, lens; opl, outer plexiform layer; pcl, photoreceptor layer; pe, pigmented epithelium; rne, retina neuroepithelium.

In the chondrocranium, the orbital cartilage grows anteroventrally from the epiphyseal bar to join the edge of the ethmoid plate (Figure 27B to D). Although the orbital cartilage appeared in the previous stage, it is only in the current stage that its rostral connection to the ethmoid plate and caudal connection to the epiphyseal bar are distinct (data not shown). The medial basihyal and basi-branial cartilages are now cartilaginous (Figure 27F and T) and the angle between the bilateral carotohyal cartilage is acute (compare Supplemental Figure 1A and C). The fifth branchial arch is distinct and carries four pairs of pharyngeal teeth (Supplemental Figure 1). The asteriscus otolith forms in the chamber of the lagena (Figure 27N and Figure 30D). The swim bladder is not yet inflated (Figure 31D and E). The first four pairs of basidorsal cartilages develop but are not yet differentiated as the Weberian apparatus (Figure 31). This stage corresponds to Kimmel stage *pec-fin* stage, on the basis of fin morphology.

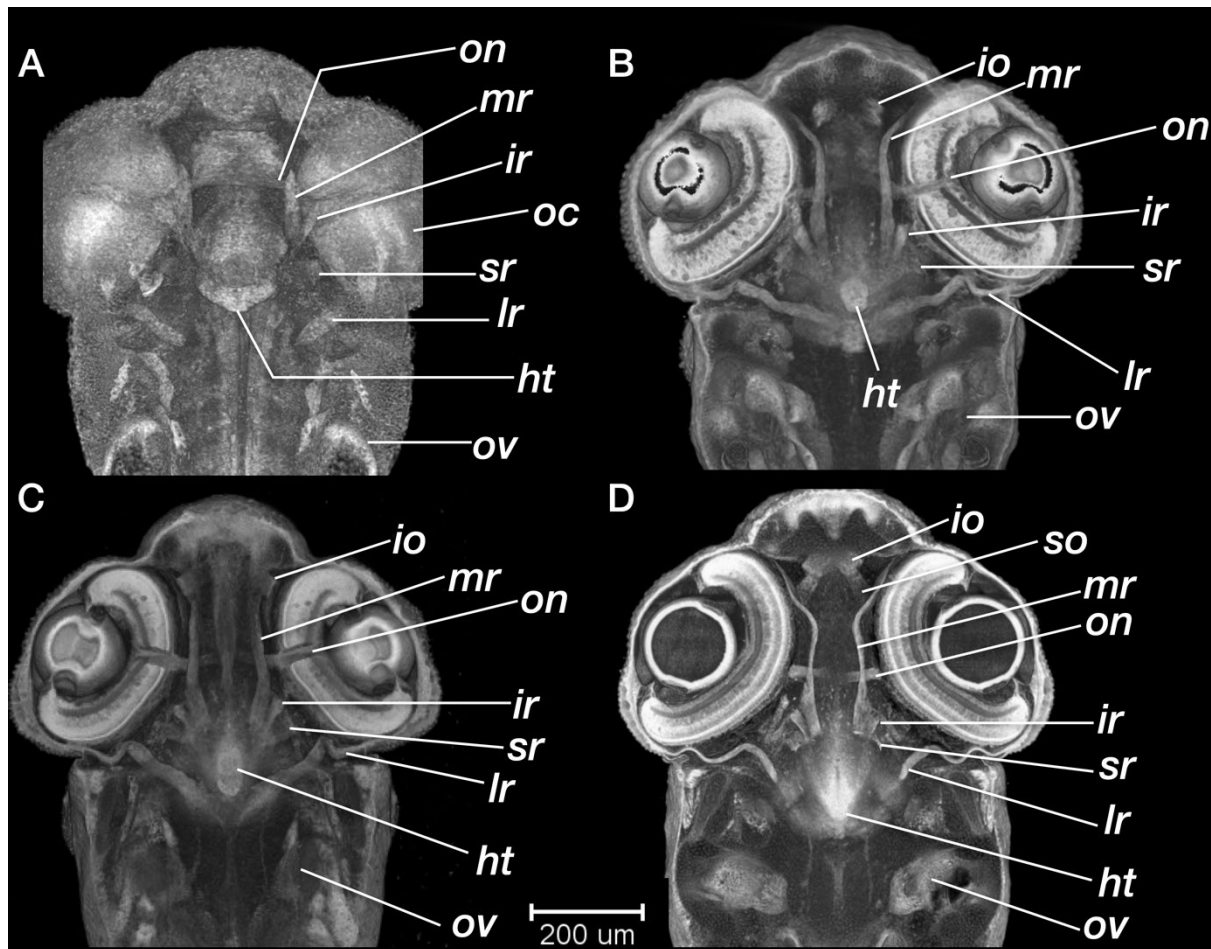


Figure 29 *Rhodeus ocellatus*, development of the extraocular muscles. A, 165 hpf B, 210 hpf C, 235 hpf D, 330 hpf. Ventral views of coronal section planes at the level of the hypothalamus. Abbreviations: ht, hypothalamus; io, inferior oblique; ir, inferior rectus.; lr, lateral rectus; mr, medial rectus; oc, optic cup; on, optic nerve; ov, otic vesicle; so, superior oblique; sr, superior rectus

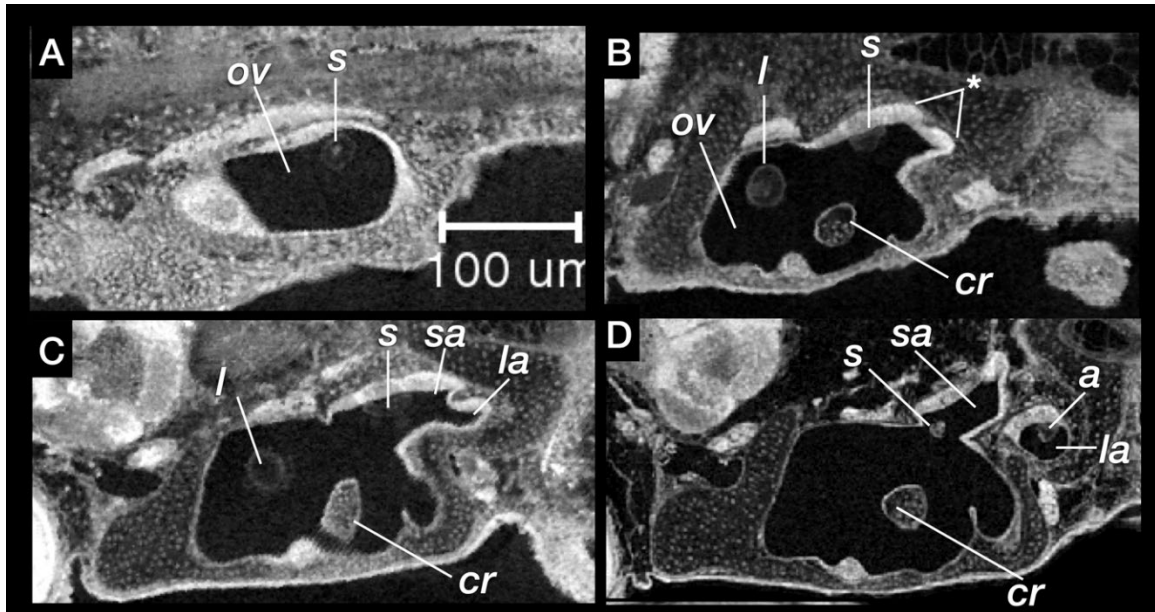


Figure 30 *Rhodeus ocellatus*, development of the pars inferior of the inner ear. Coronal sections of the ventral part of the ear. A, 165 hpf. The anterior otolith lapillus and the posterior otolith sagitta are well formed. B, 210 hpf. C, 235 hpf, the protrusion dividing the lumen into two D, 330 hpf. The asteriscus forms last in the chamber of lagena, and the saccule is separate from the utricle. Abbreviations: a, asteriscus; cr, common crus; l, lapillus; la, lagena; ov, otic vesicle; s, sagitta; sa, saccule; u, utricle; *, protrusion of saccule and lagena from the caudal margin of the otic vesicle wall.

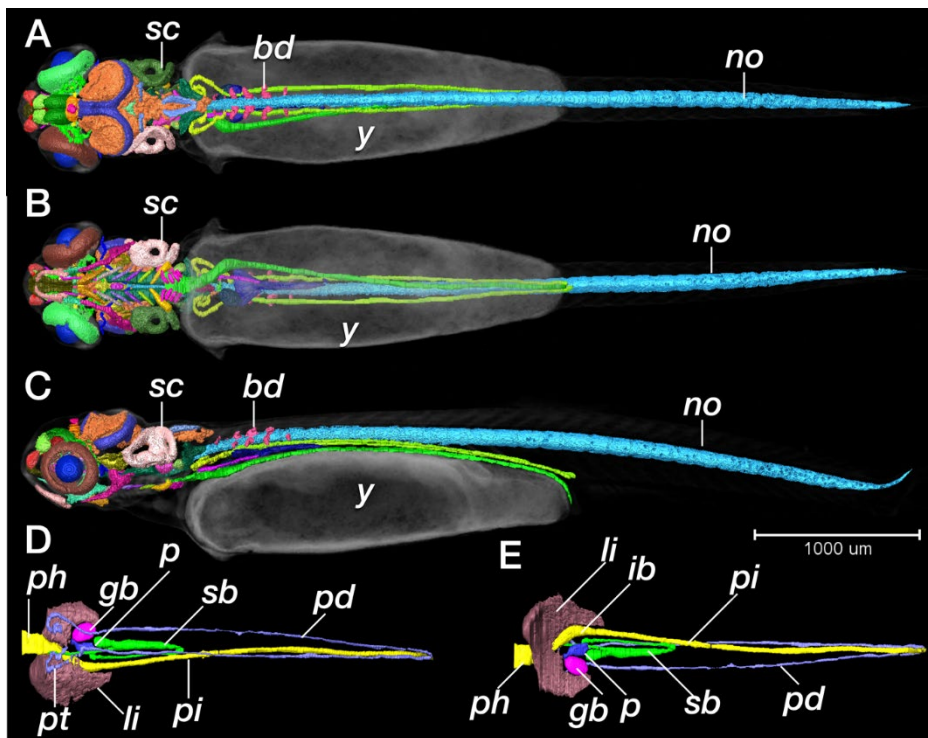


Figure 31 *Rhodeus ocellatus*, pec-fin stage. A, D, dorsal views. B, E, ventral views. C, lateral view, rostral to the left. A to C are the overviews of segmentation result visualized by surface view, background tissue (including yolk) visualized by volume rendering (greyscale color-map, transparent). D, E, segmented surface view of the digestive system the previously solid endodermal rod develops into an alimentary canal and gives rise to liver, gall bladder and pancreas buds, as well as the endodermal lining of the swim bladder. Abbreviations: bd, basidorsal cartilage; gb, gall bladder; ib, intestine bulb; li, liver; no, notochord; p, pancreas; pd, pronephric duct; ph, pharynx; pi, posterior intestine; pt, pronephric tubule; sb, swim bladder; sc, semicircular canal; y, yolk. Scale bar, 1mm.

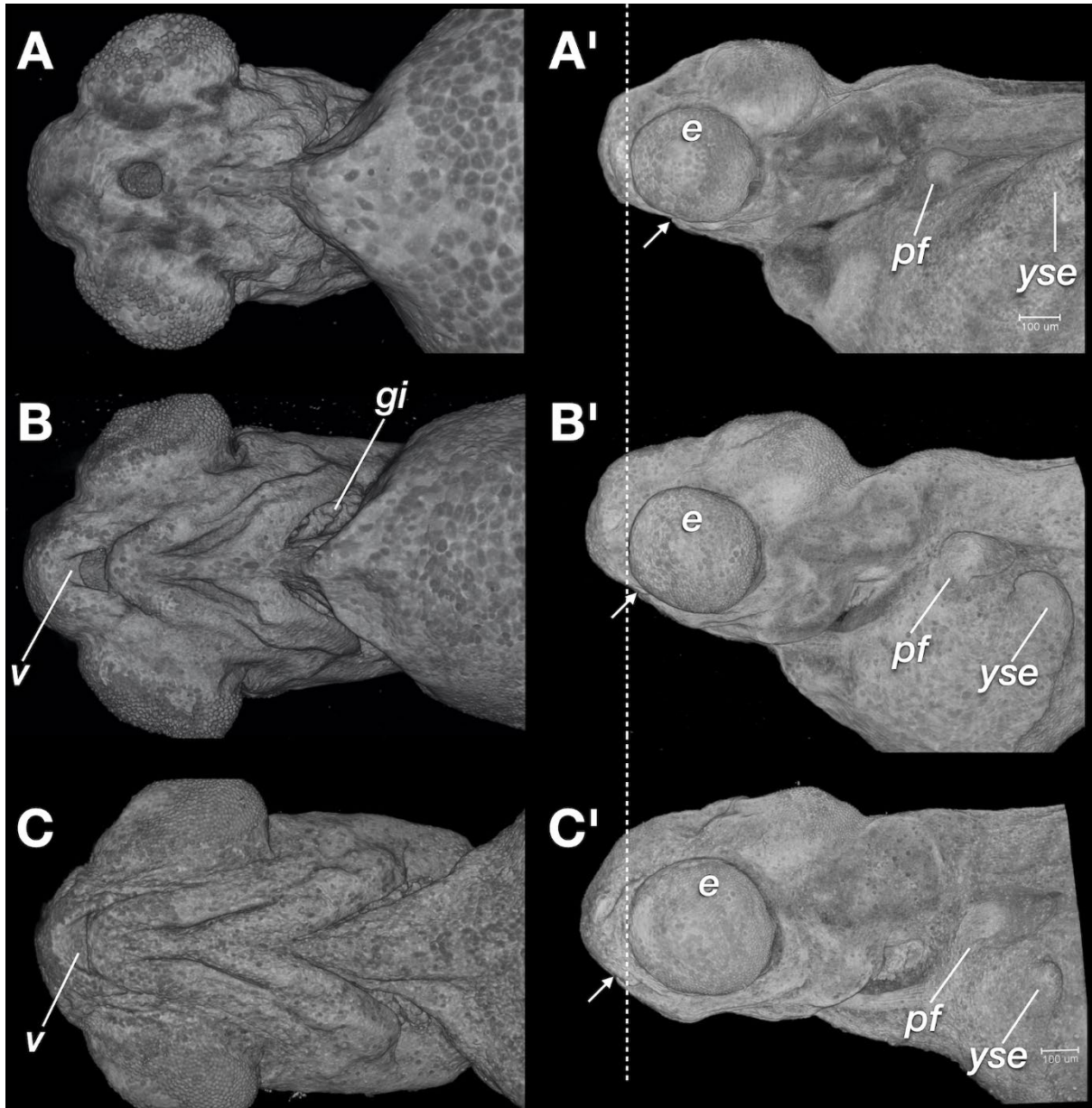
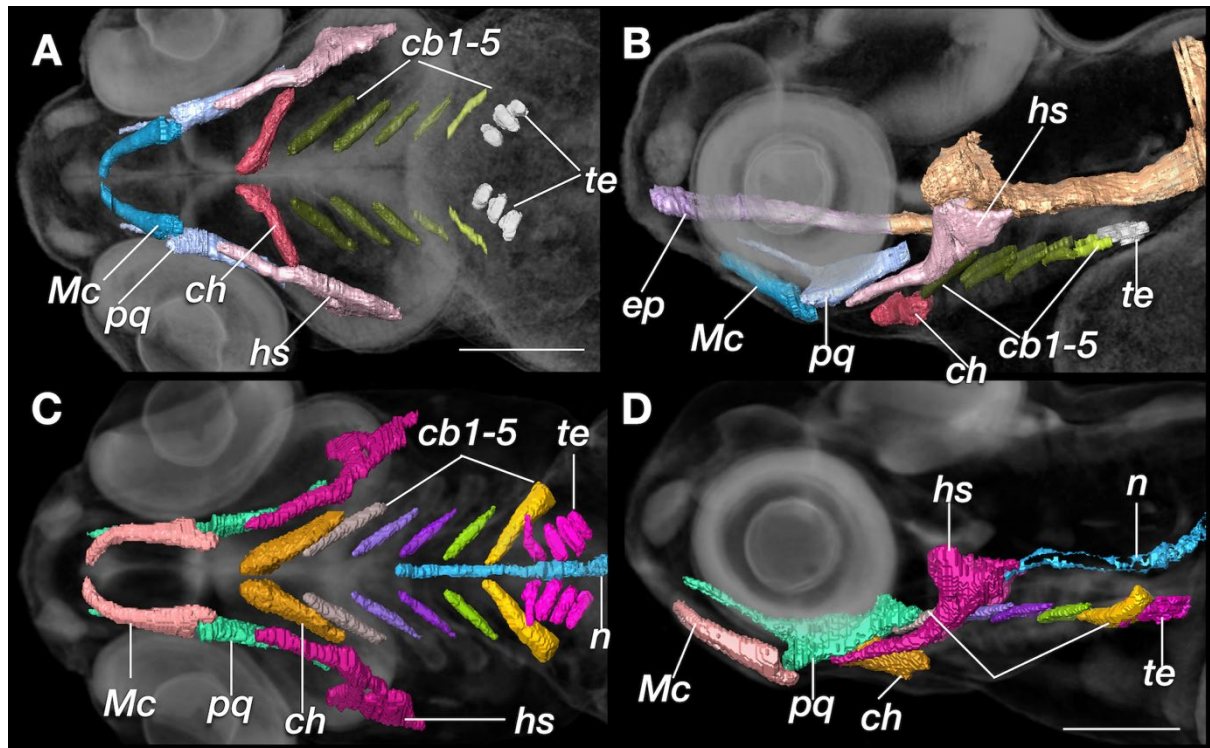


Figure 32 *Rhodeus ocellatus*, mouth protrusion and jaw extension during the organogenetic period. A, A', 210 hpf the mouth opening located ventrally, approaching the rostral margin of the eye. B, B', 235 hpf the jaw extends rostrally, now at to the rostral margin of eye cups. C, C', 330 hpf. The mouth opening has now extended further rostral, beyond the rostral margin of the eye. A, C, ventral views, A', C', left lateral views. Abbreviations: e, eye; gi, gill filaments; pf, pectoral fin bud; v, upper oral valve; yse, yolk sac extension. Dashed line, rostral margin of eye; arrows, mouth opening.

Discussion

We have described 24 stages in the development of the rosy bitterling using microCT and have made the stages comparable to the Kimmel stages for the zebrafish. Having these corresponding developmental stage series lays the foundation for our subsequent research: a comparison of the sequence of developmental events with sequences in other non-parasitic teleosts based on parsimony analysis (Ito et al., 2019; Jeffery et al., 2005). Sequence heterochrony (changes in the order in which events occur) is an important mechanism for the evolution of development (Bininda-Emonds et al., 2002; Mabee et al., 2000). Our study demonstrates the value of microCT in developmental biology. In addi-

tion to being relatively time-efficient compared with routine histology, it is a non-destructive technology. For species that were previously difficult to study because of limited material, microCT scans provide a wealth of morphological data and readily yield 3-D information.



Supplemental Figure 1 *Rhodeus ocellatus*, development of the pharyngeal cartilages. A, B, 235 hpf C, D, 330 hpf stage. Volume renderings (grayscale) with cartilage is segmented in a different color. A, C, ventral views, rostral to the left. B, D, lateral views, dorsal towards the top, rostral to the left. Abbreviations: cb, ceratobranchial cartilages; ch, ceratohyal cartilage; ep, ethmoid plate; hs, hyosymplectic; Mc, Meckel's cartilage; n, notochord.; pq, palatoquadrate; te, pharyngeal teeth. Scale bar, 200 μ m.

Position of the embryo in relation to the polarity of the chorion

According to Suzuki (1958), the time-window in which bitterling eggs can be fertilized is about 30 min after the egg has been activated when contacting water; sperm remain viable for only 7 min after contact with water. Egg activation is an irreversible process and is independent of the presence of sperm (Kunz, 2004). Once activated, the chorion becomes inflated and lifts from the egg surface (Figure 3). A funnel-shaped micropyle, a specialization of the chorion, connects the chorion with the egg surface, and serves as a passage for the sperms to fertilize the egg (Suzuki, 1961). When the female bitterling oviposits eggs inside the host mussel, these eggs are activated. Therefore, a successful fertilization requires that the male bitterling releases sperm near the host mussel within 30 min and the sperm find their way to the micropyle.

The chorion of the rosy bitterling eggs is bulb-shaped (Figure 3 and Figure 4). The micropyle is always at the narrower stalk pole (Suzuki, 1961). We observed that, during the hatching period, the head always emerges from the chorion at its wider (bulb) side (Figure 40). One explanation of the position of the micropyle could be that it facilitates fertilization. The eggs of bitterlings are deposited by the female using a long ovipositor; the eggs in each clutch are therefore arranged in a sin-

gle row in the water tube of the mussel gill (Kunz, 2004). Kunz-Ramsay's hypothesis is this: the polarity ensures that the micropyle of one egg faces the non-micropyle end of the next, to avoid sperm competition. However, we found that the embryos always hatch out from the chorion from the opposite side of the micropyle; therefore, the newly-hatched embryos are aligned in the water tube in the same orientation as the eggs, which thus reduces potential oxygen and space competition between embryos.

Notochord vacuolization is not necessary for body straightening

During the process of body elongation, especially from stages s-18 to s-32, the notochord elongates and expands in diameter because of vacuolization of the inner layer of notochordal cells. The notochord first has a typical 'stack-of-coins' appearance at the s-18 stage (Adams et al., 1990; Koehl et al., 2000), suggesting that the subsequent vacuolization of notochord plays an important role for body elongation by providing a mechanical force needed for straightening of the body along the RC axis (Stemple, 2005). Ellis, Bagwell, and Bagnat (2013) argued against this hypothesis, providing *in vivo* experimental evidence that the notochord is not necessary for embryonic straightening.

Our results are consistent with the conclusions of Ellis, Bagwell, and Bagnat (2013) because the straightening of bitterling body axis takes place during the neurula extension and neurula migration periods, both of which are complete before the notochord becomes vacuolized. We acknowledge that a temporal correlation is not sufficient proof of the causal relationship of events. However, in this case, the temporal relationship is a dependent one and therefore argues against the mechanical hypothesis.

The yolk extension forms independently of body straightening

In the zebrafish, the straightening of the body axis (from its original conformation of being curved over the yolk sac) overlaps temporally with the formation of the yolk extension (Virta, 2009). The trunk of the zebrafish straightens from the somite-13 stage to the somite-26 stage, and begins simultaneously with formation of the yolk extension (Kimmel et al., 1995; Virta & Cooper, 2009; Virta, 2009; Virta & Cooper, 2011). Virta (2009) conducted agarose immobilization of zebrafish embryos and found that the YE will form even when the trunk is prevented from straightening by the agarose.

In the bitterling, the morphogenetic movements that form the yolk extensions (YE) happen simultaneously with the straightening of the body axis. After that, extension of the YSEs dorsally occurs separately (in the somitogenesis period), without concomitant morphological changes in the body axis. For these reasons, we agree with Virta (2009) that YE formation can occur without concomitant straightening of the trunk.

Post-displacement of eye development

Our study described the development of the eye in the rosy bitterling at the microanatomic level for the first time. Compared to the zebrafish (Easter & Nicola, 1996; Schmitt & Dowling, 1994, 1999), we find that the developmental timeline of early eye morphogenesis between the zebrafish and bitterling is broadly similar. The degree of ventral displacement of the optic primordium is similar between the bitterling at the 10-somite stage (Figure 9C) and the zebrafish at the 11-12 somite stage. In the 16-17 somite stage of zebrafish development, the lens placodes appear, and this event takes place at the corresponding 28-somite stage of the bitterling (Figure 12D). However, in the zebrafish,

the lens is completely detached from the surface ectoderm at the prim-5 stage (24 hpf); this event occurred earlier in bitterling development at the 4-ovl stage (Figure 18D).

It is worth noting that retinal pigmentation begins in the zebrafish at the prim-5 stage. However, there is no sign of retinal pigmentation in the bitterling at the corresponding stage (Figure 15B'). A comparable degree of pigmentation in the bitterling does not appear until 150 hpf (Figure 15D'), a stage comparable to the prim-25 stage of the zebrafish (36 hpf). Although it is obvious that, in the bitterling, the appearance of retinal pigmentation is post-displaced compared with the development of the zebrafish, we are cautious not to draw the conclusion that the development of the eye in the bitterling is delayed. The development and maturity of the visual system, as shown in behavioral studies in the zebrafish, is based on visually-evoked startle and optokinetic responses (Easter & Nicola, 1996). These responses not only require retinal pigmentation, but also retinal lamination (Figure 28), and formation of extraocular muscles (Figure 29) at later stages.

Pre-displacement of hearing

We analyzed the process of inner ear development in the bitterling at the microanatomic level for the first time. Comparing our results with ear development in zebrafish (Bever and Fekete, 2002; Haddon and Lewis, 1996; Riley and Moorman, 2000; Whitfield et al., 2002), we find that they take place at a comparable stage, although the morphogenesis of the pars inferior of the inner ear is strikingly pre-displaced in bitterling development. Specifically, in the bitterling, the induction of the otic placode is at the 10-somite stage (Figure 9D), the same as in the zebrafish (9-10 somite stage; (Haddon and Lewis, 1996; Whitfield et al., 2002). The cavitation of the otic vesicle becomes obvious at the 28-somite stage (Figure 12G) in the bitterling and also at the corresponding stage in the zebrafish (18 somite stage). The neuroblast cells which will differentiate into the statoacoustic ganglion delaminate from the otocyst at the 35-somite stage (Figure 14G) in the bitterling as well as the corresponding 26-somite stage in the zebrafish (Haddon and Lewis, 1996; Whitfield et al., 2002).

In bitterlings, the morphogenesis of the semicircular canals begins with the protrusion of the pillars at the 1-ovl stage (Figure 21K) and then these protrusions fuse at the high-pec stage (Figure 24L). The same process happens in the zebrafish from 42-72 hpf, slightly later than in the bitterling. More striking is the separation of the lagena from the sacculolagenar pouch; this takes place during the embryonic development of bitterling at the pec-fin stage (330 hpf, 13.75 dpf), while in zebrafish, it takes place much later, during larval development (by 15 dpf; (Bever and Fekete, 2002; Whitfield et al., 2002).

The third otolith (asteriscus of the lagena), starts to form at the pec-fin stage in the bitterling, whereas the same event happens much later (9-17 dpf) in different studies of zebrafish depending on the strain (Bever and Fekete, 2002; Riley and Moorman, 2000; Whitfield et al., 2002). According to one study of otolith development and vestibular function in the zebrafish (Riley and Moorman, 2000), the utricular otolith is necessary and sufficient for vestibular function and survival in the zebrafish, whereas the sacculus and lagena otoliths function primarily in hearing. Therefore, we expect a pre-displacement of hearing development in the bitterling, which may be related to brood parasitism and development in a dark environment where hearing is more useful than vision. This in turn would also explain why visual development appears to be delayed in the bitterling.

MicroCT in developmental biology

The bitterling is not an easy species to study. Its YSEs and its large, opaque yolk mass are in contrast to the small, transparent early stages of zebrafish development. It is therefore much more difficult to observe with optical microscopy. We found that it is not feasible to manipulate differential interference (DIC) optics to count somite numbers during the somitogenesis period or trace the migration of lateral line primordia during the pharyngula period, which are key characters of staging in zebrafish embryos. In addition, the yolk mass becomes brittle when fixed, making it difficult to perform routine histology. For these reasons, three-dimensional (3D) reconstruction from serial sections is not the optimal technique for studying bitterling development.

This study has shown that application of microCT is a valuable technique for studying rosy bitterling development. The volume rendering of X-ray tomography is sufficient to display virtually the staging features of interest (compare for example the left and right columns in Figure 8). Virtual slices provide microanatomical tissue details (e.g., retinal lamination; Figure 28), and provide us with the ability to reconstruct complex three-dimensional structures that were previously only visible through dye-injection methods (e.g., the semicircular canal and alimentary tract in Figure 31).

References

- Abouheif, E., Fave, M. J., Ibarraran-Viniegra, A. S., Lesoway, M. P., Rafiqi, A. M. and Rajakumar, R.** (2014). Eco-Evo-Devo: The Time Has Come. *Ecol. Genomics Ecol. Evol. Genes Genomes* **781**, 107–125.
- Adams, D. S., Keller, R. and Koehl, M. A.** (1990). The mechanics of notochord elongation, straightening and stiffening in the embryo of *Xenopus laevis*. *Development* **110**, 115–130.
- Aldridge, D. C.** (1999). Development of European bitterling in the gills of freshwater mussels. *J. Fish Biol.* **54**, 138–151.
- Ali, S., Champagne, D. L., Spaink, H. P. and Richardson, M. K.** (2011). Zebrafish Embryos and Larvae: A New Generation of Disease Models and Drug Screens. *Birth Defects Res. Part C-Embryo Today-Reviews* **93**, 115–133.
- Babaei, F., Hong, T. L. C., Yeung, K., Cheng, S. H. and Lam, Y. W.** (2016). Contrast-Enhanced X-Ray Micro-Computed Tomography as a Versatile Method for Anatomical Studies of Adult Zebrafish. *Zebrafish* **13**, 310–316.
- Ballard, W. W.** (1981). Morphogenetic Movements and Fate Maps of Vertebrates. *Am. Zool.* **21**, 391–399.
- Bassi, A., Schmid, B. and Huisken, J.** (2015). Optical tomography complements light sheet microscopy for in toto imaging of zebrafish development. *Dev.* **142**, 1016–1020.
- Battle, H. I.** (1940). The embryology and larval development of the goldfish (*Carassius auratus* L.) from Lake Erie. *Ohio J. Sci.* **40**, 82–93.
- Belmamoune, M. and Verbeek, F. J.** (2007). Developmental anatomy ontology of zebrafish: an integrative semantic framework. *J. Integr. Bioinform.* **4**, 64–76.
- Bever, M. M. and Fekete, D. M.** (2002). Atlas of the developing inner ear in zebrafish. *Dev. Dyn.* **223**, 536–543.
- Bininda-Emonds, O. R. P., Jeffery, J. E., Coates, M. I. and Richardson, M. K.** (2002). From Haeckel to event-pairing: the evolution of developmental sequences. *Theory Biosci.* **121**, 297–320.
- Boeseman, M. J., Van der Drift, J., Van Roon, J. M., Tinbergen, N. and Ter Pelkwijk, J. J.** (1938). De bittervoorns en hun mossels. *Levende Nat.* **43**, 129–136.
- Chang, H. W.** (1948). Life history of the common Chinese bitterling, *Rhodeus ocellatus*. *Sinensia* **19**, 12–22.
- Chang, H. W. and Wu, H. W.** (1947). On the blastokinesis occurring in the egg of the common Chinese Bitterling, *Rhodeus ocellatus*. *Sinensia* **17**, 15–22.
- Chang, C. H., Li, F., Shao, K. T., Lin, Y. S., Morosawa, T., Kim, S., Koo, H., Kim, W., Lee, J. S., He, S., et al.** (2014). Phylogenetic relationships of Acheilognathidae (Cypriniformes: Cyprinoidea) as revealed from evidence of both nuclear and mitochondrial gene sequence variation: evidence for necessary taxonomic revision in the family and the identification of cryptic spec. *Mol Phylogenet Evol* **81**, 182–194.
- Ding, Y., Vanselow, D. J., Yakovlev, M. A., Katz, S. R., Lin, A. Y., Clark, D. P., Vargas, P., Xin, X., Copper, J. E., Canfield, V. A., et al.** (2019). Computational 3D histological phenotyping of whole zebrafish by X-ray histotomography. *Elife* **8**.

- Duyvené de Wit, J.** (1955). Some results of investigations into the European Bitterling, *Rhodeus amarus* BLOCH. *Japanese J. Ichthyology* **4**, 94–104.
- Easter, Jr., S. S. and Nicola, G. N.** (1996). The Development of Vision in the Zebrafish (*Danio rerio*). *Dev. Biol.* **180**, 646–663.
- Ellis, K., Bagwell, J. and Bagnat, M.** (2013). Notochord vacuoles are lysosome-related organelles that function in axis and spine morphogenesis. *J Cell Biol* **200**, 667–679.
- Folgueira, M., Bayley, P., Navratilova, P., Becker, T. S., Wilson, S. W. and Clarke, J. D. W.** (2012). Morphogenesis underlying the development of the everted teleost telencephalon. *Neural Dev.* **7**, 1–32.
- Furutani-Seiki, M. and Wittbrodt, J.** (2004). Medaka and zebrafish, an evolutionary twin study. *Mech Dev* **121**, 629–637.
- Gilbert, S. F., Bosch, T. C. G. G. and Ledón-Rettig, C.** (2015). Eco-Evo-Devo: Developmental symbiosis and developmental plasticity as evolutionary agents. *Nat. Rev. Genet.* **16**, 611–622.
- Haddon, C. and Lewis, J.** (1996). Early ear development in the embryo of the Zebrafish, *Danio rerio*. *J. Comp. Neurol.* **365**, 113–128.
- Huisken, J. and Stainier, D. Y. R. R.** (2009). Selective plane illumination microscopy techniques in developmental biology. *Development* **136**, 1963–1975.
- Ito, F., Matsumoto, T. and Hirata, T.** (2019). Frequent nonrandom shifts in the temporal sequence of developmental landmark events during teleost evolutionary diversification. *Evol. Dev.* **21**, 120–134.
- Iwamatsu, T.** (2004). Stages of normal development in the medaka *Oryzias latipes*. *Mech Dev* **121**, 605–618.
- Jeffery, J. E., Bininda-Emonds, O. R. P., Coates, M. I. and Richardson, M. K.** (2005). A new technique for identifying sequence heterochrony. *Syst Biol* **54**, 230–240.
- Kawamura, K., Ueda, T., Arai, R. and Smith, C.** (2014). Phylogenetic relationships of bitterling fishes (Teleostei: Cypriniformes: Acheilognathinae), inferred from mitochondrial cytochrome B sequences. *Zool. Sci* **31**, 321–329.
- Kim, Y. U. and Park, Y. S.** (1985). Egg development and larvae of the rose bitterling *Rhodeus ocellatus* (KNER). *Korean J. Fish. Aquat. Sci.* **18**, 586–593.
- Kim, C. H., Park, J. Y., Park, M. K., Kang, E. J., Kim, J. H. and Kim, H. S.** (2008). Minute tubercles on the skin surface of larvae in the Korean endemic bitterling, *Rhodeus pseudosericeus* (Pisces, Cyprinidae). *Ecol. Evol.* **24**, 269–275.
- Kim, H. S., Choi, H. S. and Park, J. Y.** (2018). Embryonic development characteristics and host mussel utilization of flat bitterling *Acheilognathus rhombeus* (Cyprinidae) during winter in Korea. *Environ. Biol. Fishes* **101**, 55–66.
- Kimmel, C. B., Ballard, W. W., Kimmel, S. R., Ullmann, B. and Schilling, T. F.** (1995). Stages of embryonic development of the zebrafish. *Dev. Dyn.* **203**, 253–310.
- Koehl, M. A. R., Quillin, K. J. and Pell, C. A.** (2000). Mechanical design of fiber-wound hydraulic skeletons: the stiffening and straightening of embryonic notochords. *Am. Zool.* **40**, 28–41.
- Kunz, Y. W.** (2004). *Developmental Biology of Teleost Fishes*. Dordrecht: Springer Netherlands.
- Li, F. and Arai, R.** (2010). *Rhodeus shitaiensis*, a new bitterling from China (Teleostei: Cyprinidae). *Ichthyol. Explor. Freshwaters* **21**, 303–312.
- Liu, H. Z., Zhu, Y. R., Smith, C. and Reichard, M.** (2006). Evidence of host specificity and congruence between phylogenies of bitterling and freshwater mussels. *Zool. Stud.* **45**, 428–434.
- Lowery, L. A. and Sive, H.** (2004). Strategies of vertebrate neurulation and a re-evaluation of teleost neural tube formation. *Mech. Dev.* **121**, 1189–1197.
- Mabee, P. M., Olmstead, K. L. and Cabbage, C. C.** (2000). An experimental study of intraspecific variation, developmental timing, and heterochrony in fishes. *Evolution (N. Y.)* **54**, 2091–2106.
- Masuda, K., Iuchi, I. and Yamagami, K.** (1986). Analyses of Chorion Hardening in Fish. *Zoolog. Sci.* **3**, 1043.
- Masuda, K., Murata, K., Iuchi, I. and Yamagami, K.** (1992). Some Properties of the Hardening Process in Chorions Isolated from Unfertilized Eggs of Medaka, *Oryzias latipes*. *Dev. Growth Differ.* **34**, 545–551.
- Metscher, B. D.** (2009). MicroCT for comparative morphology: simple staining methods allow high-contrast 3D imaging of diverse non-mineralized animal tissues. *BMC Physiol* **9**, 11.
- Mills, S. C. and Reynolds, J. D.** (2003). The bitterling-mussel interaction as a test case for co-evolution. *J. Fish Biol.* **63**, 84–104.
- Mueller, T. and Wullimann, M. F.** (2009). An evolutionary interpretation of teleostean forebrain anatomy. In *Brain, Behavior and Evolution.* **74**, 30–42.
- Nagata, Y. and Miyabe, H.** (1978). Development Stages of the Bitterling, *Rhodeus ocellatus ocellatus* (Cyprinidae). *Mem. Osaka Kyoiku Univ. III, Nat. Sci. Appl. Sci.* **26**, 171–181.
- Olt, A.** (1893). Lebensweise und Entwicklung des Bitterlings. *Zeitschrift für wissenschaftliche Zool.* **55**, 543–575.

- Park, J.-M. and Han, K.-H.** (2018). Early Life History of Rhodeus Fish (*R. uyekii* and *R. ocellatus*) in the Nakdong River Water System. *Dev. Reprod.* **22**, 39–53.
- Reichard, M., Smith, C. and Jordan, W. C.** (2004). Genetic evidence reveals density-dependent mediated success of alternative mating behaviours in the European bitterling (*Rhodeus sericeus*). *Mol. Ecol.* **13**, 1569–1578.
- Reichard, M., Liu, H. and Smith, C.** (2007). The co-evolutionary relationship between bitterling fishes and freshwater mussels: insights from interspecific comparisons. *Evol. Ecol. Res.* **9**, 239–259.
- Riley, B. B. and Moorman, S. J.** (2000). Development of utricular otoliths, but not saccular otoliths, is necessary for vestibular function and survival in zebrafish. *J. Neurobiol.* **43**, 329–337.
- Rouchet, R., Smith, C., Liu, H. Z., Methling, C., Douda, K., Yu, D., Tang, Q. Y. and Reichard, M.** (2017). Avoidance of host resistance in the oviposition-site preferences of rose bitterling. *Evol. Ecol.* **31**, 769–783.
- Schmitt, E. A. and Dowling, J. E.** (1994). Early-eye morphogenesis in the zebrafish, *Brachydanio rerio*. *J. Comp. Neurol.* **344**, 532–542.
- Schmitt, E. A. and Dowling, J. E.** (1999). Early retinal development in the zebrafish, *Danio rerio*: Light and electron microscopic analyses. *J. Comp. Neurol.* **404**, 515–536.
- Signore, I. A., Guerrero, N., Loosli, F., Colombo, A., Villalón, A., Wittbrodt, J. and Concha, M. L.** (2009). Zebrafish and medaka: Model organisms for a comparative developmental approach of brain asymmetry. *Philos. Trans. R. Soc. B Biol. Sci.* **364**, 991–1003.
- Smith, C. and Reichard, M.** (2013). A sperm competition model for the European bitterling (*Rhodeus amarus*). *Behaviour* **150**, 1709–1730.
- Smith, C., Reichard, M., Jurajda, P. and Przybylski, M.** (2004). The reproductive ecology of the European bitterling (*Rhodeus sericeus*). *J. Zool.* **262**, 107–124.
- Stemple, D. L.** (2005). Structure and function of the notochord: an essential organ for chordate development. *Development* **132**, 2503–2512.
- Suzuki, R.** (1958). Sperm activation and aggregation during fertilization in some fishes. V. Spermstimulating factor on the vegetal pole. *Embryologia (Nagoya)*. **34**, 18–23.
- Suzuki, R.** (1961). Sperm activation and aggregation during fertilization in some fishes. VII. Separation of the sperm-stimulating factor and its chemical nature. *Jap. J. Zool* **13**, 79–100.
- Tankersley, R. A.** (1996). Multipurpose Gills: Effect of Larval Brooding on the Feeding Physiology of Freshwater Unionid Mussels. *Invertebr. Biol.* **115**, 243.
- Tsai, H.-Y. Y., Chang, M., Liu, S.-C. C., Abe, G. and Ota, K. G.** (2013). Embryonic development of goldfish (*Carassius auratus*): A model for the study of evolutionary change in developmental mechanisms by artificial selection. *Dev. Dyn.* **242**, 1262–1283.
- Van Slyke, C. E., Bradford, Y. M., Westerfield, M. and Haendel, M. A.** (2014). The zebrafish anatomy and stage ontologies: representing the anatomy and development of *Danio rerio*. *J. Biomed. Semantics* **5**, 12.
- Virta, V. C.** (2009). *Yolk extension ontogenesis: a novel evolutionary and developmental module of the teleostean phylotypic period*. University of Washington.
- Virta, V. C. and Cooper, M. S.** (2009). Ontogeny and phylogeny of the yolk extension in embryonic cypriniform fishes. *J Exp Zool B Mol Dev Evol* **312B**, 196–223.
- Virta, V. C. and Cooper, M. S.** (2011). Structural components and morphogenetic mechanics of the zebrafish yolk extension, a developmental module. *J. Exp. Zool. Part B Mol. Dev. Evol.* **316 B**, 76–92.
- Weber, M., Mickoleit, M. and Huisken, J.** (2014). Multilayer Mounting for Long-term Light Sheet Microscopy of Zebrafish. *J. Vis. Exp.* 51119.
- Weinhardt, V., Shkarin, R., Wernet, T., Wittbrodt, J., Baumbach, T. and Loosli, F.** (2018). Quantitative morphometric analysis of adult teleost fish by X-ray computed tomography. *Sci. Rep.* **8**, 16531.
- Werneburg, I.** (2009). A Standard System to Study Vertebrate Embryos. *PLoS One* **4**, e5887.
- Whitfield, T. T., Riley, B. B., Chiang, M.-Y. and Phillips, B.** (2002). Development of the zebrafish inner ear. *Dev. Dyn.* **223**, 427–458.
- Wiepkema, P. R.** (1962). An Ethological Analysis of the Reproductive Behaviour of the Bitterling (*Rhodeus Amarus* Bloch). *Arch. Néerlandaises Zool.* **14**, 103–199.
- Wong, M. D., Dorr, A. E., Walls, J. R., Lerch, J. P. and Henkelman, R. M.** (2012). A novel 3D mouse embryo atlas based on micro-CT. *Development* **139**, 3248–3256.
- Wullmann, M. F. and Puelles, L.** (1999). Postembryonic neural proliferation in the zebrafish forebrain and its relationship to prosomeric domains. *Anat. Embryol. (Berl)*. **199**, 329–348.
- Xiong, F., Ma, W., Hiscock, T. W., Mosaliganti, K. R., Tentner, A. R., Brakke, K. A., Rannou, N., Gelas, A., Souhait, L., Swinburne, I. A., et al.** (2014). Interplay of Cell Shape and Division Orientation Promotes Robust Morphogenesis of Developing Epithelia. *Cell* **159**, 415–427.

Chapter 3 Developmental neuroanatomy of the rosy bitterling *Rhodeus ocellatus* (Teleostei: Cypriniformes)

Wenjing Yi¹, Thomas Mueller², Martin Rücklin³, and Michael K. Richardson¹

1, Institute of Biology, University of Leiden, Sylvius Laboratory, Sylviusweg 72,
2333BE, Leiden, the Netherlands.

2, Division of Biology, Kansas State University, 340 Ackert Hall, Manhattan, KS 66506-
4901, Kansas, United States.

3, Vertebrate Evolution, Development and Ecology, Naturalis Biodiversity Center,
Postbus 9517, 2300 RA Leiden, The Netherlands.

Manuscript under revision at *Journal of Comparative Neurology*

Abstract

Bitterlings are a group of teleost fish (Cypriniformes: Acheilanthidae) that notable for their brood parasitic lifestyle. Bitterling embryos develop as parasites inside the gill chamber of their freshwater mussel hosts. However, little is known about brain development of this valuable model for evolutionary adaptation of parasitism. Here, we have imaged the development of the brain of the rosy bitterling, *Rhodeus ocellatus*, at four embryonic stages of 165, 185, 210, 235 hpf using micro-Computed tomography (microCT) with a specific focus on developmental regionalization and brain ventricular organization. We have given a detailed neuroanatomical account of the development of the brain divisions with reference to *The Atlas of Early Zebrafish Brain Development* and the prosomeric model. Segmentation and three-dimensional visualization of the ventricular system were performed in order to clarify changes in the longitudinal brain axis as a result of cephalic flexure during development. The results show that during early embryonic and larval development, histological differentiation, tissue boundaries, periventricular proliferation zones, and ventricular spaces are all detectable by microCT. Importantly, our approach is validated by the fact that the profile of CT values displayed here in the bitterling brain are consistent with genoarchitecture identified in previous neurodevelopmental. Distinct developmental heterochrony of the precocious development of the inferior lobe are seen in the rosy bitterling compared to the zebrafish.

Introduction

Bitterlings, a group of freshwater teleosts, have been established as valuable model species in behavioral, population and evolutionary ecology due to their brood parasitic life history. Their peculiar life style involves the laying of eggs by the bitterling in a host mussel, a phenomenon that has been recognized for more than a century (Boeseman et al., 1938; Chang, 1948; Duyvené de Wit, 1955; Kitamura et al., 2012; Mills and Reynolds, 2003; Olt, 1893; Reichard et al., 2007; Rouchet et al., 2017; Smith, 2016; Wiepkema, 1962). Noll (1877) was the first to show that the embryos of European bitterling (*Rhodeus amarus*) develop in the gill chamber of their host mussel. This location provides a sheltered environment which protects the developing embryos from potential predators (Aldridge, 1999; Liu et al., 2006; Reichard et al., 2007; Smith et al., 2004). We (Yi et al., 2021) have recently compared developmental sequences of the rosy bitterling (*Rhodeus ocellatus*) to the zebrafish (*Danio rerio*); the latter is a non-parasitic teleost which lays its eggs into the open water (Kimmel et al., 1995; Lawrence, 2007). That study confirmed the relative pre-displacement of hatching, and the relative delay of development of the pectoral fins, in the bitterling.

The specialized ontogeny of the bitterling, and its brood parasitic lifestyle, make it a potentially interesting model for the study of developmental mechanisms underlying brain evolution. In this study, we generated an atlas of the developing bitterling brain as a reference for cross-species comparisons. To build a foundation for such comparisons, we related the bitterling brain development with published data of the zebrafish. The comparison to the zebrafish is useful for two reasons: Firstly, the zebrafish is firmly established as a genetic model system that has been most thoroughly investigated with regard to embryonic, postembryonic, and larval stages (Mueller and Wullimann, 2003; Mueller and Wullimann, 2016; Mueller et al., 2006; Wullimann, 2009; Wullimann and Knipp, 2000; Wullimann and Mueller, 2004). Secondly, both, the bitterling and the zebrafish belong to the group of carp-like (cyprinid) teleosts with very similar adult brain anatomy yet, as we show, distinct developmental heterochronies. A developmental stage atlas of the bitterling brain as visualized in this study, provides a foundation to examine the molecular mechanisms underlying these heterochronies.

In the vertebrates, the central nervous system, including its anteriormost part, the brain, develops from the neural tube (Richardson and Wright, 2003; Schmitz et al., 1993; Wullimann, 2009). In teleosts, including bitterlings, the development of the neural tube involves secondary neurulation (Schmitz et al., 1993). The definitive neural tube is filled with cerebrospinal fluid (Lowery and Sive, 2009). The neural tube caudal to the brain is the spinal cord, and has a narrow lumen called the central canal. The brain has an inflated, irregular lumen which form a series of brain ventricles (Korzh, 2018). In general, the vertebrate brain consists of four parts: (1) the secondary prosencephalon, (2) the diencephalon, (3) the mesencephalon, and (4) the rhombencephalon. Correspondingly, the brain ventricular system has been divided into the 4th ventricle (the lumen of the rhombencephalon); the mesencephalic ventricle; the 3rd ventricle (the lumen of diencephalon proper); and the prosencephalic ventricle (including the telencephalic ventricle and the hypothalamic part of the classic diencephalic ventricle; Nieuwenhuys and Puelles, 2016).

In this study we used the prosomeric model of Puelles and Rubenstein (2003) for dividing neuromeres in the secondary prosencephalon as well as for defining other brain divisions. In general, the prosomeric model alongside its recognition of longitudinal zones and transverse neuromeres forms a powerful paradigm for vertebrate cross-species comparisons. One reason for this is that the

model is based on conserved molecular and developmental characteristics that allow a consistent demarcation of the CNS into developmental units (morphogenetic entities) along the neuraxis of a range of vertebrate species. Applying the prosomeric model for the development of the zebrafish brain, it has been demonstrated that cellular processes, i.e., proliferation, migration and differentiation, can be used to define prosomeric units in teleosts (Mueller and Wullimann, 2003; Mueller and Wullimann, 2016; Mueller et al., 2006; Wullimann, 2009; Wullimann and Knipp, 2000; Wullimann and Mueller, 2004).

The prosomeric model analyzes brain regions along the general brain axis and according to the mediolateral extent of brain regions. Longitudinally, the neural tube has four compartments divided by the *sulcus limitans* that was first defined by Wilhelm His, Sr. (His Wilhelm, 1895); reviewed by Puelles (2019). The four compartments are: the roof plate dorsally, the alar plate dorsolaterally, the basal plate ventrolaterally, and the floor plate ventrally.

According to Nieuwenhuys and Puelles (2016), the rhombencephalon consists of twelve neuromeres (rhombomeres, isthmus or r0 plus r1-r11) in longitudinal series. In cyprinids like the Goldfish (*Carassius auratus*), the rostral rhombomeres two to six (r2-r6) correspond to the mammalian pons, whereas the caudal rhombomeres seven to eight (r7-8) correspond to the mammalian medulla oblongata (Gilland et al., 2014; Rahmat and Gilland, 2019). The rostral rhombomeres r2-r6 form clearly segmented neural clusters while the caudal r7-r8 lack a precise morphological delineation (Ma et al., 2009). The zebrafish r8 is twice as large as the rostral rhombomeres, composed by multiple crypto- or pseudo rhombomeres that can be delimited only molecularly similar to the avian brain (Cambronero and Puelles, 2000). The rostral subdivision of neuromeres is more complex, because bending of the neural tube (the cephalic flexure, Hauptmann and Gerster, 2000; Mueller and Wullimann, 2009) has made the definition of the longitudinal neuraxis more difficult (Mueller and Wullimann, 2009; Puelles, 2019; Vernier, 2017; Wullimann and Rink, 2002).

Here, we visualize the development of the rosy bitterling (*Rhodeus ocellatus*) brain using micro-Computed tomography (microCT, x-ray microscopy or μ CT) with a specific focus on developmental regionalization and brain ventricular organization. MicroCT is a widely used high-resolution, non-destructive, three-dimensional (3D) imaging technique (Babaei et al., 2016; Metscher, 2009a) that just recently has been introduced to study development (Wong et al., 2015). The contrast of CT scans is based on absorption of x-ray radiation passed through the sample. Conventionally, highly mineralized structures like bones and teeth have higher attenuation coefficient (CT value or Hounsfield units), and are brighter and easier to recognize than soft tissues. For the visualization of the latter, a treatment with contrast agents is needed. In this work, we used phosphotungstic acid (Metscher, 2009b), which allows discrimination of soft tissues such as muscles, nerves, and blood vessels. In this study, we extend MicroCT techniques to the developing fish brain. Our goal is to establish microCT and 3D visualizations as complementary methods for cross-species comparisons of structural characteristics of both developing and mature brains. In fact, our results indicate that microCT is useful to quantitatively analyze, for example, ventricular spaces, and white matter versus proliferative and postmitotic cell masses.

Materials and Methods

Sample preparation

Embryos of six developmental stages of 135, 150, 165, 185, 210, 235 *hpf* (hours post fertilization; Table 1) were obtained by *in vitro* fertilization following the method of Nagata and Miyabe (1978). Embryos were staged according to Yi et al. (2021). Embryos were incubated in a temperature-controlled incubator (22.5 ± 1 °C) and fixed in 3% paraformaldehyde (pFA) and 1% glutaraldehyde (GA). Digital microphotographs of fixed samples were obtained with a CCD (charge-coupled device) camera connected to stereo microscope (Nikon SMZ1500). For x-ray contrast enhancement, embryos were stained for at least 24 h in 0.3% phosphotungstic acid (PTA) dissolved in 70% ethanol. Samples were then brought back to 70% ethanol without PTA and mounted in low-melting point agarose for non-shift scanning in pipette tips.

Table 1 Sample information and microCT scanning parameters.

Age (hpf)	Stage name	Pixel size (μm)	Voltage (keV/W)	Exp. time (sec.)	Intensity
135	2-ovl	2.19	40/3	4	5000-9000
150	1-ovl	2.0615	40/3	4.5	5000-10000
165	1-ovl/pec-bud	0.9765	40/3	17	5000-8500
185	pec-bud	0.9989	80/7	3	5000-6300
210	high-pec	1.4582	40/3	9.5	5000-10000
235	long-pec	1.4299	40/3	8.5	5000-10000

Note: for each stage, we scanned at least two specimens. The stage names follow Yi et al. (2021). For the pec-bud stage at 185 hpf, we also tried a lower resolution scan with the voltage set to 40/3 keV/W. We found no practical difference in image quality between scans at 80/7 keV/W and 40/3 keV/W. Therefore, we decided to use the less time-consuming option for this stage, namely scanning with the higher voltage but shorter exposure time. Key: Dev, developmental; hpf, hours post fertilization; Exp, exposure; keV, kiloelectron volt.

MicroCT scanning

Attenuation-based microtomographic images were acquired using a Xradia 520 Versa 3D X-ray microscope (Zeiss), with the x-ray tube voltages source set at 80/7 or 40/3 keV/W (keV: kiloelectron volts). A thin LE1 filter was used to avoid beam hardening artifacts. During the CT scanning, the sample was placed on a rotation table and projection images are acquired over an angular range of 180 degree. To obtain high resolution images, a CCD (charge-coupled device) optical objective with 4x was applied in the scan. Images were acquired with voxel (volumetric 3D pixels after reconstruction) sizes of 1-1.5 μm, and tomographic reconstructions were made with the resident software (XMReconstructor). Reconstructed images were exported as TIFF and loaded into Avizo version 9.5 (Thermo Fisher Scientific) for 3D visualization.

3D visualization

The reconstructed volume was viewed “slice by slice” as virtual sections using the *Slice* module in the Avizo software (Version: 9.5; Thermo Fisher Scientific). A computational module *Resample transformed image* was applied to register images to the orthogonal direction of the anatomical axis. *Ortho View* was used for interactive orthogonal views in *xy*, *yz* and *xz* axis simultaneously. The *Volume rendering* module was used for 3D view. Values of colormap and opacity degree were optimized in the settings of rendering. Scalebars were added using the *Scalebars* module.

Annotations on 2D slices

To generate a developmental atlas, serial virtual transverse sections were taken in rostrocaudal sequence from the olfactory bulb to the medulla oblongata. The section plane was settled parallel to the deep ventricular sulcus between telencephalon and diencephalon (the anterior intraencephalic sulcus or AIS). To keep a consistent prosomeric axis annotation, we visualize the transverse section from the rostral to caudal, the coronal section from dorsal to ventral, the sagittal section from medial to lateral along the general body axis (Figure 1f). Labels were added to each section in the Adobe InDesign software (Version: 15.0.2; Adobe Systems Inc., San José, California). For anatomical terms see the list of abbreviation. In general, and to facilitate cross-species comparisons, we adopted anatomical terms were adopted from the *Atlas of Early Zebrafish Brain Development* (Mueller and Wullimann, 2005, 2016).

Segmentation of brain ventricles

Segmentation of the brain ventricle was conducted in Avizo in two steps. First, a rough segmentation based on greyscale threshold was achieved semi-automatically and polished by using *Smooth labels* and *Remove islands* filters. These segmentation results were checked slice-by-slice and were corrected manually. The *Generate Surface* module was used to extract surfaces from the segmentation results. Brain ventricles were colored in yellow using the *Surface view* module, while the rest of the cranial tissues are in semi-transparent using the *Volume rendering* module. The segmented model of the brain ventricles was captured in dorsal, ventral, lateral, and rostral views and saved in TIFF format, annotated in Adobe InDesign.

Results

We have studied the developmental stages of 165, 185, 210, 235 *hpf* (hours post fertilization) of the brain in the rosy bitterling (*Rhodeus ocellatus*) using microCT. Throughout this study we have used the stage table of development of the rosy bitterling generated by Yi et al. (2021). To avoid confusion regarding the anatomical orientation, we follow Herget et al., (2014) and use the term rostral, caudal, dorsal and ventral as in classical descriptions for the linear axial system of the embryonic body. For the topological position, prosomeric position and considering the curved neuraxis, we use the terms anterior, posterior, alar and basal as alternatives (Figure 1f). The anterior and posterior of the transverse neuromeres has to regarding the bending neural axis. Our results are divided into two sections. First, we illustrated the development of the ventricular system. Second, we compiled a developmental atlas of the bitterling brain.

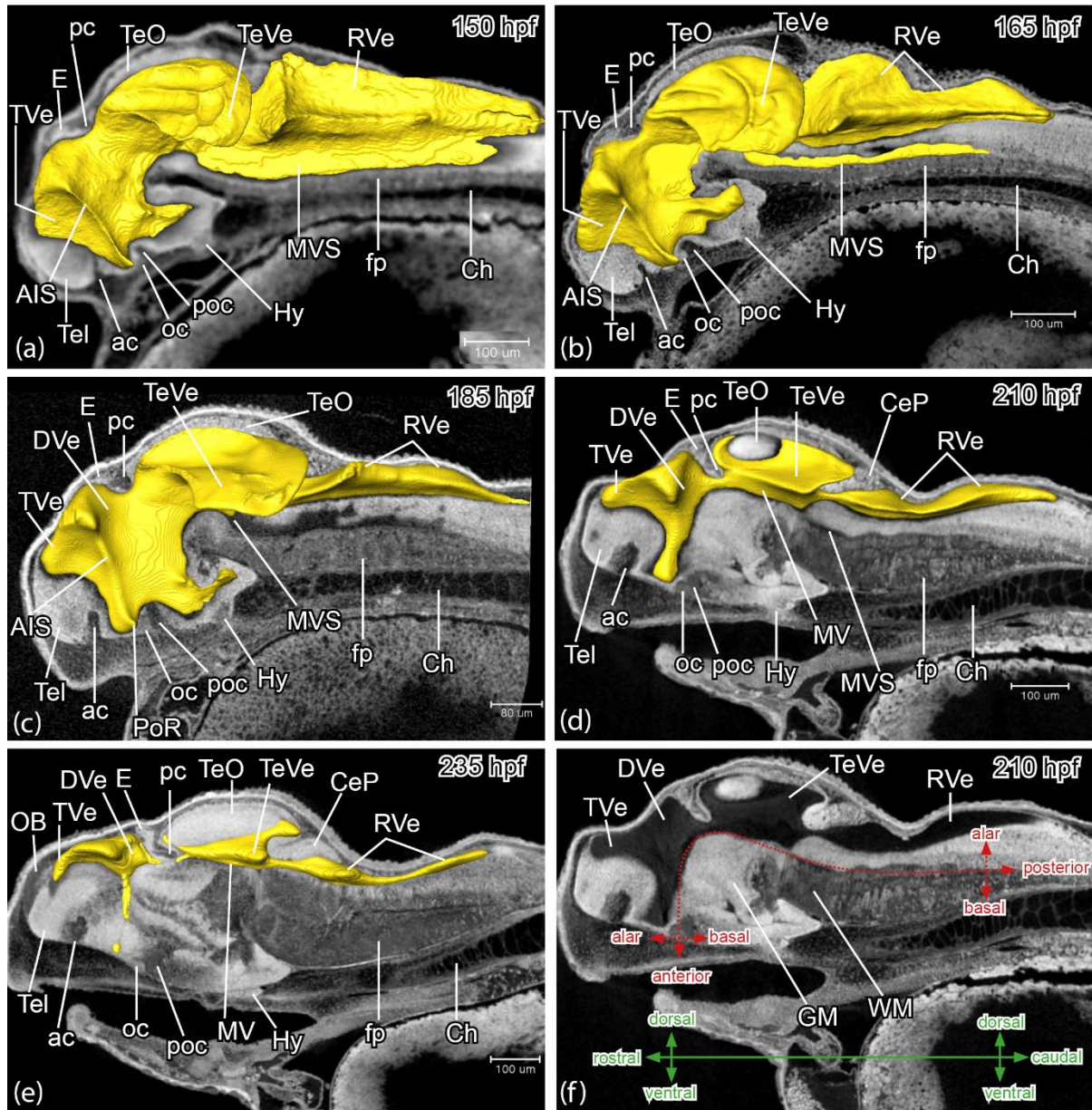


Figure 1 *Rhodius ocellatus*, development of the brain ventricular system, microCT images, dorsal to the top, head to the left. (a-e) virtual midsagittal sections overlaid with surface view of manually-segmented brain ventricles, and showing the distinct ridge of the anterior intraencephalic sulcus (AIS) and progressive compartmentalization of the ventricular system (a-e). (f) virtual midsagittal section illustrating the black lumen of the brain ventricle, a bright white periventricular layer of gray matter (GM), and a gray peripheral layer of white matter (WM). The red dotted line indicates the neuraxis, with anterior, posterior, alar and basal topological direction for the curved axis. The green axes refer to the linear axial system apply to the brain parts with the terms rostral, caudal, dorsal, and ventral. The (a) stage 1-ovl, 150 hpf. (b) stage 1-ovl/pec-bud, 165 hpf. (c) stage pec-bud, 185 hpf. (d, f) stage high-pec, 210 hpf. (e) stage long-pec, 235 hpf. For annotations, see Table 2 List of Abbreviations. Scale bars = 100 μm (a, b, d, e, f); 80 μm (c).

A. Development of the brain ventricular system of the rosy bitterling

General description

The greyscale values we observed on virtual microCT sections depend on certain properties of the tissue such as dye precipitation, tissue density, and cell type. In the brain, the gray matter generally appeared brighter than the white matter (for example, compare the telencephalon and anterior commissure in Figure 1, Tel and ac). The white matter with its myelinated axons and tracts yielded greyscale values typical of low-density soft tissues (Figure 1, ac, poc, pc). In contrast, the brain ventricle, essentially a hollow space filled with cerebrospinal fluid (CSF), showed a lower density than the grey or white of the brain. It was visible in CT scans as the darkest part (Figure 1a-f, rendered in yellow color in Figure 1a-e). Therefore, the radiological appearance of the brain presented itself as a three-partitioned structure each separated by clear boundaries: (1) a black lumen (ventricle), (2) a bright white periventricular layer of gray matter, and (3) a gray peripheral layer of white matter (Figure 1f).

The forebrain ventricle divides dorsally by the position of the anterior intraencephalic sulcus (AIS) into the anterior telencephalic ventricle (TVe) and the posterior diencephalic ventricle proper (DVe or the 3rd ventricle; Figure 1). During the eversion of the telencephalic ventricle, the dorsal part of the AIS showed concomitant enlargement (Figure 1). Around the preoptic recess (PoR), the optic recess region (ORR) was recognizable, bordered by the anterior commissure (ac) and postoptic (poc) commissures (see locations of ac, poc and PoR in Figure 1c). The hypothalamic ventricle topographically locates caudal (topologically basal) to the optic recess region, and topologically anterior to the 3rd ventricle, including the lateral recess (LR) and the posterior recess (PR; Figure 2).

The lumen of the mesencephalon ventricle contains the paired tectal ventricle (TeVe), the median ventricle (MV), and the median ventricular sulcus (MVS) (Puelles, 2019). The TeVe projects dorsolaterally from the median ventricle (Figure 3a), covered by the subarea of the alar plate of the midbrain (optic tectum). A transiently visible median ventricular sulcus (MVS) branches off from the ventral bottom of the median ventricle and shows separately at the floor plate area (Figure 3b, inset in the upper right corner). The median ventricle extends caudally to the rhombencephalic ventricle (RVe or the 4th ventricle; Figure 3; García-Lecea et al., 2017; Korzh, 2018).

STAGE 1-ovl/pec-bud, 165 hpf

In the rosy bitterling, the ventricular inflation is completed at stage 165 hpf (compare Figure 1a, b). The rhombencephalic ventricle (RVe) is diamond-shaped (rhombic) in dorsal and rostral aspects (Figure 3a and c). The bilateral tectal ventricles (TeVe) resemble scallop shells (Figure 3a). The telencephalic ventricle is triangular in rostral aspect (Figure 3d). A pair of oval fossae appear caudal-ventral to the midbrain (Figure 3c, of). These fossae are occupied by the rostral cerebellar thickenings, which develop into the valvula cerebelli of the adult (Wullimann and Knipp, 2000). The lateral recess (LR) and the posterior recess (PR) of the hypothalamic ventricle are in shallow groves (Figure 2a).

STAGE pec-bud, 185 hpf

Width of the rhombencephalic ventricle (RVe) decreases to less than half of the tectal ventricles (TeVe) width (Figure 4a). The RVe gradually flattens along its dorsal-ventral axis (compare 3b and 4b). The dorsal surface of the TeVe appeared smoother due to a further developed optic tectum (mammalian superior colliculus) and torus semicircularis (mammalian inferior colliculus; Figure 4a).

There is a deep midline ridge separates left and right TeVe (Figure 4a, d). The preoptic recess (PoR) compressed, reduction in width (compare Figure 3c and 4c). The oval fossae enlarge with the growth of the rostral cerebellar thickening (compare Figure 3c and 4c). The lateral recess and posterior recess extend outward and become observable (Figure 2b).

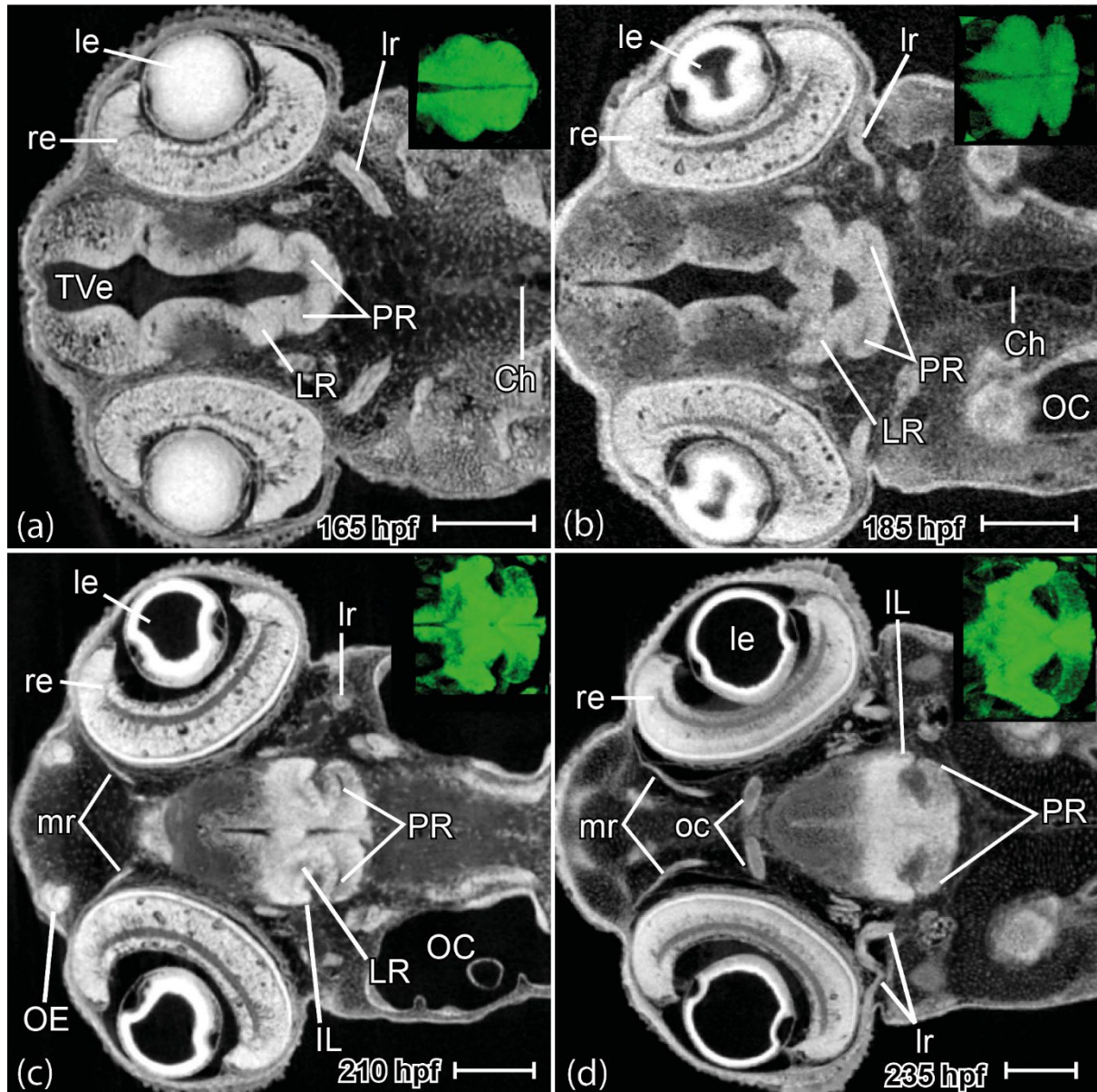


Figure 2 *Rhodeus ocellatus*, development of the lateral recess and posterior recess in the hypothalamus region. Virtual coronal sections, head to the left. At the right upper corner is the 3D volume rendering of the hypothalamus region seen from the dorsal side. (a) stage 1-ovl/pec-bud, 165 hpf. (b) stage pec-bud, 185 hpf. (c) stage high-pec, 210 hpf. (d) stage long-pec, 235 hpf. For annotations, see Table 2 List of Abbreviations. Scale bars = 100 μ m.

STAGE high-pec, 210 hpf.

Compared to earlier stages, the brain ventricles appeared compressed at 210 hpf (compare Figure 4a and 5a). However, the dorsal ventricle of the anterior intraencephalic sulcus (AIS) appeared expanded probably due to the eversion of the telencephalic ventricle (Tve). The tectal lobes grow larger and adhesion between the right and left lobes emergent in the midline; therefore, the deep midline ridge of the TeVe appeared compressed rostrally (Figure 5b). The lateral recess (LR) extends

basalward to flange the posterior recess (PR), around the lateral recess forms the inferior lobe (IL, Figure 2c; Bloch et al. 2019).

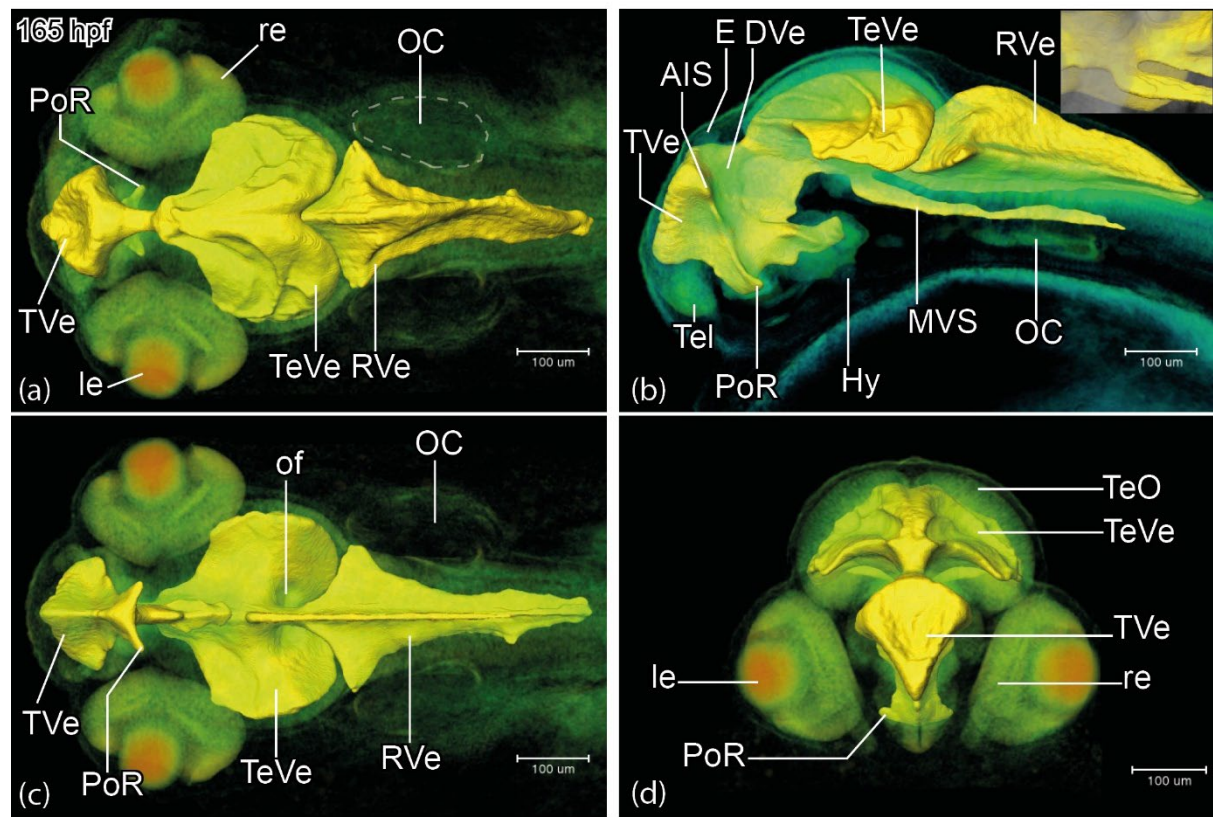


Figure 3 *Rhodnius ocellatus*, brain ventricular system at the stage 1-ovl/pec-bud, 165 hpf. (a-d) microCT images, the pseudo-colour volume rendering of the head region overlaid with a surface view of the manually-segmented brain ventricles. (a-d) dorsal, lateral, ventral, and rostral views, respectively. The inset in the upper right corner in (b) illustrates the median ventricular sulcus (MVS) branches off from the ventral bottom of the median ventricle of the mesencephalon. For annotations, see Table 2 List of Abbreviations. Scale bars = 100 µm.

STAGE long-pec, 235 hpf.

The rhombencephalic ventricle (RVe) can be divided into two portions, a rostral rhomboid opening with very thin roof plate tenting over, and a caudal elongated ventricle between the rhombic lips (RL; Figure 6a). The rostral view of the telencephalic ventricle (TVe) gradually deepens from a triangle into a T-shape (Figure 6d). Compared to earlier stages, the tectal ventricles (TeVe) are further compressed and separated from the median ventricle (Figure 6b). The lateral recess (LR) extends more basalward (compare Figure 2c and d), the inferior lobe (IL) enlarged considerable. The posterior recess (PR) extends alarward (Figure 2d).

B. Developmental atlas of the rosy bitterling brain

We noticed that there were cell clusters in periventricular locations that appeared brighter than the adjacent gray matter (eg. Figure 7j). The distribution of these cell clusters was highly consistent with the distribution of proliferation zones detected during neurogenesis in the zebrafish (Mueller and Wullmann, 2005, 2016). This fact has allowed us in this study to map proliferation zones of the developing bitterling brain and delineate brain territories. Therefore, the delineation of anatomical structures is based on three types of observation: (1) topological relationship to proliferation zones; (2) relative location to annotated brain ventricles (see previous section) and other landmarks such as

commissures and fiber tracts; (3) gray scale values in virtual slices. For example, the zona limitans intrathalamica (Zli) can be demarcated by its dark appearance from the surrounding bright white thalamic tissues (Figure 7g, h).

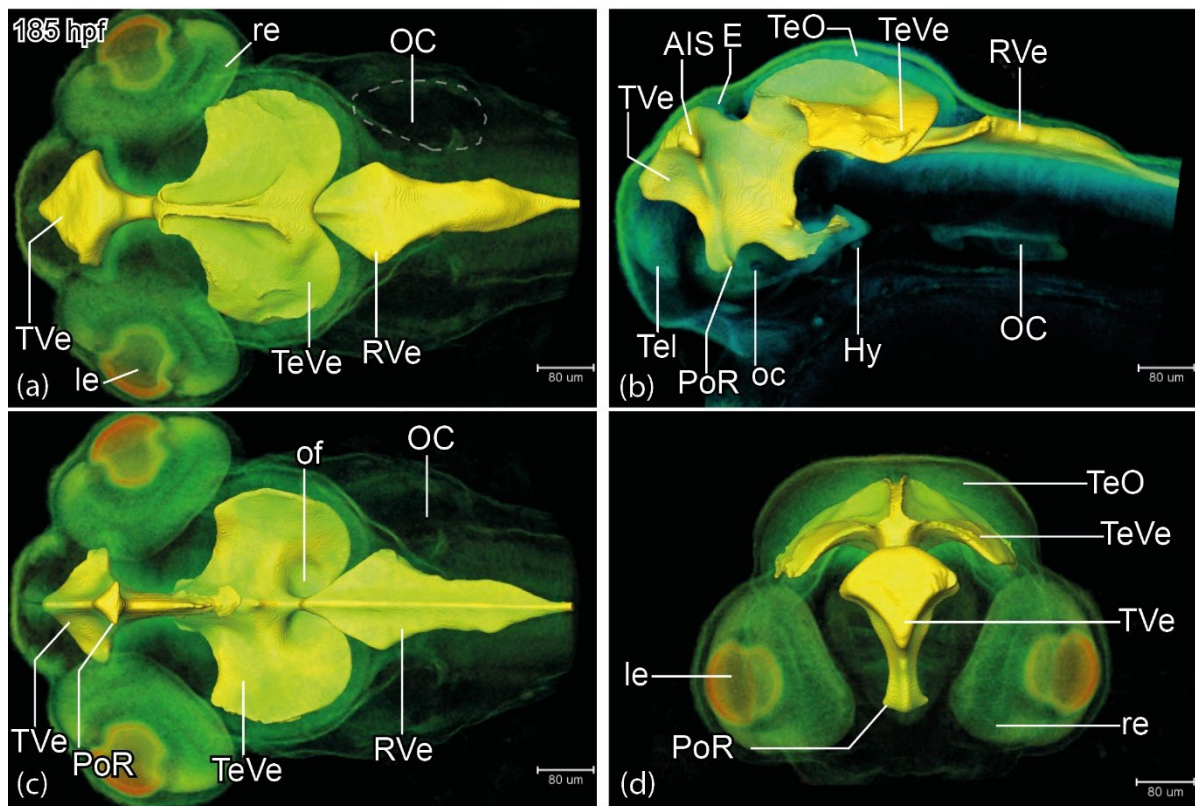


Figure 4 *Rhodeus ocellatus*, brain ventricular system at the stage pec-bud, 185 hpf. (a-d) microCT images, the pseudo-colour volume rendering of the head region overlaid with a surface view of the manually-segmented brain ventricles. (a-d) dorsal, lateral, ventral, and rostral views, respectively. For annotations, see Table 2 List of Abbreviations. Scale bars = 80 μm .

Secondary prosencephalon

Rostral to the telencephalic region, the olfactory epithelium (OE) is very bright, clearly visible from the 1-ovl/pec fin stage (165 hpf, Figure 7a). At the long-pec stage (235 hpf) the olfactory epithelium develops into a bow-shaped structure surrounding the lumen of the olfactory pits (Figure 10a). The olfactory epithelium (OE) is connected to the olfactory bulb (OB) through the easily recognizable olfactory nerve (ON; Figure 7c, 9b and 10b). The olfactory bulb (OB) is characterized by its glomerular structure (Figure 7a, 8a, 9a and 10a; Dynes and Ngai 1998).

The telencephalic ventricle is located at the dorsum of the pallium. The tela choroidea is in the roof of the ventricle. The periventricular proliferation zones of the subpallium (S) and pallium (P) in our samples appeared distinctively bright in virtual transverse sections. At the long-pec stage (235 hpf), the bright subpallial cell clusters were separated by distinct, dark boundaries (dashed line in Figure 10d), corresponding to the dorsal and ventral subdivisions of the subpallium (Sd and Sv). The

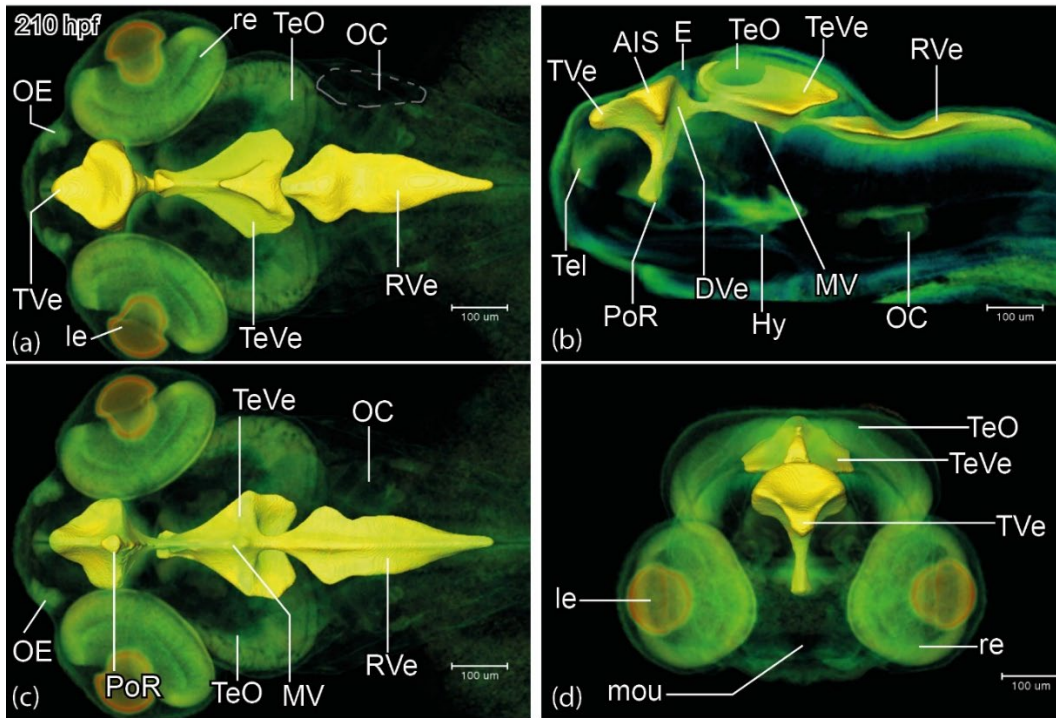


Figure 5 *Rhodnius ocellatus*, brain ventricular system at the stage high-pec, 210 hpf. (a-d) microCT images, the pseudo-colour volume rendering of the head region is overlaid with a surface view of the manually-segmented brain ventricles. (a-d) dorsal, lateral, ventral, and rostral views, respectively. For annotations, see Table 2 List of Abbreviations. Scale bars = 100 μm .

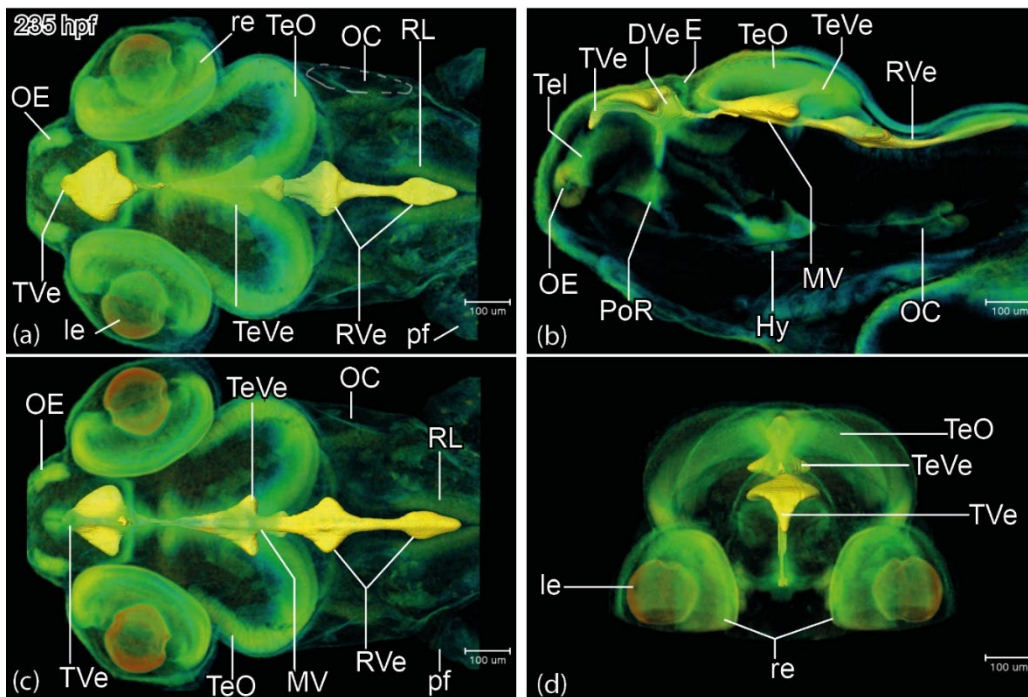


Figure 6 *Rhodnius ocellatus*, brain ventricular system at the stage long-pec, 235 hpf. (a-d) microCT images, the pseudo-colour volume rendering of the head region is overlaid with a surface view of the manually-segmented brain ventricles. (a-d) dorsal, lateral, ventral, and rostral views respectively. For annotations, see Table 2 List of Abbreviations. Scale bars = 100 μm .

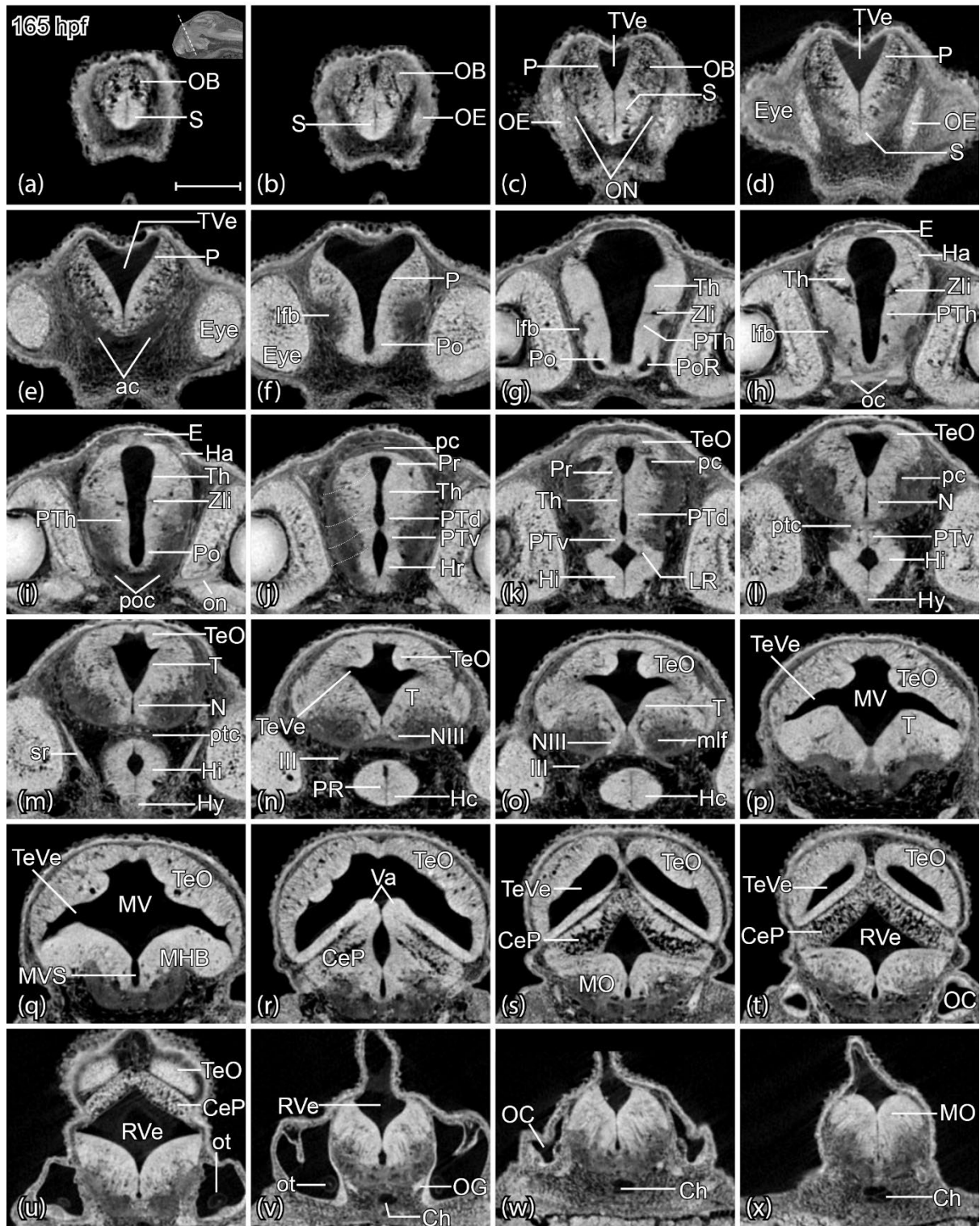


Figure 7 *Rhodnius ocellatus*, brain cross-sectional anatomy, stage 1-ovl/pec-bud, 165 hpf. (a-x) microCT images, virtual sections, transverse plane, dorsal towards the top, sections from rostral to caudal, direction of section plane indicated in inset in (a). For annotations, see Table 2 List of Abbreviations Scale bars = 100 μ m.

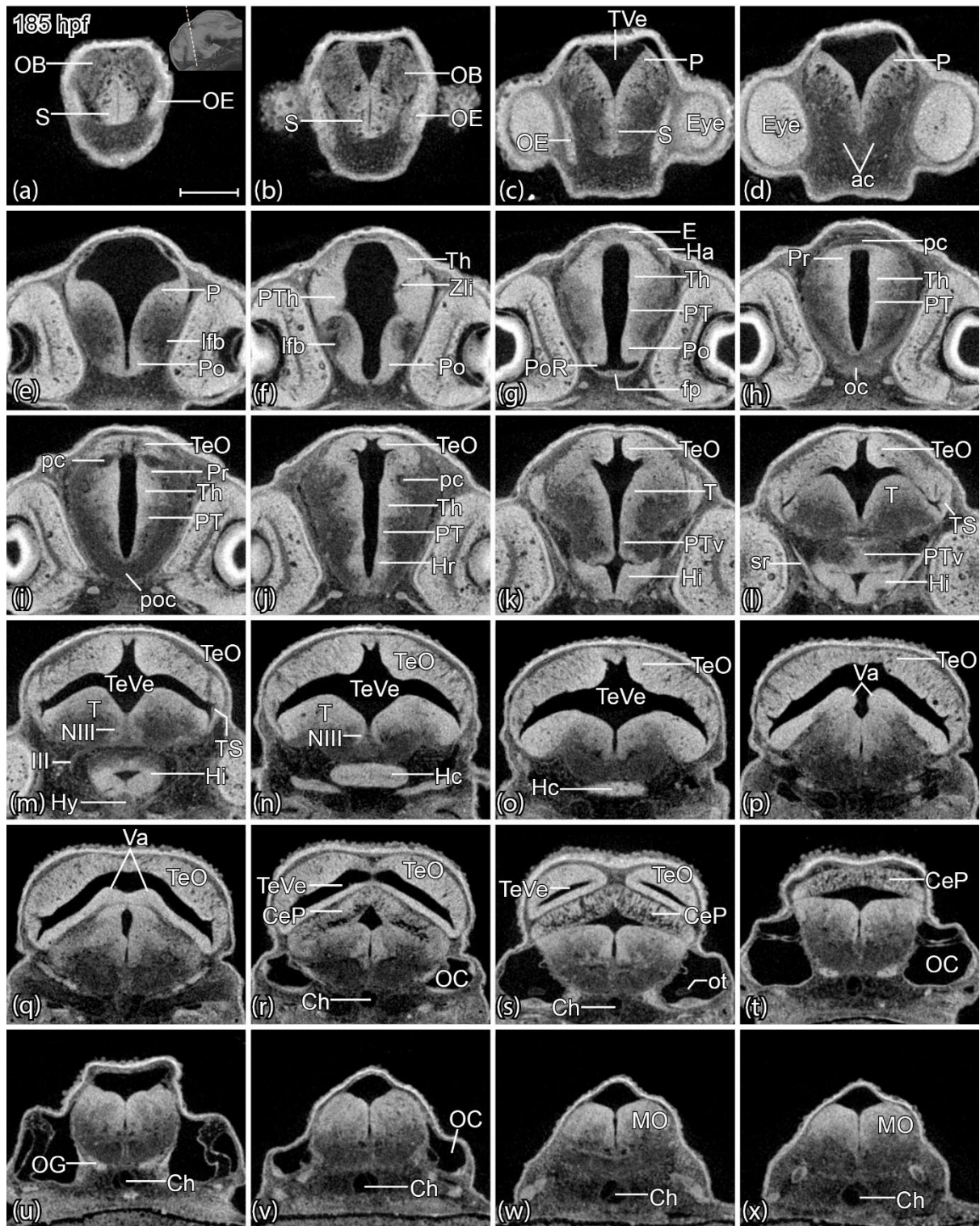


Figure 8 *Rhodnius ocellatus*, brain cross-sectional anatomy, stage pec-bud, 185 hpf. (a-x) microCT images, virtual sections, transverse plane, dorsal towards the top, sections from rostral to caudal, direction of section plane indicated in inset in (a). For annotations, see Table 2 List of Abbreviations. Scale bars = 100 μ m.

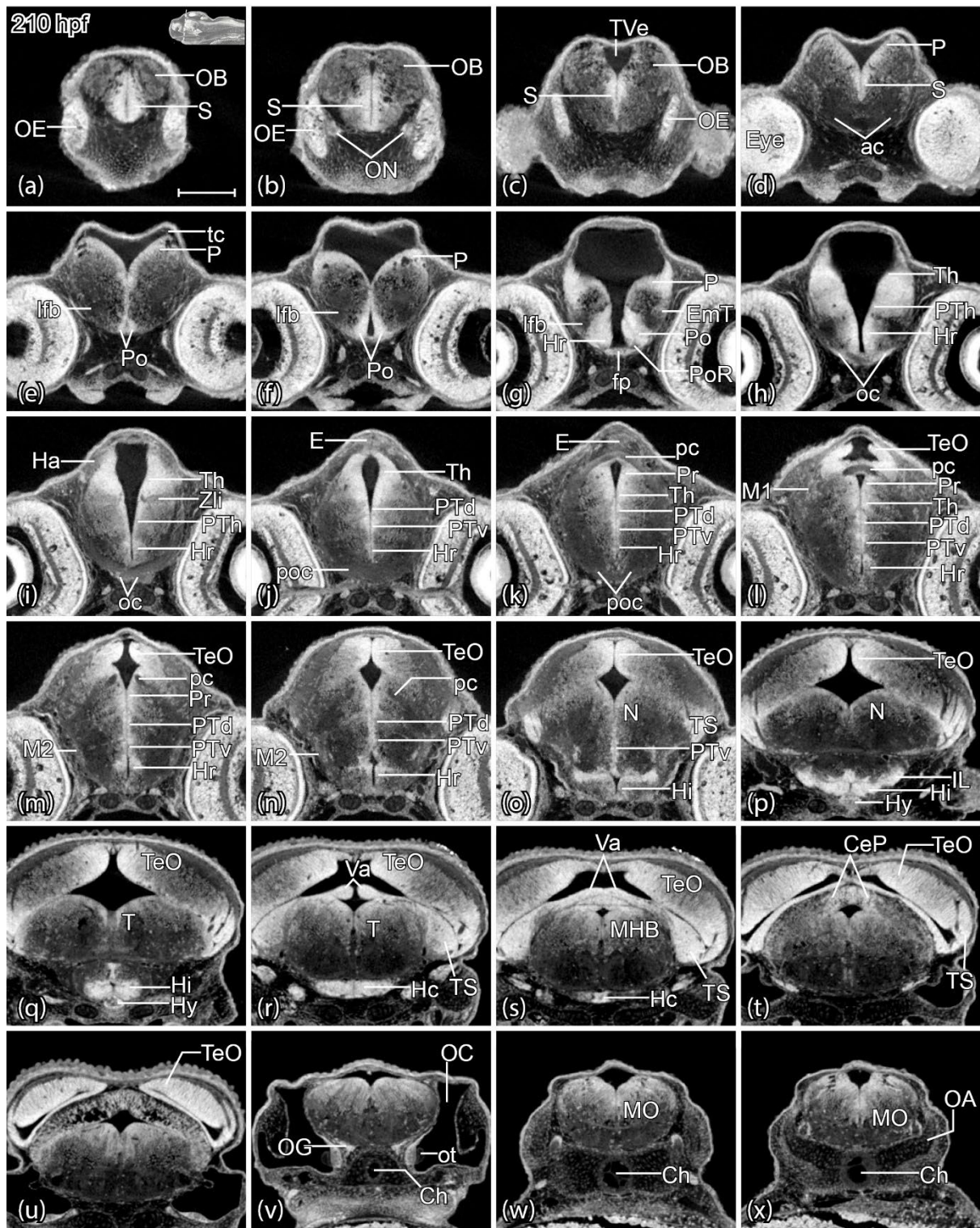


Figure 9 *Rhodnius ocellatus*, brain cross-sectional anatomy, stage high-pec, 210 hpf. (a-x) microCT images, virtual sections, transverse plane, dorsal towards the top, sections go from rostral to caudal, direction of section plane indicated in inset in (a). For annotations, see Table 2 List of Abbreviations. Scale bars = 100 μ m.

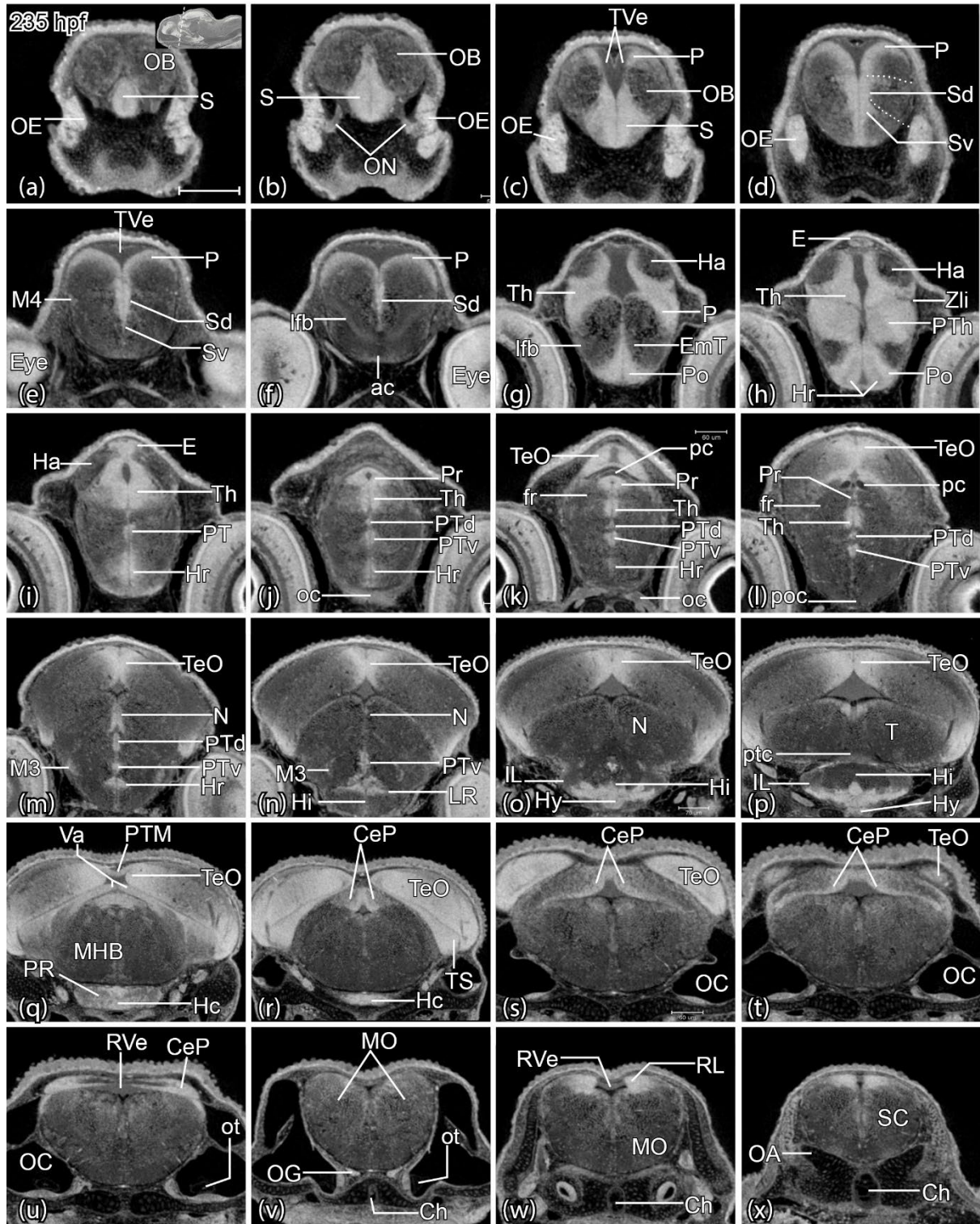


Figure 10 *Rhodnius ocellatus*, brain cross-sectional anatomy, stage long-pec, 235 hpf. (a-x) microCT images, virtual sections, transverse plane, dorsal towards the top, sections go from rostral to caudal, direction of section plane indicated in inset in (a). For annotations, see Table 2 List of Abbreviations. Scale bars = 100 μ m.

zones of pallial proliferation consist of a few cell rows, and are visible as a pair of arches flanking the dorsal subpallium (Figure 7c, 8c, 9d, 10c). The telencephalic migrated area (M4) was recognizable as nonventricular proliferation cell clusters at the margin of the lateral subpallium (Figure 10e).

Immediately caudal to the subpallium, the anterior commissure (ac) and the lateral fore-brain bundle (lfb) appeared as a dark fiber bundle crossing the rostral end of the forebrain (Figure 7e,f, 8d,e, 9d,e, 10f). We define the anterior commissure (ac) and the postoptic commissure (poc) as the boundaries of the preoptic region (Po) in this study. This region recently also has been considered the alar hypothalamus (aHyp) or the optic recess region (ORR) (Affaticati et al., 2015; Schredelseker and Driever, 2020; Slack, 2005). The proliferation zone of the preoptic region (Po) was easy to identify based on its triangular shape that surrounded the optic recess. The Po proliferation zone was broad on its ventral side and thins out dorsally (Figure 7f, 8e, 9e, 10g). The optic chiasma (oc) which has a bright, thick appearance, decussates in the midline (Figure 7h, 8h, 9h, 10j); it marks the anterior end of the neural axis.

In the basal hypothalamic region, the hypophysis topologically locates acroterminal (anterior) to the hypothalamus (Figure 2). It projects from the ventral midline of the brain (Figure 2). Like in the zebrafish developmental brain atlas, we divided the basal hypothalamus into the following regions: (i) the intermediate hypothalamus (Hi) near the hypophysis and including the inferior lobe (IL); (ii) the rostral hypothalamus (Hr) near the rostral end; and (iii) the caudal hypothalamus (Hc) near the caudal end. The hypothalamus encloses the hypothalamic ventricles including the lateral recess (LR) in the Hi and posterior recess (PR) in the Hc. This division is consistent with those classically used for describing the zebrafish hypothalamus (Wullimann et al., 1996; Manoli and Driever, 2014; Biran et al., 2015; Mueller and Wullimann, 2016; Muthu et al., 2016).

However, it should be noted that recent molecular studies in zebrafish improved the comparative interpretation of the teleostean hypothalamus and its evolutionary relationships with the mammalian hypothalamus (Baeuml et al., 2019; Herget et al., 2014). Likewise, gene expression in the PR tuberal region of embryonic zebrafish revealed homology with two domains of the mammalian hypothalamus, the TuV (tuberal region, ventral part) and TuI (tuberal region, intermedia part). Therefore, Schredelseker and Driever (2020) proposed to refer to this region as PRR (posterior recess region) to show its teleost specific phylogeny. Due to the fact, that our analysis in the rosy bitterling is based on purely anatomical microCT data, however, we were not able to relate our findings with those recent ones. For this purpose, future studies are required that analyze appropriate gene expression patterns in bitterlings.

Diencephalon

The prosomeric model divides the diencephalon, from caudal to rostral, into alar and basal plate derivatives. In this model, the pretectum (aP1), the thalamus proper (aP2), and the prethalamus (aP3) form the alar plate portions of the diencephalon (Lauter et al., 2013). In contrast, the proliferation zones of the nucleus of the medial longitudinal fasciculus (N; bP1), and the dorsal (bP2) and ventral (bP3) posterior tegmentum (PT; Mueller and Wullimann, 2005, 2016) form the corresponding basal plate derivatives.

Along the roof plate of the diencephalon, the most prominent structure is the epiphysis (E), a swelling in the dorsal midline of the brain (Figure 7h, 8g, 9j, 10i). The habenular nuclei (Ha) are located one each side of it (Figure 7h, 8g, 9i, 10i) and show discrete cell clusters from the pec-bud stage (185 hpf) onwards (Figure 8g). Notice that the fasciculus retroflexus (fr) appeared in our microCT photographs in the form of distinctive, dark fiber-bundles in the gray matter (Figure 10k, i). It originates from the habenular nuclei and connects to the interpeduncular nucleus across isthmus (r0) and rhombomere 1 (Akle et al., 2012). In the prosomeric model, the fasciculus retroflexus is used to delimit pretegmentum (P1) and thalamus (P2; Akle et al., 2012; Lauter et al., 2013; Puellas, 2019). We use the caudal end of the posterior commissure as the caudal boundary of the pretegmentum (P1), which divides the diencephalic area and the mesencephalic area (Figure 7j, 8h, 9l, 10k)

In the thalamic region, we identified the zona limitans intrathalamica (Zli) as a dark band (Figure 7i, 8f, 9i, 10h) that marks out the boundary between prethalamus (P3) and thalamus (P2). Therefore, we annotated the separate periventricular proliferation zones of prethalamus (PTh) and thalamus (Th) in the transverse virtual section based on their topological relationships (anterior vs. posterior) and Zli landmark (e.g., Figure 10j).

The thalamic eminence (EmT) is a relatively complex region of in the diencephalon and most often viewed in the prosomeric model as anterior portion of the prethalamus (hence often termed “prethalamic eminence”, PThE). However, while the EmT (or PThE) generates glutamatergic derivatives, the prethalamus proper forms predominantly GABAergic territories. In addition, some recent studies in zebrafish and tetrapods indicated that the EmT/PThE contributes to telencephalic territories such as the medial extended amygdala and newly identified nucleus of the lateral olfactory tract (Alonso et al., 2020; Porter and Mueller, 2020; Vicario et al., 2017). Due to the lack of molecular expression patterns, we stayed conservative in our analyses and placed the EmT topologically anterior to the prethalamus and posterior to the preoptic region similar as has been described for larval zebrafish (Wullimann and Mueller, 2004). It abuts the lateral forebrain bundle (Mueller, 2012) which is identifiable in our CT scans (Figure 7f, 8e, 9e, 10f). Molecular markers such as Tbr-1 are needed to validate our annotations (Wullimann, 2009; Wullimann and Mueller, 2004).

Note that the PT has distinct PTd and PTv proliferation zones (eg. Figure 10k). The neural axis is flexed here (i.e., at the cephalic flexure) and so the dorsal-ventral topology, in the virtual transverse sections, actually corresponds to the anterior-posterior axis of the neural tube.

Mesencephalon and rhombencephalon

The boundary between the diencephalon and mesencephalon defined dorsally by the posterior end of the posterior commissure and ventrally by anterior margin of the oculomotor nerve root (Moreno et al., 2016). In the tegmentum, we were able to identify the oculomotor nerve (III), which typically projects ventrolaterally from the oculomotor nucleus (NIII) and exits at the ventral surface of the brain (e.g., Figure 7n and o). The proliferation cluster of the oculomotor nucleus (NIII), and the basal plate of the mesencephalon, are thereby demarcated.

In the prosomeric model, the mesencephalon contains two mesomeres, m1 and m2 from anterior to posterior. the tectal gray, optic tectum (mammalian superior colliculus), and torus semicircularis (mammalian inferior colliculus) constitute thealar plate of m1. The oculomotor nucleus (NIII) represents the basal plate of m1.

We noticed two pairs of tectal membrane thickenings which invaginate into the tectal ventricle toward the tegmentum at the 1-ovl/pec-bud stage on 165 hpf (Figure 7q and r). During development, the boundaries between these thickenings gradually disappears as they growth together (Figure 8o and 9o). The tectal proliferation zones are distinct. At the 1-ovl/pec-bud stage (165 hpf) and the pec-bud stage (185 hpf), the tectal region appears as a large, bright field with the microCT (Figure 7o and 8l). Beginning with the high-pec stage (210 hpf), the rostral tectal proliferation becomes restricted to one mediadorsal cluster and two bilateral clusters (Figure 9o and 10n). These lateral and medial proliferation zones merge in the midline at caudal levels and form a continuous cap of tectal proliferation (e.g., Figure 9t).

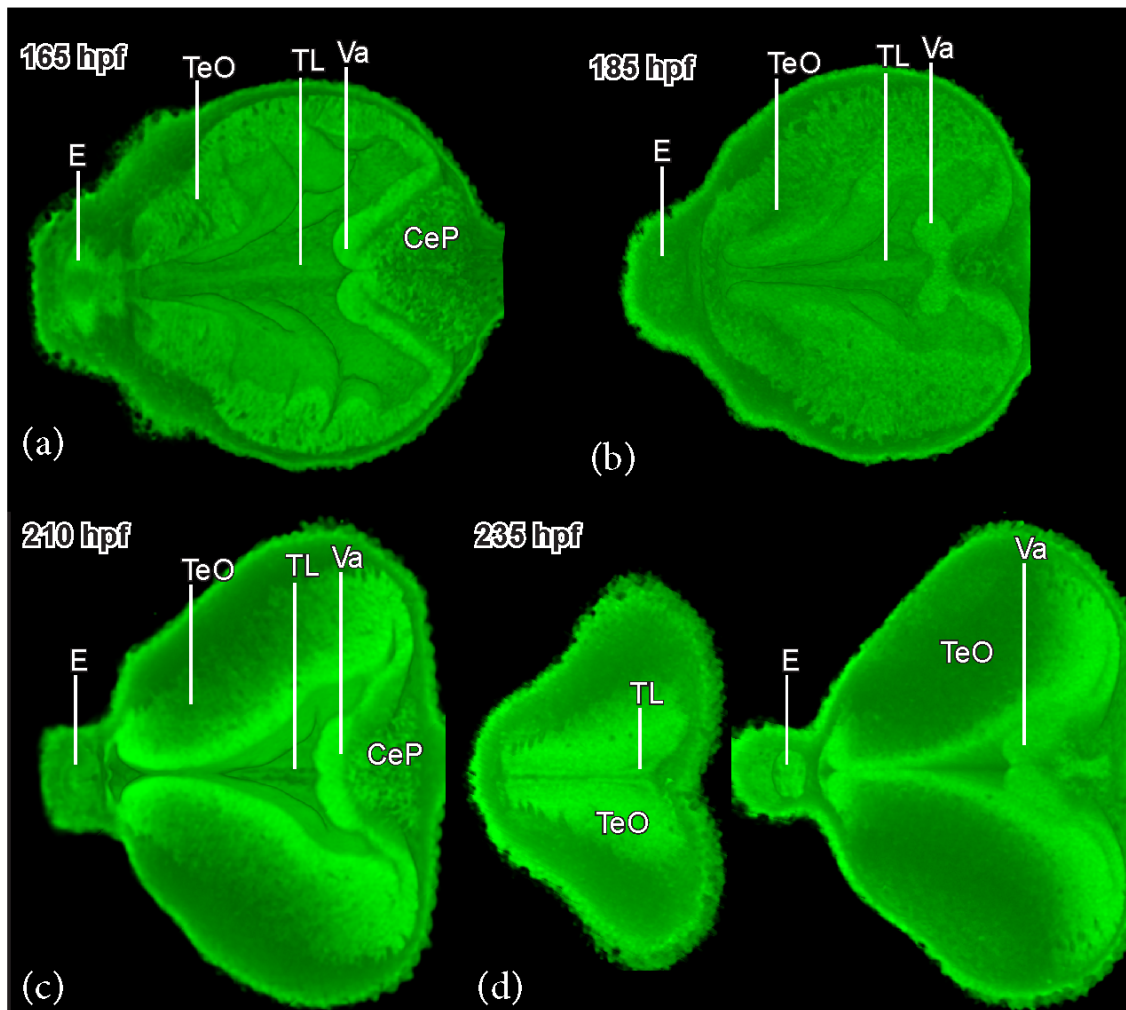


Figure 11 *Rhodeus ocellatus*, development of the torus longitudinalis. Virtual dissection, head to the left. (a) stage 1-ovl/pec-bud, 165 hpf. (b) stage pec-bud, 185 hpf. (c) stage high-pec, 210 hpf. (d) stage long-pec, 235 hpf. For annotations, see Table 2 List of Abbreviations.

The torus longitudinalis (TL) is a specialized brain region exclusive to ray-finned fish (Folgueira et al., 2020; Wullimann, 1994). We identified the TL from rostral to caudal along the medial margins of the optic tectum. Virtual horizontal sections through the optic tectum horizontally from the level of epiphysis and the rostral cerebellar thickening, revealed the TL can be seen at the top of the mesencephalic ventricle (Figure 11).

The r0, or isthmus, is at the midbrain-hindbrain boundary (MHB) region. The MHB is composed of the posterior tectal membrane and the rostral cerebellar thickenings (the valvula cerebelli; Wullmann and Knipp, 2000); appeared bright throughout the developmental period (Figure 7r, 8q, 9r, 10q). The cerebellar plate appeared bright only at its basal and medial aspects (e.g., Figure 10t and u). The trochlear nucleus (NIV) topologically belongs to r0. It is easier to identify the trochlear decussation (DIV) and the commissure cerebelli (Ccer) in the midsagittal section (Figure 12a-d) in the valvula cerebelli (Va). Then follow the caudolaterally projection of the trochlear axon in the horizontal section (Figure 12e) until it exits the brain as the trochlear nerve (IV, Figure 12f) between torus semicircularis and rhombencephalon. The axon tract of the trochlear nucleus delineates the boundary between r0 and r1.

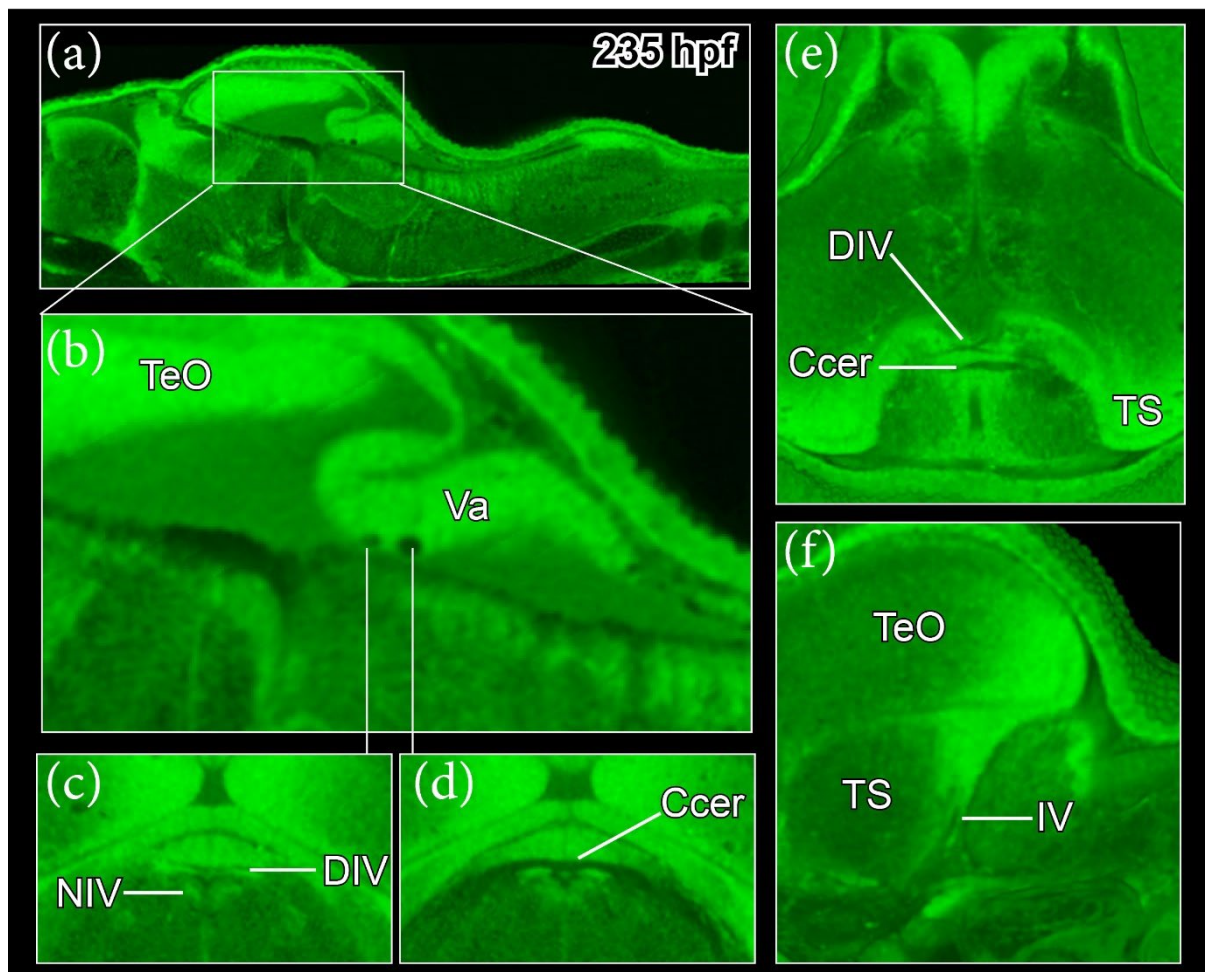


Figure 12 *Rhodeus ocellatus*, trochlear nerve, stage long-pec, 235 hpf. (a-f) microCT images, virtual sections. (a and b) midsagittal plane, head to the left, dorsal towards the top. (c and d) transverse plane, dorsal towards the top. (e) horizontal plane, head towards the top. (f) parasagittal plane, head to the left, dorsal towards the top. For annotations, see Table 2 List of Abbreviations.

The fasciculus retroflexus (fr) of teleosts innervates the interpeduncular nucleus (NIn). Thus, we used the white matter tract of the fr to identify the NIn in the bitterling embryo (Figure 13a). According to Lorente-Cánovas et al. (2012), the interpeduncular nucleus is at the basal plate across isthmus (r0) and r1. The r1 is devoid of cranial motor neurons (Nieuwenhuys and Puelles, 2016), therefore, we used the posterior margin of the interpeduncular nucleus as a landmark for the boundary between r1 and r2.

In the more caudal rhombencephalic region, the roof plate is a thin layer of tela choroidea, which is visible in microCT scans because it remains intact during the procedure (e.g., Figure 7x). The dorsal medullary proliferation zone is broad and expands ventrally up to the high-pec stage on 210 hpf (Figure 7v, 8v, and 9v), but at the long-pec stage (235 hpf) it becomes more restricted, forming the rhombic lip proliferation zone (Figure 10w).

The boundaries between rhombomeres from r2 to r8 are visible in early bitterling embryos at 135 hpf (Figure 14), but soon become less visible at least from the 1-ovl/pec fin stage at 165 hpf. However, teleost fish retain a segmented pattern of reticulospinal neurons through embryonic to adult (Gilland et al., 2014). For example, the large bilateral Mauthner neurons (M) is the marker of r4 (Eaton and Farley, 1973; Moens and Prince, 2002). By slicing the embryo of 135 hpf at the transverse level of r4, it is determined that the Mauthner cell reside near the central of rhombomere 4 rather than at the segmental boundaries (Figure 14). The rhombomeric segments of the older embryo (235 hpf, Figure 13a to k) were thereby identified by assuming that each reticulospinal neuronal cluster is located in the center of each rhombomeres.

The nerve roots of the cranial nerves are also reliable landmarks of rhombomeres. By tracing the projection of cranial nerves, we identified the trigeminal nerve root (V) in r2 (Figure 13e), the facial (VII) and the accompanying vestibulo-cochlear nerves in r4 (Figure 13g), the abducens root (VI) in r5 (Figure 13h), the glossopharyngeal root (IX) in r7 (Figure 13j), and the vagus root (X) in r8 (Figure 13k). The r2 was also labeled by somata of the anterior trigeminal motor neuron (NVa, Figure 13e) and the r3 by the posterior trigeminal motor neuron (NVp, Figure 13f). The facial motor neuron (NVII) is distinct in r6 (Figure 13i).

DISCUSSION

Brain imaging and 3D visualization of neuroanatomy

To gain insight into the complex morphogenesis of the bitterling brain, we analyzed the formation of the brain ventricular system in 3D from the stage 1-ovl (150 hpf) to long-pec (235 hpf) of bitterling development. We combined annotations of brain functional subdivisions and morphological landmarks, based on microCT scanning results and on the literature for the zebrafish embryo. We found that 3D visualization with microCT scanning protocols were extremely useful for the study of the rosy bitterling and provide an updating of imaging modalities for morphological and anatomical analyses in this non-model organism. A systematic application of microCT may help provide an essential foundation for future comparative studies of the teleost brain.

Our study provides 3D reconstruction of brain ventricles in the bitterling, showing similar organization to the zebrafish larval ventricular system as visualized by dye-injection into the hindbrain ventricle (Lowery and Sive, 2005). We have also defined boundaries of brain ventricle subdivisions based on published anatomical landmarks (Turner et al., 2012). Furthermore, we found that the flexure of the neuraxis is easily visualized continuously from the rostral tip of the brain to the spinal cord. Understanding the cephalic flexure is crucial because it has a drastic effect on the topology of the brain, especially in the highly complex secondary prosencephalon (Hauptmann and Gerster, 2000; Puellas, 2019). It has been shown that the mechanism of brain ventricle development is highly con-

versed across vertebrate (Lowery and Sive, 2009). The cerebrospinal fluid in the brain ventricular system could contribute to specialization of the early brain because the production and flow of cerebrospinal fluid performs an important role in homeostasis of the central nervous system (Fame et al., 2016).

In contrast to other vertebrates, actinopterygian fish like teleosts lack a pair of lateral ventricles in the telencephalon (Wullimann and Rink, 2002). Instead, they show a T-shaped midline telencephalic ventricle that is the result of a morphogenetic process called 'eversion' (Mueller and Wullimann, 2009). Our 3D models showed that in the rosy bitterling, the anterior intraencephalic sulcus (AIS) develops much earlier than the eversion of the telencephalic ventricle, and expansion of the dorsal ventricular surface of the AIS is synchronous with the eversion process. Our results are consistent with the telencephalic ventricle morphogenesis described in zebrafish (Folgueira et al., 2012). Initially, we could visualize the generation of the deep ventricular sulcus (AIS); followed by an anterolateral eversion of the telencephalic neuroepithelium.

We found distinct periventricular cell clusters in the gray matter with higher greyscale values than the surrounding tissue. Their distribution pattern was highly consistent with the distribution of proliferation zones described during neurogenesis of zebrafish (Mueller and Wullimann, 2003; Mueller and Wullimann, 2016; Mueller et al., 2006; Wullimann, 2009; Wullimann and Knipp, 2000; Wullimann and Mueller, 2004). It is possible, for example, that newly postmitotic neurons appear brighter than most of the postmitotic cell masses in more peripheral positions, remote from the periventricular proliferation zones. The result of immunohistochemistry for the neurotransmitter GABA (γ -aminobutyric acid) in zebrafish (Mueller and Wullimann, 2016; Mueller et al., 2006; Panganiban and Rubenstein, 2002), and PCNA (proliferation cell nuclear antigen) for proliferation patterns (Wullimann and Knipp, 2000; Wullimann and Mueller, 2004; Wullimann and Puelles, 1999) are consistent with our interpretation of the proliferation zones.

This study will hopefully pave the way to more detailed analyses of the bitterling brain. We hope that it will also prove valuable in studies using the growing number of fish models (and even non-fish models). Application of microCT 3D imaging provides a heuristic model of the brain, an extremely complex anatomical region. Importantly, our approach is validated by the fact that the profile of CT values displayed here in the bitterling brain are consistent with genoarchitecture identified in previous neurodevelopmental studies. For example, our annotation of the zona limitans intrathalamica (ZLI) is extremely close to the highly conserved expression pattern of the gene *sonic hedgehog* (*shh*; Vieira et al., 2005; Mueller et al., 2006; Scholpp et al., 2006). In addition, microCT allows time-efficient imaging of intact brains while providing a resolution (micron level) sufficient for displaying critical landmarks, groups of neurons such as proliferation zones versus postmitotic cell masses and white matter tracts. These histological characteristics are critical for detecting landmarks and visualize structural features as means to describe developmental neuroanatomy. However, the resolution of microCT is inferior to light microscopy of either histological brain sections or light sheet microscopy-based imaging of fluorescence-stained intact brains. It is also lower resolution than Synchrotron imaging, whose resolution reaches the sub-micron level, and therefore permits quantitative histological phenotyping (Ding et al., 2019). Neurons and neuropils in the central nervous system can be selectively stained with the salts of metallic elements including gold, silver, platinum and mercury chloride

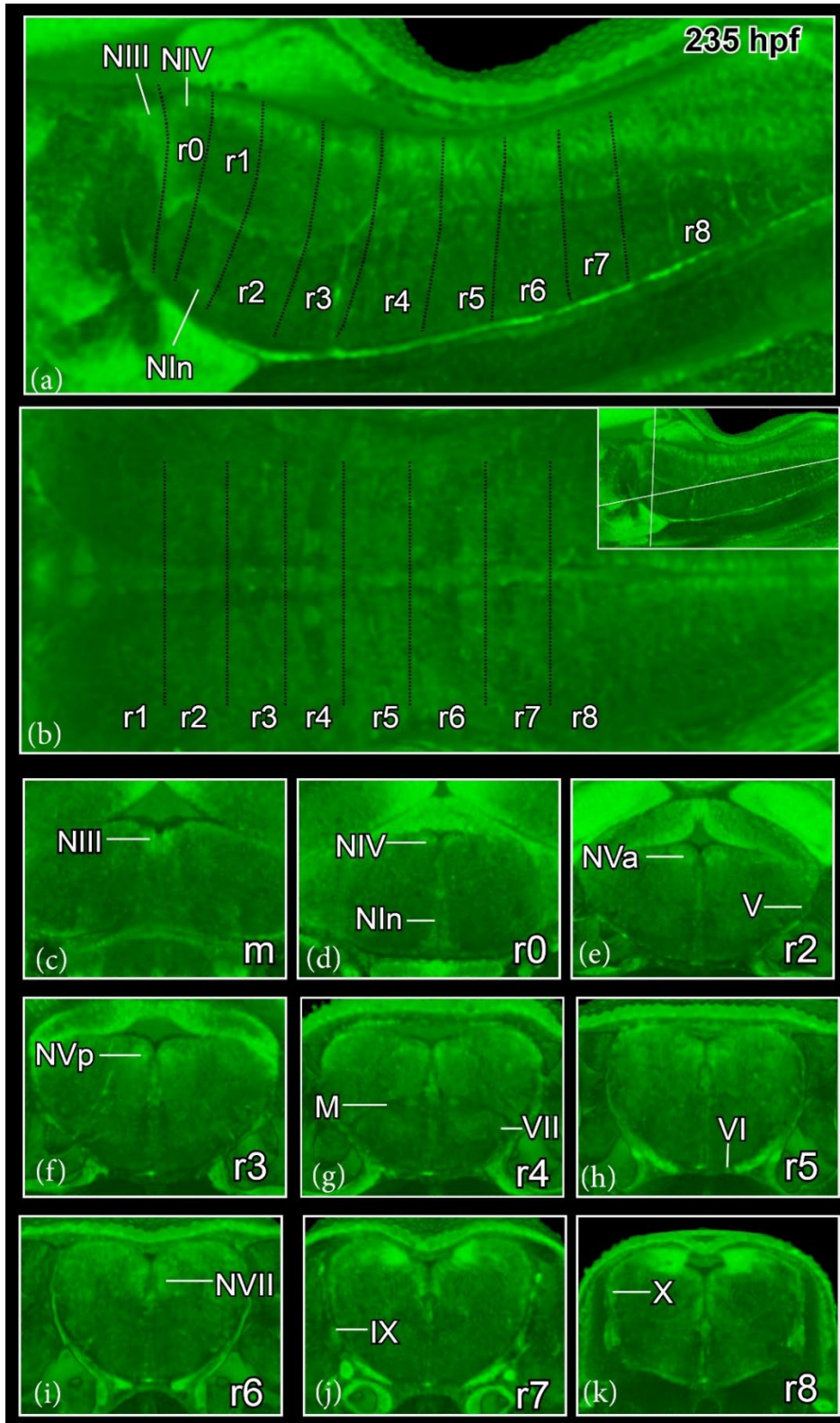


Figure 13 *Rhodnius ocellatus*, hindbrain segmentation, stage long-pec, 235 hpf. (a) microCT images, virtual sections, midsagittal plane, dorsal towards the top, head to the left. The black dash line indicates the rhombomeric boundaries. (b) horizontal plane, head to the left, direction of section plane indicated in inset at the upper right corner. (c-k) transverse plane, dorsal towards the top, sections go from the rostral to caudal, direction of section plane indicated in inset in (b). For annotations, see Table 2 List of Abbreviations.

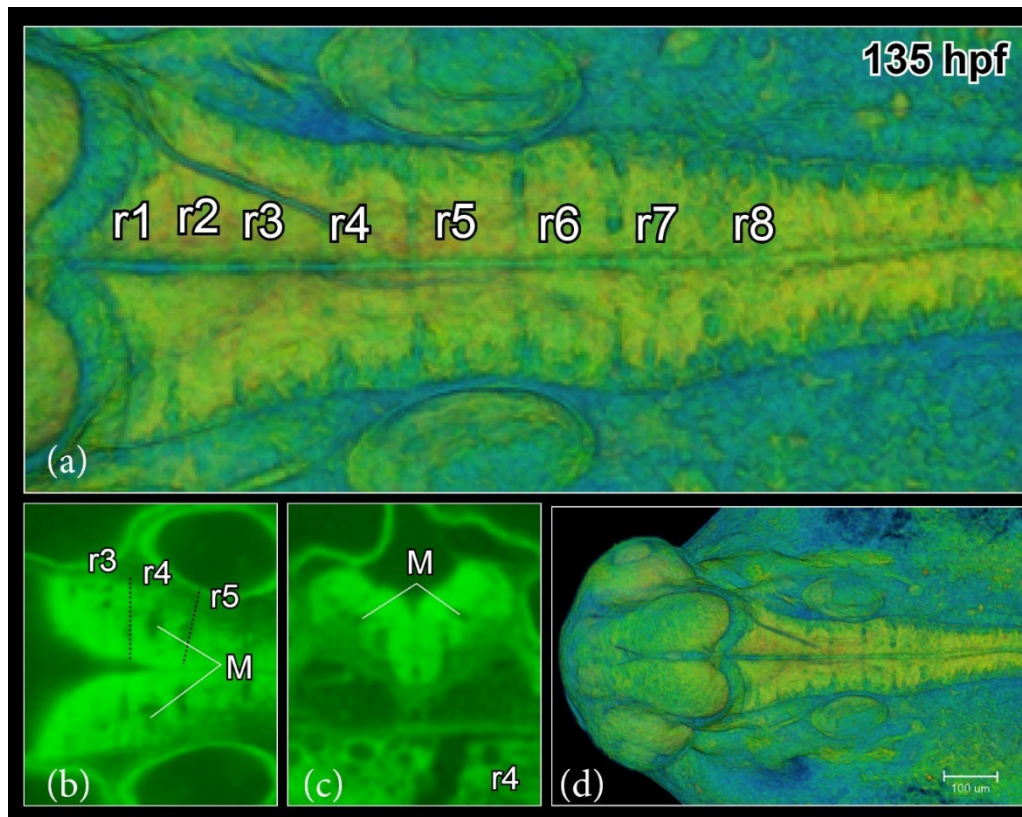


Figure 14 *Rhodeus ocellatus*, hindbrain segmentation, 135 hpf. (a and d) microCT images, volume rendering, show boundaries between rhombomeres. (b) virtual section, horizontal plane, head to the left, show the location of the Mauthner cell at the centre of r4. (c) virtual section, transverse plane, dorsal towards the top. For annotations, see Table 2 List of Abbreviations.

(Keklikoglou et al., 2019; Mizutani and Suzuki, 2012), which can compensate for the inability to use antibodies in combination with microCT. In summary, MicroCT imaging produces lower resolution than some imaging modalities, but has the special advantage that complex 3D models can be produced without the need for time-consuming reconstruction from histological material. The specimens imaged with microCT can be subsequently run through paraffin histology if needed.

Comparison of developmental stages between bitterling and zebrafish

The phylogenetic relationship of the rosy bitterling and the well-studied zebrafish are very close (Cypriniformes: Cyprinidae; Mayden et al., 2009). It allows for a relatively straight forward interspecies comparison of their brain development. The process of brain ventricle inflation, flexion of the neuroaxis, and establishment of prosomeric units, happens in bitterling as the same as in the zebrafish. Specifically, the 165 hpf bitterling brain and 30 hpf zebrafish brain are in the same process of brain ventricle inflation and have a similar degree of flexion of the neuroaxis. We noticed stratification of the proliferation zones of the diencephalic region (Pr, Th, PTd, PTv) is consistent between the 185 hpf bitterling brain and 36 hpf zebrafish brain.

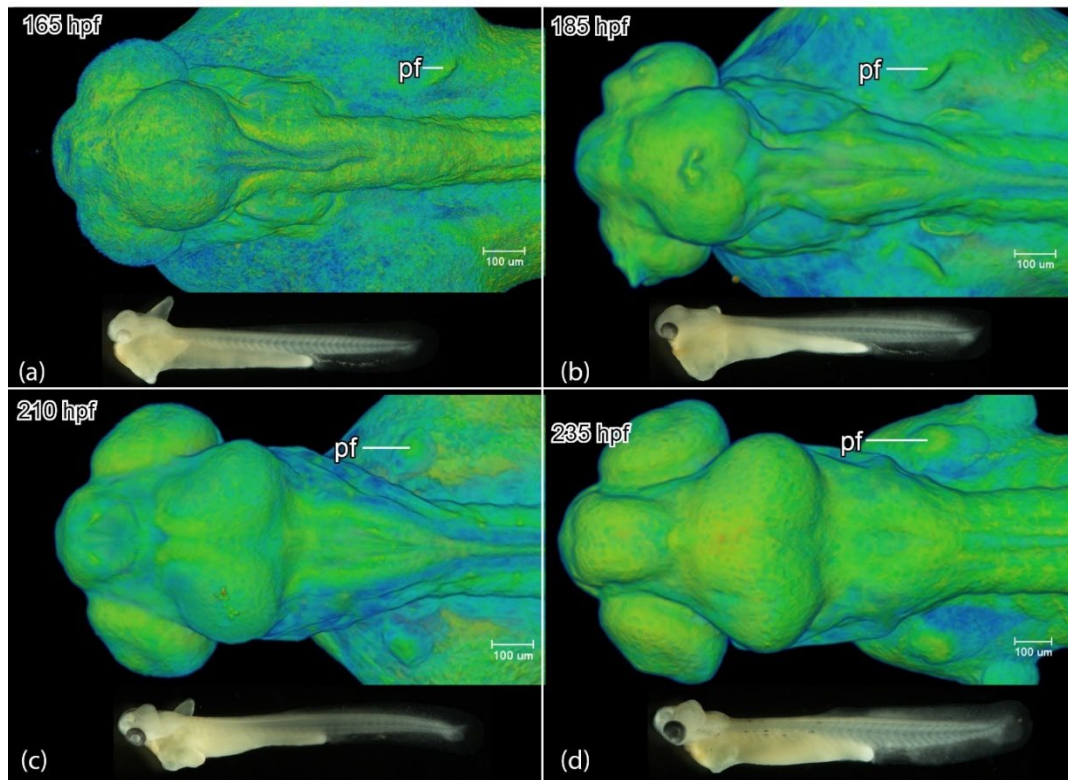


Figure 15 *Rhodeus ocellatus*, development of the brain region and the pectoral fin bud. Dorsal view of the head region microCT images, pseudo-colored volume-renderings, rostral to the left. Lateral view of the embryo, photomicrographs, rostral to the left. (a) 1-ovl/pec-bud, 165 hpf; (b) pec-bud, 185 hpf; (c) high-pec, 210 hpf; (d) long-pec 235 hpf. For annotations, see Table 2 List of Abbreviations.

However, distinct developmental heterochronies detected between bitterling and zebrafish brains. The bitterling shows precocious development of the inferior lobe and basalward extension of the lateral recess in the hypothalamic region (Figure 2): the inferior lobe is remarkable so early at the long-pec stage (235 hpf in bitterling, Figure 15; 48 hpf in zebrafish). The long-pec stage is defined by the development of the pectoral fin bud, when the pectoral fin bud of both species grows significantly to the distal end, and the bud height grows to twice of the width at the bud base (Kimmel et al., 1995; Yi et al., 2021). In zebrafish, the inferior lobe has not developed at the long-pec stage; it is identifiable until 5 days post fertilization (Bloch et al., 2019). In teleost fish, the inferior lobe is known as a multi-sensory integration center that involved in gustatory (Rink and Wullimann, 1998; Wullimann, 2020), visual (Butler et al., 1991), and octavolateralis system (Yang et al., 2007). Further studies can use the detailed descriptions of the bitterling brain developmental atlas provided here, to uncover the underlying regulatory mechanisms that control such heterochronic development.

Table 2 List of Abbreviations

Abbreviation	Anatomical terms
ac	anterior commissure
AIS	anterior intraencephalic sulcus
Ccer	commissure cerebelli
CeP	cerebellar plate
Ch	notochord
DIV	trochlear decussation
DVe	diencephalic ventricle
E	epiphysis
EmT	eminencia thalami
fp	floor plate
fr	fasciculus retroflexus
GM	gray matter
Ha	habenula
Hc	caudal hypothalamus
Hi	intermediate hypothalamus
Hr	rostral hypothalamus
Hy	hypophysis
III	oculomotor nerve
IL	inferior lobe of hypothalamus
IV	trochlear nerve
IX	glossopharyngeal nerve
le	lens
lfb	lateral forebrain bundle
LR	lateral recess of hypothalamic ventricle
lr	lateral rectus muscle
M	Mauthner neurons
M1	pretectal migrated area
M2	posterior tubercular migrated area
M3	EmT migrated area
M4	telencephalic migrated area
MHB	midbrain-hindbrain boundary
mlf	medial longitudinal fascicle
mou	mouth
MV	median ventricle of the mesencephalic ventricle
MVS	median ventricular sulcus of the mesencephalic ventricle
N	region of the nucleus of the medial longitudinal fascicle
NIII	oculomotor nucleus
NIn	interpeduncular nucleus
NIV	trochlear nucleus
NVa	rostral trigeminal motor neuron
NVII	facial motor neuron
NVp	caudal trigeminal motor neuron
OA	occipital arch
OB	olfactory bulb
oc	optic chiasma
OC	otic capsule

OE	olfactory epithelium
of	oval fossae
OG	octaval ganglion (VIII)
ON	olfactory nerve
on	optic nerve
ot	otolith
P	pallium
pc	posterior commissure
pf	pectoral fin
Po	preoptic region
poc	postoptic commissure
PoR	preoptic recess
PR	posterior recess of hypothalamic ventricle
Pr	pretectum
ptc	posterior tubercular commissure
PTd	dorsal part of posterior tuberculum
PTH	prethalamus
PTM	posterior tectal membrane
PTv	ventral part of posterior tuberculum
r	rhombomere
re	retina
RL	rhombic lip
RVe	rhombencephalic ventricle
S	subpallium
SC	spinal cord
Sd	dorsal subpallium
sr	superior rectus muscle
Sv	ventral subpallium
T	midbrain tegmentum
tc	tela choroidea
Tel	telencephalon
TeO	tectum opticum
TeVe	tectal ventricle
Th	thalamus
TL	torus longitudinalis
tpc	tract of posterior commissure
TS	torus semicircularis
TVe	telencephalic ventricle
V	trigeminal nerve
Va	valvula cerebelli
VI	abducens nerve
VII	facial nerve
WM	white matter
X	vagus nerve
Zli	zona limitans intrathalamica

References

- Affaticati, P., Yamamoto, K., Rizzi, B., Bureau, C., Peyri ras, N., Pasqualini, C., Demarque, M. and Vernier, P.** (2015). Identification of the optic recess region as a morphogenetic entity in the zebrafish forebrain. *Sci. Rep.* **5**, 8738.
- Akle, V., Guelin, E., Yu, L., Brassard-Giordano, H., Slack, B. E. and Zhdanova, I. V.** (2012). F-Spondin/spon1b Expression Patterns in Developing and Adult Zebrafish. *PLoS One* **7**, e37593.
- Aldridge, D. C.** (1999). Development of European bitterling in the gills of freshwater mussels. *J. Fish Biol.* **54**, 138–151.
- Alonso, A., Trujillo, C. M. and Puelles, L.** (2020). Longitudinal developmental analysis of prethalamic eminence derivatives in the chick by mapping of Tbr1 in situ expression. *Brain Struct. Funct.* **225**, 481–510.
- Babaei, F., Hong, T. L. C., Yeung, K., Cheng, S. H. and Lam, Y. W.** (2016). Contrast-Enhanced X-Ray Micro-Computed Tomography as a Versatile Method for Anatomical Studies of Adult Zebrafish. *Zebrafish* **13**, 310–316.
- Baeuml, S. W., Biechl, D. and Wullimann, M. F.** (2019). Adult islet1 Expression Outlines Ventralized Derivatives Along Zebrafish Neuraxis. *Front. Neuroanat.* **13**, 19.
- Bloch, S., Thomas, M., Colin, I., Galant, S., Machado, E., Affaticati, P., Jenett, A. and Yamamoto, K.** (2019). Mesencephalic origin of the inferior lobe in zebrafish. *BMC Biol.* **17**, 22.
- Boeseman, M. J., Van der Drift, J., Van Roon, J. M., Tinbergen, N. and Ter Pelkwijk, J. J.** (1938). De bittervoorns en hun mossels. *Levende Nat.* **43**, 129–136.
- Butler, A. B., Wullimann, M. F. and Northcutt, R. G.** (1991). Comparative cytoarchitectonic analysis of some visual pretectal nuclei in teleosts. *Brain. Behav. Evol.* **38**, 92–114.
- Cambronero, F. and Puelles, L.** (2000). Rostrocaudal nuclear relationships in the avian medulla oblongata: A fate map with quail chick chimeras. *J. Comp. Neurol.* **427**, 522–545.
- Chang, H. W.** (1948). Life history of the common Chinese bitterling, *Rhodeus ocellatus*. *Sinensia* **19**, 12–22.
- Ding, Y., Vanselow, D. J., Yakovlev, M. A., Katz, S. R., Lin, A. Y., Clark, D. P., Vargas, P., Xin, X., Copper, J. E., Canfield, V. A., et al.** (2019). Computational 3D histological phenotyping of whole zebrafish by X-ray histotomography. *Elife* **8**, e44898.
- Duyven  de Wit, J.** (1955). Some results of investigations into the European Bitterling, *Rhodeus amarus* BLOCH. *Japanese J. Ichthyology* **4**, 94–104.
- Dynes, J. L. and Ngai, J.** (1998). Pathfinding of olfactory neuron axons to stereotyped glomerular targets revealed by dynamic imaging in living zebrafish embryos. *Neuron* **20**, 1081–1091.
- Eaton, R. C. and Farley, R. D.** (1973). Development of the Mauthner Neurons in Embryos and Larvae of the Zebrafish, *Brachydanio rerio*. **1973**, 673–682.
- Fame, R. M., Chang, J. T., Hong, A., Aponte-Santiago, N. A. and Sive, H.** (2016). Directional cerebrospinal fluid movement between brain ventricles in larval zebrafish. *Fluids Barriers CNS* **13**, 11.
- Folgueira, M., Bayley, P., Navratilova, P., Becker, T. S., Wilson, S. W. and Clarke, J. D. W.** (2012). Morphogenesis underlying the development of the everted teleost telencephalon. *Neural Dev.* **7**, 32.
- Folgueira, M., Riva-Mendoza, S., Ferre o-Galm n, N., Castro, A., Bianco, I. H., Anad n, R. and Y nez, J.** (2020). Anatomy and Connectivity of the Torus Longitudinalis of the Adult Zebrafish. *Front. Neural Circuits* **14**, 1–20.
- Garc a-Lecea, M., Gasanov, E., Jedrychowska, J., Kondrychyn, I., Teh, C., You, M.-S. and Korzh, V.** (2017). Development of Circumventricular Organs in the Mirror of Zebrafish Enhancer-Trap Transgenics. *Front. Neuroanat.* **11**, 114.
- Gilland, E., Straka, H., Wong, T. W., Baker, R. and Zottoli, S. J.** (2014). A hindbrain segmental scaffold specifying neuronal location in the adult goldfish, *Carassius auratus*. *J. Comp. Neurol.* **522**, 2446–2464.
- Hauptmann, G. and Gerster, T.** (2000). Regulatory gene expression patterns reveal transverse and longitudinal subdivisions of the embryonic zebrafish forebrain. *Mech. Dev.* **91**, 105–118.
- Herget, U., Wolf, A., Wullimann, M. F. and Ryu, S.** (2014). Molecular neuroanatomy and chemoarchitecture of the neurosecretory preoptic-hypothalamic area in zebrafish larvae. *J. Comp. Neurol.* **522**, 1542–1564.
- His Wilhelm** (1895). *Die anatomische Nomenclatur. Nomina anatomica*. Veit.
- Keklikoglou, K., Faulwetter, S., Chatzinikolaou, E., Wils, P., Brecko, J., Kva ek, J., Metscher, B. and Arvanitidis, C.** (2019). Micro-computed tomography for natural history specimens: a handbook of best practice protocols. *Eur. J. Taxon.* **522**, 1–55.
- Kimmel, C. B., Ballard, W. W., Kimmel, S. R., Ullmann, B. and Schilling, T. F.** (1995). Stages of embryonic development of the zebrafish. *Dev. Dyn.* **203**, 253–310.

- Kitamura, J., Nagata, N., Nakajima, J. and Sota, T.** (2012). Divergence of ovipositor length and egg shape in a brood parasitic bitterling fish through the use of different mussel hosts. *J. Evol. Biol.* **25**, 566–573.
- Korzh, V.** (2018). Development of brain ventricular system. *Cell. Mol. Life Sci.* **75**, 375–383.
- Lauter, G., Söll, I. and Hauptmann, G.** (2013). Molecular characterization of prosomeric and intraprosomeric subdivisions of the embryonic zebrafish diencephalon. *J. Comp. Neurol.* **521**, 1093–1118.
- Lawrence, C.** (2007). The husbandry of zebrafish (*Danio rerio*): A review. *Aquaculture*.
- Liu, H. Z., Zhu, Y. R., Smith, C. and Reichard, M.** (2006). Evidence of host specificity and congruence between phylogenies of bitterling and freshwater mussels. *Zool. Stud.* **45**, 428–434.
- Lorente-Cánovas, B., Marín, F., Corral-San-Miguel, R., Hidalgo-Sánchez, M., Ferrán, J. L., Puellas, L. and Aroca, P.** (2012). Multiple origins, migratory paths and molecular profiles of cells populating the avian interpeduncular nucleus. *Dev. Biol.* **361**, 12–26.
- Lowery, L. A. and Sive, H.** (2005). Initial formation of zebrafish brain ventricles occurs independently of circulation and requires the *nanog* and *snakehead/atp1a1a.1* gene products. *Development* **132**, 2057–2067.
- Lowery, L. A. and Sive, H.** (2009). Totally tubular: the mystery behind function and origin of the brain ventricular system. *BioEssays* **31**, 446–458.
- Ma, L. H., Punnamoottil, B., Rinkwitz, S. and Baker, R.** (2009). Mosaic *hoxb4a* neuronal pleiotropism in zebrafish caudal hindbrain. *PLoS One* **4**, e5944.
- Mayden, R. L., Chen, W.-J., Bart, H. L., Doosey, M. H., Simons, A. M., Tang, K. L., Wood, R. M., Agnew, M. K., Yang, L., Hirt, M. V., et al.** (2009). Reconstructing the phylogenetic relationships of the earth's most diverse clade of freshwater fishes—order Cypriniformes (Actinopterygii: Ostariophysi): A case study using multiple nuclear loci and the mitochondrial genome. *Mol. Phylogenet. Evol.* **51**, 500–514.
- Metscher, B. D.** (2009a). MicroCT for comparative morphology: simple staining methods allow high-contrast 3D imaging of diverse non-mineralized animal tissues. *BMC Physiol.* **9**, 11.
- Metscher, B. D.** (2009b). MicroCT for developmental biology: a versatile tool for high-contrast 3D imaging at histological resolutions. *Dev Dyn* **238**, 632–640.
- Mills, S. C. and Reynolds, J. D.** (2003). The bitterling-mussel interaction as a test case for co-evolution. *J. Fish Biol.* **63**, 84–104.
- Mizutani, R. and Suzuki, Y.** (2012). X-ray microtomography in biology. *Micron* **43**, 104–115.
- Moens, C. B. and Prince, V. E.** (2002). Constructing the hindbrain: Insights from the zebrafish. *Dev. Dyn.* **224**, 1–17.
- Moreno, N., Morona, R., López, J. M. and González, A.** (2016). The Diencephalon and Hypothalamus of Nonmammalian Vertebrates: Evolutionary and Developmental Traits. In *Evolution of Nervous Systems: Second Edition*, pp. 409–426.
- Mueller, T.** (2012). What is the Thalamus in Zebrafish? *Front. Neurosci.* **6**, 64.
- Mueller, T. and Wullimann, M. F.** (2003). Anatomy of neurogenesis in the early zebrafish brain. *Dev. Brain Res.* **140**, 137–155.
- Mueller, T. and Wullimann, M. F.** (2009). An Evolutionary Interpretation of Teleostean Forebrain Anatomy. *Brain. Behav. Evol.* **74**, 30–42.
- Mueller, T. and Wullimann, M. F.** (2016). *Atlas of Early Zebrafish Brain Development*. Second ed. Elsevier.
- Mueller, T., Vernier, P. and Wullimann, M. F.** (2006). A phylotypic stage in vertebrate brain development: GABA cell patterns in zebrafish compared with mouse. *J. Comp. Neurol.* **494**, 620–634.
- Nagata, Y. and Miyabe, H.** (1978). Development Stages of the Bitterling, *Rhodeus ocellatus ocellatus* (Cyprinidae). *Mem. Osaka Kyoiku Univ. III, Nat. Sci. Appl. Sci.* **26**, 171–181.
- Nieuwenhuys, R. and Puellas, L.** (2016). *Towards a New Neuromorphology*. Cham: Springer International Publishing.
- Noll, C. F.** (1877). Gewohnheiten und Eierlegen des Bitterlings. *Zool. Garten* **18**, 351–379.
- Olt, A.** (1893). Lebensweise und Entwicklung des Bitterlings. *Zeitschrift für wissenschaftliche Zool.* **55**, 543–575.
- Panganiban, G. and Rubenstein, J. L. R.** (2002). Developmental functions of the *Dlx* homeobox genes. *Development* **129**, 4371–4386.
- Porter, B. A. and Mueller, T.** (2020). The Zebrafish Amygdaloid Complex – Functional Ground Plan, Molecular Delineation, and Everted Topology. *Front. Neurosci.* **14**, 608.
- Puelles, L.** (2019). Survey of Midbrain, Diencephalon, and Hypothalamus Neuroanatomic Terms Whose Prosomeric Definition Conflicts With Columnar Tradition. *Front. Neuroanat.* **13**, 20.
- Puelles, L. and Rubenstein, J. L. R.** (2003). Forebrain gene expression domains and the evolving prosomeric model. *Trends Neurosci.* **26**, 469–476.

- Rahmat, S. and Gilland, E.** (2019). Hindbrain neurovascular anatomy of adult goldfish (*Carassius auratus*). *J. Anat.* **235**, 783–793.
- Reichard, M., Liu, H. and Smith, C.** (2007). The co-evolutionary relationship between bitterling fishes and freshwater mussels: insights from interspecific comparisons. *Evol. Ecol. Res.* **9**, 239–259.
- Richardson, M. K. and Wright, G. M.** (2003). Developmental transformations in a normal series of embryos of the sea lamprey *Petromyzon marinus* (Linnaeus). *J. Morphol.* **257**, 348–363.
- Rink, E. and Wullimann, M. F.** (1998). Some forebrain connections of the gustatory system in the goldfish *Carassius auratus* visualized by separate Dil application to the hypothalamic inferior lobe and the torus lateralis. *J. Comp. Neurol.* **394**, 152–170.
- Rouchet, R., Smith, C., Liu, H. Z., Methling, C., Douda, K., Yu, D., Tang, Q. Y. and Reichard, M.** (2017). Avoidance of host resistance in the oviposition-site preferences of rose bitterling. *Evol. Ecol.* **31**, 769–783.
- Schmitz, B., Papan, C. and Campos-Ortega, J. A.** (1993). Neurulation in the anterior trunk region of the zebrafish *Brachydanio rerio*. *Roux's Arch. Dev. Biol.* **202**, 250–259.
- Scholpp, S., Wolf, O., Brand, M. and Lumsden, A.** (2006). Hedgehog signalling from the zona limitans intrathalamica orchestrates patterning of the zebrafish diencephalon. *Development* **133**, 855–864.
- Schredelseker, T. and Driever, W.** (2020). Conserved Genoarchitecture of the Basal Hypothalamus in Zebrafish Embryos. *Front. Neuroanat.* **14**, 3.
- Slack, J. M. W.** (2005). *Essential Developmental Biology (2nd ed.)*. Oxford, UK: BlackWell Publishing Ltd.
- Smith, C.** (2016). Bayesian inference supports the host selection hypothesis in explaining adaptive host specificity by European bitterling. *Oecologia* **183**, 1–11.
- Smith, C., Reichard, M., Jurajda, P. and Przybylski, M.** (2004). The reproductive ecology of the European bitterling (*Rhodeus sericeus*). *J. Zool.* **262**, 107–124.
- Turner, M. H., Ullmann, J. F. P. and Kay, A. R.** (2012). A method for detecting molecular transport within the cerebral ventricles of live zebrafish (*Danio rerio*) larvae. *J. Physiol.* **590**, 2233–2240.
- Vernier, P.** (2017). The Brains of Teleost Fishes. In *Evolution of Nervous Systems*, pp. 59–75. Elsevier.
- Vicario, A., Mendoza, E., Abellán, A., Scharff, C. and Medina, L.** (2017). Genoarchitecture of the extended amygdala in zebra finch, and expression of FoxP2 in cell corridors of different genetic profile. *Brain Struct. Funct.* **222**, 481–514.
- Vieira, C., Garda, A. L., Shimamura, K. and Martinez, S.** (2005). Thalamic development induced by Shh in the chick embryo. *Dev. Biol.* **284**, 351–363.
- Wiepkema, P. R.** (1962). An Ethological Analysis of the Reproductive Behaviour of the Bitterling (*Rhodeus Amarus* Bloch). *Arch. Néerlandaises Zool.* **14**, 103–199.
- Wong, M. D., Van Eede, M. C., Spring, S., Jevtic, S., Boughner, J. C., Lerch, J. P. and Mark Henkelman, R.** (2015). 4D Atlas of the Mouse Embryo for Precise Morphological Staging. *Dev.* **142**, 3583–3591.
- Wullimann, M. F.** (1994). The teleostean torus longitudinalis: A short review on its structure, histochemistry, connectivity, possible function and phylogeny. *Eur. J. Morphol.* **32**, 235–242.
- Wullimann, M. F.** (2009). Secondary neurogenesis and telencephalic organization in zebrafish and mice: a brief review. *Integr. Zool.* **4**, 123–133.
- Wullimann, M. F.** (2020). Neural origins of basal diencephalon in teleost fishes: Radial versus tangential migration. *J. Morphol.* **281**, 1133–1141.
- Wullimann, M. F. and Knipp, S.** (2000). Proliferation pattern changes in the zebrafish brain from embryonic through early postembryonic stages. *Anat. Embryol. (Berl.)* **202**, 385–400.
- Wullimann, M. F. and Mueller, T.** (2004). Identification and Morphogenesis of the Eminentia Thalami in the Zebrafish. *J. Comp. Neurol.* **471**, 37–48.
- Wullimann, M. F. and Puelles, L.** (1999). Postembryonic neural proliferation in the zebrafish forebrain and its relationship to prosomeric domains. *Anat. Embryol. (Berl.)* **199**, 329–348.
- Wullimann, M. F. and Rink, E.** (2002). The teleostean forebrain: A comparative and developmental view based on early proliferation, Pax6 activity and catecholaminergic organization. *Brain Res. Bull.* **57**, 363–370.
- Yang, C.-Y., Xue, H.-G., Yoshimoto, M., Ito, H., Yamamoto, N. and Ozawa, H.** (2007). Fiber connections of the corpus glomerulosum pars rotunda, with special reference to efferent projection pattern to the inferior lobe in a percomorph teleost, tilapia (*Oreochromis niloticus*). *J. Comp. Neurol.* **501**, 582–607.
- Yi, W., Rücklin, M., Poelmann, R. E., Aldridge, D. C. and Richardson, M. K.** (2021). Normal stages of embryonic development of a brood parasite, the rosy bitterling *Rhodeus ocellatus* (Teleostei: Cypriniformes). *J. Morphol.* **282**, 783–819.

Chapter 4 Spatial and temporal expression of marker genes during early brain regionalization in the rosy bitterling (*Rhodeus ocellatus*)

Wenjing Yi, Michael K. Richardson

Institute of Biology, University of Leiden, Sylvius Laboratory, Sylviusweg 72, 2333BE, Leiden, the Netherlands.

Manuscript in preparation

Abstract

During early brain development, the neural tube is partitioned into forebrain, midbrain and hind-brain regions and further subdivided into radial, longitudinal and transverse units. This regionalization is associated with the position-specific expression of developmental control genes. We investigated early brain regionalization in the rosy bitterling (*Rhodeus ocellatus*), a teleost, by examining the expression pattern of marker genes *dlx2a*, *fgf8a*, *msx3*, *pax6a*, *shha*, and *sox9b* using whole-mount *in situ* hybridization. The developmental stages examined were 10-somite, 30-somite, 5-ovl and the prim-3 stages. Our results indicate that the subdivision of brain regions has started at the 10-somite stage. At the 30-somite stage, differentiation on the DV axis has started and segmentation of the neuromeres along the AP axis is completed. At the 5-ovl and prim-3 stages, there are three and five streams of migratory neural crest cells, respectively. The cephalic flexure becomes apparent at the prim-3 stage. We compared the observed gene expression patterns in the bitterling with those in the zebrafish (*Danio rerio*). The comparison shows that transcriptional heterochrony is found between the brain and trunk region between the bitterling and the zebrafish.

Introduction

The adult brain has an extremely complex structure. None the less, features of this structure are conserved across the vertebrate subphylum. The brain develops from the embryonic neural tube (Lumsden and Krumlauf, 1996). An early sign of regionalization of the neural tube is the partitioning of its anterior end into three brain vesicles arranged in anteroposterior sequence: the forebrain (prosencephalon), midbrain (mesencephalon) and hindbrain (rhombencephalon). Subsequently, the forebrain is subdivided into the telencephalon and diencephalon, and the hindbrain is subdivided into the metencephalon and myelencephalon (Mueller and Wullimann, 2016; Puelles and Rubenstein, 2003). Further regionalization events produce prosomeres in the prosencephalon (Murakami et al., 2001; Puelles and Rubenstein, 2003) and rhombomeres 1 to 7 in the rhombencephalon (Moens and Prince, 2002; Murakami et al., 2001; Trevarrow et al., 1990). This regionalization provides the foundation for neuronal differentiation and axonal outgrowth (Hanneman et al., 1988; Mendelson, 1986; Metcalfe et al., 1986; Moens and Prince, 2002; Wilson et al., 1990).

The assignment of regional identity in the neural tube, as outlined above, is accompanied by the position-specific expression of developmental genes in so-called 'signalling centers' (Gibbs et al., 2017; Reifers et al., 1998; Rhinn and Brand, 2001). Of these, the midbrain-hindbrain boundary (MHB) or isthmus organizer (IsO) is the most extensively-studied. The MHB is composed of the posterior membrane of the tectal ventricle and the rostral cerebellar thickening (Wullimann and Knipp, 2000). The expression of the zebrafish *fgf8a* in the MHB is associated with planar induction during mes- and rhombencephalon development (Gibbs et al., 2017; Puelles, 2019; Reifers et al., 1998).

The anterior neural ridge (ANR) is a forebrain signaling center. It lies at the junction between the anterior neural plate and anterior non-neural ectoderm. The expression of *fgf8a* in the ANR is essential for induction of the telencephalon (Shanmugalingam et al., 2000). The zona limitans intrathalamica (ZLI) is a neuroepithelial domain in the alar plate of the diencephalon which separates the prethalamus from the thalamus. Expression of *shha* in the ZLI alone is sufficient for diencephalic differentiation in zebrafish (Jeong et al., 2007; Scholpp et al., 2006; Vieira et al., 2005). In the hindbrain area, r4 is the earliest rhombomere to develop; it is also a signaling center. r4 promotes the development of adjacent rhombomeres, thus supporting the propagation of hindbrain segmental patterns (Maves et al., 2002).

Spatially-restricted gene expression related to these various signaling centers define transverse and longitudinal segmental boundaries in the neural tube (Hauptmann and Gerster, 2000; Lauter et al., 2013). For example, the subdivisions of the diencephalic region can be visualized in terms of gene expression patterns. According to the *updated prosomeric model* (Puelles, 2019; Puelles and Rubenstein, 2003; Wullimann and Rink, 2002), the alar plate of the diencephalon is divided into regions called P1 (pretectum), P2 (thalamus), and P3 (prethalamus). Stable *pax6a* expression is an early marker of the pretectum as well as a P1 marker, defining the forebrain-midbrain boundary (Krauss et al., 1991a; Murakami et al., 2001; Puschel et al., 1992). The gene *dlx2a* is a P3 marker whose expression is restricted to the prethalamus, mainly in the cells of the ventricular zone (Mueller et al., 2008). The mesencephalon is devoid of *pax6a* expression. The transcription factor *sox9b*, a molecular marker for the tegmentum (Chiang et al., 2001; Li et al., 2002), is expressed on the ventral side of the mesencephalon.

In the hindbrain, several genes show segmental expression patterns. The expression domain of *pax6a* extends from r2 to the posterior hindbrain region (Krauss et al., 1991b; Puschel et al., 1992). Cranial neural crest cells are derived from adjacent r1, 2, 4, and 6. The odd-numbered r3 and 5 do not give rise to migratory neural crest cells (Graham et al., 1993). In the zebrafish, *sox9b* is expressed in neural crest progenitors; its expression is downregulated after the neural crest cells start migrating (Li et al., 2002; Plavicki et al., 2014). *dlx2a* is expressed in migratory neural crest cells (Akimenko et al., 1994; Panganiban and Rubenstein, 2002; Piotrowski and Nüsslein-Volhard, 2000). Its expression marks out distinct segmented streams of neural crest cells migrating towards the primordia of all seven pharyngeal arches (Rocha et al., 2020).

Highly conserved gene expression patterns are the foundation of the emergent concept of a *neural genoarchitecture*. This concept describes the neuroanatomy of the brain, including its anatomical boundaries, in terms of discrete gene expression domains (Puelles and Ferran, 2012; Schredelseker and Driever, 2020). Here, we used whole-mount *in situ* hybridization (WISH) to profile the spatial and temporal expression of selected marker genes (Table 1) in the bitterling fish (*Rhodeus ocellatus*). Our aim is to visualize early brain development and regionalization. The expression patterns have been compared with those in the zebrafish in order to detect temporal shifts in the gene expression (transcriptional heterochrony (Richardson et al., 2009). We then examine whether transcriptional heterochrony might provide an explanation for phenotypic evolution as suggested by (Bickelmann et al., 2012).

Materials and Methods

Rhodeus ocellatus embryos

Rhodeus ocellatus embryos, synchronized in developmental age, were produced by the Martin Reichard Lab of the Institute of Vertebrate Biology in Brno, Czech Republic by IVF (*in vitro* fertilization). After fixation of the embryos of various developmental stages in 4% paraformaldehyde (pFA) in phosphate buffered saline (PBS), they were dehydrated in graded methanol and stored in 100% methanol (MeOH) at -20°C. The developmental staging of the embryos was based on Nagata and Miyabe (Nagata and Miyabe, 1978) and on the staging table in Chapter 2 of this thesis.

Zebrafish embryos

Zebrafish (*Danio rerio*) embryos (AB/TL line) were collected from the fish facility of the Institute of Biology Leiden. The eggs were fertilized by 1:1 spawning (single crossing) at the beginning of the light period (14 hr light/10 hr dark). The fertilized eggs were collected and incubated in egg water (containing 60 µg/mL “Instant Ocean” sea salts) at 28.5 °C. Embryos were collected at 12, 24, 36 and 48 hpf (hours post fertilization). After collection, the embryos were immediately fixated in 4% pFA in PBS. Fixed embryos were dehydrated step-wise in graded methanol and stored in 100% methanol at -20 °C. Developmental stages were determined according to Kimmel *et al.* (Kimmel et al., 1995).

Whole-mount *in situ* hybridization

The digoxigenin-labeled antisense RNA probes used on *R. ocellatus* embryos were synthesized from plasmids containing PCR products of a major part of the coding sequences of genes *shha*, *fgf8a*,

pax6a, *msx3*, *sox9b*, *dlx2a* of *D. rerio*, using cDNA retro-transcribed from embryonic mRNA of *R. ocellatus* template. Whole-mount *in situ* hybridization (WISH) was performed according to (Thisse and Thisse, 2014).

Table 1 List of developmental marker genes used in this research

Gene Name	Family	Expression pattern	Reference
<i>dlx2a</i>	Distal-less homeobox 2a Homeobox genes	Forebrain segmental boundaries	(Mueller, Wullimann, & Guo, 2008; Renz et al., 2011; Stock, 2006; C. Thisse & Thisse, 2005; Wullimann, 2009)
<i>fgf8a</i>	Fibroblast growth factor 8a Growth factors	Midbrain/hindbrain boundary (MHB) or isthmus	(Albertson & Yelick, 2005; Nechiporuk, Linbo, Poss, & Raible, 2006; Ornitz & Itoh, 2015; Rhinn & Brand, 2001; B. Thisse et al., 2001; Wurst, Bally-Cuif, & Bally-Cuif, 2001)
<i>msx3</i>	Muscle segment polarity homeobox 3 Homeobox genes	Dorsal part of central nervous system	(Bendall & Abate-Shen, 2000; Ekker et al., 1997; C. Thisse & Thisse, 2005)
<i>pax6a</i>	Paired box 6a Pair rule genes	Eye and forebrain development; segmental organization of the hindbrain	(B. Thisse et al., 2001; C. Thisse & Thisse, 2005; Zhang, Boa-Amponsem, & Cole, 2017)
<i>shha</i>	Sonic hedgehog a Growth factors	Floorplate and zona limitans intrathalamica (Zli)	(Jeong et al., 2007; Zhang et al., 2017)
<i>sox9b</i>	SRY (sex determining region Y) box 9b Transcription factors	Early neural crest	(Chiang et al., 2001; Li, Zhao, Wang, Zhao, & Meng, 2002; B. Thisse & Thisse, 2004; Yan et al., 2005)

Results

Bitterling expression pattern

Stage 10-somite: early brain regionalization

At 10-somite stage (30 hpf), the bitterling embryo has just hatched out from the chorion and has 10-12 somites. The neural tube is differentiated into a brain primordium and narrower spinal cord primordium. The optic primordia extend laterally from the future diencephalon so that the outline of the head in dorsal view is arrowhead shaped. In the bitterling, there is strong expression of *fgf8a* at this stage, indicating onset of forebrain regionalization and the induction of the telencephalon (Figure 1A and D). The *pax6a* gene is expressed in the diencephalic part of the forebrain, non-overlapping with the telencephalic *fgf8a* expression (Figure 1B and E). The region from midbrain to r2 is devoid of *pax6a* expression (Figure 1B and E), and so the forebrain-midbrain boundary is indicated by the posterior margin of the *pax6a* diencephalic expression domain. There is strong expression of *fgf8a* in the MHB (isthmus organizer).

In the hindbrain, expression of *msx3* is located laterodorsally of the neural ectoderm (Figure 1C and F), in contrast to the ventromedial expression of *pax6a* and *fgf8a*. These three genes all present a segmental expression pattern in the hindbrain. *pax6a* has the highest intensity at r2, *fgf8a* is strongly expressed at r1 and r4, and *msx3* is expressed most strongly from the MHB to the posterior hindbrain, with weaker expression in r3.

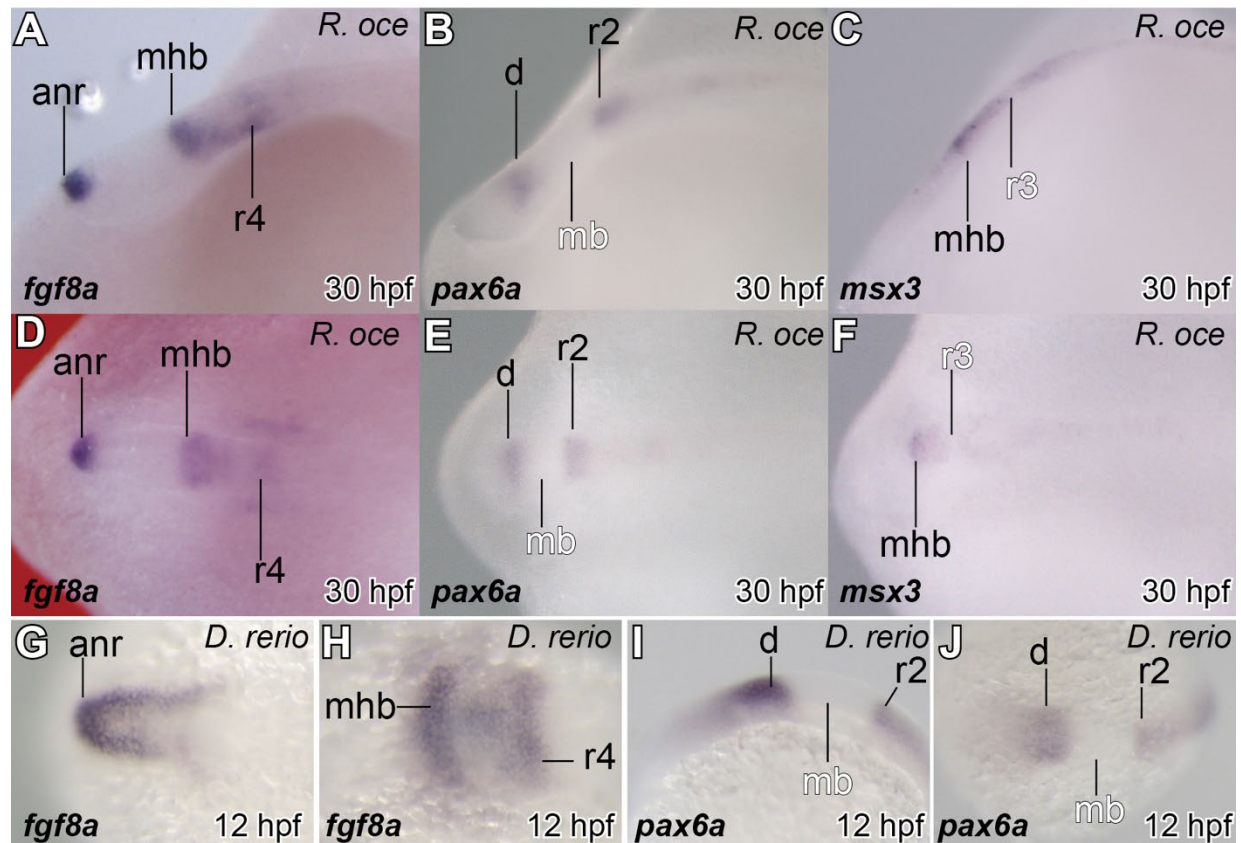


Figure 1 Gene expression patterns demonstrate early brain regionalization in the rosy bitterling (*R. oce*) and zebrafish (*D. rerio*). A to C, and I, lateral view, head to the left. D to H, and J, dorsal view, head to the left. Key for all figures in this chapter: anr, anterior neural ridge; fb, forebrain; mb, midbrain; hb, hindbrain; mhb, midbrain-hindbrain boundary; t, telencephalon; d, diencephalon; sp, subpallium; r1-7, rhombomeres; pr, preotic; po, postotic; re, retina; le, lens; ot, otic vesicle; tg, tegmentum; zli, zona limitans intrathalamica; hp, hypothalamus; pt, pretectum; ce, cerebellum; s1-5, cell streams; op, olfactory placode; of, optic fissure; fp, floor plate.

Stage 30-somite: specification of neural crest cells

At this stage (which is approximately 50 hpf) the somite number is 30 (the maximum number in this species is 35), the optic rudiment is distinctly cup-shaped, and the rhombomeres are visible as seven bulges. Compared with the previous stage, *fgf8a* expression is limited to the telencephalic regions and the MHB, and this gene is no longer expressed in the rhombomeres (Figure 2A and D). The expression of *pax6a* persists in the diencephalon and the proximal part of the retina (Figure 2B and E). The gene *sox9b* has four bilateral expression domains at the axial level of forebrain, anterior hindbrain, preotic, and postotic region of the hindbrain respectively (Figure 2C and F). The expression of *dlx2a* at the preotic level marks an early stage of neural crest migration (Figure 2G and H).

Stage 5-ovl: migration of neural crest cells

This stage (approximately 70 hpf) is the end of somitogenesis period. The somite has reached the maximum number. The hindbrain neural tube shows a cavity, the fourth ventricle. The expression of *fgf8a* is limited to the MHB, in the region where the tectum forms a fold that deeply invaginates towards the midline (Figure 3A and D). The gene *pax6a* shows strongest hybridization in the dorsal di-encephalon and the proximal retina (Figure 3B and E). The expression domains of *sox9b* and *pax6a* in the forebrain and midbrain are adjacent but non-overlapping. For example, *pax6a* is not expressed in the midbrain, while *sox9b* is expressed in the ventral region of the midbrain, marking out the tegmentum (Figure 3C and F). In the optic region, *pax6a* is expressed not only in the retina, but also in the lens placode; by contrast, *sox9b* is expressed only in the proximal portion of the retina. The hindbrain expression of *sox9b* is located on the ventral boundaries of r4/r5, r5/r6, and r6/r7. Expression of *sox9b* in the neural crest cells disappears. The anterior boundary of *pax6a* expression in hindbrain is still located at r2.

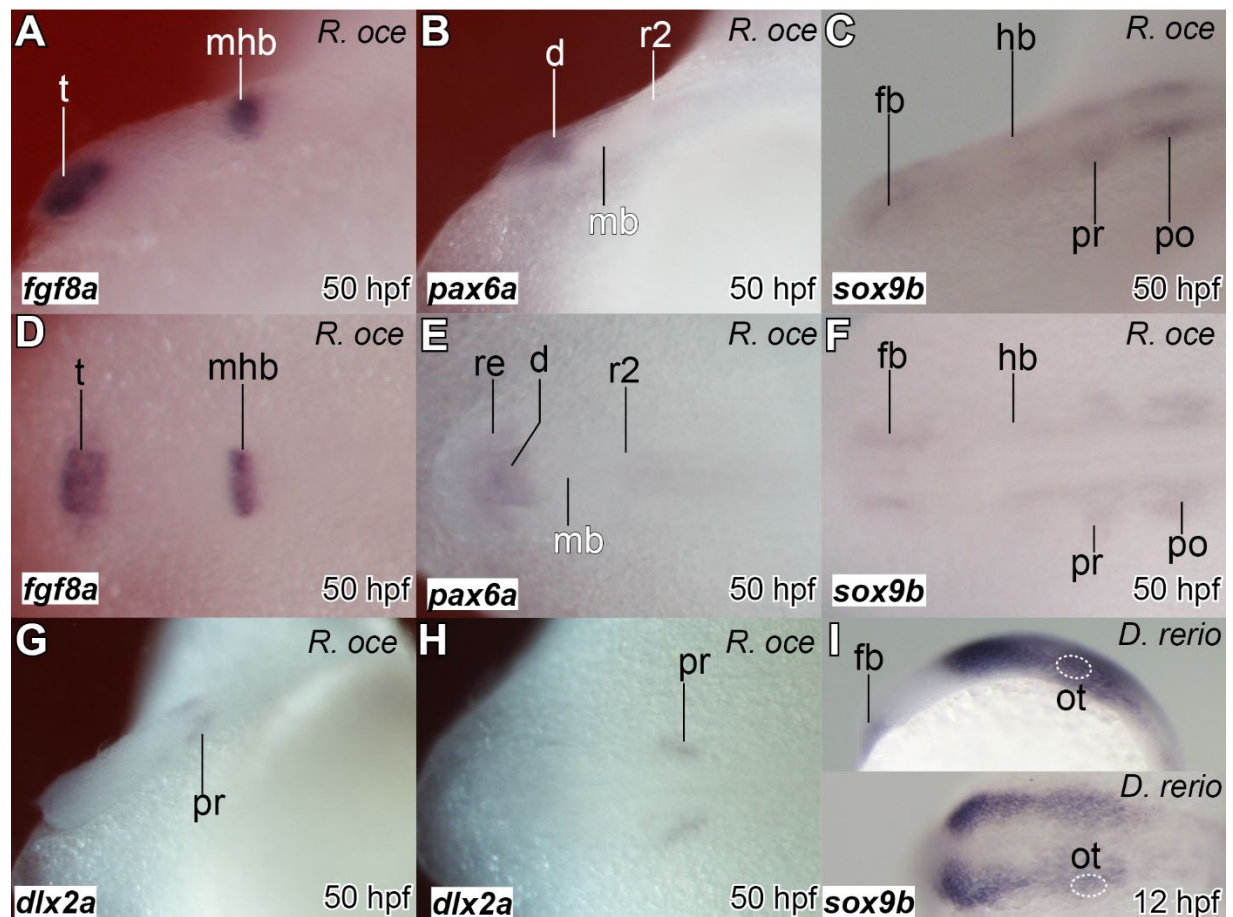


Figure 2 Gene expression and early neural crest specification in the rosy bitterling (*R. oce*) and zebrafish (*D. rerio*). A to C, G, and I (upper), lateral view, head to the left. D to F, H and I (lower), dorsal view, head to the left. See Fig. 1 for abbreviations.

At this stage, *dlx2a* has a telencephalic expression domain in the subpallium; and a diencephalic domain in the periventricular zone of the prethalamus (Figure 3G and J). The gene *shha* is expressed in the hypothalamus, and its floor plate expression bifurcated rostrally in the diencephalic region, marking the Zli boundary between the thalamus and the prethalamus (Figure 3H and K). The gene

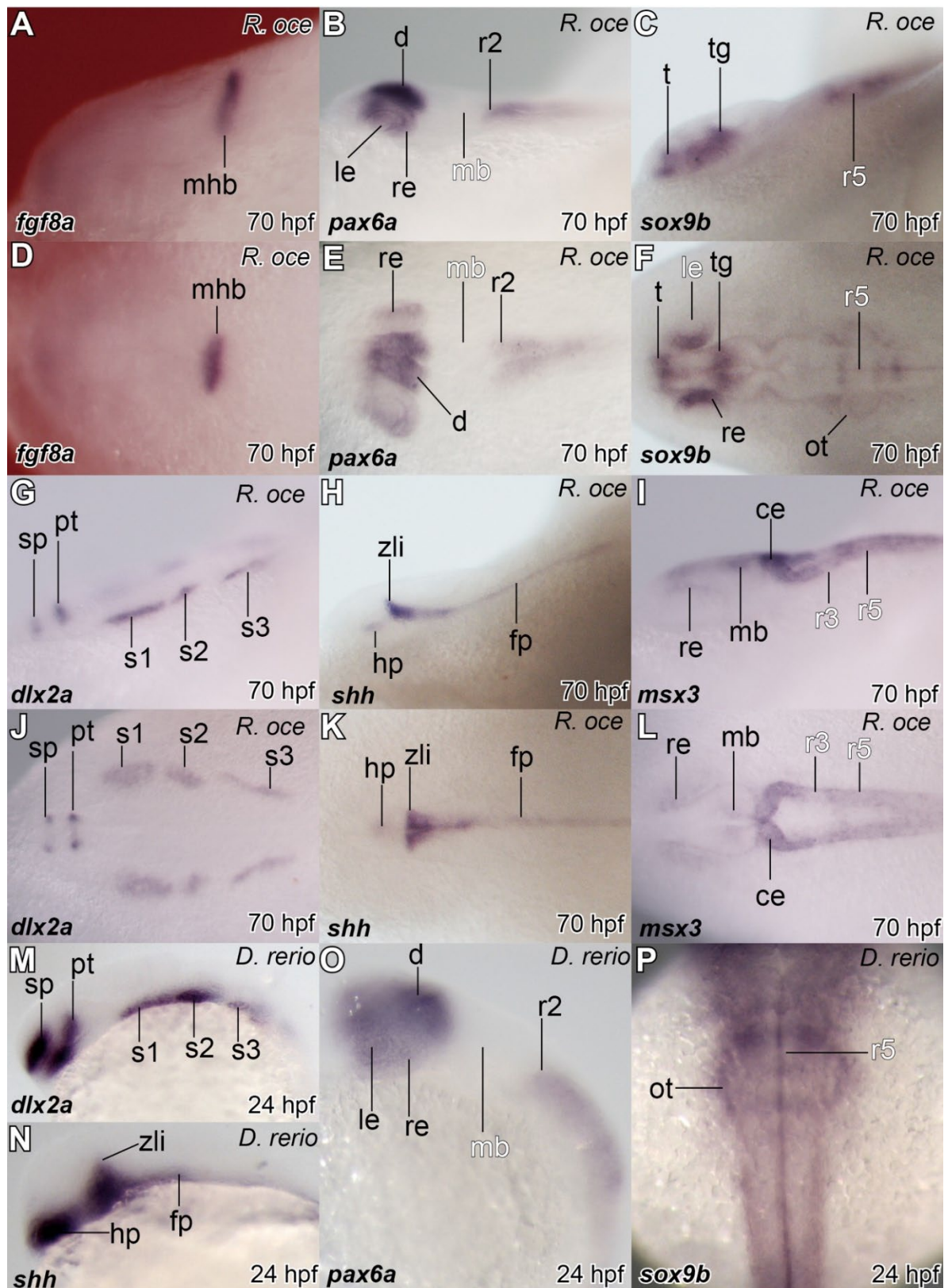


Figure 3 Gene expression and early neural crest migration in the rosy bitterling (*R. ocea*) and zebrafish (*D. rerio*). A to C, G to I, M to O, lateral view, head to the left. D to F, J to L, and P, dorsal view, head to the left. See Fig. 1 for abbreviations.

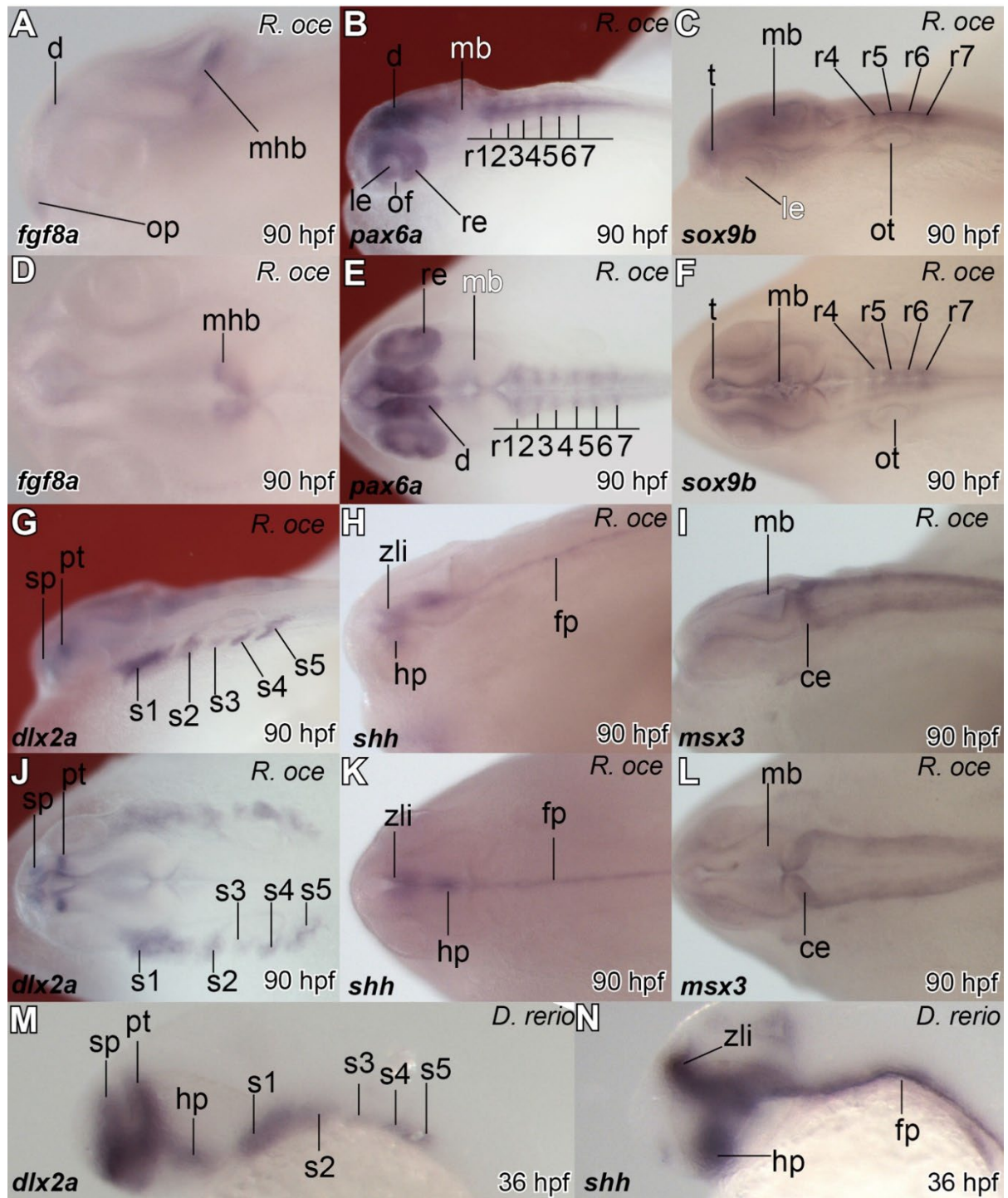


Figure 4 Gene expression and flexure of the neuraxis in the rosy bitterling (*R. ocea*) and zebrafish (*D. rerio*). A to C, G to I, M and N, lateral view, head to the left. D to F, J to L, dorsal view, head to the left. See Fig. 1 for abbreviations.

msx3 showed sporadic expressions on the dorsal side of the midbrain and retina. In the hindbrain, *msx3* probe hybridizes to the entire dorsal rhombencephalon except r3 and r5 where hybridization is weak or absent (Figure 3I and L).

Stage prim-3: cephalic flexure

At 90 hpf, the leading posterior end of the posterior lateral line primordium is at the axial level of myotome 3, and the stage is named accordingly as prim-3. New expression domains of *fgf8a* appear in the olfactory placode and the dorsal diencephalon (Figure 4A and D). The expression of *pax6a* persists in the retina and lens. In the hindbrain, *pax6a* has a new expression pattern, now marking intersegmental boundaries of the rhombomeres from r1 to r7 (Figure 4B and E). The alar plate of the rhombencephalon and basal plate of the r3 and r5 show hybridization with *msx3* (Figure 4F and I).

With the advance of the cephalic flexure, the longitudinal *shha* expression domain is displaced ventrad (Figure 4H and K). There are five streams of neural crest cells as indicated by expression of *dlx2a* (Figure 4G and J). The first and second streams are migrating to the mandibular and hyoid arches, respectively. The posterior three postotic streams are migrating to the 3rd, 4th, and the common primordium of the 5-7th pharyngeal arches.

Comparison between bitterling and zebrafish expression patterns

Comparing the expression patterns between the bitterling and zebrafish, we find that the zebrafish expression domain of *fgf8a* (Figure 1G and H) and *pax6a* (Figure 1I and J) at 6-somite stage (12 hpf) is similar to those of the bitterling at the 10-somite stage (30 hpf). However, the ANR expression of the zebrafish was more extensive (Figure 1G) than in the bitterling (Figure 1D). Expression of *sox9b* in the zebrafish at the 6-somite stage (Figure 2I) and in the bitterling at the 30-somite stage (50 hpf, Figure 2C and F) are similar; located bilaterally along the neural tube but is not yet subdivided into distinct domains (Figure 2I)

The expression of *dlx2a* in the migratory neural crest is similar between the zebrafish and bitterling. At the prim-5 stage in the zebrafish (24 hpf; Figure 3M and N) and 5-ovl stage of bitterling (70 hpf; Figure 3G and J) both species present three streams: two preotic streams migrating to the mandibular and hyoid arches, and one postotic stream migrating to 3-7th pharyngeal arches. At later stages, *dlx2a* shows expression in five NCC streams in both species (at the prim-25 stage in zebrafish, which is approximately 36 hpf; Figure 4M) and at prim-3 in the bitterling, which is approximately 90 hpf; Figure 4G and J). Expression of *pax6a* and *sox9b* is similar in zebrafish (at the prim-5 stage; Figure 3O and P) and the bitterling (at the 5-ovl stage). The longitudinal expression of *shha* has become displaced ventrad in the zebrafish at prim-25 stage (36 hpf; Figure 4N) and the bitterling at prim-3 stage (90 hpf; Figure 4H and K).

Discussion

Early brain development in the bitterling

This is the first study of brain development in a bitterling analyzed through gene expression patterns. At the 10-somite stage, there are no discernible anatomical boundaries in the brain. The MHB at this stage is discernible by microCT, but is distinctly marked by *fgf8a* expression (Figure 5). At this stage, the non-overlapping expression domains of *fgf8a* and *pax6a* indicate that the subdivision of the prosencephalon into telencephalon and diencephalon is underway.

Similarly, while there are no rhombomeres discernible by microCT in the 10-somite bitterling, *fgf8a* expression at this stage demarcates r1 and r4, and *msx3* demarcates r3; segmentation of the hind-brain is therefore already in progress. At the 30-somite stage, diminished expression of *fgf8a* and *pax6a* suggest that the segmentation of the rhombencephalon along the AP axis is complete. The appearance and initial migration of neural crest cells indicated by *sox9b* and *dlx2a* expression indicates that the differentiation of the hindbrain region on the DV axis has started at the 30-somite stage.

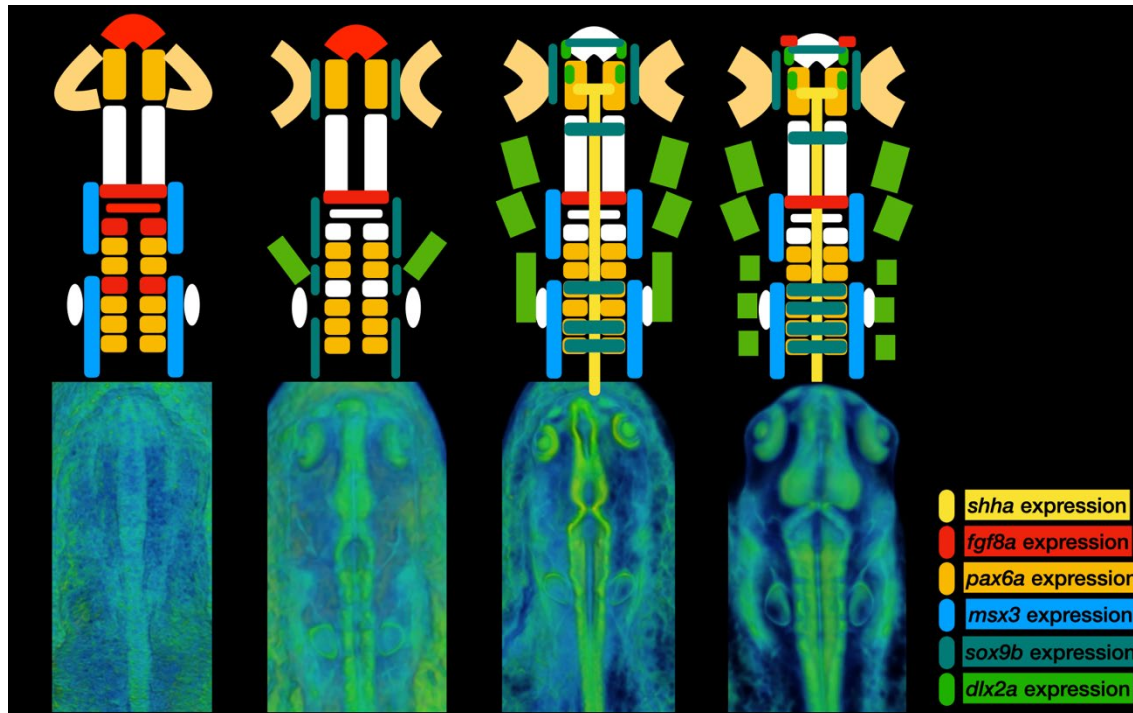


Figure 5 **Gene expression patterns and brain regionalization in the bitterling.** From left to right: stage 30 hpf, 50 hpf, 70 hpf, and 90 hpf. The upper images are color-coded schematics of gene expression domains. The lower images are volume renderings from microCT of embryos at the same developmental stage as the corresponding schematic. Dorsal views, rostral is to the top.

Transcriptional heterochrony between bitterling and the zebrafish

We identify three developmental periods of brain development that are extremely similar in the bitterling and zebrafish, namely: 10-somite to 6-somite, 5-ovl to prim-5, and prim-3 to prim-25 periods. Especially noteworthy in this comparative context is the expression of *dlx2a*. Its expression changes from demarcating 3 NCC streams to 5, and this represents a particularly useful comparative landmark because it is a transition that can be quantified. In the zebrafish, the 5 NCC streams do not appear until prim-17 (30 hpf), but in the bitterling they appear as early as prim-3. The prim number is based on the migration of the posterior lateral line primordium in the trunk. Therefore, the brain of a prim-3 bitterling corresponds to the development degree of a prim-17 zebrafish, while the trunk corresponds to an earlier prim-3 zebrafish.

In the zebrafish, truncal expression of *dlx2a* is apparent in pectoral fin bud at the prim-17 stage. A similar expression of *dlx2a* in the pectoral fin bud does not appear in the bitterling until the 1-ovl stage (150 hpf). A possible explanation for this discrepancy in relative timing is that

development is modular, such that each module develops autonomously and can evolve its own independent timing in different species. Just as there are different time zones on the earth, the time zone of the brain region could be a few hours earlier than the trunk region between zebrafish and bitterling.

References

- Akimenko, M. A., Ekker, M., Wegner, J., Lin, W. and Westerfield, M.** (1994). Combinatorial expression of three zebrafish genes related to distal-less: part of a homeobox gene code for the head. *J. Neurosci.* **14**, 3475–3486.
- Bickelmann, C., Mitgutsch, C., Richardson, M. K., Jiménez, R., de Bakker, M. A. G., Sánchez-Villagra, M. R., Jimenez, R., de Bakker, M. A. G. and Sanchez-Villagra, M. R.** (2012). Transcriptional heterochrony in talpid mole autopods. *Evodevo* **3**, 16.
- Chiang, E. F. L., Pai, C. I., Wyatt, M., Yan, Y. L., Postlethwait, J. and Chung, B. chu** (2001). Two sox9 genes on duplicated zebrafish chromosomes: Expression of similar transcription activators in distinct sites. *Dev. Biol.* **231**, 149–163.
- Gibbs, H. C., Chang-Gonzalez, A., Hwang, W., Yeh, A. T. and Lekven, A. C.** (2017). Midbrain-hindbrain boundary morphogenesis: At the intersection of wnt and Fgf signaling. *Front. Neuroanat.* **11**, 1–17.
- Graham, A., Heyman, I. and Lumsden, A.** (1993). Even-numbered rhombomeres control the apoptotic elimination of neural crest cells from odd-numbered rhombomeres in the chick hindbrain. *Development* **119**, 233–45.
- Hanneman, E., Trevarrow, B., Metcalfe, W. K., Kimmel, C. B. and Westerfield, M.** (1988). Segmental pattern of development of the hindbrain and spinal cord of the zebrafish embryo. *Development* **103**, 49–58.
- Hauptmann, G. and Gerster, T.** (2000). Regulatory gene expression patterns reveal transverse and longitudinal subdivisions of the embryonic zebrafish forebrain. *Mech. Dev.* **91**, 105–118.
- Jeong, J. Y., Einhorn, Z., Mathur, P., Chen, L., Lee, S., Kawakami, K. and Guo, S.** (2007). Patterning the zebrafish diencephalon by the conserved zinc-finger protein Fezl. *Development* **134**, 127–136.
- Kimmel, C. B., Ballard, W. W., Kimmel, S. R., Ullmann, B. and Schilling, T. F.** (1995). Stages of embryonic development of the zebrafish. *Dev. Dyn.* **203**, 253–310.
- Krauss, S., Johansen, T., Korzh, V. and Fjose, A.** (1991). Expression pattern of zebrafish pax genes suggests a role in early brain regionalization. *Nature* **353**, 267–270.
- Krauss, S., Johansen, T., Korzh, V., Moens, U., Ericson, J. U. and Fjose, A.** (1991). Zebrafish pax[zf-a]: a paired box-containing gene expressed in the neural tube. *EMBO J.* **10**, 3609–3619.
- Lauter, G., Söll, I. and Hauptmann, G.** (2013). Molecular characterization of prosomeric and intraprosomeric subdivisions of the embryonic zebrafish diencephalon. *J. Comp. Neurol.* **521**, 1093–1118.
- Li, M., Zhao, C., Wang, Y., Zhao, Z. and Meng, A.** (2002). Zebrafish sox9b is an early neural crest marker. *Dev. Genes Evol.* **212**, 203–206.
- Lumsden, A. and Krumlauf, R.** (1996). Patterning the Vertebrate Neuraxis. *Science* **274**, 1109–1115.
- Maves, L., Jackman, W. and Kimmel, C. B.** (2002). FGF3 and FGF8 mediate a rhombomere 4 signaling activity in the zebrafish hindbrain. *Development* **129**, 3825–37.
- Mendelson, B.** (1986). Development of reticulospinal neurons of the zebrafish. I. Time of origin. *J. Comp. Neurol.* **251**, 160–171.
- Metcalfe, W. K., Mendelson, B. and Kimmel, C. B.** (1986). Segmental homologies among reticulospinal neurons in the hindbrain of the zebrafish larva. *J. Comp. Neurol.* **251**, 147–159.
- Moens, C. B. and Prince, V. E.** (2002). Constructing the hindbrain: Insights from the zebrafish. *Dev. Dyn.* **224**, 1–17.
- Mueller, T. and Wullimann, M. F.** (2016). *Atlas of Early Zebrafish Brain Development*. Second ed. Elsevier.
- Mueller, T., Wullimann, M. F. and Guo, S. U.** (2008). Early Teleostean Basal Ganglia Development Visualized by Zebrafish GAD67 Gene Expression. *Comp. Gen. Pharmacol.*
- Murakami, Y., Ogasawara, M., Sugahara, F., Hirano, S., Satoh, N. and Kuratani, S.** (2001). Identification and expression of the lamprey Pax6 gene: evolutionary origin of the segmented brain of vertebrates. *Development* **128**, 3521–31.

- Nagata, Y. and Miyabe, H.** (1978). Development Stages of the Bitterling, *Rhodeus ocellatus ocellatus* (Cyprinidae). *Mem. Osaka Kyoiku Univ. III, Nat. Sci. Appl. Sci.* **26**, 171–181.
- Panganiban, G. and Rubenstein, J. L. R.** (2002). Developmental functions of the Distal-less/Dlx homeobox genes. *Development* **129**, 4371–4386.
- Piotrowski, T. and Nüsslein-Volhard, C.** (2000). The Endoderm Plays an Important Role in Patterning the Segmented Pharyngeal Region in Zebrafish (*Danio rerio*). *Dev. Biol.* **225**, 339–356.
- Plavicki, J. S., Baker, T. R., Burns, F. R., Xiong, K. M., Gooding, A. J., Hofsteen, P., Peterson, R. E. and Heideman, W.** (2014). Construction and characterization of a sox9b transgenic reporter line. *Int. J. Dev. Biol.* **58**, 693–699.
- Puelles, L.** (2019). Survey of Midbrain, Diencephalon, and Hypothalamus Neuroanatomic Terms Whose Prosomeric Definition Conflicts With Columnar Tradition. *Front. Neuroanat.* **13**, 20.
- Puelles, L. and Ferran, J. L.** (2012). Concept of neural genoarchitecture and its genomic fundament. *Front. Neuroanat.* **6**, 47.
- Puelles, L. and Rubenstein, J. L. R.** (2003). Forebrain gene expression domains and the evolving prosomeric model. *Trends Neurosci.* **26**, 469–476.
- Püschel, A. W., Gruss, P. and Westerfield, M.** (1992). Sequence and expression pattern of pax-6 are highly conserved between zebrafish and mice. *Development* **114**, 643–51.
- Reifers, F., Böhli, H., Walsh, E. C., Crossley, P. H., Stainier, D. Y. and Brand, M.** (1998). Fgf8 is mutated in zebrafish acerebellar (ace) mutants and is required for maintenance of midbrain-hindbrain boundary development and somitogenesis. *Development* **125**, 2381–2395.
- Rhinn, M. and Brand, M.** (2001). The midbrain-hindbrain boundary organizer. *Curr. Opin. Neurobiol.* **11**, 34–42.
- Richardson, M. K., Gobes, S. M. H., van Leeuwen, A. C., Polman, J. A. E., Pieau, C., Sanchez-Villagra, M. R. and Sánchez-villagra, M. R.** (2009). Heterochrony in limb evolution: developmental mechanisms and natural selection. *J Exp Zool B Mol Dev Evol* **312**, 639–664.
- Rocha, M., Singh, N., Ahsan, K., Beiriger, A. and Prince, V. E.** (2020). Neural crest development: insights from the zebrafish. *Dev. Dyn.* **249**, 88–111.
- Scholpp, S., Wolf, O., Brand, M. and Lumsden, A.** (2006). Hedgehog signalling from the zona limitans intrathalamica orchestrates patterning of the zebrafish diencephalon. *Development* **133**, 855–864.
- Schredelseker, T. and Driever, W.** (2020). Conserved Genoarchitecture of the Basal Hypothalamus in Zebrafish Embryos. *Front. Neuroanat.* **14**, 3.
- Shanmugalingam, S., Houart, C., Picker, A., Reifers, F., Macdonald, R., Barth, A., Griffin, K., Brand, M. and Wilson, S. W.** (2000). Ace/Fgf8 is required for forebrain commissure formation and patterning of the telencephalon. *Development* **127**, 2549–61.
- Thisse, B. and Thisse, C.** (2014). *In Situ Hybridization on Whole-Mount Zebrafish Embryos and Young Larvae. In Methods in Molecular Biology*, pp. 53–67.
- Trevarrow, B., Marks, D. L. and Kimmel, C. B.** (1990). Organization of hindbrain segments in the zebrafish embryo. *Neuron* **4**, 669–679.
- Vieira, C., Garda, A.-L., Shimamura, K. and Martinez, S.** (2005). Thalamic development induced by Shh in the chick embryo. *Dev. Biol.* **284**, 351–363.
- Wilson, S. W., Ross, L. S., Parrett, T. and Easter, S. S.** (1990). The development of a simple scaffold of axon tracts in the brain of the embryonic zebrafish, *Brachydanio rerio*. *Development* **108**, 121–45.
- Wullmann, M. F. and Knipp, S.** (2000). Proliferation pattern changes in the zebrafish brain from embryonic through early postembryonic stages. *Anat. Embryol. (Berl)*. **202**, 385–400.
- Wullmann, M. F. and Rink, E.** (2002). The teleostean forebrain: A comparative and developmental view based on early proliferation, Pax6 activity and catecholaminergic organization. *Brain Res. Bull.* **57**, 363–370.

Chapter 5 Pre-hatching early embryonic development in the rosy bitterling (*Rhodeus ocellatus*)

Wenjing Yi¹, Martin Reichard², Martin Rücklin³, and Michael K. Richardson¹

1, Institute of Biology, University of Leiden, Sylvius Laboratory, Sylviusweg 72, 2333BE, Leiden, the Netherlands.

2, Institute of Vertebrate Biology, Czech Academy of Sciences, Kvetna 8, 603 65 Brno, Czech Republic.

3, Vertebrate Evolution, Development and Ecology, Naturalis Biodiversity Center, Postbus 9517, 2300 RA Leiden, The Netherlands

Manuscript in preparation

Abstract

Bitterlings are Cynipid fish of the subfamily Acheilognathinae. All bitterlings have a brood-parasitic early life history, in which embryos parasitise the internal gill space of fresh-water unionid mussels (Unionidae). Our aim in this study is to examine early stages of development in this species in detail because they are otherwise known only from a few descriptive studies. We hypothesise that early development in the bitterling will show modifications related to brood parasitism. We have examined the expression of the genes *fgf8a*, *krt8*, *msx3* and *ctslb* by whole-mount *in situ* hybridization (WISH) in early pre-hatching development and hatching of the rosy bitterling (*Rhodeus ocellatus*). We find that a unique aspect of bitterlings among teleosts is their modified pattern of convergent-extension movements during gastrulation and neurulation. This leads to the rostro-caudal inversion of the embryo in the chorion, a phenomenon referred to as blastokinesis. Further, we suggest that blastokinesis in the rosy bitterling is functional because it provides optimal positioning of the post-hatching embryo in the gill space of the host mussel. More generally, our study provides an example of variation in yolk shape and egg size consistent with the concept of developmental penetrance of adaptations on later stages.

Introduction

The rosy bitterling (*Rhodeus ocellatus*, Kner, 1866) is a teleost fish of the carp and minnow family (Cyprinidae). Together with approximately 70 other species of bitterling, it belongs to the subfamily Acheilognathinae (Cheng et al., 2014; Kawamura et al., 2014). All Acheilognathinae have a brood parasitic life history, and development is similar in the entire group (Smith et al., 2004). During the mating season (April to June) female bitterlings develop long ovipositors, that they use to deposit their eggs into the gills of a living mussel through its exhalant siphon (Awata et al., 2019; Chang, 1948; Chang and Wu, 1947; Khlopova and Kul'bachnyi, 2013; Olt, 1893; Smith et al., 2014).

After deposition of the eggs by the female into the mussel, the male releases sperm into the inhalant siphon of the mussel. The incoming water current then transfers the spermatozoa through the gills, where it fertilizes the eggs. Once the eggs are hatched, the larvae reside inside the mussel. There, the larvae compete with their host for oxygen (Spence and Smith, 2013). After approximately one month, the larvae are able to free themselves from the interlamellar space, migrate to the exhalant cavity at the gill base and leave their host (Aldridge, 1999; Chang, 1948; Leung, 2014; Smith, 2016; Suzuki, 2006).

An important question in bitterling evo devo is: from what stage of development does rosy bitterling show adaptations to the brood parasitic life-style? In addressing this question, we note already some derived conditions at the earliest stages post-laying. The fresh eggs of rosy bitterling eggs have a characteristic morphology. Unlike most teleost eggs, which are approximately spherical (Kunz, 2004), the rosy bitterling spawns long, spindle-shaped eggs. The eggs are also relatively large compared to other carp species (Aldridge, 1999; Kim and Park, 1985). The fertilized egg has a characteristic shape like a balloon, with an enlarged, spherical vegetal hemisphere and a small, tubular animal hemisphere (Chang, 1948). Another bitterling specialization is the shape of the yolk sac. Its anterior portion expands into a pair of widened yolk sac extensions (YSEs) immediately after hatching, eventually giving the whole embryo the shape of an arrowhead (Arai, 1988; Nagata and Miyabe, 1978; Virta and Cooper, 2009b).

Chang and Wu (1947) described in detail a phenomenon: the rostro-caudal inversion of the embryo in the chorion which they called 'blastokinesis'. The blastokinesis is autonomous, in the sense that it is not subject to external forces such as gravity or the internal pressure of the chorion (Chang and Wu, 1947). According to Chang and Wu (1947), the whole process of blastokinesis takes place over 5.5 hours (at 27-29 °C). It begins at a stage just before the closure of the blastopore, and ends at the initial phase of YSEs formation when there are 10-12 somite pairs. Then, the embryos begin to hatch. Those authors also noticed that, after the closure of the blastopore, the embryo grows conspicuously in length and blastokinesis takes place more slowly than in the first 2.5 h.

The rosy bitterling (*R. ocellatus*) is the only teleost species that has been to show blastokinesis during early development. Blastokinesis proper is more familiar to researchers of insect development (Panfilio, 2008; Panfilio, 2009). As suggested by Needham (1942), blastokinesis in insects may agitate the yolk material, facilitating the supply of yolk nutrients to the embryo. At present, it is not clear whether blastokinesis in these two taxa are homologous or convergent evolution, and this uncertainty provides additional motivation for further research on blastokinesis in the bitterling.

In Chapter 2 we hypothesized that blastokinesis was caused by the processes of gastrulation, neurulation and somitogenesis. Therefore, we named stages before the closure of blastopore as convergence, extension and migration, and indexed later stages by somite number. Here, we have studied the expression of highly conserved marker genes by whole-mount *in situ* hybridization (WISH) to visualize the early pre-hatching development of *R. ocellatus* and test that hypothesis. Convergent extension (CE) is a collective cell movement, a highly conserved developmental process in all metazoans (Tada and Heisenberg, 2012). CE results in the narrowing and lengthening of an embryonic field along a defined axis (Williams and Solnica-Krezel, 2020). FGF signaling, including *fgf8a*, has an essential role in the coordination of cell movements during gastrulation and neurulation (Dorey and Amaya, 2010). The neural plate undergoes CE movements, which result in lengthening and narrowing of the neural plate along the anterior-posterior and medial-lateral axes. Convergence of the neural plate can be identified by the specific expression domain of the gene *msx3* (Phillips et al., 2006).

We have also use time-lapse photography, histology and microCT methods to analyze the early development of bitterling, to explore the phenomenon of blastokinesis and its possible adaptive significance. To examine the cellular composition of the YSEs we studied the expression of the genes *krt8* and *ctslb*. The gene *krt8* is an epidermal marker for keratinocyte differentiation (Eisenhoffer et al., 2017; Imboden et al., 1997). The expression of *ctslb* is a reliable marker for the hatching gland cells (Vogel and Gerster, 1997).

Materials and Methods

Rhodeus ocellatus embryos

Rhodeus ocellatus embryos of synchronized developmental age were provided by the Reichard lab of the Institute of Vertebrate Biology in Brno, Czech Republic by IVF (*in vitro* fertilization). After fixation of the embryos of various developmental stages in 4%PFA, they were dehydrated step-wise in methanol and stored in 100% methanol (MeOH) at -20°C. The developmental staging of the embryos was based on Nagata and Miyabe (Nagata & Miyabe, 1978) and on the staging table from the Chapter 2 of this thesis. Two or three replicates were used for each stage.

Danio rerio embryos

Embryos of the zebrafish *Danio rerio* (AB/TL line) were collected in the fish facility of the Institute of Biology Leiden. The eggs were fertilized by 1:1 spawning (single crossing) at the beginning of the light period (14 h light, 10 h dark). The fertilized eggs were collected and incubated in egg water (containing 60 µg/ml “Instant Ocean” sea salts) at 28.5 °C. After collection, the embryos were immediately fixated in 4% paraformaldehyde (pFA). Fixed embryos were dehydrated step-wise in MeOH and stored in 100% MeOH at -20 °C. The developmental stages were determined according to Kimmel *et al.* (Kimmel et al., 1995). For each stage, ten replicates were used.

Whole-mount *in situ* hybridization

Whole-mount *in situ* hybridization (WISH) was performed according to the protocol of Thisse *et al.*, (2004).

MicroCT

The following protocol is based on Metscher (2009), and Babaei, Hong et al. (2016). The fixative was 3% pFA and 1% glutaraldehyde in 0.1mol l⁻¹ phosphate buffered saline (PBS), pH 7.0 at 4 °C overnight. After rinsing in PBS (2 x 10 min), specimens were stained with iodine-potassium iodide (1% iodine in 2% potassium iodide) for 12 h or phosphotungstic acid (0.3% phosphotungstic acid in 70% ethanol) for ≥ 24 h. Staining was carried out on a rotary mixer at 6 revolutions per minute. After staining, the embryos were stored at 4 °C in 70% ethanol. Samples were immobilized in 1% low melting-point agarose, sealed with paraffin oil and parafilm, and stabilized in a polystyrene tube during scanning.

The raw data for 3-D imaging of the samples were acquired using an Xradia 520 Versa 3-D X-ray microscope (Zeiss). The X-ray source was set to 80/7 or 40/3 (keV/W). A thin LE1 filter was used to avoid beam hardening artifacts. To obtain high resolution images, a CCD (charge-coupled device) optical objective (4x) was used. The isotropic voxel size for overview scanning of the whole embryo was 2-3 μm. For detailed scanning of the head region, the isotropic voxel size was set to < 1.5 μm. Each sample was rotated 180+fan degrees along the anterior-posterior (AP) axis. The projection images acquired were checked for sample drifting then reconstructed if of acceptable quality.

3D-reconstructions and annotation

Virtual sections were created from the microCT data and were assembled with Avizo software (Avizo 9.5, Thermo Scientific™) using volume rendering for 3D visualization.

Results

Convergence- extension is the first phase of blastokinesis

From the onset of gastrulation, *fgf8a* early expression is in the marginal cells around the entire periphery of the blastoderm (Fig. 1A). At the mid-gastrula stage, a dorsoventral gradient expression appears in the marginal region (Fig. 1B), marking the establishment of the dorsoventral axis of the embryo. At this stage, the strongest expression of *fgf8a* is in the embryonic shield, the teleost equivalent of Spemann's organizer (Fürthauer et al., 1997), located at the dorsal midline (Fig. 1C). Along the dorsal midline, towards the animal pole, two transverse bands of weak hybridization are recognizable as the bilateral hindbrain primordia (Fig. 1C and D).

According to Chang and Wu (1947), at the beginning of blastokinesis, the embryo starts to migrate on the yolk ball gradually, the head passing the animal pole and migrating to the opposite side; the whole embryo thereby becomes hook-shaped. The blastopore has not yet closed (Fig. 2A, and on this basis, the embryo is at an equivalent stage as that depicted in Fig. 1D in Chang and Wu (1947).

The expression of *fgf8a* at this stage marks the progress of gastrulation. Its dorsoventral expression gradient persists up to the closure of blastopore, when it surrounds the yolk plug (Figure 2A). We have noted (in Chapter 2) that the yolk plug of the bitterling embryo is located not at the vegetal pole but dorsal to it, a position resulting from the asymmetry of convergence and extension movements between the dorsal and ventral blastoderm during gastrulation. The zebrafish embryo presents a similar picture, except that the zebrafish yolk plug is located ventral to the vegetal pole

(Kimmel et al., 1995). The rostral expression domains of *fgf8a* in the hindbrain primordia fuse in the midline because of convergence extension movements (Fig. 2A).

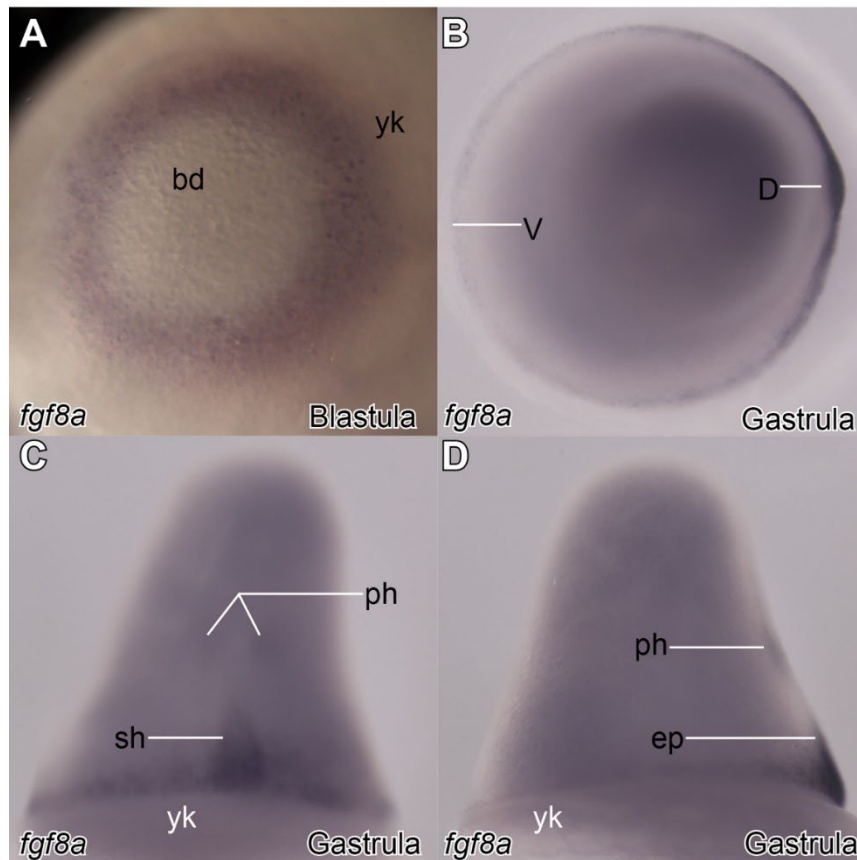


Figure 1 Expression of *fgf8a* during the blastula and gastrula period of the rosy bitterling. A, animal pole view, blastula stage, 6 hpf. B, C, and D, mid-gastrula stage, 15 hpf. B, animal pole view, dorsal at left. C, dorsal view, animal pole up. D, lateral view, animal pole up, dorsal at left. Key: bd, blastoderm; yk, yolk; D, dorsal; V, ventral; ph, presumptive hindbrain territory; sh, shield; ep, epiblast.

As blastokinesis advances, the embryo has migrated half-way up the yolk mass, being symmetrically doubled over either side of the animal pole; the blastopore is now closed (Fig. 2B, comparable in stage to Fig. 1E in Chang and Wu (1947)). The expression of *msx3* marks the boundary between the dorsal neural ectoderm, and the ventral non-neural ectoderm, and indicates the dorsal-ventral differentiation of the neural ectoderm. The rostral expression domains of *msx3* at the mid-brain axial level are confluent in the midline, indicating the formation of the neural keel (Fig. 2C). The caudal expression pattern of *msx3* shows bilateral domains, indicating that the lateral neural plate has not yet converged in the midline at this axial level (Fig. 2D). In transverse sections (Fig. 3) it can be seen that the neuroectoderm has formed the neural plate in the midline. It has thickened in the dorsoventral axis to form the triangular neural keel at rostral axial levels (Fig. 3A) but remains as a flat neural plate caudally (Fig. 3B). The chordal mesoderm and somitic mesoderm undergo initial differentiation (Fig. 3B).

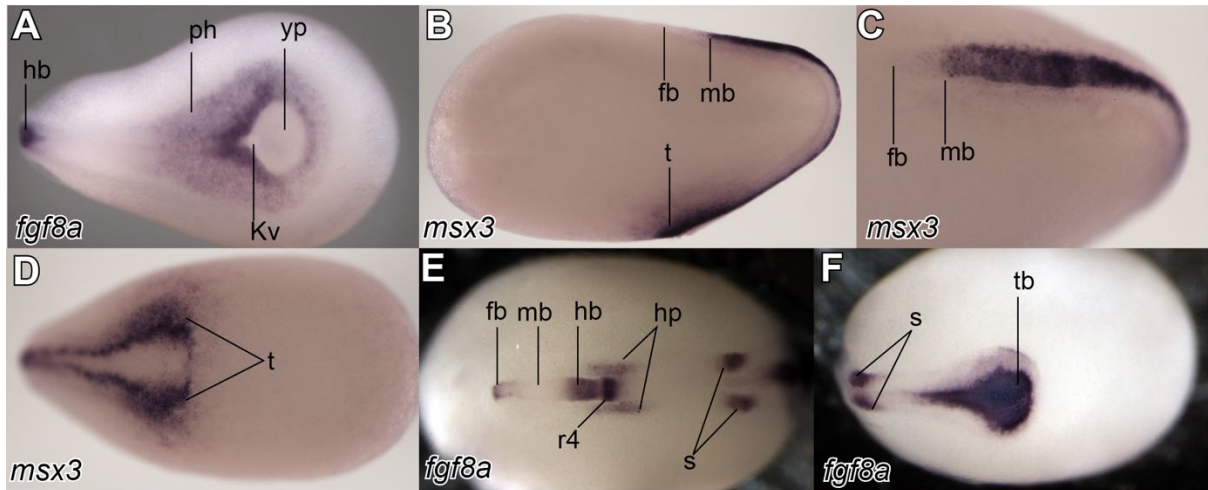


Figure 2 **Gene expression during the neurulation and somitogenesis periods of the rosy bitterling.** A, dorsal view, head to the left, 90% epiboly stage, 22.5 hpf. B, C and D, migration stage, 24.2 hpf; B is lateral view, dorsal up; C is dorsal view of head region, head to the left; D is dorsal view of the tail part, tail to the right. E and F, dorsal view of head and tail region respectively, head to the left, 3-somite stage, 25.5 hpf. Key: hb, hindbrain; ph, paraxial hypoblast; Kv, Kupffer's vesicle; yp, yolk plug; fb, forebrain; mb, midbrain; t, tail; r4, rhombomere 4; hp, heart primordia; s, somite; tb, tail bud. Stages according to Yi et al. (2021).

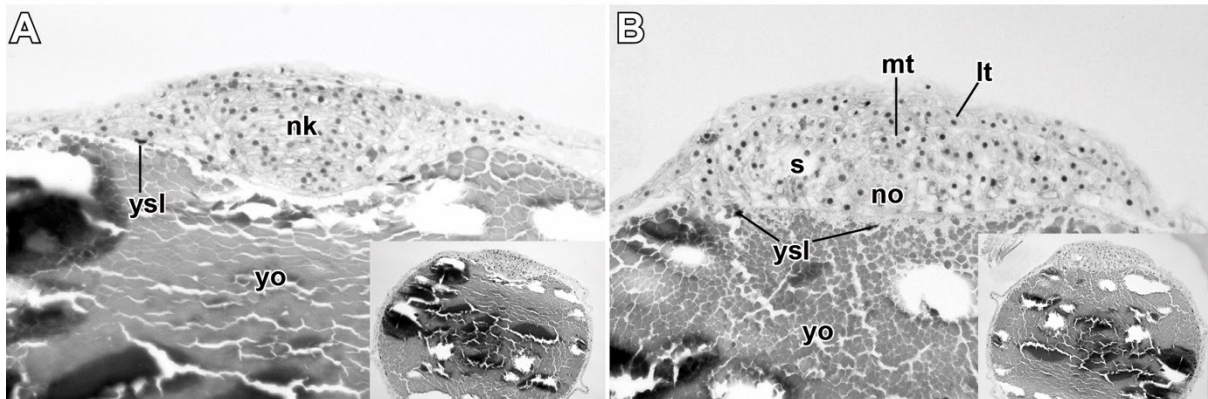


Figure 3 **Transverse sections through the dorsal side of a rosy bitterling embryo at the migration stage.** 24 hpf, H&E staining. The embryo lies symmetrically over either side of the animal pole. A and B are on opposite sides of the same section, dorsal up. A, the neural keel (nk) becomes visible at rostral axial levels. B, the neural plate at the caudal level, the median thickening (mt) of the neural plate immediately adjacent to the notochord (no), the lateral thickening (lt) overlay on somitic mesoderm (s). Key: ysl, nucleus of yolk syncytial layer; yo, yolk mass.

Body elongation during somitogenesis is the second phase of blastokinesis

With the progress of blastokinesis, the head of the embryo approaches the vegetal pole (Fig. 2E) and the tail approaches the animal pole (Fig. 2F). At the 3-somite stage *fgf8a* expression is seen in the forebrain, hindbrain, lateral plate mesoderm, somitic mesoderm and tailbud (Fig. 2E and F). Hybridization in the forebrain is particularly intense in the anterior neural ridge. The hindbrain expression extends from the presumptive MHB (midbrain-hindbrain boundary) to r4 (rhombomere 4), where it shows intense hybridization. Expression in the lateral plate mesoderm, bilaterally at the axial level of r4, indicates the induction of the cardiogenic fields. Segmental expression marks out the newly formed somites. The expression in the tailbud region is uniform, with no indication of a dorsal-ventral gradient in expression.

At the end of blastokinesis (the somite-6 stage), the YSEs project from the body in the ventral-dorsal direction; the yolk constriction on the ventral surface is prominent (Figure 4A, comparable to Fig. 1F in Chang and Wu (1947)). At this stage, the expression of *fgf8a* is similar to the previous stage except that segmental expression in hindbrain becomes more obvious. There is now expression in r1, r2 and r4 but not in r3 (Fig. 4B). The expression of *fgf8a* in the differentiated somites becomes more restricted to the anterior somite border of somites 1-6. During the hatching period, at the 10-somite stage, the YSEs become more prominent (compare Figure 4B and D), and the rostral protrusion of the YE (yolk extension) appears. Hybridization of *fgf8a* in the hindbrain decreases, while the expression intensity at the MHB is still high. Hybridization to the anterior neural ridge of the forebrain domain appears stronger than the previous stage.

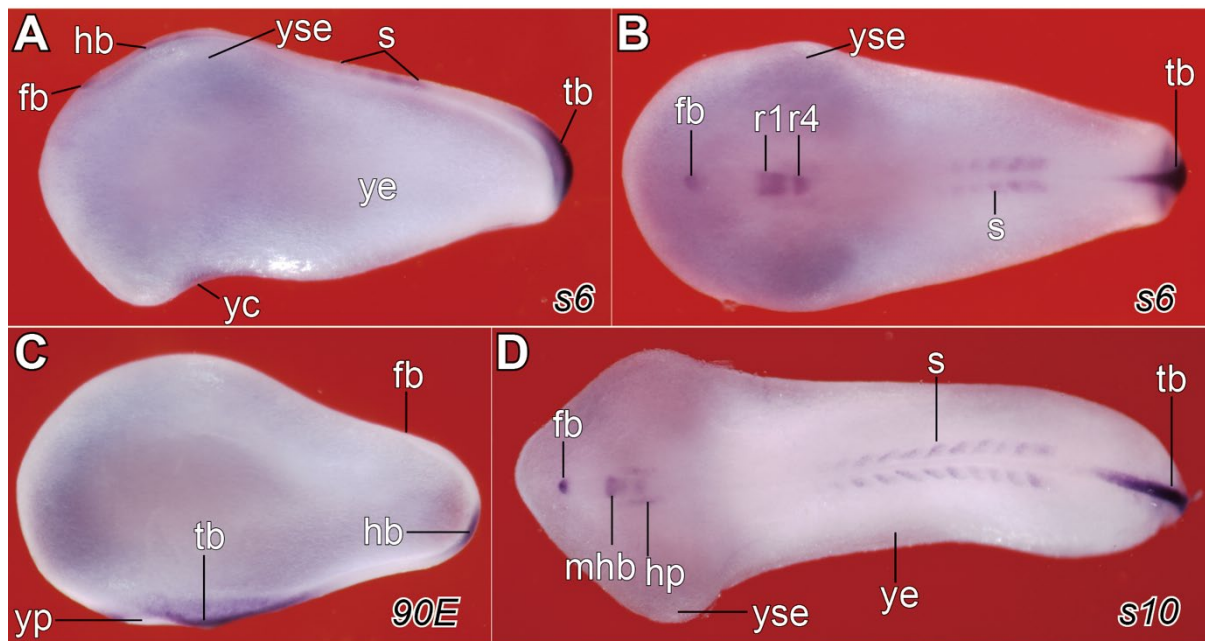


Figure 4 Expression of *fgf8a* in the rosy bitterling embryo showing the elongation of embryo. A and C, lateral aspect, head to the left. B and D, dorsal aspect, head to the left. A and B, 6-somite stage, 27 hpf. C, 90% epiboly stage, 22.5 hpf. D, 10-somite stage, 30 hpf. Comparing A and C, it can be seen that the hindbrain region is displaced from the animal pole towards the vegetal pole. Compare B and D for the elongation of the embryo trunk before and after hatching. Key: fb, forebrain; hb, hindbrain; tb, tail bud; r1, rhombomere 1; r4, rhombomere 4; yp, yolk plug; yc, yolk constriction; ye, yolk extension; yse, yolk sac extension; mhb: midbrain-hindbrain boundary; tb, tail bud; hp, heart primordium; s, somite.

Hatching of the embryo from the vegetal end of the chorion

Using time-lapse video recording of live embryos, we observed the hatching of embryos from the chorion. The process of hatching is very rapid, taking only 1 – 2 min. We hypothesize that the vegetal pole of the chorion is ruptured due to an increase in internal pressure, resulting in turn from the growing rostral protrusion of the YE (Fig. 5A to C). The expression of *krt8* in the bitterling embryo is restricted to the rostral protrusion of YE and YSEs before and after the hatching events at 29 hpf and 31 hpf (Fig. 5D to I). By contrast, *krt8* is expressed in the zebrafish embryo in the epidermis over the whole embryo up to 48 hpf (Fig. 5J to L). We suggest that the high local expression of *krt8* in the bitterling on the rostral protrusion of the YE and YSEs is related to cell aggregation and advanced keratinocyte differentiation. This in turn may facilitate the rupture of the chorion.

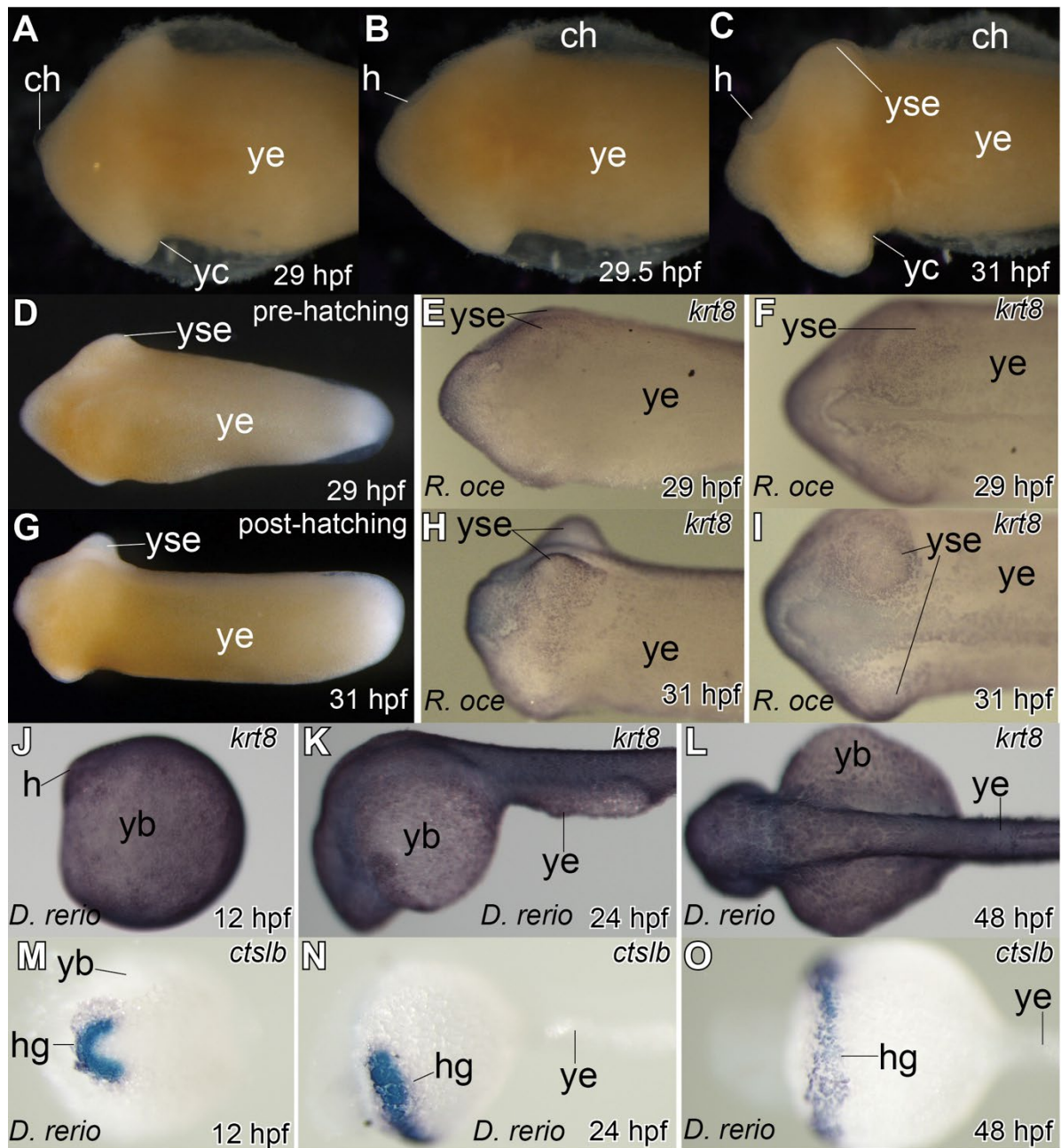


Figure 5 Gene expression in the rosy bitterling during the hatching period. All with head to the left. A to C, lateral view of bitterling embryos showing the hatching process. By 29 hpf, embryo before hatching with intact chorion (A); 30 min later, head and the anterior yolk extension protrudes from the chorion (B); by 31 hpf, the yolk sac extension (yse) and yolk constriction (yc) protrude from the chorion (C). D to I show *krt8* expression in *R. ocellatus* before and after hatching. Notice that the hybridization is particularly strong at the anterior yolk extension and the bilateral yolk sac extensions. J to L present the ubiquitous expression of *krt8* during zebrafish (*Danio rerio*) embryonic development. M to O present the specific expression of *ctslb* marking out the hatching gland cells of the zebrafish embryo. Key: ch, chorion; h, head; yc, yolk constriction; ye, yolk extension; yse, yolk sac extension; yb, yolk ball; hg, hatching gland.

We find no expression of *ctslb* in bitterling embryos during the hatching event (3-, 10- and 35-somite stages, data not shown). However, we find intense expression of *ctslb* in pre-hatching stages in the zebrafish (Fig. 5M to O). This result is consistent with our hypothesis that the hatching

of bitterlings is purely physical, with no involvement of a hatching-gland enzyme. Therefore, we conclude that the rupture site of the chorion is not random, but is consistently at the vegetal pole, in front of the rostral protrusion of the YE.

Blastokinesis determines the orientation of the post-hatching embryo in the host mussel

In the dissected host mussel, the main parasitic site of the bitterling embryo is the interlamellar space (Fig. 6A). This space is divided into parallel water tubes by the interlamellar junction (Fig. 6B). From our observations, the animal pole of the newly oviposited egg is always towards the opening of the water tube at the dorsal side of the host mussel (Fig. 6B). During blastokinesis, the orientation of embryo changes so that the head moves gradually to the vegetal pole (Fig. 6C). Consequently, when the embryo hatches out rostrally at the vegetal end, the newly hatched embryo is oriented towards the blind end of the water tube at the ventral side of the host mussel (Fig. 6E).

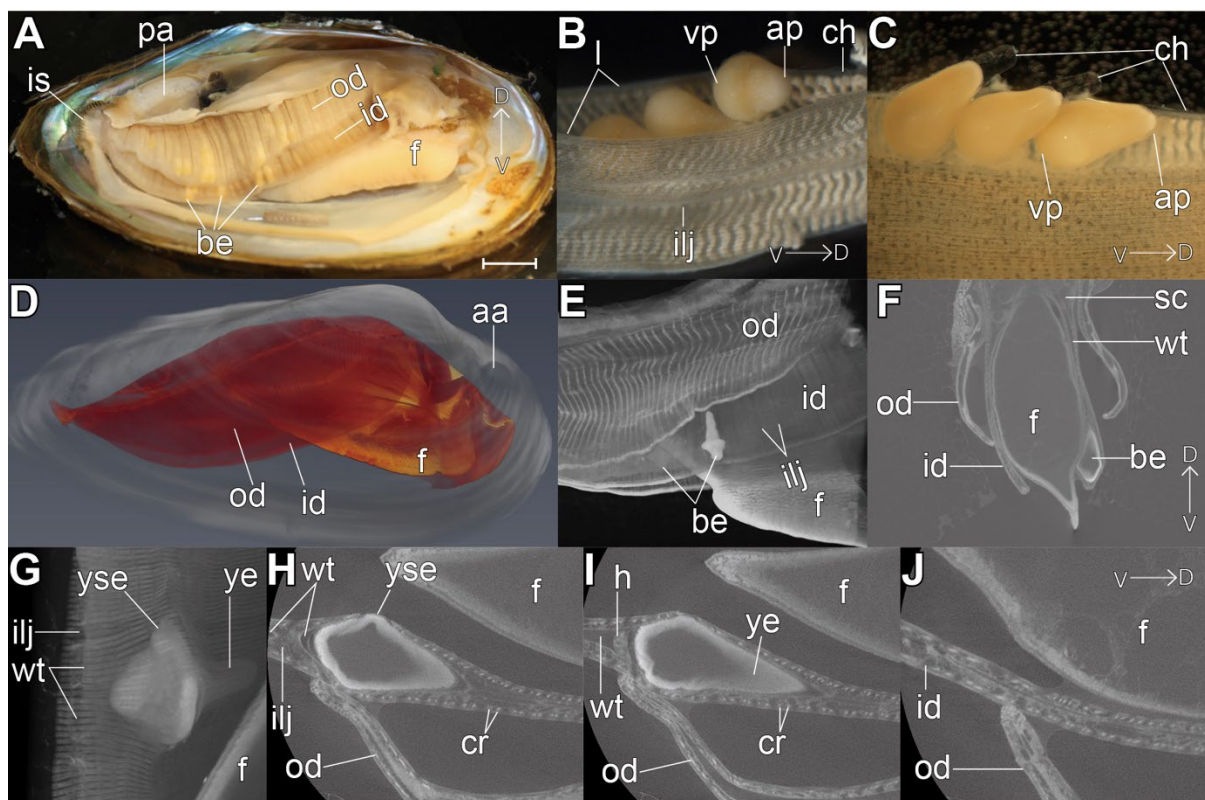


Figure 6 Rosy Bitterling embryos in the interlamellar space of the host mussel (*Anodonta anatine*). A shows a host mussel gravid with bitterling embryos, the right shell removed, dorsal up, anterior to the right. B and C are macro photographs of the gill lamellae occupied by bitterling embryos. Notice that the pre-hatching embryos are oriented with their animal pole dorsal to the gill lamellae. D, microCT reconstruction of an intact mussel. The internal soft tissue is pseudo-colored, dorsal up, anterior to the right. E to J is microCT scan results of a gravid host mussel. E and G, volume rendering view of mussel gills and bitterling embryos. F, transverse virtual section of the mussel gill lamellae, dorsal up. H to J, coronal virtual section of the bitterling embryo, head to the left. Keys: is, inhalant siphon; pa, posterior abductor muscle; aa, anterior abductor muscle; f, foot; be, bitterling embryo; od, outer demibranchs; id, inner demibranchs; wt, water tube; l, gill lamellae; ap, animal pole of bitterling embryo; vp, vegetal pole of bitterling embryo; ilj, interlamellar junction; h, head; ye, yolk extension; yse, yolk sac extension; sc, suprabranchial chamber; cr, chitinous rods. The dorsal-ventral body axis of the mussel is indicated by an arrow from V towards D. Scale bar in A is 10 mm.

Compared with a non-parasitized mussel (Fig. 6D), the gills of bitterling host-mussels have irregular folds and the interlamellar space is obviously dilated (Fig. 6E and F). At the site occupied by the bitterling embryo, 2-3 water tubes are merged to form a large chamber (Fig. 6G and J) because of the growth of YSEs. We also found damage to the interlamellar junction and broken lamellar filaments surrounding the enlarged YSEs (Fig. 6G). The gill filaments are closely attached to the yolk sac of the bitterling embryo, leaving no space for movements of the embryo before the YSEs disappear (Fig. 6H to J). Therefore, the bitterling post-hatching embryo is held in the gill water tube in this position for 3-4 weeks until the yolk mass has been totally consumed and the YSEs have disappeared.

Discussion

We have examined the unique blastokinesis process and early embryonic development of the bitterling *R. ocellatus* for the first time using molecular markers. Our data suggest that the blastokinesis in bitterlings is actually the convergent-extension movement during gastrulation and neurulation, followed by body elongation during somitogenesis. We also provide evidence that blastokinesis is functional, because it provides a secure body direction of post-hatching embryos in the water tube of the host mussel.

Now we can answer the question we posed in the introduction: what is the relationship between insect blastokinesis and bitterling blastokinesis? In short, these two types of blastokinesis are functionally different. In bitterlings, the distinct advantage of blastokinesis is related to the body direction during hatching, and does not function in agitating the yolk mass. We also show that, in the bitterling, the changes of embryo direction are like a 'front-flip' on the yolk mass, in contrast to the 'back flip' seen in insects (e.g., milkweed bug, *Oncopeltus fasciatus*; Panfilio, 2008). Therefore, it is difficult to find homology in regulatory genes. However, we suggest that blastokinesis may be related to the large quantity of yolk amount in bitterlings because it does not occur in *Drosophila melanogaster* (the fruit fly), the embryos of which have very reduced extraembryonic tissue (Panfilio, 2008; Saenko et al., 2008).

We have shown that yolk plug closure in the rosy bitterling and the zebrafish embryos takes place opposite the vegetal pole (dorsally vs. ventrally), indicating that the ventral blastoderm lip migrates faster than the dorsal lip in the bitterling. In zebrafish, the migration of the blastoderm is called epiboly (Délot et al., 1999; Fürthauer et al., 1997; Kimmel et al., 1995; Li et al., 2007; Xiong et al., 2014). We speculate that epiboly in the bitterling shows differences in migration rate compared to the zebrafish that may be related to the shape of the yolk. Our hypothesis is that the specialised shape and size of the bitterling yolk affects the diffusion of molecular signals that regulate the dorsal-ventral differentiation during convergence and extension. The body orientation during hatching is important in at least two respects.

First, if the opening of the chorion and the body orientation are random, then it may sometimes happen by chance that post-hatching embryos inside the water tube are aligned head-to-head. This orientation may be maladaptive if it leads to competition between embryos for oxygen and space. As we have shown in this study, all bitterling embryos hatch from the vegetal side of the chorion, opposite to the site of micropyle, and all are oriented in the same direction. We suggest that this arrangement allows all embryos to make the most effective use of the interlamellar space.

Second, the hatched embryos always have their heads directed towards the blind end of the gill filaments. In the eulamellibranch gill, the water runs into the partitioned water tubes through ostia. Inside each water tube, water moves dorsally and empties into the suprabranchial chamber, then out to the environment from the excurrent siphon (Medler and Silverman, 2001; Medler et al., 1999). It has been reported that mussels can eject premature bitterling embryos by a sudden burst of high velocity water flow (Mills and Reynolds, 2003; Reichard et al., 2007; Rouchet et al., 2017). With their heads facing the blind end, embryos can either resist ejection by being anchored to the gill filament via their wing-like YSEs (during the early developmental period) or can swim against the water current (when capable of movement).

The bitterling embryo provides an example how small modifications in yolk shape and egg size affect morphogenetic movements of the extraembryonic tissue (the yolk sac and YSEs) during gastrulation and somitogenesis. And these subtle shifts are amplified to produce an adaptive variation known as blastokinesis. This is in consistent with the concept of developmental penetrance of adaptations (Bickelmann et al., 2012; Richardson, 1999). This theory states that evolutionary adaptations appearing at later stages of development, can result from the modification of early stages of development.

References

- Aldridge, D. C.** (1999). Development of European bitterling in the gills of freshwater mussels. *J. Fish Biol.* **54**, 138–151.
- Arai, R.** (1988). *Acheilognathus melanogaster*, a senior synonym of *A. moriokae*, with a revision of the genera of the subfamily Acheilognathinae (Cypriniformes, Cyprinidae). *Bull Nat Sci Mus Tokyo Ser A* **14**, 199–213.
- Awata, S., Sasaki, H., Goto, T., Koya, Y., Takeshima, H., Yamazaki, A. and Munehara, H.** (2019). Host selection and ovipositor length in eight sympatric species of sculpins that deposit their eggs into tunicates or sponges. *Mar. Biol.* **166**, 59.
- Bickelmann, C., Mitgutsch, C., Richardson, M. K., Jiménez, R., de Bakker, M. A. G., Sánchez-Villagra, M. R., Jimenez, R., de Bakker, M. A. G. and Sanchez-Villagra, M. R.** (2012). Transcriptional heterochrony in talpid mole autopods. *Evodevo* **3**, 16.
- Chang, H. W.** (1948). Life history of the common Chinese bitterling, *Rhodeus ocellatus*. *Sinensia* **19**, 12–22.
- Chang, H. W. and Wu, H. W.** (1947). On the blastokinesis occurring in the egg of the common Chinese Bitterling, *Rhodeus ocellatus*. *Sinensia* **17**, 15–22.
- Cheng, P., Yu, D., Liu, S., Tang, Q. and Liu, H.** (2014). Molecular phylogeny and conservation priorities of the subfamily Acheilognathinae (Teleostei: Cyprinidae). *Zool. Sci* **31**, 300–308.
- Délot, E., Kataoka, H., Goutel, C., Yan, Y.-L., Postlethwait, J., Wittbrodt, J. and Rosa, F. M.** (1999). The BMP-related protein Radar: a maintenance factor for dorsal neuroectoderm cells? *Mech. Dev.* **85**, 15–25.
- Dorey, K. and Amaya, E.** (2010). FGF signalling: diverse roles during early vertebrate embryogenesis. *Development* **137**, 3731–3742.
- Eisenhoffer, G. T., Slattum, G., Ruiz, O. E., Otsuna, H., Bryan, C. D., Lopez, J., Wagner, D. S., Bonkowsky, J. L., Chien, C. Bin, Dorsky, R. I., et al.** (2017). A toolbox to study epidermal cell types in zebrafish. *J Cell Sci* **130**, 269–277.
- Fürthauer, M., Thisse, C. and Thisse, B.** (1997). A role for FGF-8 in the dorsoventral patterning of the zebrafish gastrula. *Development* **124**, 4253–64.
- Imboden, M., Goblet, C., Korn, H. and Vríz, S.** (1997). Cytokeratin 8 is a suitable epidermal marker during zebrafish development. *C R Acad Sci III* **320**, 689–700.
- Kawamura, K., Ueda, T., Arai, R. and Smith, C.** (2014). Phylogenetic relationships of bitterling fishes (Teleostei: Cypriniformes: Acheilognathinae), inferred from mitochondrial cytochrome B sequences. *Zool. Sci* **31**, 321–329.
- Khlopova, A. V. and Kul'bachnyi, S.** (2013). Histological structure of the female gonads and ovipositor of the European bitterling, *Rhodeus amarus* (Bloch, 1782) (Cyprinidae: Acheilognathinae). *Acta Zool.* **94**, 355–363.
- Kim, Y. U. and Park, Y. S.** (1985). Egg development and larvae of the rose bitterling *Rhodeus ocellatus* (KNER). *Korean J. Fish. Aquat. Sci.* **18**, 586–593.

- Kimmel, C. B., Ballard, W. W., Kimmel, S. R., Ullmann, B. and Schilling, T. F.** (1995). Stages of embryonic development of the zebrafish. *Dev. Dyn.* **203**, 253–310.
- Kunz, Y. W.** (2004). *Developmental Biology of Teleost Fishes*. Dordrecht: Springer Netherlands.
- Leung, T. L. F.** (2014). Fish as parasites: An insight into evolutionary convergence in adaptations for parasitism. *J. Zool.* **294**, 1–12.
- Li, Z., Korzh, V. and Gong, Z.** (2007). Localized rbp4 expression in the yolk syncytial layer plays a role in yolk cell extension and early liver development. *BMC Dev. Biol.* **7**, 117.
- Medler, S. and Silverman, H.** (2001). Muscular Alteration of Gill Geometry in vitro: Implications for Bivalve Pumping Processes. *Biol. Bull.* **200**, 77–86.
- Medler, S., Thompson, C. C., Dietz, T. H. and Silverman, H.** (1999). Ionic effects on intrinsic gill muscles in the freshwater bivalve, *Dreissena polymorpha*. *Comp. Biochem. Physiol. - A Mol. Integr. Physiol.* **122**, 163–172.
- Mills, S. C. and Reynolds, J. D.** (2003). The bitterling-mussel interaction as a test case for co-evolution. *J. Fish Biol.* **63**, 84–104.
- Nagata, Y. and Miyabe, H.** (1978). Development Stages of the Bitterling, *Rhodeus ocellatus ocellatus* (Cyprinidae). *Mem. Osaka Kyoiku Univ. III, Nat. Sci. Appl. Sci.* **26**, 171–181.
- Needham, J.** (1942). *Biochemistry and morphogenesis*. Cambridge: University Press.
- Olt, A.** (1893). Lebensweise und Entwicklung des Bitterlings. *Zeitschrift für wissenschaftliche Zool.* **55**, 543–575.
- Panfilio, K. A.** (2008). Extraembryonic development in insects and the acrobatics of blastokinesis. *Dev. Biol.* **313**, 471–491.
- Panfilio, K. A.** (2009). Late extraembryonic morphogenesis and its zenRNAi-induced failure in the milkweed bug *Oncopeltus fasciatus*. *Dev. Biol.* **333**, 297–311.
- Phillips, B. T., Kwon, H. J., Melton, C., Houghtaling, P., Fritz, A. and Riley, B. B.** (2006). Zebrafish msxB, msxC and msxE function together to refine the neural-nonneural border and regulate cranial placodes and neural crest development. *Dev. Biol.* **294**, 376–390.
- Reichard, M., Liu, H. and Smith, C.** (2007). The co-evolutionary relationship between bitterling fishes and freshwater mussels: insights from interspecific comparisons. *Evol. Ecol. Res.* **9**, 239–259.
- Richardson, M. K.** (1999). Vertebrate evolution: The developmental origins of adult variation. *BioEssays* **21**, 604–613.
- Rouchet, R., Smith, C., Liu, H. Z., Methling, C., Douda, K., Yu, D., Tang, Q. Y. and Reichard, M.** (2017). Avoidance of host resistance in the oviposition-site preferences of rose bitterling. *Evol. Ecol.* **31**, 769–783.
- Saenko, S. V., French, V., Brakefield, P. M. and Beldade, P.** (2008). Conserved developmental processes and the formation of evolutionary novelties: examples from butterfly wings. *Philos Trans R Soc L. B Biol Sci* **363**, 1549–1555.
- Smith, C.** (2016). Bayesian inference supports the host selection hypothesis in explaining adaptive host specificity by European bitterling. *Oecologia* **183**, 1–11.
- Smith, C., Reichard, M., Jurajda, P. and Przybylski, M.** (2004). The reproductive ecology of the European bitterling (*Rhodeus sericeus*). *J. Zool.* **262**, 107–124.
- Smith, C., Warren, M., Rouchet, R. and Reichard, M.** (2014). The function of multiple ejaculations in bitterling. *J. Evol. Biol.* **27**, 1819–1829.
- Spence, R. and Smith, C.** (2013). Rose bitterling (*Rhodeus ocellatus*) embryos parasitize freshwater mussels by competing for nutrients and oxygen. *Acta Zool.* **94**, 113–118.
- Suzuki, N.** (2006). Egg and larval development of the bitterling, *Rhodeus pseudosericeus* (Cyprinidae). *Japanese J. Ichthyol.* **53**, 47–54.
- Tada, M. and Heisenberg, C.-P.** (2012). Convergent extension: using collective cell migration and cell intercalation to shape embryos. *Development* **139**, 3897–3904.
- Virta, V. C. and Cooper, M. S.** (2009). Ontogeny and phylogeny of the yolk extension in embryonic cypriniform fishes. *J. Exp. Zool. Part B Mol. Dev. Evol.* **312**, 196–223.
- Vogel, A. M. and Gerster, T.** (1997). Expression of a zebrafish Cathepsin L gene in anterior mesendoderm and hatching gland. *Dev. Genes Evol.* **206**, 477–479.
- Williams, M. L. K. and Solnica-Krezel, L.** (2020). Cellular and molecular mechanisms of convergence and extension in zebrafish. In *Current Topics in Developmental Biology*, pp. 377–407. Academic Press Inc.
- Xiong, F., Ma, W., Hiscock, T. W., Mosaliganti, K. R., Tentner, A. R., Brakke, K. A., Rannou, N., Gelas, A., Souhait, L., Swinburne, I. A., et al.** (2014). Interplay of Cell Shape and Division Orientation Promotes Robust Morphogenesis of Developing Epithelia. *Cell* **159**, 415–427.

Chapter 6 Summary and discussion

A tribute to landmark researches

Compared with modern results the wonder is, not that these early workers made mistakes, but that they made so few. (De Beer, 1937: p. 14)

Wenjing Yi, Michael K. Richardson

Institute of Biology, University of Leiden, Sylvius Laboratory, Sylviusweg 72, 2333BE, Leiden, the Netherlands.

Manuscript in preparation

In this chapter, we summarize the results of this thesis while reviewing previous landmark researches, and discuss how the results of this thesis connect scattered fragments from the past. The bitterlings, a special group of species that have drawn the attention of biologist, have been known for more than a century (Boeseman et al., 1938; Chang, 1948; Chang and Wu, 1947; Duyvené de Wit, 1955; Kitamura et al., 2012; Methling et al., 2018; Mills and Reynolds, 2003; Olt, 1893; Reichard et al., 2007; Rouchet et al., 2017; Smith, 2016; Wiepkema, 1962). Among all the biologist that focussed on bitterlings, Olt (1893) was the first to describe the developmental stages of the European bitterling embryo (*Rhodeus amarus*). His illustrations of the changing shapes of the yolk are still regarded as classics. **Chapter 2** of this thesis is a tribute to Olt's staging series (Olt, 1893) and to the work of Kim & Park (1985) and Nagata & Miyabe (1978).

I want to emphasize again the importance of staging descriptions for understanding development. Franz Keibel set up a paradigm for embryonic research by presenting normal plates, tables, and stages (Hopwood, 2007; Keibel, 1895). These provide detailed developmental data in a standard way that helps in the analysis of differences between ontogeny and phylogeny (Bininda-Emonds et al., 2002). The staging system is a way to organizing embryonic development and is the cornerstone of developmental and evolutionary research (Iwamatsu, 2004; Kunz, 2004; Richardson and Keuck, 2002; Wong et al., 2015). Development is a dynamic process. As Wilhem Roux wrote, 'Development is Change' (Roux, 1894). International cooperation and cross-disciplinary collaboration are possible only when staging characters are established, providing a specific time window for cross-species comparative studies (Kimmel et al., 1995; Signore et al., 2009; Werneburg, 2009). Our complete stage series of the bitterling species *R. ocellatus* In **Chapter 2** is a response to the call of Duyvené de Wit (1955) for realizing a broad research scheme including comparative embryology, endocrinology, ethology and taxonomy.

In **Chapter 3**, we described the neuroanatomy of bitterling for the first time, filling the gaps in the previous embryonic research in various bitterling taxa. Combined with the molecular analysis of brain early development in **Chapter 4**, brain development in the rosy bitterling is compared with that in the zebrafish. We found that there is a timing difference between head development and trunk development in the rosy bitterling vs. the zebrafish. Compared with previous bitterling embryonic research that focussed on phylogeny and classification (Kim, 2020; Suzuki, 2006; Suzuki and Hibiya, 1984a; Suzuki et al., 1989b), I have introduced the zebrafish (*Danio rerio*) as a comparison species to study developmental heterochrony. By taking advantage of the knowledge of the genetic background of the zebrafish (Kudoh et al., 2001; Thisse and Thisse, 2014; Thisse et al., 2004), and its development (Mork and Crump, 2015; Virta and Cooper, 2011; Whitfield et al., 2002), I have tried to provide an insight to the conserved aspects of teleost development while highlighting synapomorphies of the bitterling.

Olt (1893) mentioned that the embryos that he found in the mussel gills were, without exception, oriented with their heads towards the blind end of the gill, and their tails oriented towards the gill duct. In this way, the bitterling can remain safely in the gill by means of its wing-like YSEs. Olt (1893) believed that the embryo's orientation is caused by gravity; by contrast, Chang & Wu (1947) refuted the gravity hypothesis through experiments. The research of (Chang and Wu, 1947) is an important landmark because it pioneers the study of the morphogenesis of *R. ocellatus*. Those authors

proposed that blastokinesis is the reason for embryo's rotation in the chorion. The rotation occurs in the same way, no matter how the influence of gravity changes.

In **Chapter 5**, I studied blastokinesis by means of molecular markers: *fgf8a*, a marker of the embryonic shield; and *msx3*, a marker of the neural ectoderm boundary. My conclusion is that bitterling-specific blastokinesis is convergent with insect blastokinesis. Compared to the well-known blastokinesis of insects (Panfilio, 2008; Panfilio et al., 2006), the direction of embryo displacement during bitterling blastokinesis is reversed. Thus, there is a 'backflip' in the milkweed bug (*Oncopeltus fasciatus*) vs. a 'frontflip' in the rosy bitterling. The bitterling-specific blastokinesis is essentially a convergent extension process (D'Amico and Cooper, 2001; Tada and Heisenberg, 2012). It is noticeable that the convergent extension migration of cells in the rosy bitterling takes place on an irregular yolk mass shaped like an inverted balloon. Therefore, I speculate that the special features of bitterling blastokinesis are related to changes in the axial orientation of the cells as they migrate over the irregular yolk mass.

In the future, my research outlook will be: 1) to introduce more closely-related species to the species pool, including *Tanakia* and *Acheilognatus* sp. For these sister groups, thorough embryonic research is necessary to facilitate comparative studies and help us answer how they have adapted to their brood parasitic life history. One thing that needs special investigation is the molecular regulation mechanism of YSEs development; 2) to trace cell migration *in toto* during the blastokinesis period, and at the same time manipulate the expression of genes that control the axial migration of cells using gene editing.

Techniques to study bitterling development

In this thesis, I applied a variety of techniques to study the development of a single species. Therefore, it is necessary to summarize the advantages of different techniques and integrate them into a combined protocol for future studies. I recommend time-lapse video as the first step of any embryonic research. It is useful for the recording of dynamic processes, for example heart rate, tracking body movements and tracing the establishment of the blood circulation (**Chapter 2**). More importantly, tracking the hatching moment of the rosy bitterling in real time helped me hypothesize that the hatching process is mechanical rather than enzymatic. In addition, by regularly recording embryo dynamics before hatching, I became aware of the body rotation movements inside the chorion, a part of the bitterling-specific blastokinesis, which is otherwise easily overlooked (**Chapter 5**).

MicroCT is helpful for the observation of external morphology and morphological staging characters. Numerically indexed characters such as somite number (from counting the somite/myotome boundaries) and prim number (by discerning the leading, posterior end of the posterior lateral line primordium during its caudal migration) were only observable with the help of MicroCT (**Chapter 2**). The three-dimensional (3-D) images obtained by microCT are like a spatial navigation system, and are extremely useful for anatomical analyses of the complex brain structures. To gain insight into the morphogenesis of the bitterling brain, I analyzed the formation of the brain ventricular system in three-dimension from stage *1-ovl* to *long-pec* (**Chapter 3**). Furthermore, microCT has the capacity to indicate the location of proliferative zones. It provides an updating of traditional modalities (e.g., histology) for future comparative studies of the teleost brain.

I also note the limitations of microCT. First of all, the virtual sections have a limited resolution, much less than that of conventional histological sections (Figure 1.). Secondly, tissue specific staining is not currently feasible in routine microCT.

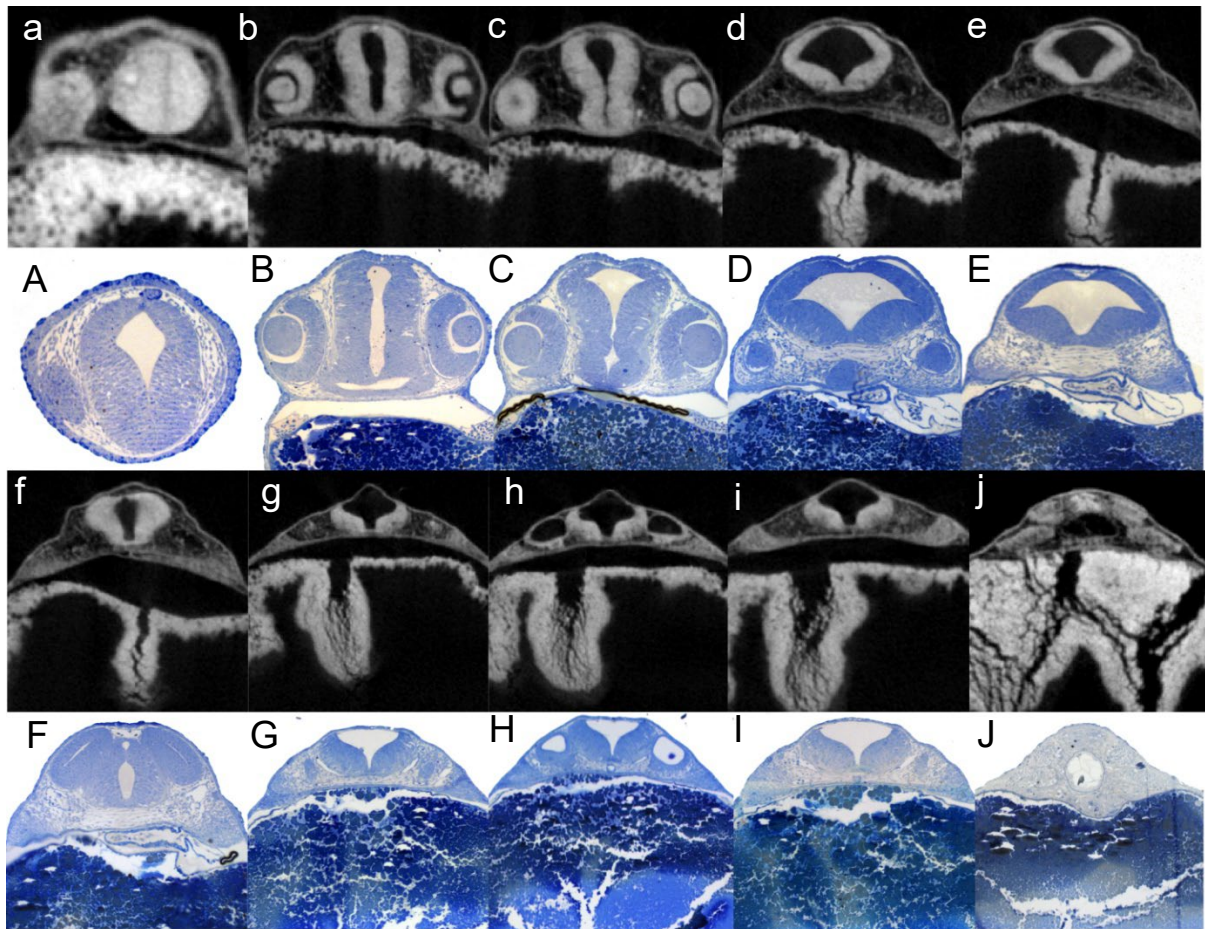


Figure 1 *Rhodeus ocellatus*, virtual microCT sections compared to histological sections. a to j: microCT virtual sections, 78.5 hpf. A to J: epon embedded sample stained with toluidine blue, 3 dpf. Transverse sections from rostral to caudal at the level of olfactory placode (a and A), optic stalk and forebrain ventricle (b and B), optic cup (c and C), midbrain ventricle (d, e and D, E), midbrain hindbrain boundary (f and F), hindbrain ventricle (g and G), otic vesicle (h and H), notochord (i and I), and myotome (j and J).

Nonetheless, microCT is time-efficient, non-destructive and the counter staining using PTA is reversible and does not preclude subsequent histological staining (Keklikoglou et al., 2019). In terms of technical procedures, CT scanning is highly recommended as the next step of *in vivo* research, to be used before routine histology or other destructive methods. Our study demonstrates the value of microCT in developmental biology. For species, like the rosy bitterling, that were previously difficult to study because of limited material, microCT scans provide a wealth of morphological data and readily yield 3-D information. In addition, microCT has the capacity of visualizing and analyzing specimen digitally, which facilitate data sharing and the reuse of the digital data for comparative studies (Davies et al., 2017).

Wholemout *in situ* hybridization (WISH) is the technique I used to study temporal and special gene expression patterns during bitterling development. In **Chapter 4**, the brain segmental boundaries are marked by discrete gene expression domains the early embryo. At these early stages,

boundaries are not discernible using microCT or histology. For example, the midbrain-hindbrain boundary (MHB) is distinctly marked by *fgf8a* expression in the early embryo at 30 hpf (hatching). The initial migration of the neural crest cells marked by the *dlx2a* expression, began at 50 hpf. These genoarchitectonic boundaries are based on highly conserved gene expression patterns, which are related directly to the causal mechanisms that create the relevant morphological subdivisions (Puelles and Ferran, 2012; Schredelseker and Driever, 2020). WISH therefore provides an opportunity to understand the causal mechanisms from genomic control to the boundaries that were defined by gross morphology (e.g., ventricular sulci and cytoarchitecture).

The molecular marker method also provides an opportunity for understanding the blastokinesis (**Chapter 5**), and early embryonic development of the bitterling *R. ocellatus*. The expression data suggest that blastokinesis in bitterlings is based on the convergent-extension movements of the blastoderm cells during gastrulation and neurulation. Our study can potentially identify candidate genes that regulate blastokinesis, but functional studies are needed to make the identification definitive. My hypothesis is that blastokinesis is morphogenetic movement which results from collective cell migration on the anterior-posterior and dorsal-ventral axes. In most cases, the hatching embryo is located with its head towards the vegetal side, as a result of the cell migration. Heterochrony (a change in developmental timing) can potentially modify blastokinesis; by prolonging or delaying convergent extension movement, it is possible that the embryo could hatch from the animal pole of the chorion or the head could only migrate halfway.

In summary, innovative research techniques have brought us new perspectives and have updated our understanding of the development of bitterlings. In the future, new techniques such as *in toto* imaging (Bassi et al., 2015), which is capable of quantitative analysis of cell shape changes and the orientation of cell divisions, will provide an opportunity to understand the regulation of blastokinesis. However, embryonic development is dynamic and complex process. Before observing embryos at single-cell resolution, I recommend starting with time lapse observations and constructing a 3D model in order to form a global view.

Summary of the comparison with zebrafish development

In **chapters 2, 3 and 4**, we compared heterochrony (changes in development timing) and transcriptional heterochrony (changes in the timing of gene expression) between the rosy bitterling and the zebrafish. The comparison indicated evolutionary adaptations related to the bitterling's brood parasitic lifestyle. These adaptations are summarized as follows:

I identified developmental delays in retinal pigmentation and pectoral fin development (in *R. ocellatus* compared to the zebrafish *D. rerio*). Possible explanations for these delays are: 1) the bitterling embryos and larvae develop in a dark, enclosed and sheltered environment, with no need for retinal photosensitivity. This is comparable, perhaps to the lack of retinal pigmentation in cave fish (Yamamoto et al., 2004). 2) **the** motility of bitterling is restricted while they are developing in the gill water-tube of their host mussel, and the fin is therefore effectively functionless.

A developmental advance is conspicuous in the development of the inner ear. The morphogenesis of the semicircular canals, the separation of the lagena from the sacculolagenar pouch and the formation of the asteriscus otolith are all pre-displaced in bitterling development. This

predisplacement may be related to embryonic development in a dark environment where hearing is more useful than vision. This in turn would also explain why visual development appears to be delayed in the bitterling.

For transcriptional heterochrony, if I just compare the expression patterns and timing in the brain region, there are comparable developmental stages in the bitterling and zebrafish. But if the comparison expands to the whole embryo, including the pectoral fin bud and myotomes, such comparable developmental stages do not exist. It is obvious that the development of pectoral fins lags behind the development of the brain in both species. My explanation is that development is modular; each module has its independent rhythm or autonomous growth. Just as there are different time zones on the earth, the time zone of the brain region is several hours earlier than the trunk region. Even the ticking of the clock may be faster or slower. The high level of timing changes (heterochrony) between developmental modules is an important evolutionary mechanism that has been shown to underlie phenotypic evolution (Bininda-Emonds et al., 2002; Bininda-Emonds et al., 2003; Olaf R. P. et al., 2003; Richardson, 1995).

References

- Bassi, A., Schmid, B. and Huisken, J.** (2015). Optical tomography complements light sheet microscopy for in toto imaging of zebrafish development. *Dev.* **142**, 1016–1020.
- Bininda-Emonds, O. R. P. P., Jeffery, J. E., Coates, M. I. and Richardson, M. K.** (2002). From Haeckel to event-pairing: the evolution of developmental sequences. *Theory Biosci.* **121**, 297–320.
- Bininda-Emonds, O. R. P., Jeffrey, J. E. and Richardson, M. K.** (2003). Is Sequence Heterochrony an Important Evolutionary Mechanism in Mammals? *J. Mamm. Evol.* **10**, 335–361.
- Boeseman, M. J., Van der Drift, J., Van Roon, J. M., Tinbergen, N. and Ter Pelkwijk, J. J.** (1938). De bittervoorns en hun mossels. *Levende Nat.* **43**, 129–136.
- Chang, H. W.** (1948). Life history of the common Chinese bitterling, *Rhodeus ocellatus*. *Sinensia* **19**, 12–22.
- Chang, H. W. and Wu, H. W.** (1947). On the blastokinesis occurring in the egg of the common Chinese Bitterling, *Rhodeus ocellatus*. *Sinensia* **17**, 15–22.
- D’Amico, L. A. and Cooper, M. S.** (2001). Morphogenetic domains in the yolk syncytial layer of axiating zebrafish embryos. *Dev. Dyn.* **222**, 611–624.
- Davies, T. G., Rahman, I. A., Lautenschlager, S., Cunningham, J. A., Asher, R. J., Barrett, P. M., Bates, K. T., Bengtson, S., Benson, R. B. J., Boyer, D. M., et al.** (2017). Open data and digital morphology. *Proc. R. Soc. B Biol. Sci.* **284**, 20170194.
- De Beer, G. R.** (1937). *The development of the vertebrate skull*. Oxford: Clarendon Press.
- Duyvené de Wit, J.** (1955). Some results of investigations into the European Bitterling, *Rhodeus amarus* BLOCH. *Japanese J. Ichthyology* **4**, 94–104.
- Hopwood, N.** (2007). A history of normal plates, tables and stages in vertebrate embryology. *Int. J. Dev. Biol.* **51**, 1–26.
- Iwamatsu, T.** (2004). Stages of normal development in the medaka *Oryzias latipes*. *Mech Dev* **121**, 605–618.
- Keklikoglou, K., Faulwetter, S., Chatzinikolaou, E., Wils, P., Brecko, J., Kvaček, J., Metscher, B. and Arvanitidis, C.** (2019). Micro-computed tomography for natural history specimens: a handbook of best practice protocols. *Eur. J. Taxon.* 1–55.
- Kim, H. S.** (2020). Minute tubercles in bitterling larvae: Developmental dynamic structures to prevent premature ejection by host mussels. *Ecol. Evol.* **10**, 5840–5851.
- Kim, Y. U. and Park, Y. S.** (1985). Egg development and larvae of the rose bitterling *Rhodeus ocellatus* (KNER). *Korean J. Fish. Aquat. Sci.* **18**, 586–593.
- Kimmel, C. B., Ballard, W. W., Kimmel, S. R., Ullmann, B. and Schilling, T. F.** (1995). Stages of embryonic development of the zebrafish. *Dev. Dyn.* **203**, 253–310.
- Kitamura, J., Nagata, N., Nakajima, J. and Sota, T.** (2012). Divergence of ovipositor length and egg shape in a brood parasitic bitterling fish through the use of different mussel hosts. *J. Evol. Biol.* **25**, 566–573.

- Kudoh, T., Tsang, M., Hukriede, N. A., Chen, X., Dedekian, M., Clarke, C. J., Kiang, A., Schultz, S., Epstein, J. A., Toyama, R., et al.** (2001). A gene expression screen in zebrafish embryogenesis. *Genome Res.* **11**, 1979–1987.
- Kunz, Y. W.** (2004). *Developmental Biology of Teleost Fishes*. Dordrecht: Springer Netherlands.
- Methling, C., Douda, K., Liu, H., Rouchet, R., Bartáková, V., Yu, D., Smith, C. and Reichard, M.** (2018). Energetic costs in the relationship between bitterling and mussels in East Asia. *Biol. J. Linn. Soc.* **125**, 750–759.
- Mills, S. C. and Reynolds, J. D.** (2003). The bitterling-mussel interaction as a test case for co-evolution. *J. Fish Biol.* **63**, 84–104.
- Mork, L. and Crump, G.** (2015). Zebrafish Craniofacial Development. In *Current Topics in Developmental Biology*, pp. 235–269.
- Nagata, Y. and Miyabe, H.** (1978). Development Stages of the Bitterling, *Rhodeus ocellatus ocellatus* (Cyprinidae). *Mem. Osaka Kyoiku Univ. III, Nat. Sci. Appl. Sci.* **26**, 171–181.
- Olaf R. P., B.-E., Jonathan E., J. and Richardson, M. K.** (2003). Inverting the hourglass: quantitative evidence against the phylotypic stage in vertebrate development. *Proc. R. Soc. London. Ser. B Biol. Sci.* **270**, 341–346.
- Olt, A.** (1893). Lebensweise und Entwicklung des Bitterlings. *Zeitschrift für wissenschaftliche Zool.* **55**, 543–575.
- Panfilio, K. A.** (2008). Extraembryonic development in insects and the acrobatics of blastokinesis. *Dev. Biol.* **313**, 471–491.
- Panfilio, K. A., Liu, P. Z., Akam, M. and Kaufman, T. C.** (2006). *Oncopeltus fasciatus* zen is essential for serosal tissue function in kataropsis. *Dev. Biol.* **292**, 226–243.
- Puelles, L. and Ferran, J. L.** (2012). Concept of neural genoarchitecture and its genomic fundament. *Front. Neuroanat.* **6**, 47.
- Reichard, M., Liu, H. and Smith, C.** (2007). The co-evolutionary relationship between bitterling fishes and freshwater mussels: insights from interspecific comparisons. *Evol. Ecol. Res.* **9**, 239–259.
- Richardson, M. K.** (1995). Heterochrony and the phylotypic period. *Dev Biol* **172**, 412–421.
- Richardson, M. K. and Keuck, G.** (2002). Haeckel's ABC of evolution and development. *Biol. Rev. Camb. Philos. Soc.* **77**, 495–528.
- Rouchet, R., Smith, C., Liu, H. Z., Methling, C., Douda, K., Yu, D., Tang, Q. Y. and Reichard, M.** (2017). Avoidance of host resistance in the oviposition-site preferences of rose bitterling. *Evol. Ecol.* **31**, 769–783.
- Schredelseker, T. and Driever, W.** (2020). Conserved Genoarchitecture of the Basal Hypothalamus in Zebrafish Embryos. *Front. Neuroanat.* **14**, 3.
- Signore, I. A., Guerrero, N., Loosli, F., Colombo, A., Villalón, A., Wittbrodt, J. and Concha, M. L.** (2009). Zebrafish and medaka: Model organisms for a comparative developmental approach of brain asymmetry. *Philos. Trans. R. Soc. B Biol. Sci.* **364**, 991–1003.
- Smith, C.** (2016). Bayesian inference supports the host selection hypothesis in explaining adaptive host specificity by European bitterling. *Oecologia* **183**, 1–11.
- Suzuki, N.** (2006). Egg and larval development of the bitterling, *Rhodeus pseudosericeus* (Cyprinidae). *Japanese J. Ichthyol.* **53**, 47–54.
- Suzuki, N. and Hibiya, T.** (1984). Development of Eggs and Larvae of Two Bitterlings, *Rhodeus atremius* and *R. suigensis* (Cyprinidae). *Japanese J. Ichthyol.* **31**, 287–296.
- Suzuki, N., Umezawa, K., Yabe, T. and Murai, H.** (1989). Development of the Bitterling, *Paracheilognathus-Himantegus* (Cyprinidae), with a Note on Minute Tubercles on the Skin Surface. *Japanese J. Ichthyol.* **36**, 318–326.
- Tada, M. and Heisenberg, C.-P.** (2012). Convergent extension: using collective cell migration and cell intercalation to shape embryos. *Development* **139**, 3897–3904.
- Thisse, B. and Thisse, C.** (2014). In Situ Hybridization on Whole-Mount Zebrafish Embryos and Young Larvae. In *Methods in Molecular Biology*, pp. 53–67.
- Thisse, B., Heyer, V., Lux, A., Alunni, V., Degraeve, A., Seiliez, I., Kirchner, J., Parkhill, J. P. and Thisse, C.** (2004). Spatial and temporal expression of the zebrafish genome by large-scale in situ hybridization screening. *Methods Cell Biol* **77**, 505–519.
- Virta, V. C. and Cooper, M. S.** (2011). Structural components and morphogenetic mechanics of the zebrafish yolk extension, a developmental module. *J. Exp. Zool. Part B Mol. Dev. Evol.* **316 B**, 76–92.
- Werneburg, I.** (2009). A Standard System to Study Vertebrate Embryos. *PLoS One* **4**, e5887.
- Whitfield, T. T., Riley, B. B., Chiang, M.-Y. and Phillips, B.** (2002). Development of the zebrafish inner ear. *Dev. Dyn.* **223**, 427–458.
- Wiepkema, P. R.** (1962). An Ethological Analysis of the Reproductive Behaviour of the Bitterling (*Rhodeus Amarus* Bloch). *Arch. Néerlandaises Zool.* **14**, 103–199.

Wong, M. D., Van Eede, M. C., Spring, S., Jevtic, S., Boughner, J. C., Lerch, J. P. and Mark Henkelman, R. (2015). 4D Atlas of the Mouse Embryo for Precise Morphological Staging. *Dev.* **142**, 3583–3591.

Yamamoto, Y., Stock, D. W. and Jeffery, W. R. (2004). Hedgehog signalling controls eye degeneration in blind cavefish. *Nature* **431**, 844–847.

Addendum

Nederlandse samenvatting

Curriculum vitae

List of publications

Nederlandse samenvatting

We ontwikkelden de bittervoorn als een uniek, goed bestudeerd modelorganisme op het gebied van de evolutionaire ecologie van broedparasitisme. De bittervoorn-mosselrelatie, interspecifieke mosselgastheervoorkeur en mosselkieuwstructuur worden in detail bestudeerd om de ontwikkelingsadaptatie van bittervoornembryo's in reactie op hun mosselgastheren te helpen begrijpen. Onze complete reeks van ontwikkelingsstadia van de bittervoornsoort *R. ocellatus* in **Hoofdstuk 2** is een nieuw, op karakter gebaseerd systeem dat compatibel is met het veelgebruikte stadiëringsstelsel voor zebrafissen. Met time-lapse-video hebben we de dynamische processen van het uitkomen van het moment van de roze bittervoorn in realtime gedemonstreerd, wat aangeeft dat het arceringsproces eerder mechanisch dan enzymatisch is.

In **Hoofdstuk 3** beschreven we voor het eerst de neuroanatomie van de bittervoorn, waarmee we de hiaten opvulden in het eerdere embryonale onderzoek in verschillende bitterlingtaxa. Gecombineerd met de moleculaire analyse van de vroege hersenontwikkeling in **Hoofdstuk 4**, wordt de hersenontwikkeling in de roze bittervoorn vergeleken met die in de zebrafis. De vergelijking wees op evolutionaire aanpassingen die verband houden met de broedparasitaire levensstijl van de bittervoorn. We identificeerden ontwikkelingsachterstanden in retinale pigmentatie en borstvinontwikkeling bij *R. ocellatus* in vergelijking met de zebrafis *D. rerio*. De morfogenese van de halfcirkelvormige kanalen, de scheiding van de lagena van de sacculolagenaire zak en de vorming van de asteriscus otoliet zijn allemaal vooraf verplaatst in de ontwikkeling van bittervoornjes. Deze aanpassingen kunnen verband houden met de embryonale ontwikkeling in een donkere omgeving waar horen nuttiger is dan zien. Dit zou op zijn beurt ook verklaren waarom de visuele ontwikkeling vertraagd lijkt te zijn in de bittervoorn.

In **Hoofdstuk 5** hebben we het morfogenetische proces van blastokinese in het embryo van de bittervoorn bestudeerd, en de mogelijke relatie met broedparasitisme. We hebben ons gericht op de vroege ontwikkeling vóór het uitkomen en het uitkomen van de roze bittervoorn. We hebben de expressie van ontwikkelingsregulerende genen *fgf8a*, *msx3*, *krt8* en *ctslb* geprofileerd door middel van whole-mount *in situ* hybridisatie (WISH). We visualiseerden morfogenetische bewegingen tijdens gastrulatie en neurulatie, en het proces van lichaamsverlenging tijdens somitogenese. We concludeerden dat blastokinese bij de roze bittervoorn functioneel is omdat het zorgt voor een optimale positionering van het embryo na het uitkomen in de kieuwruimte van de gastheermossel. Meer in het algemeen biedt onze studie een voorbeeld van variatie in dooivorm en eigrootte in overeenstemming met het concept van ontwikkelingspenetratie van aanpassingen in latere stadia.

In dit proefschrift heb ik een verscheidenheid aan technieken toegepast om de ontwikkeling van een enkele soort te bestuderen. Ik raad time-lapse-video aan als de eerste stap van elk embryonaal onderzoek. MicroCT is nuttig voor de observatie van externe morfologie en morfologische stadiëringskarakters. De driedimensionale (3D) beelden die door microCT worden verkregen, zijn als een ruimtelijk navigatiesysteem en uiterst nuttig voor anatomische analyses van de complexe hersenstructuren. Bovendien heeft microCT het vermogen om de locatie van proliferatieve zones tijdens vroege hersenontwikkeling aan te geven. Het biedt een update van traditionele modaliteiten voor toekomstige vergelijkende studies van de teleost-hersenen.

Curriculum vitae

Wenjing Yi was born on November 11th 1988 in Zigui, a town in Hubei Province of China. After completing secondary education at the No.1 Middle School (Zigui) in 2007, she attended Huazhong Agriculture University to study aquaculture and got her Bachelor's degree in 2011. During this period, she studied artificial breeding and the reproduction of the mandarin fish *Siniperca chuatsi* and the Chinese sturgeon *Acipenser sinensis*. She started her postgraduate study under the supervision of Prof. Jianzhong Shen in the same university with a full scholarship, co-supervised by Prof. E Zhang in the Institute of Hydrobiology, Chinese Academy of Science (CAS). During this period, she became interested in the evolution and biodiversity from the investigation of fish resources in the Dongting Lake system. To specialize herself in the field of taxonomy, she performed a taxonomic revision of the genus *Vanmanenia* (hillstream loach) in South China and the genus *Rhodeus* (bitterling) throughout mainland China. In 2014, she started her PhD at the Institute of Biology of Leiden University under the supervision of Prof. Dr. M. K. Richardson and co-supervision of Dr. M. Rücklin (Naturalis). Her PhD project, entitled "Evolutionary developmental biology of bitterling fish", is described in this thesis.

List of publications

Yi, W., Mueller, T., Rücklin, M., & Richardson, M. K. Developmental neuroanatomy of the rosy bitterling *Rhodeus ocellatus* (Teleostei: Cypriniformes). *Manuscript submitted*.

Yi, W., Rücklin, M., Poelman, R., Aldridge, D. C., & Richardson, M. K. (2021). Normal stages of embryonic development of a brood parasite, the rosy bitterling *Rhodeus ocellatus* (Teleostei: Cypriniformes). *Journal of Morphology*, 282, 783–819.

Yu, Y., Yi, W., Ma, Z., Yang, R., & Shen, J. (2016). The complete mitochondrial genome of *Rhodeus fangi* (Cypriniformes, Cyprinidae, Acheilognathinae). *Mitochondrial DNA*, 27(1), 284–285.

Yi, W. J., Zhang, E., & Shen, J. Z. (2014). *Vanmanenia maculata*, a new species of hillstream loach from the Chang-Jiang basin, South China (Teleostei: Gastromyzontidae). *Zootaxa*, 3802, 85.